EPR Measurements and Redox Chemistry of Fine Particulate Matter

Alexander Filippi

Dissertation

zur Erlangung des Grades

Doktor rerum naturalium (Dr. rer. nat.)

im Promotionsfach Chemie

am Fachbereich Chemie, Pharmazie und Geowissenschaften

der Johannes Gutenberg-Universität in Mainz

Max Planck Graduate Center

Dezember, 2020

I hereby declare that I wrote the dissertation submitted without any unauthorized external assistance and used only sources acknowledged in the work. All textual passages which are appropriated verbatim or paraphrased from published and unpublished texts as well as all information obtained from oral sources are duly indicated and listed in accordance with bibliographical rules. In carrying out this research, I complied with the rules of standard scientific practice as formulated in the statutes of Johannes Gutenberg-University Mainz to insure standard scientific practice.

Abstract

Redox chemistry influences many processes including atmospheric aging as well as adverse health effects of ambient particulate matter (PM). By atmospheric processing and emissions, PM composition undergoes constant change, where condensed-phase and gas-phase molecules interact in multiphase processes including redox- and radical reactions. Upon deposition of PM in the human airways, redox-active constituents may induce oxidative stress in the lung. The term oxidative stress describes a condition in which the formation of reactive species (RS) outcompetes the regulation capacity of natural antioxidants, potentially resulting in oxidation of biomolecules, inflammation, and even cell death or tissue damage. Herein RS include radicals like $^{\bullet}OH$ and $O_2^{-\bullet}$ as well as non-radical species like H_2O_2 and NO_2^-. Due to the complexity of online measurements in airborne particles and the short lifetimes of many radicals, there is a lack of understanding about the atmospheric relevance and reaction rates of many of these redox reactions involving PM. Therefore, in this PhD project electron paramagnetic resonance (EPR) spectroscopy was used to explore some of these processes in PM. This technique is particularly suitable to study radical reactions as it enables the retrieval of qualitative as well as quantitative information about radicals. The concrete research studies in this thesis focused on the following aspects:

(1) Characterization of the impact synthetic cerium oxide nanoparticles (CeNPs) have on OH radical concentrations in a surrogate lung fluid (SLF). Therein, the potential of these particles to produce $^{\bullet}OH$ – a particularly harmful RS - in suspensions was tested against their antioxidant activity using spin-trapping and EPR spectroscopy. According to the investigations, CeNPs exhibit predominantly antioxidant properties in SLF, which mimics physiologically relevant conditions. Furthermore, the particle size has a pronounced impact on this activity, with smaller particles showing a stronger effect. This size-dependent antioxidant activity is attributed to the higher concentration of active surface CeO_2 species, which influence $^{\bullet}OH$ concentrations in solution by heterogeneous redox reactions.

(2) Elucidation of the role of highly oxygenated molecules (HOMs) play in the RS formation of PM upon suspension in aqueous solution. The concentration of HOMs in ambient PM and laboratory-generated secondary organic aerosol (SOA) were quantified using mass spectrometry and radical formation in aqueous solution was studied by EPR spin-trapping. For ambient PM a positive correlation of HOMs abundance with the radical formation in pure water was observed. Among laboratory-generated particles biogenic precursors formed SOA with a higher radical yield than SOA from anthropogenic precursors. The results indicate that HOMs could play a significant role in the production of RS by PM.

(3) Identification of key chemical molecules that determine the production of reactive species by ambient particulate matter from different environments. While there is some understanding that aerosols from clean and polluted environments differ in their potential to generate RS in solution, convincing links to specific PM constituents are missing. Radical and H_2O_2 yields from dissolution of PM confirm differences in the RS production potential by filter samples from a remote forest and two urban sites. Further results indicate that the specific proportions of different RS concentrations measured for the three sites can be reasonably mimicked using only transition metals, organic hydroperoxide, H_2O_2, humic-, and fulvic acids as PM surrogate mixtures. This suggests that these very abundant constituents could be of central importance for the RS yields of PM.

(4) Investigation of the occurrence of environmentally persistent free radicals (EPFR) in remote and urban environments and their distribution within PM of different size between 10 nm and 10 µm.

EPFR are molecular structures that were identified as constituents of ambient PM and also of other environmental samples like soil and microplastic. The understanding of this class of pollutants is still limited due to a shortage of data about their concentration and spatial distribution. The results demonstrate, that EPFR occur not only in populated areas but also in remote regions with limited anthropogenic influence. Among the filter samples from different environments the abundance of EPFR is highly correlated with PM mass concentration. Moreover, in urban air samples, the size-resolved EPFR distribution reveals a pronounced maximum in the sub-micrometer size range, while remote regions have a more variable EPFR size distribution. Based on these insights, the deposition of EPFR in human airways was modeled, whereby the results show that most of the radicals potentially deposit deep in the lung, because they are concentrated in particulate matter smaller than 1 µm.

(5) Determination how prevalent EPFR are indoor air, house dust, and on indoor surfaces, as well as how EPFR interact with gas-phase oxidants. In a coordinated study in Mainz, indoor and outdoor samples were collected simultaneously. Concentrations of EPFR in indoor air were found to be linked with concentrations in outdoor air. The results further demonstrate that the number of EPFR in surface films and house dust exceeds the total amount of EPFR in PM substantially for typical indoor settings. Exposure experiments of those samples indicate that there may be interactions between EPFR and typical gas-phase oxidants (e.g. O_3 and NO_2). Therewith EPFR could be involved in redox reactions and represent a reactivity reservoir in PM as well as other condensed phases indoors.

Zusammenfassung

Redoxchemie ist essentiell für viele Prozesse rund um Feinstaub, dazu zählt die chemische Veränderung von Partikeln in der Atmosphäre sowie auch die schädlichen Gesundheitsauswirkungen von Feinstaub. Die Zusammensetzung von Feinstaub ändert sich permanent durch den Einfluss von Emissionen und atmosphärischem Prozessieren. Für die zu Grunde liegenden Multiphasenprozesse spielen Redox- und insbesondere Radikalreaktionen zwischen Molekülen in der Gas- und Partikelphase eine zentrale Rolle. Beim Einatmen von Feinstaub setzten sich viele Partikel in der Lunge ab und redoxaktive Bestandteile können oxidativen Stress verursachen. Die Bezeichnung oxidativer Stress beschreibt einen Zustand, in dem die Menge an reaktiven Spezies (RS) die regulative Kapazität von Antioxidantien überschreitet, was zur Beschädigung von Biomolekülen und Zellen sowie zu Entzündungsreaktion führen kann. Zu RS zählen in diesem Kontext Radikale wie $^{\bullet}OH$ und $O_2^{-\bullet}$ genauso wie nicht radikalische Spezies wie H_2O_2 und NO_2^-. Da es äußerst komplex ist direkte Messungen in Feinstaub durchzuführen und auch wegen des kurzen Lebenszyklus‘ von Radikalen, gibt es einen Mangel an Ratenkonstanten und Verständnis über die atmosphärische Relevanz von vielen Redoxreaktionen unter Beteiligung von Feinstaub. Aus diesem Grund wurden im Rahmen dieser Doktorarbeit mittels Elektronen Spin Resonanz (EPR) Spektroskopie Redoxprozesse im Zusammenhang mit Feinstaub untersucht. Diese Technik ist besonders geeignet zur Beobachtung von Radikalreaktionen, da sie quantitative und qualitative Einblicke durch die direkte Messung von Radikalen ermöglicht. Die spezifischen Forschungsprojekte, welche im Rahmen dieser Arbeit behandelt wurden, lauten wie folgt:

(1) Charakterisierung des Einflusses den synthetische Cerdioxid Nanopartikeln auf die Konzentration von OH Radikalen in einem Lungenfluid Surrogat (SLF) haben. Dabei konnte gezeigt werden, dass CeO_2 Nanopartikel eine betont antioxidative Wirkung in SLF haben, wobei dieses Medium physiologische Bedingungen simulieren soll. Außerdem zeigten die Ergebnisse eine starke Abhängigkeit der Aktivität von der Partikelgröße, wobei kleinere Nanopartikel einen deutlich stärkeren Effekt hatten. Diese Größenabhängigkeit steht im Zusammenhang mit der Zunahme des Anteils aktiver CeO_2 Spezies an der Oberfläche bei kleineren Partikeln. Diese können mit reaktiven Spezies in Lösung über heterogene Redoxreaktionen interagieren.
(2) Untersuchung des Einflusses den stark oxidierte organische Molekülen (HOMs) auf die Bildung von RS in wässriger Lösung haben. Zu diesem Zweck wurden Feinstaub aus Umgebungsluft sowie synthetisch generierte sekundäre, organische Aerosole (SOA) gesammelt. Anschließend wurden diese Proben auf ihren Gehalt an HOMs mittels Massenspektrometrie und auf ihr Potential zur Bildung von Radikalen mittels EPR Spin-trapping untersucht. Dabei wurde eine positive Korrelation zwischen der Häufigkeit von HOMs und der Bildung von Radikalen in wässriger Lösung aufgedeckt. Im Vergleich von verschiedenen SOA wurde beobachtet, dass Feinstaub aus typischen biologischen Ausgangsmolekülen mehr Radikale produzierte als solcher aus anthropogenen Ausgangsmolekülen. Die Ergebnisse deuten darauf hin, dass HOMs einen substantiellen Beitrag zur Produktion von RS aus Feinstaub leisten.
(3) Identifizierung von Molekülen mit zentraler Bedeutung für die Produktion von RS durch Feinstaub aus verschiedenen Umgebungen. Denn obwohl angenommen wird, dass sich Feinstaub aus sauberen und verschmutzten Regionen in seinen Eigenschaften unterscheidet, fehlt immer noch das Verständnis, welche konkreten Feinstaubbestandteile hauptsächlich für die Produktion on RS verantwortlich sind. Es konnte anhand von Radikal- und H_2O_2 Bildung in wässriger Lösung bestätigt werden, dass es Unterschiede im Potential zur RS Bildung zwischen Filterproben aus einem abgelegenen Wald und zwei urbanen Orten gibt. Des Weiteren konnte demonstriert werden,

dass das ortspezifische Verhältnis der Produktion verschiedener RS experimentell simuliert werden kann. Zu diesem Zweck war es ausreichend unterschiedliche Mischungen von Übergangsmetallen, organischen Hydroperoxiden, H_2O_2, Huminsäuren und Fulvinsäuren als herzustellen. Diese Resultate suggerieren, dass diese häufig vorkommenden Bestandteile von Feinstaub eine zentrale Bedeutung für die RS Produktion durch Feinstaub haben könnten.

(4) Erfassung der Häufigkeit von Environmentally persistent free radicals (EPFR) in abgelegenen und urbanen Umgebungen, sowie deren Verteilung in Feinstaub verschiedener Größe zwischen 10 nm und 10 µm. EPFR sind molekulare Strukturen die als Bestandteil von Feinstaub und auch in Bodenproben sowie Mikroplastik gefunden wurden. Das Wissen über diese Substanzgruppe ist auf Grund von fehlenden Daten über deren Konzentration und Verteilung begrenzt. Die Ergebnisse zeigen, dass EPFR nicht nur in bevölkerten Regionen auftreten, sondern auch in sehr abgelegenen, von Menschen kaum berührten Umgebungen. Die Häufigkeit von EPFR korreliert, beim Vergleich unterschiedlicher Umgebungen, sehr eng mit der Menge an Feinstaub in der Luft. In urbanen Räumen zeigt die Größenverteilung, dass die meisten EPFR in Feinstaub mit weniger als 1 µm Durchmesser auftreten. Im Gegensatz dazu ist die Größenverteilung an abgelegenen Orten variabler. Auf Basis dieser Resultate wurde ermittelt, wie viele EPFR sich beim Einatmen in den Atemwegen absetzen. Die Ergebnisse deuten darauf hin, dass der Großteil der EPFR bis in die Lunge vordringt, weil sie in Partikeln kleiner als 1 µm sind.

(5) Bestimmung von EPFR Konzentrationen in Raumluft, Hausstaub und auf Oberflächen. Außerdem wurde die Interaktion von EPFR mit Oxidantien aus der Gasphase untersucht. In einer systematischen Studie wurden in Mainz parallel Proben drinnen und draußen genommen. Dabei zeigt sich, dass die Konzentration von EPFR in Raumluft häufig eng mit der Konzentration draußen zusammenhängt. Außerdem konnte demonstriert werden, dass die Mengen an EPFR in Hausstaub und Oberflächen die absolute Menge an EPFR in Feinstaub in einem typischen Raum deutlich übersteigt. Die Exposition der gesammelten Proben mit kontrollierten Mengen an O_3 und NO_2 gibt Hinweise darauf, dass EPFR mit diesen gasförmigen Oxidantien interagieren. Damit könnte es sein, dass EPFR ein Reaktivitätsreservoir sind und an Redoxreaktionen in Räumen beteiligt sind.

Contents

1. Introduction

1.1 Health Effects of Air Particulate Matter

Ambient aerosol particles are a large public health problem of global concern (Organization, 2016; West et al., 2016; Cohen et al., 2017; Lelieveld et al., 2020). The occurrence of this particulate matter (PM) is linked to numerous diseases of the respiratory tract, the cardiovascular system, and beyond (Schraufnagel et al., 2019; Lelieveld et al., 2019). These adverse health effects have been connected to oxidative stress in the lung, induced upon airway deposition of PM (Huang et al., 2012; Lakey et al., 2016). Therein oxidative stress describes a condition in which an excessive amount of oxidants is generated, that outcompetes the protective capacity of biological antioxidants. Ultimately, this may lead to inflammation processes and oxidative damage to biomolecules (Sies, 2017). Accordingly, the ability of PM to generate such reactive oxidants determines its potential health impacts. This is sometimes described as the oxidative potential of PM. More concretely, studies mostly focus on particulate matter smaller than 2.5 µm ($PM_{2.5}$), which can penetrate deep into the airways (World-Health-Organization, 2006). To describe the oxidative potential of $PM_{2.5}$, it is crucial to understand its composition and the contribution of different constituents. Accordingly, many studies have investigated single constituents as well as ambient $PM_{2.5}$ for their oxidative potential (Nawrot et al., 2009). In these reports, transition metal ions like iron, copper, and manganese as well as redox-active organic compounds like quinones and organic peroxides are frequently reported to correlate closely with the oxidative potential of $PM_{2.5}$ (Valavanidis et al., 2005; Lyu et al., 2018; Calas et al., 2018). A recent kinetic modeling study has demonstrated that only a few of these PM constituents could account for the majority of oxidative potential (Lakey et al., 2016). Nevertheless, due to the complex and highly variable composition of ambient aerosols, a detailed chemical understanding of the interactions between PM constituents with airway interfaces is missing.

Particulate matter is generated by a variety of emission sources: suspension of dust, sea salt, biological particles, or soot from combustion processes, but also by condensation of gaseous compounds like volatile organic compounds, NO_2, SO_2, and many more (Seinfeld and Pandis, 2016). Some studies have focused on differentiating adverse health effects of PM based on varying emission sources (Künzli et al., 2000; Rohr and Wyzga, 2012; Lelieveld et al., 2015). From these investigations, some combustion processes like traffic or residential fuel burning are standing out as PM sources with potentially increased health relevance, but data on this subject remain controversial. More direct connections are established to certain properties of PM, as measured by aerosol instrumentation. Among them, especially black carbon (BC) seems to be critical for adverse health effects (Highwood and Kinnersley, 2006; Janssen et al., 2011; Magalhaes et al., 2018). BC is identified based on its light-absorbing optical properties, it consists mostly of carbonaceous material often connected to combustion processes (Andreae and Gelencsér, 2006). Due to the potential to robustly detect and monitor this species as well as its toxicity, BC is now also a frequently used air quality indicator.

Another critical factor for PM toxicity is its size distribution. Ambient air often contains suspended particulate matter in the size range from less than 10 nm (e.g. molecular clusters) to more than 10 µm (e.g. pollen grains). As mentioned above, $PM_{2.5}$ is monitored based on the understanding that these small particles are more health relevant than larger ones, but the size distribution among particles smaller 2.5 µm has strong implications for its deposition behavior (Carvalho et al., 2011). Accordingly, many studies have looked into this subject and revealed the importance of ultrafine particles smaller than ~200 nm for systemic

oxidative stress and diseases (Araujo et al., 2008; Valavanidis et al., 2008; Stone et al., 2017). Therefore, it is vital to characterize not only the abundance but also the distribution of particle constituents and properties across the whole size range of ambient PM. Especially, as the size of particles determines its surface area and therewith the fraction of constituents, that can either biophysically interact with the airway interface or dissolve in the lung fluid. This step, after impaction of ambient particles in the epithelial lung fluid (ELF), is an area of ongoing research, wherein the following questions are of critical importance: what fraction of PM is dissolving (Wang et al., 2003); which constituents are more likely to dissolve (Ma et al., 2018); to what extent do ultrafine particles penetrate through the epithelial barrier (Martinelli et al., 2013); are insoluble (surface) constituents of PM relevant for redox chemistry and therewith oxidative stress in the ELF (Fang et al., 2017); what is the composition of PM indoors, where we spend most of our lifetime (Szalai, 1972; Abbatt and Wang, 2020)?

1.2 Reactive Species

Molecules with a short chemical lifetime, which play a role in redox processes of biologic systems, are frequently referred to by the term reactive species (RS) (Sies, 2017). It includes short-lived free radicals like OH, O_2^-, and organic radicals, but also comparatively stable species like H_2O_2, O_3, and nitrogen oxides (NO_x). Under consideration of this wide range of stabilities, the term RS can be perceived as misleading, because it seems to be defined by a common range of reactivity. Nonetheless, this range is not restricted to a certain half-life time, but wide and flexible in order to encompass all transient species that are relevant in biological metabolisms. Accordingly, hydroxyl radicals, which react almost diffusion controlled with most molecules (Arangio et al., 2015), and H_2O_2, which has substantial steady-state concentrations in cells (Sies, 2017), belong to this same group. Due to the variability in reactivity and the different properties of these species, a number of different measurement techniques for single RS or groups are used depending on the aim of the study: e.g. EPR spectroscopy for the detection of free radicals, UV-vis spectroscopy with and without dyes, electrochemical methods, or indirect detection of non-reactive end products (Halliwell and Gutteridge, 2015; Seinfeld and Pandis, 2016; Bates et al., 2019).

In ambient aerosols, RS play a crucial role in atmospheric processing and aging. Especially O_3, OH, and NO_x are key oxidants in the gas phase as well as the particle phase. They influence secondary particle formation, particle growth, and the chemical composition of aerosols (Seinfeld and Pandis, 2016). Furthermore, the levels of O_3 and NO_x in ambient air are common air quality metrics, due to their adverse health effects. These health effects are associated with their reactive and oxidizing properties, but epidemiological studies indicate, that the impact of these gas-phase oxidants is comparatively small under ambient conditions compared to the effect of PM (Cohen et al., 2017; Lelieveld et al., 2020).

Apart from this destructive role as damaging oxidants, RS are also important signaling molecules in biochemical systems (Alfadda and Sallam, 2012). In this context, they are produced by proteins to send messages to other compartments in cells or even across tissues. Among others, this is important for parts of the immune system, inflammation reactions, muscle activity, and many other cell biological functions (Halliwell and Gutteridge, 2015). Due to this ambivalent role of RS – as damaging oxidants and vital signal messengers – oxidative stress also fulfills an important role, which is why it is crucial to investigate the balance between RS and antioxidants (Sies, 2017).

1.3 CeO_2 Nanoparticles

Synthetic nanomaterials are widespread in numerous applications and research enterprises. They have comparable sizes to ultrafine ambient PM (< 100 nm) and are often designed to serve as redox interfaces (Karakoti et al., 2010). Accordingly, some toxicological properties may be similar between synthetic and ambient particulate matter (Krug and Wick, 2011). Whereby synthetic nanomaterials typically have a defined composition as well as known physicochemical properties. This allows more straight forward interpretation of their behavior without the complex interplay of various constituents being characteristic for ambient PM.

An example of such nanomaterials are cerium dioxide nanoparticles (CeNPs), which attract substantial interest due to their redox properties and potential use in the treatment of various diseases (Rajeshkumar and Naik, 2018). The distinct ability of cerium in CeNPs to change their oxidation state between Ce^{3+} and Ce^{4+} enables such particles to effectively interact with RS (Dunnick et al., 2015). In accordance with this, studies have observed antioxidant activities by CeNPs, e.g. direct scavenging of ·OH, NO·, and $OONO^-$ (Xue et al., 2011; Dowding et al., 2012; Dowding et al., 2013). Furthermore, enzyme-like activities were found, mimicking the catalytic reactions of catalase- and superoxide dismutase (Yang et al., 2016). Those reactions are influenced by the cerium oxidation state on surfaces, pH, oxidant levels, and Ce ligand concentrations (Grulke et al., 2014). Contrary to these effects, some studies suggested that CeNPs may promote oxidative stress and inflammatory signaling responses by RS generation (Wason et al., 2013; Park et al., 2008). CeNPs have very low solubility at neutral pH (Plakhova et al., 2016) and can be produced in high purity with a homogenous composition (Korschelt et al., 2018). Therefore, CeNPs represent a good model to investigate the effect of insoluble, nanometer-sized, redox-active constituents of PM on RS budgets in physiological environments.

1.4 Environmentally Persistent Free Radicals

Environmentally persistent free radicals (EPFR) are molecules that typically constitute of a transition metal center and the radical intermediate of a polycyclic aromatic molecule (e.g. semiquinone) (Vejerano et al., 2018). Their stability is at least several hours at room temperature, but the half-life time and exact molecular composition are heterogeneous (Gehling and Dellinger, 2013). The occurrence of EPFR has been observed first in aerosols originating from cigarette smoke (Church and Pryor, 1985), later also in ambient PM (Dellinger et al., 2001). A wide range of EPFR concentrations has been found in PM from urban and suburban environments (Xu et al., 2019). Different combustion processes have been identified as EPFR sources, among them traffic, industrial activities, waste incineration, and residential heating (Wang et al., 2019; Chen et al., 2019a). Mechanistic studies suggest, that in combustion processes polycyclic aromatic compounds interact with transition metal ions, forming stable metal-organic radical complexes containing phenoxy- and semiquinone residues (Dellinger et al., 2007; Vejerano et al., 2018). Other EPFR sources include room temperature oxidation of organic molecules by ozone or transition metals (Borrowman et al., 2016; Patterson et al., 2017) and photochemical reactions in PM (Chen et al., 2019b; Li et al., 2020). Nevertheless to this date, there is a clear shortage of information about the ambient concentrations and sources of EPFR in different environmental settings.

Besides the abundance, observations have revealed information about the properties of EPFR: the lifetime of this class of compounds is diverse, ranging from hours to months (Gehling and Dellinger, 2013; Chen et al., 2019a). The spectral properties are relatively conserved in a small range of g-values (2.0023-2.0048), which is an indication for semiquinone type organic radicals. Therein, the varying oxidation degree

determines the exact deviation from the free electron g-value (Xu et al., 2019). Furthermore, the influence of EPFR on multiphase reactions in ambient aerosols has been a matter of rising interest (Khachatryan et al., 2011; Li et al., 2016; Zhao et al., 2019a; Deng et al., 2020). These studies have revealed, that the formation of RS by EPFR could play a role in the degradation of organic molecules in the particle phase. Therein, EPFR reportedly react either in solution or as catalysts on multiphase interfaces producing different RS (e.g. $^{\bullet}OH$ and $O_2^{-\bullet}$), which may subsequently lead to oxidation of other compounds.

Moreover, EPFR have been connected to a number of biochemical inflammation pathways (Balakrishna et al., 2009; Reed et al., 2014; Jaligama et al., 2018; Harmon et al., 2018), suggesting that they may play a role in the health effects of PM. More concretely, these reports suggest that EPFR related RS formation results in antioxidant depletion, enzyme deactivation, and altered gene expression, which was demonstrated in cell culture as well as animal models. Even though it remains unclear whether these effects are induced directly by EPFR or its constituents in another form, these findings encourage more in-depth studies on this topic.

1.5 Research Objectives

Investigating the role and reactivity of radicals in airborne particles is important to better understand multiphase processes and the health effects of fine particulate matter. To pursue these challenges, the doctoral project aimed to apply EPR spectroscopy to constrain factors that influence the production of RS during the suspension of particulate matter in liquid solutions. Secondly, aims to deepen the understanding of EPFR occurrence and their role in particle phase reactivity. The detailed activities and research questions were as follows:

1) Develop an understanding of how surface properties and surface area per unit mass influence the redox activity of CeNPs under physiological conditions.
2) Elucidate radical formation of secondary organic molecules in PM and the effect of oxidation degree. Find a way to connect insights into the molecular structure of organic matter in PM with their potential to produce specific reactive species.
3) Achieve an improved understanding of the influence of key molecular constituents on the production of reactive species PM from different sources.
4) Investigate concentrations of EPFR in PM from remote regions compared to urban areas to achieve insights how the concentration and size distribution of EPFR vary between sites of different pollution levels.
5) Investigate EPFR occurrence in indoor environments compared to outdoors, more specifically in household aerosols, on surfaces, and in house dust. Test the applicability of EPFR concentration as an indicator for particle phase reactivity.

2. Methods

2.1 Electron Paramagnetic Resonance Spectroscopy

Electron paramagnetic resonance (EPR) spectroscopy enables the qualitative and quantitative analysis of molecules containing unpaired electrons (Gerson and Huber, 2003; Weil and Bolton, 2007). Therein, a sample is exposed to a strong external magnetic field, resulting in Zeeman splitting of the spin energy states associated with electrons (Figure 1). Subsequently, electromagnetic radiation is channeled through the sample, which can induce transitions between two spin states under resonance conditions. The thereby induced difference between ingoing and outgoing microwave radiation intensity can be measured, resulting in quantitative information about the number of spins and thus unpaired electrons in the sample. Qualitative information about the molecular structure can be retrieved from hyperfine splitting patterns as well as from the point of resonance of the energy gap between the two spin states and the wavelength of the microwave radiation at a specific magnetic field strength. Therein the resonance point depends on the molecule-specific g-value, which for most organic molecules is close to the g-value of a free electron in vacuum ($g = 2.00232$). It is mostly determined by the electron orbital magnetic moment resulting from spin-orbit coupling. The hyperfine splitting results mostly from spin-nuclei coupling with magnetic nuclei in close proximity of the unpaired electron. Therein the magnitude of the splitting is also characteristic for certain spin-nuclei couples.

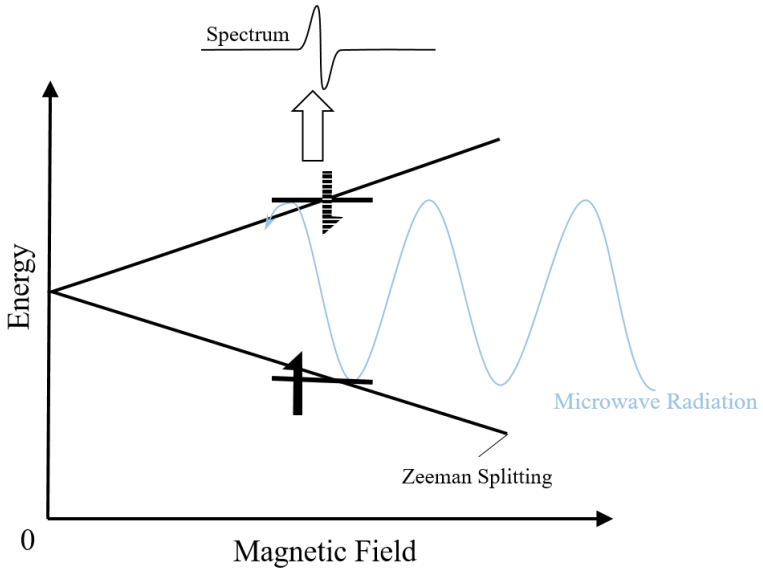

Figure 1: *Schematic illustration of the operating principle of EPR spectroscopy: Microwave radiation induces - at the point of resonance between the energy gap and the wavelength of the radiation - a transition of the spin state and therewith loses energy.*

Standard EPR spectrometers typically require relatively stable concentrations of spins in the range of at least 10^{-7}-10^{-9} mol L^{-1} (Hawkins and Davies, 2014). In order to account for physicochemical considerations and ensure a sufficient concentration, EPR is mainly applied to solid and liquid samples. Whereby liquid solutions pose special challenges due to varying spin-lattice interactions. Additionally, many molecules with unpaired spins in solution exhibit short lifetimes, preventing the formation of substantial steady-state concentrations. This is true for short-lived radicals like $^{\bullet}OH$, superoxide, and transient organic radicals, which typically cannot be measured directly by EPR. In order to overcome this hurdle, the so-called spin-

trapping technique can be applied: Therein small organic molecules are added to the sample. These dyes can react with short-lived species to semi-stable radicals, which accumulate in detectable concentrations (Davies, 2016). A wide range of such spin-traps is commercially available, with differences in their specificity and efficiency of trapping certain RS (Hawkins and Davies, 2014). For instance, nitrone spin-traps (e.g. 5, 5-dimethyl-1-pyrroline-N-oxide short DMPO or 5-tertbutoxycarbonyl-5-methyl-1-pyrroline-N-oxide short BMPO) are frequently used because of their ability to react with a variety of species including C-, O-, N-, and S-centered radicals. On the other hand, the resulting adducts reveal only limited information about the molecular structure of the initial radical. This is due to the comparatively large distance between the radical carrying nitroxide group and the point, where the RS is bound to the spin trap. Conversely, nitroso spin-traps deliver more qualitative information about the radical by hyperfine splitting patterns, but they can often only be applied to C-centered radicals. Consequently, it is crucial to carefully choose the measurement conditions including the selection of the right spin trap when needed.

The application of EPR spectroscopy in atmospheric sciences requires further considerations beyond the aspects outlined above. Therein the main challenge arises from the complexity of environmental samples, consisting of a multitude of molecules and phase states (Seinfeld and Pandis, 2016). Another important aspect to consider is the low mass of ambient PM, because therewith concentrations of any substance of interest are either low or PM needs to be collected for an extensive amount of time. Also, the mass of the substrate or filter used for collection of PM can be orders of magnitude higher than the collected particles, which can result in substantial matrix effects. Approaches to account for these challenges can be grouped in the following fields of action:

1. Considerations before or during sampling of PM
2. Sample pretreatment and preparation
3. Measurement conditions

To collect PM for EPR measurements, filters or sample substrates should be chosen, which are as thin as possible and free of transition metals. The thickness is crucial because it can reduce matrix effects and enable the preparation of a small sample, which fits into the most sensitive region of the cavity and is homogenous in the PM amount at each point of the sample. Transition metals and other impurities can yield EPR signals, which potentially interfere with the signal of interest, or during extraction may leach into the solution and participate in redox chemistry. For better reproducibility of direct measurements of PM on a filter, it can be helpful to incubate samples under a dry N_2 atmosphere to prevent matrix effects of humidity or changes in gas phase composition. Sample preparation for spin-trapping studies of PM should be done without the influence of light, in pure and degassed solvents following strict time protocols. Generally, during such experiments, it should be kept in mind that not only RS can interact with spin-traps, but also other reagents like iron or copper species can induce unintended side reactions. In order to improve sensitivity and reproducibility, it can be helpful to cool down samples and ensure a stable N_2 atmosphere within the cavity and in the sample. Instrumental settings like the modulation amplitude may be used to fine-tune between sensitivity and signal resolution depending on the requirements.

2.2 Collection of Suspended Particulate Matter

When sampling ambient PM for analysis, one can aim to collect the total amount of suspended particles (TSP) or separate particles based on their size or aerodynamic diameter (Heard, 2006; Seinfeld and Pandis, 2016). Collection of TSP is typically performed using at least one filter, through which the ambient aerosol is sucked, with a minimum path length from the air inlet to the filter material. On the filter material

individual particles can be deposited by the following mechanisms: Filtration of particles that are too large to penetrate through the pores; impaction of particles with high inertia prohibiting them to follow the gas stream; diffusion of very small particles away from the air stream, if it results in adsorption to the filter material. PM segregation into different size intervals is usually based on the direct relationship of particle aerodynamic diameter and inertia: to collect PM smaller than a defined threshold like $PM_{2.5}$ the geometry and air stream velocity are designed in a specific way, that particles larger than this cut-off are depositing on an interface above the actual substrate. It is also possible to stack multiple of such interfaces and thereby segregate PM into many different size fractions.

For any kind of PM sampler, it is crucial to take into consideration the design of the inlet and flow velocity because particles can also be lost in pipes. Shortly, the same mechanisms as during deposition on filters play a role: very large particles may not fit through the air inlet and on any point where the airflow is not in vertical orientation particles may be deposited due to inertia especially at angles. Moreover, the longer the inlet line the more small particles diffuse to the pipe walls. Additionally, electrostatic charges of the pipe may cause charged particles to be directed away from their flow direction, accordingly conductive pipes should be used. Lastly, the flow velocity and pipe diameter determine whether the air flows in a laminar shape or turbulent. The velocity should be slow enough to ensure a laminar flow, therewith minimizing depositional losses to the wall, but at the same time fast enough to reduce diffusion losses.

3. Results

3.1 Overview

The results of this PhD project are presented in the form of 5 manuscripts for publication in peer-reviewed journals (3 first author and 2 coauthored), which are enclosed in following chapters. Two of these papers are already published in leading, international journals of the field, one is currently under review on an open-access preprint server, and two will be submitted soon.

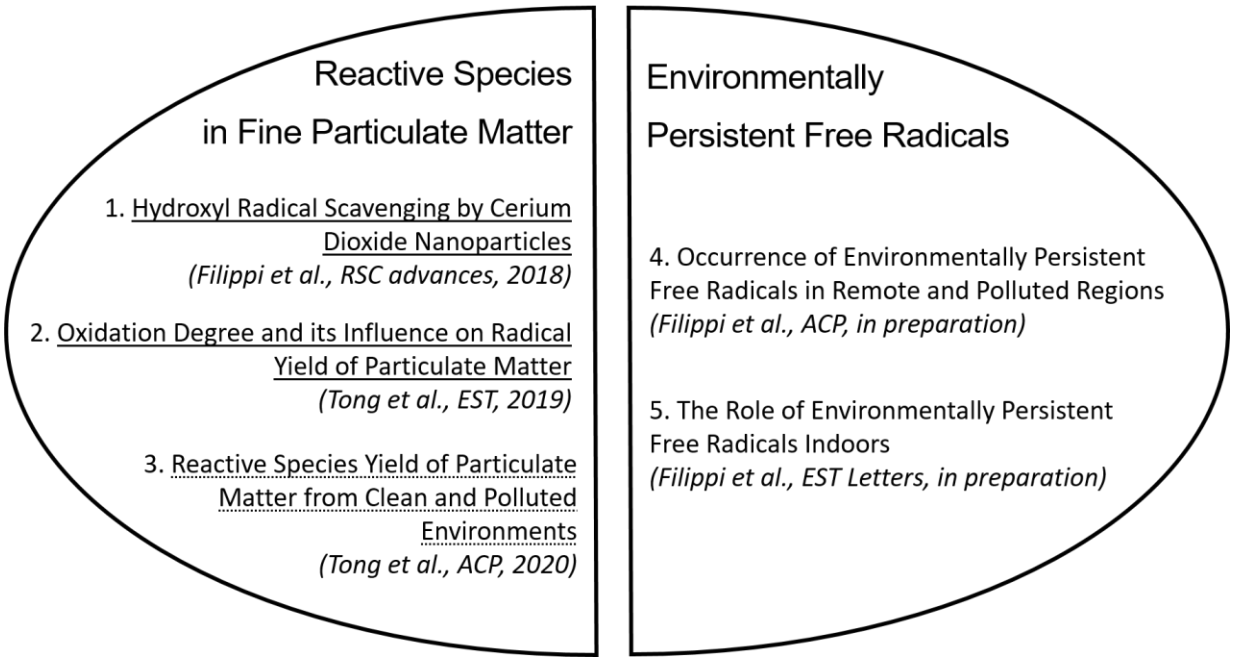

Figure 2*: Overview of studies prepared in the context of the PhD project. Manuscripts listed on the left focus on reactive species in solution studied with EPR spin-trapping, manuscripts on the right focus on condensed phase environmentally persistent free radicals. Solid underlined titles are published in peer-reviewed journals, the dotted underlined title is currently under review, and non-underlined titles shall be submitted soon.*

3.2 Hydroxyl Radical Scavenging by Cerium Dioxide Nanoparticles

This chapter has been published as research paper in *RSC advances*. As first author of this manuscript I have performed a significant share of the experiments myself, coordinated the different characterizations, and contributed a large part to the compilation and integration of the findings. More concretely I performed the experiments with cerium nanorods in surrogate lung fluid and also some of the EPR spin-trapping experiments with cerium nanoparticles of different size. Furthermore, I established and coordinated the collaboration with Karsten Korschelt, Wolfgang Tremel, and Tobias Reich. This enabled the incorporation of nanorods into the study and secured the characterizations of our nanoparticles by TEM, BET, and XPS. Moreover, I provided the first draft of the publication, created the figures, organized the editing among the coauthors, and contributed to the revision following reviewer comments.

Antioxidant activity of cerium dioxide nanoparticles and nanorods in scavenging hydroxyl radicals

RSC Advances, **9(20)**, 11077-11081, (2019).

Alexander Filippi,[‡, 1] Fobang Liu,[‡, 1, 2] Jake Wilson,[1] Steven Lelieveld,[1] Karsten Korschelt,[3] Ting Wang,[1, 4] Yueshe Wang,[4] Tobias Reich,[5] Ulrich Pöschl,[1] Wolfgang Tremel,[3] and Haijie Tong.[1]

[1] Multiphase Chemistry Department, Max Planck Institute for Chemistry, Mainz, 55128, Germany

[2] School of Chemical and Biomolecular Engineering, Georgia Institute of Technology, Atlanta, Georgia 30332, USA

[3] Institute for Inorganic Chemistry and Analytical Chemistry, Johannes Gutenberg University Mainz, Mainz, 55128, Germany

[4] State Key Laboratory of Multiphase Flow in Power Engineering, Xi'an Jiaotong University, Xi'an 710049, China

[5] Institute of Nuclear Chemistry, Johannes Gutenberg University Mainz, Mainz, 55099, Germany

RSC Advances

PAPER

View Article Online
View Journal | View Issue

Cite this: *RSC Adv.*, 2019, **9**, 11077

Antioxidant activity of cerium dioxide nanoparticles and nanorods in scavenging hydroxyl radicals†

Alexander Filippi,‡[a] Fobang Liu,‡[ab] Jake Wilson,[a] Steven Lelieveld,[a] Karsten Korschelt,[c] Ting Wang,[ad] Yueshe Wang,[d] Tobias Reich,[e] Ulrich Pöschl,[a] Wolfgang Tremel[c] and Haijie Tong*[a]

Received 24th January 2019
Accepted 4th April 2019

DOI: 10.1039/c9ra00642g

rsc.li/rsc-advances

Cerium oxide nanoparticles (CeNPs) have been shown to exhibit antioxidant capabilities, but their efficiency in scavenging reactive oxygen species (ROS) and the underlying mechanisms are not yet well understood. In this study, cerium dioxide nanoparticles (CeNPs) and nanorods (CeNRs) were found to exhibit much stronger scavenging activity than ·OH generation in phosphate buffered saline (PBS) and surrogate lung fluid (SLF). The larger surface area and higher defect density of CeNRs may lead to higher ·OH scavenging activity than for CeNPs. These insights are important to understand the redox activity of cerium nanomaterials and provide clues to the role of CeNPs in biological and environmental processes.

Reactive oxygen species (ROS) generally describe reduction products of oxygen molecules, including H_2O_2 and hydroxyl radicals (·OH).[1] ROS play a central role in biological processes exerting both beneficial and adverse health effects.[2] Several studies have looked into the redox balance between ROS and antioxidants[3] as well as the underlying mechanisms.[4] Among all ROS, ·OH is considered as one of the most reactive species; it can attack biomolecules and cause irreversible damage.[5] Thus, experimental quantification and abiotic regulation of ·OH under physiologically relevant conditions is an important yet challenging task.

In the last decade, cerium dioxide nanoparticles (CeNPs) have drawn much attention due to their redox properties[6] and potential therapeutic applications (such as treating cardiac ischemia).[7–9] Efforts have been made to explore the potential use of CeNPs as medicine.[7,10,11] The ability of CeNPs in switching the oxidation state of Ce^{3+} and Ce^{4+} makes it a good candidate to mediate ROS.[6,12] Direct scavenging of ·OH (process ① in Scheme 1), NO·, and $OONO^-$ by CeNPs have been investigated.[13–16] Moreover, previous studies indicated that CeNPs have catalase- and superoxide dismutase (SOD)-like effects (processes ③ and ⑤ in Scheme 1).[17,18] Both effects are closely correlated with the Ce^{3+} and Ce^{4+} surface concentrations, pH, H_2O_2 and chelating ligand concentrations.[19–23]

In contrast to research about the antioxidant activity of CeNPs, inhalable CeNPs have been detected in ambient air and concerns have been raised about their potential adverse health effect.[24,25] Besides this, additional studies suggested that CeNPs can induce oxidative stress, inflammatory signaling response, and cell death upon generating ROS (processes ④–⑥ in Scheme 1) or ROS-messengers.[26–30] Given the controversies about the beneficial and toxic effects of CeNPs, it is necessary to distinguish the anti- and prooxidant activities of CeNPs under physiologically relevant conditions.[31] In this study, we compared the

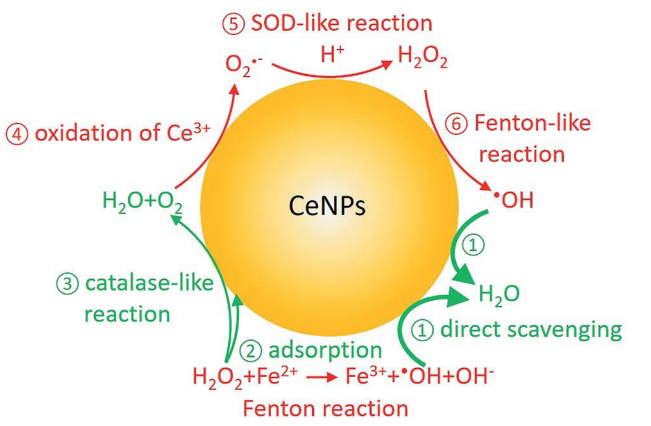

Scheme 1 Fenton reaction and reactive oxygen chemistry of CeNPs. Red and green colors indicate ROS formation and scavenging processes, respectively.

[a]*Multiphase Chemistry Department, Max Planck Institute for Chemistry, Mainz, 55128, Germany. E-mail: h.tong@mpic.de*

[b]*School of Chemical and Biomolecular Engineering, Georgia Institute of Technology, Atlanta, Georgia 30332, USA*

[c]*Institute for Inorganic Chemistry and Analytical Chemistry, Johannes Gutenberg University Mainz, Mainz, 55128, Germany*

[d]*State Key Laboratory of Multiphase Flow in Power Engineering, Xi'an Jiaotong University, Xi'an 710049, China*

[e]*Institute of Nuclear Chemistry, Johannes Gutenberg University Mainz, Mainz, 55099, Germany*

† Electronic supplementary information (ESI) available. See DOI: 10.1039/c9ra00642g

‡ Both authors contributed equally to this work.

·OH formation and scavenging ability of commercial CeNPs (∅ 25 and 50 nm) and homemade cerium nanorods (CeNRs) with different physicochemical properties in phosphate buffered saline (PBS) buffer, antioxidant solutions, and a surrogate lung fluid (SLF). The SLF was used to mimic the key interface between human respiratory tract and inhaled air.

Fig. 1 shows the size, morphology, surface composition, and mass normalized surface area of CeNPs and cerium dioxide nanorods (CeNRs). More information about the applied techniques, sample handling and instrument settings is compiled in Sections S1–S5.† Fig. 1A and B indicate that CeNPs (∅ 50 nm) and CeNPs (∅ 25 nm) have a heterogeneous size distribution with average diameters of <50 nm and <25 nm respectively. Moreover, samples of these commercial CeNPs contain predominantly cubic NPs. In contrast, the morphology of CeNRs (Fig. 1C) is more uniform with a length of ~100 nm. Details about the CeNRs can be found from our previous study.[32] In addition to the detection of size and morphology, the specific surface areas of the cerium nanoparticles were determined to be 24.8 ± 0.4 m^2 g^{-1} (∅ 50 nm CeNPs) (Fig. 1D), 39.2 ± 0.7 m^2 g^{-1} (∅ 25 nm CeNPs) (Fig. 1E), and 106.5 ± 2.4 m^2 g^{-1} (CeNRs) (Fig. 1F). Moreover, the similar Ce 3d XPS spectra of CeNPs (∅ 50 nm) (Fig. 1G), CeNPs (∅ 25 nm) (Fig. 1H), and CeNRs (Fig. 1I) indicate that the distribution of the cerium surface oxidation states (Ce^{3+} and Ce^{4+}) on these NPs are quite similar. The six most prominent peaks of these spectra are attributable to Ce^{4+} ions.[33] This indicates that Ce^{4+} was the dominant cerium species in all three samples. The peak fittings (dashed lines) in panels G, H and I are based on the method by Maslakov *et al.*.[33] The fitting based deconvolution of Ce 3d XPS spectra indicates that the concentration of surface Ce^{3+} in all these samples is <3%. Such a low abundance of surface Ce^{3+} is also supported by the absence of a shoulder peak of Ce 4f electrons at ~1.1 eV in the XPS valence band spectrum of the CeNRs samples (Fig. S3†). Furthermore, the deconvolution of the XPS spectrum of the O 1s region of the NPs (Fig. S2 and Table S3†) indicates that the CeNRs surface contains a much higher concentration of hydroxide than CeNPs. This may correlate with the synthesis method of CeNRs using NaOH as reagent[34] and may play a role in the higher ·OH scavenging activity of CeNRs. These differences in chemical composition, morphology, and surface area between CeNPs and CeNRs may result in variations of their redox activity.

Fig. 2 shows the trapping mechanism of 5-*tert*-butoxycarbonyl-5-methyl-1-pyrroline-*N*-oxide (BMPO, panel A) and EPR spectra of aqueous mixtures of Fe^{2+}, H_2O_2, SLF, and CeNPs (panel B). Fig. 2A shows that BMPO can react with OH radicals and form a BMPO–OH radical adduct. In this way, short lifetime radicals can be probed and characterized by electron paramagnetic resonance (EPR) spectroscopy (EMXplus10/12, Bruker, Germany, see details in Section S5 and Table S4†). The grey dashed lines in panel B indicate the characteristic hyperfine splitting of BMPO–OH, in agreement with previous assignment.[35] The peak intensities of the spectra in Fig. 2B decrease in the order A (Fe^{2+} + H_2O_2) > B (Fe^{2+} + H_2O_2 + CeNPs) > C (Fe^{2+} + H_2O_2 + SLF) > D (Fe^{2+} + H_2O_2 + CeNPs + SLF). This implies that the amount of ·OH decreases accordingly. Based on the spin-counting method,[32] we quantified the concentration of BMPO–OH in these solutions. The results are shown in Fig. 3 and Tables S5–S7.†

Fig. 3A and B show the positive correlation of ·OH yields of CeNPs (∅ 50 nm) without (black circles) and with the addition of H_2O_2 (black triangles) under different CeNPs (∅ 50 nm) loading conditions. In the absence of H_2O_2, 0.1–30 mg mL^{-1}

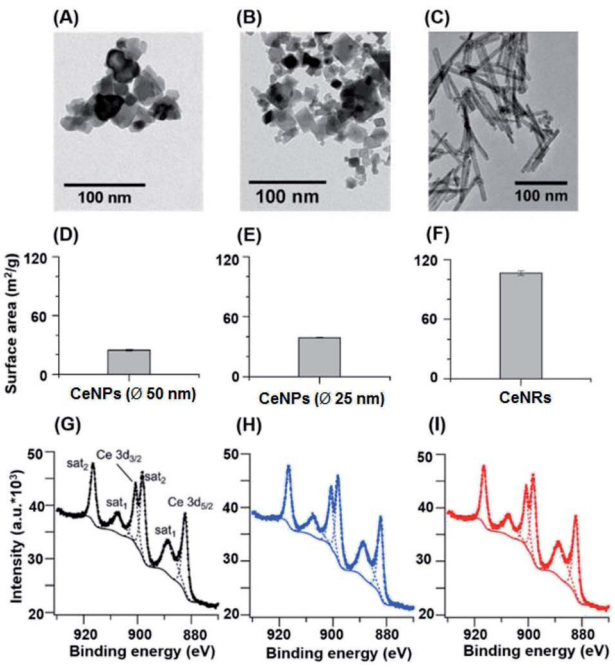

Fig. 1 Physicochemical characteristics of CeNPs (∅ 50 nm) (A, D, and G), CeNPs (∅ 25 nm) (B, E, and H), and CeNRs (C, F, and I). (A–C) TEM images. (D–F) Surface areas determined by BET. (G–I) Ce 3d XPS spectra. The error bars in panels (D–F) represent standard deviations based on three replicates. The dashed lines in panels (G–I) are fitting curves.

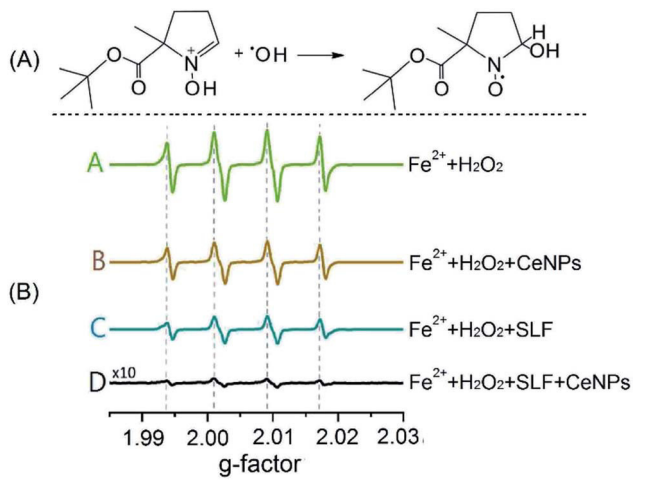

Fig. 2 (A) Reaction mechanism of the spin-trapping agent BMPO with a hydroxyl radical. (B) EPR spectra of the BMPO-radical adduct in different aqueous mixtures. The four peaks (dotted lines) are characteristic of BMPO–OH adducts. The concentrations of Fe^{2+}, H_2O_2, and CeNPs (∅ 50 nm) are 1 mM, 10 mM, and 10 mg mL^{-1}, respectively.

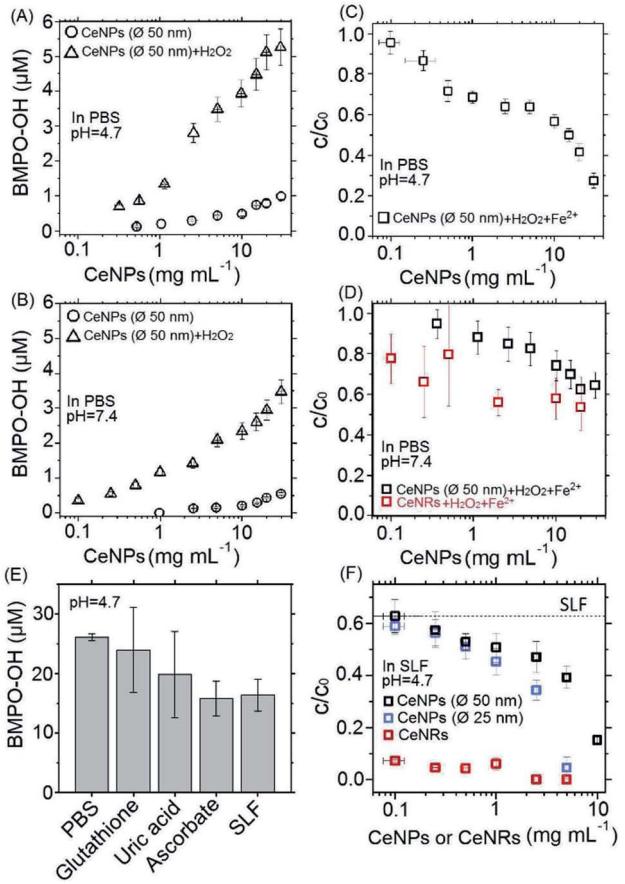

Fig. 3 Concentrations (A, B, and E) or remaining fractions (C, D, and F) of BMPO–OH in different aqueous mixtures. (A) and (B) Concentrations of BMPO–OH formed by pure CeNPs (∅ 50 nm) (○) or their mixtures within H_2O_2 (Δ) in pH = 4.7 (A) and 7.4 (B) PBS. (C) and (D) Remaining fraction (c/c_0) of BMPO–OH without (c_0) and with (c) mixing CeNPs (∅ 50 nm) or CeNRs (□) with 1 mM Fe^{2+} and 10 mM H_2O_2 in pH = 4.7 (C) and 7.4 (D) PBS. (E) Concentration of BMPO–OH formed by Fenton reactions in neutral PBS, antioxidant solutions, and SLF. (F) c/c_0 of BMPO–OH with and without mixing CeNPs (∅ 50 nm) (□), CeNPs (∅ 25 nm) (□), and CeNRs (□) with 1 mM Fe^{2+} and 10 mM H_2O_2 in pH = 4.7 SLF. The values of c_0 in panels B, D and F are ~53, ~17, and ~26 μM. The *x*-axis errors in panels A, B, C, D, and F represent uncertainties from weighing and pipetting. All the *y*-errors represent standard deviation of more than three replicates.

CeNPs (∅ 50 nm) can generate 0–0.8 and 0–0.5 μM ·OH in pH = 4.7 (Fig. 3A) and 7.4 (Fig. 3B) PBS, respectively. The generation of ·OH by pure CeNPs (∅ 50 nm) in acidic PBS is consistent with previous hypothesis that acid can catalyze the ·OH formation by CeNPs.[36] In contrast to pure CeNPs (∅ 50 nm), mixtures of 0.1–30 mg mL^{-1} CeNPs (∅ 50 nm) with 10 mM of H_2O_2 can generate 0–5 (pH = 4.7) and 0–3 μM (pH = 7.4) ·OH, which also shows a positive correlation with the loading of CeNPs (∅ 50 nm) as shown in Fig. 3A and B. These hydroxyl radicals may be formed through Fenton-like reactions initiated by CeNPs:[37] $H_2O_2 + Ce^{3+} \rightarrow Ce^{4+} + \cdot OH + OH^-$.

To evaluate the ·OH scavenging activity of CeNPs in aqueous solution, we measured the ·OH yield by mixtures of CeNPs (∅ 50 nm) or CeNRs, Fe^{2+}, and H_2O_2 in acidic and neutral PBS. Fig. 3C and D show that the ·OH concentration decreased with increasing CeNPs or CeNRs loading, characterized by the decreasing remaining OH radical concentration. In the absence of CeNPs, Fenton reactions of 1 mM Fe^{2+} and 10 mM H_2O_2 generated ~53 and ~17 μM ·OH in pH = 4.7 (Fig. 3C) and 7.4 (Fig. 3D) PBS. At 30 mg mL^{-1} CeNPs (∅ 50 nm), concentration of ·OH decreased to 15 μM (pH = 4.7) and 11 μM (pH = 7.4), respectively (Tables S5 and S6†). In contrast to CeNPs, CeNRs exhibited higher ·OH scavenging efficiency, with 20–50% of ·OH to be scavenged by 0.1–20 mg mL^{-1} CeNRs. This implies that the scavenging activity of CeNPs (∅ 50 nm) is more pronounced under acidic conditions. The decrease of ·OH concentration may be induced by the following processes: first, CeNPs (∅ 50 nm) or CeNRs could scavenge ·OH directly (process ① in Scheme 1).[13] Second, the adsorption of H_2O_2 on CeNPs (∅ 50 nm) or CeNRs surfaces (like process ② in Scheme 1) may decrease the available H_2O_2 concentration.[38] In this case, due to the lower availability of the H_2O_2 precursor, the amount of ·OH formed by Fenton reactions will decrease. Third, the surface-bound H_2O_2 can be decomposed *via* catalase-like reactions (process ③ in Scheme 1).[21] This process will form H_2O and O_2 rather than ·OH. Beyond these two pathways, iron ion-initiated redox processes may also influence the measured ·OH concentrations. For instance, it has been suggested that upon interaction with the surface of CeNPs, Fe^{2+} can enhance the dissolution of Ce^{3+} and cause the formation of 6-line ferrihydrite, which can increase the colloidal stability of the CeNPs.[39] Such a reaction may alter the redox activity of CeNPs (∅ 50 nm) or CeNRs.

Recently Baldim *et al.*[38] measured the H_2O_2 surface adsorption potential of CeNPs with different sizes. They found that 5–28 nm diameter CeNPs could adsorb 2–20 H_2O_2 molecules nm^{-2}, depending on the surface composition of the nanomaterial. We used the adsorption potential from Baldim *et al.* and estimated that only <1% of H_2O_2 (~8 μM) can be adsorbed on the surface of the CeNPs. Therefore, the surface adsorption of H_2O_2 by CeNPs cannot fully explain the reduction of ·OH concentration in Fig. 3. Furthermore, Pirmohamed *et al.*[21] observed a H_2O_2 decomposition rate of ~2.7 nmol min^{-1} through catalase-like reactions. Based on this value, we estimate that a concentration of 0.1 mg mL^{-1} of CeNPs would result in a H_2O_2 loss of <2% in our studies. Therefore, we suggest the direct scavenging process (① in Scheme 1), rather than the surface adsorption (② in Scheme 1) and catalase-like (③in Scheme 1) processes to be the dominant reduction pathways of ·OH.

Fig. 3E shows the ·OH scavenging activity of typical epithelial lung fluid antioxidants and a surrogate lung fluid (SLF). Here, 0.1 mM of glutathione, 0.1 mM of uric acid, and 0.2 mM of ascorbate solutions could scavenge ~8%, ~14%, and ~39% of hydroxyl radicals originating from Fenton reactions of 1 mM Fe^{2+} and 10 mM H_2O_2 in PBS. The SLF showed a similar activity as 0.2 mM ascorbate, *i.e.* the ·OH scavenging activities of individual antioxidants are not additive and decrease in the order ascorbate > uric acid > glutathione. This trend is consistent with previous findings.[38]

To assess the antioxidant activity of CeNPs under quasi-physiological conditions, we explored the ·OH scavenging activity of CeNPs and CeNRs in SLF. Fig. 3F shows the hydroxyl radical yield by Fenton reactions in SLF as a function of the CeNPs (∅ 25 and 50 nm) and CeNRs loading. As the loading of CeNPs (∅ 50 nm) increased from 0.1 to 10 mg mL^{-1}, the concentration of ·OH in SLF decreased by 38–85%. Within the same loading range, the CeNPs (∅ 25 nm) exhibited a similar efficiency. Whereas at higher loadings (1–5 mg mL^{-1}), the ·OH scavenging potential of CeNPs (∅ 25 nm) was 9–55% higher than that of their 50 nm counterparts. In contrast to CeNPs, the CeNRs showed a much higher ·OH scavenging efficiency. Even with a loading as low as 0.1 mg mL^{-1}, the CeNRs could reduce 88% of the ·OH. For CeNRs loadings that exceeded 1 mg mL^{-1}, no ·OH could be observed. The trend of the ·OH scavenging efficiency according to CeNRs > CeNPs (∅ 25 nm) >CeNPs (∅ 50 nm) is in the same order as the surface area of these NPs (Fig. 1D–F). Given the low abundance of Ce^{3+} on fresh CeNPs and CeNRs surface (Fig. 1G–H), we suggest that substantial amount of Ce^{3+} may be formed upon interactions of NPs with water.[13] The larger surface area of CeNRs may increase the density of Ce^{3+} per unit particle mass and subsequently their ·OH scavenging activity. Previous works showed that CeNRs are prone to expose their (110) facets to reactive species.[34] These facets were described as reactive "hybrid structures" between the (111) and (100) surfaces of CeNPs. Furthermore, the distinct crystallographic surface structure of CeNRs may act as binding site for reactive species (·OH and H_2O_2) exerting peroxidase-like effects. Additionally, Fe^{2+}-dependent reactive oxygen chemistry may contribute to the observed ·OH scavenging processes.[39] Finally, it has been suggested that glutathione could interact with CeNPs and influence the redox couple of Ce^{3+}/Ce^{4+}.[40]

It is worthy to note that a real physiologic environment is more complicated than SLF. A large number of redox chemistry processes may alter the agglomeration and distribution of CeNPs and relevant materials,[41] which may eventually influence its properties including ·OH scavenging efficiency and SOD-like characteristics.[42] Thus, characterizing CeNPs or their functionalized derivatives in more realistic environments will be beneficial and promising in follow-up studies.

Conclusions

In this study, we compared the ability of CeNPs and CeNRs in scavenging hydroxyl radicals (·OH) under physiologically relevant conditions. We found that CeNPs and CeNRs exert high ·OH scavenging activity in both PBS and SLF. In SLF, the ·OH scavenging potential of CeNPs increased 4-fold as the loading increases from 0.1 to 10 mg mL^{-1}. In the same loading range, CeNRs showed 5–50-fold higher ·OH scavenging potential than CeNPs, which may be attributable to the higher surface area and defect density of CeNRs. Furthermore, we found the scavenging activity of CeNPs is pH-dependent, exhibiting higher scavenging efficiency under lower pH condition. The observed ·OH scavenging efficiency of CeNPs and CeNRs in SLF took into account the effect of antioxidants at concentrations close to the epithelial lung fluid, reflecting the redox activity of CeNPs and CeNRs under more realistic *in vitro* conditions than previous studies. These findings are of critical importance for a better understanding of the relative ROS scavenging efficiency of CeNPs comparing to conventional antioxidants. Moreover, these results are also important for making accurate dose–response curves predicting the toxicity or antioxidant characteristics of CeNPs or their functionalized derivatives in biological and environmental processes.

Conflicts of interest

There are no conflicts to declare.

Acknowledgements

This work was funded by the Max Planck Society, the Deutsche Forschungsgemeinschaft (DFG), and the National Natural Science Foundation of China (No. 51576160). We thank Jakob Drebert for his support of the XPS measurements. Open Access funding provided by the Max Planck Society.

Notes and references

1 A. A. Alfadda and R. M. Sallam, *J. Biomed. Biotechnol.*, 2012, **2012**, 936486.
2 C. C. Winterbourn, *Nat. Chem. Biol.*, 2008, **4**, 278–286.
3 B. Poljsak, D. Suput and I. Milisav, *Oxid. Med. Cell. Longevity*, 2013, **2013**, 956792.
4 S. B. Nimse and D. Pal, *RSC Adv.*, 2015, **5**, 27986–28006.
5 A. Phaniendra, D. B. Jestadi and L. Periyasamy, *Indian J. Clin. Biochem.*, 2015, **30**, 11–26.
6 A. Karakoti, S. Singh, J. M. Dowding, S. Seal and W. T. Self, *Chem. Soc. Rev.*, 2010, **39**, 4422–4432.
7 J. M. Perez, A. Asati, S. Nath and C. Kaittanis, *Small*, 2008, **4**, 552–556.
8 S. Rajeshkumar and P. Naik, *Biotechnol. Rep.*, 2018, **17**, 1–5.
9 M. Culcasi, L. Benameur, A. Mercier, C. Lucchesi, H. Rahmouni, A. Asteian, G. Casano, A. Botta, H. Kovacic and S. Pietri, *Chem.-Biol. Interact.*, 2012, **199**, 161–176.
10 C. Walkey, S. Das, S. Seal, J. Erlichman, K. Heckman, L. Ghibelli, E. Traversa, J. F. McGinnis and W. T. Self, *Environ. Sci.: Nano*, 2015, **2**, 33–53.
11 C. K. Kim, T. Kim, I. Y. Choi, M. Soh, D. Kim, Y. J. Kim, H. Jang, H. S. Yang, J. Y. Kim and H. K. Park, *Angew. Chem., Int. Ed.*, 2012, **51**, 11039–11043.
12 K. M. Dunnick, R. Pillai, K. L. Pisane, A. B. Stefaniak, E. M. Sabolsky and S. S. Leonard, *Biol. Trace Elem. Res.*, 2015, **166**, 96–107.
13 Y. Xue, Q. Luan, D. Yang, X. Yao and K. Zhou, *J. Phys. Chem. C*, 2011, **115**, 4433–4438.
14 J. M. Dowding, T. Dosani, A. Kumar, S. Seal and W. T. Self, *Chem. Commun.*, 2012, **48**, 4896–4898.
15 J. M. Dowding, S. Seal and W. T. Self, *Drug Delivery Transl. Res.*, 2013, **3**, 375–379.
16 W. He, Y. Liu, W. G. Wamer and J. J. Yin, *J. Food Drug Anal.*, 2014, **22**, 49–63.

17 C. Korsvik, S. Patil, S. Seal and W. T. Self, *Chem. Commun.*, 2007, **10**, 1056–1058.
18 Y. Yang, Z. Mao, W. Huang, L. Liu, J. Li, J. Li and Q. Wu, *Sci. Rep.*, 2016, **6**, 35344.
19 B. C. Nelson, M. E. Johnson, M. L. Walker, K. R. Riley and C. M. Sims, *Antioxidants*, 2016, **5**, 15–36.
20 E. Grulke, K. Reed, M. Beck, X. Huang, A. Cormack and S. Seal, *Environ. Sci.: Nano*, 2014, **1**, 429–444.
21 T. Pirmohamed, J. M. Dowding, S. Singh, B. Wasserman, E. Heckert, A. S. Karakoti, J. E. King, S. Seal and W. T. Self, *Chem. Commun.*, 2010, **46**, 2736–2738.
22 V. K. Ivanov, A. B. Shcherbakov and A. V. Usatenko, *Russ. Chem. Rev.*, 2009, **78**, 855–871.
23 V. Patel, M. Singh, E. L. H. Mayes, A. Martinez, V. Shutthanandan, V. Bansal, S. Singh and A. S. Karakoti, *Chem. Commun.*, 2018, **54**, 13973–13976.
24 C. Guo, S. Robertson, R. J. M. Weber, A. Buckley, J. Warren, A. Hodgson, J. Z. Rappoport, K. Ignatyev, K. Meldrum, I. Römer, S. Macchiarulo, J. K. Chipman, T. Marczylo, M. O. Leonard, T. W. Gant, M. R. Viant and R. Smith, *Nanotoxicology*, 2019, 1–18.
25 S. Dekkers, L. Ma-Hock, I. Lynch, M. Russ, M. R. Miller, R. P. Schins, J. Keller, I. Römer, K. Küttler and V. Strauss, *Inhalation Toxicol.*, 2018, **30**, 273–286.
26 A. Srinivas, P. J. Rao, G. Selvam, P. B. Murthy and P. N. Reddy, *Toxicol. Lett.*, 2011, **205**, 105–115.
27 E. J. Park, J. Choi, Y. K. Park and K. Park, *Toxicology*, 2008, **245**, 90–100.
28 H. J. Eom and J. Choi, *Toxicol. Lett.*, 2009, **187**, 77–83.
29 E.-J. Park, W.-S. Cho, J. Jeong, J.-h. Yi, K. Choi, Y. Kim and K. Park, *J. Health Sci.*, 2010, **56**, 387–396.
30 M. S. Wason, J. Colon, S. Das, S. Seal, J. Turkson, J. Zhao and C. H. Baker, *Nanomedicine*, 2013, **9**, 558–569.
31 H. Zhang, X. He, Z. Zhang, P. Zhang, Y. Li, Y. Ma, Y. Kuang, Y. Zhao and Z. Chai, *Environ. Sci. Technol.*, 2011, **45**, 3725–3730.
32 K. Korschelt, R. Schwidetzky, F. Pfitzner, J. Strugatchi, C. Schilling, M. von der Au, K. Kirchhoff, M. Panthofer, I. Lieberwirth, M. N. Tahir, C. Hess, B. Meermann and W. Tremel, *Nanoscale*, 2018, **10**, 13074–13082.
33 K. I. Maslakov, Y. A. Teterin, A. J. Popel, A. Y. Teterin, K. E. Ivanov, S. N. Kalmykov, V. G. Petrov, P. K. Petrov and I. Farnan, *Appl. Surf. Sci.*, 2018, **448**, 154–162.
34 K. Herget, P. Hubach, S. Pusch, P. Deglmann, H. Gotz, T. E. Gorelik, I. A. Gural'skiy, F. Pfitzner, T. Link, S. Schenk, M. Panthofer, V. Ksenofontov, U. Kolb, T. Opatz, R. Andre and W. Tremel, *Adv. Mater.*, 2017, **29**, 1603823.
35 H. Tong, P. S. J. Lakey, A. M. Arangio, J. Socorro, F. Shen, K. Lucas, W. H. Brune, U. Poschl and M. Shiraiwa, *Environ. Sci. Technol.*, 2018, **52**, 11642–11651.
36 W. Lin, Y. W. Huang, X. D. Zhou and Y. Ma, *Int. J. Toxicol.*, 2006, **25**, 451–457.
37 A. D. Bokare and W. Choi, *J. Hazard. Mater.*, 2014, **275**, 121–135.
38 V. Baldim, F. Bedioui, N. Mignet, I. Margaill and J. F. Berret, *Nanoscale*, 2018, **10**, 6971–6980.
39 X. Liu, J. R. Ray, C. W. Neil, Q. Li and Y. S. Jun, *Environ. Sci. Technol.*, 2015, **49**, 5476–5483.
40 F. Rollin-Genetet, C. Seidel, E. Artells, M. Auffan, A. Thiery and C. Vidaud, *Chem. Res. Toxicol.*, 2015, **28**, 2304–2312.
41 A. Nel, T. Xia, L. Madler and N. Li, *Science*, 2006, **311**, 622–627.
42 J. Wu, X. Wang, Q. Wang, Z. Lou, S. Li, Y. Zhu, L. Qin and H. Wei, *Chem. Soc. Rev.*, 2019, **48**, 1004–1076.

Supporting Information

Antioxidant activity of cerium dioxide nanoparticles and nanorods in scavenging hydroxyl radicals

Alexander Filippi,[a†] Fobang Liu,[a,b†] Jake Wilson,[a] Steven Lelieveld,[a] Karsten Korschelt,[c] Ting Wang,[d,a] Yueshe Wang,[d] Tobias Reich,[e] Ulrich Pöschl,[a] Wolfgang Tremel,[c] Haijie Tong*[a]

[a] Multiphase Chemistry Department, Max Planck Institute for Chemistry, Mainz, 55128, Germany

[b] School of Chemical and Biomolecular Engineering, Georgia Institute of Technology, Atlanta, Georgia 30332, USA

[c] Institute for Inorganic Chemistry and Analytical Chemistry, Johannes Gutenberg University Mainz, Mainz, 55128, Germany

[d] State Key Laboratory of Multiphase Flow in Power Engineering, Xi'an Jiaotong University, Xi'an 710049, China

[e] Institute of Nuclear Chemistry, Johannes Gutenberg University Mainz, Mainz, 55099, Germany

† Both authors contributed equally to this work

*Corresponding author:

Dr. Haijie Tong

E-mail: h.tong@mpic.de

Table of Contents

Section S1. Materials and solution samples

The Ø 25 (544841) and Ø 50 nm (700290) diameter CeNPs were purchased from Sigma Aldrich and used as received without further purification. Homemade CeNRs were synthesized along the method described by Korschelt et al..[1] Briefly 0.08 M cerium (III) nitrate hexahydrate was mixed with 4.8 M sodium hydroxide for 30 min. Then, the reaction mixture was dried at 373 K for 24 h and cooled down to room temperature. Later on, the precipitates were isolated and washed with water and ethanol. Finally, the CeNRs were heated at 333 K for 24 h. These CeNRs have the advantages of low costs, environmental compatibility, and long-term stability,[1] exhibiting enzyme activity comparable to native jack bean urease[1] and quorum-sensing-regulatory properties similar to natural or engineered vanadium haloperoxidases and halogenases.[2] All the commercial CeNPs and homemade CeNRs were stored in closed vessels at room temperature until analysis.

The composition of surrogate lung fluid (SLF) is shown in Table S1. Therein the concentrations of ascorbate (11140, Sigma Aldrich), citric acid (C0759, Sigma Aldrich), glutathione (G4251, Sigma Aldrich), uric acid (U2625, Sigma Aldrich), and sodium chloride (443824T, VWR) are 0.2, 0.3, 0.1, 0.1, and 114 mM, respectively.[3] The pH was adjusted by using different molar ratios of sodium phosphate dibasic (71269, Fluka) and potassium phosphate monobasic (11594, Alfa Aesar). The total concentration of PO_4^{3-} is 10 mM. The pH values were measured using a S210 pH meter (Mettler Toledo). All the suspensions were always prepared and used freshly.

The loading of CeNPs in different suspensions is in the range of 0.1-30 mg mL^{-1}. The composition of different aqueous mixture samples is shown in Table S1. Briefly, the measured solution samples include:

1) Suspensions containing CeNPs (Ø 50 nm) and phosphate buffer (PBS).

2) Suspensions containing CeNPs (Ø 50 nm), PBS, and H_2O_2.

3) Suspensions containing CeNPs (Ø 50 nm), PBS, H_2O_2, and Fe^{2+}.

4) Suspensions containing CeNPs or CeNRs, antioxidants, PBS, H_2O_2, and Fe^{2+}.

Table S1. Summary of the spin trapping EPR experiments performed in this study.

Solutions	Component	Fenton reagents	Particle type	Effect on $OH^{\cdot}$ yield*	
				pH=4.7	pH=7.4
PBS	10 mM mixture of Na_2HPO_4 and KH_2PO_4	No	CeNPs (Ø 50 nm)	+	+
PBS		Only H_2O_2	CeNPs (Ø 50 nm)	++	+
PBS		H_2O_2 + Fe^{2+}	CeNPs (Ø 50 nm)	---	--
SLF	10 mM Na_2HPO_4 and KH_2PO_4 0.2 mM ascorbate 0.3 mM citric acid 0.1 mM glutathione 0.1 mM uric acid 114 mM NaCl	H_2O_2 + Fe^{2+}	CeNPs (Ø 50 nm)		-
SLF		H_2O_2 + Fe^{2+}	CeNPs (Ø 25 nm)		-
SLF		H_2O_2 + Fe^{2+}	CeNRs		---

* Note: the '+' and '-' represent the positive and negative effects of CeNPs or CeNRs in H_2O_2 formation, respectively. The number of the '+' and '-' indicates the extent of the effects by these NPs.

Section S2. Transmission electron microscope (TEM) analysis

The particle size and shape of the CeNPs and CeNRs were characterized using a TEM (FEI Tecnai G2 Spirit).[1] The TEM images of these nanoparticles were taken with an acceleration voltage of 120 kV and a LaB6 kathode.

Section S3. Brunauer-Emmett-Teller (BET) measurement

The surface area of CeNPs and CeNRs was determined through the BET method. A gas adsorption setup Autosorb-6B from Quantachrome with nitrogen as carrying gas has been used. The measurement was conducted at 77 K. Triplicates have been made for each type of nanoparticles.

Section S4. XPS measurement

X-ray photoelectron spectrometry (XPS) measurements were conducted to detect the surface composition of CeNPs and CeNRs. A XPS spectrometer (SPECS GmbH, Germany) equipped with a twin-anode X-ray source XR 50, a hemispherical energy analyzer PHOIBOS 100 and 5 channeltron detectors has been used for this study. The CeNPs or CeNRs particles were pressed into indium foil without any additional prior treatment. Non-monochromatized Al Kα radiation (1486.6 eV) was used to record the XPS spectra. The software CasaXPS (Casa Software Ltd., UK) was used for data evaluation. More information about the analysis steps can be found in a previous study.[4] XPS measurements where conducted with a pressure inside the analyzer chamber of about 10^{-8} mbar. The survey scan was recorded at a constant analyzer pass energy E_p = 50 eV. High-resolution spectra of Ce 3d and O 1s were recorded with E_p = 13 eV. Ten sweeps of each spectrum were averaged. Fifty sweeps in the region of the outer valence molecular orbitals (OVMO) were measured with E_p = 30 eV. Data analysis steps to produce the spectra in Fig. 1 and Fig. S2 included satellite subtraction from Al Kα radiation and Shirley background calculation. Since the spectra did not show any C 1s intensity, the binding energy of the Ce $3d_{5/2}$ peak of CeO_2 was set to 882.3 eV to correct for surface charging. The line shape for fitting the individual components was GL (60). The only constrain used in the fits of the Ce 3d spectra concerned the full-width-at-half-maximum (FWHM) of the individual peaks. In the Ce 3d spectra, that are composed of the $3d_{5/2}$ and $3d_{3/2}$ doublets with two associated satellite peaks each, the FWHM of the corresponding pairs of peaks were independently fitted. Peak areas and positions were adjustable parameters during all fits. The quantitative analysis of the O 1s components for the three different types of nanomaterials used in this study can be found in Table S3. Clearly the abundance of surface hydroxide is much higher in the nanorods than in the commercial CeNPs. The electron binding energies are display in Table S2.

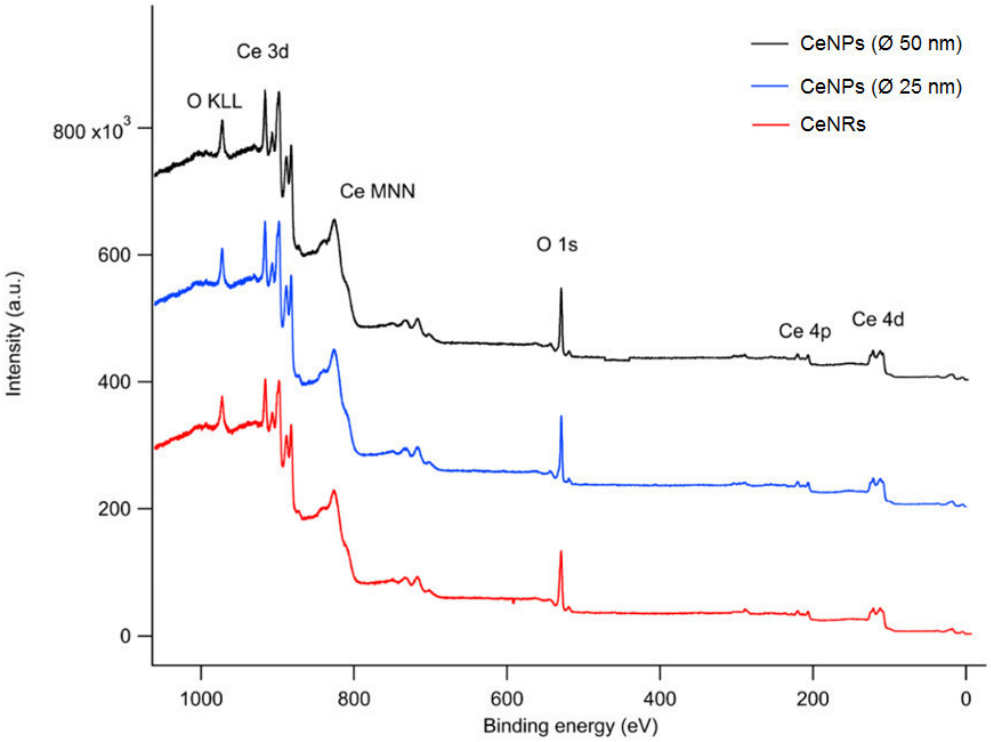

Fig. S1 XPS survey scan of the three different CeNPs and CeNRs samples.

Table S2. Electron binding energies E_b (eV) for all three types of CeO_2 nanoparticles. The FWHM is shown in parenthesis.

CeO_2	Ce $3d_{5/2}$*	Sat_1	Sat_2	O 1s (CeO_2)	O 1s (OH^-)
CeNPs (Ø 50 nm)	882.3 (2.5)	888.1 (5.8)	898.0 (2.3)	529.2 (1.4)	531.0 (1.9)
CeNPs (Ø 25 nm)	882.3 (2.4)	888.1 (5.7)	898.0 (2.3)	529.2 (1.4)	531.8 (2.8)
CeNRs	882.3 (2.6)	887.8 (6.0)	897.9 (2.5)	528.8 (1.5)	530.5 (2.5)

* E_b of Ce $3d_{5/2}$ in CeO_2 was set to 882.3 eV[4] to correct for electrostatic sample charging. The error in E_b equals ±0.1 eV. Sat_1 and Sat_2 are the charge-transfer and shake-up satellites associated to Ce $3d_{5/2}$, respectively.

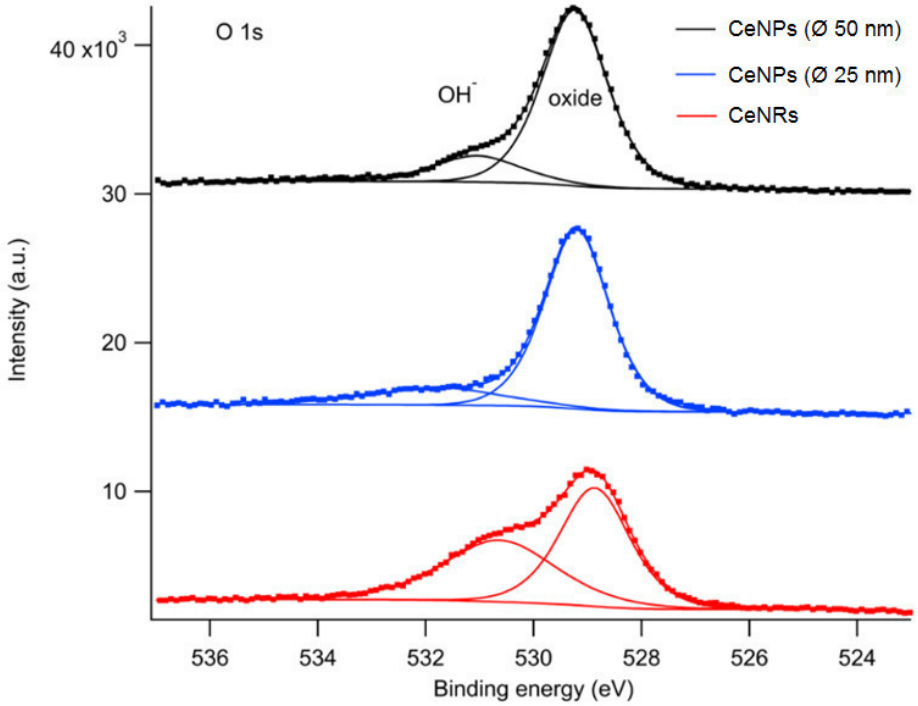

Fig. S2 XPS spectrum of the O 1s region of the three different nanoparticles. The CeNRs show significantly more OH^- groups[5] associated with the transition metal surface.

Table S3. Relative intensities (%) of the O 1s components and the oxygen coefficient *x* in CeO_{2-x} for different CeO_2 nanoparticles.

CeO_2	O 1s - CeO_2 (%)	O 1s - OH^- (%)	x^*
CeNPs (Ø 50 nm)	83	17	2.0
CeNPs (Ø 25 nm)	84	16	2.1
CeNRs	54	46	1.7

* The oxygen coefficient was calculated from the relative O 1s (oxide) and Ce $3d_{5/2}$ intensities, assuming that *x* equals 2.0 in sample CeNPs (Ø 50 nm). The relative error is approximately ±5%.

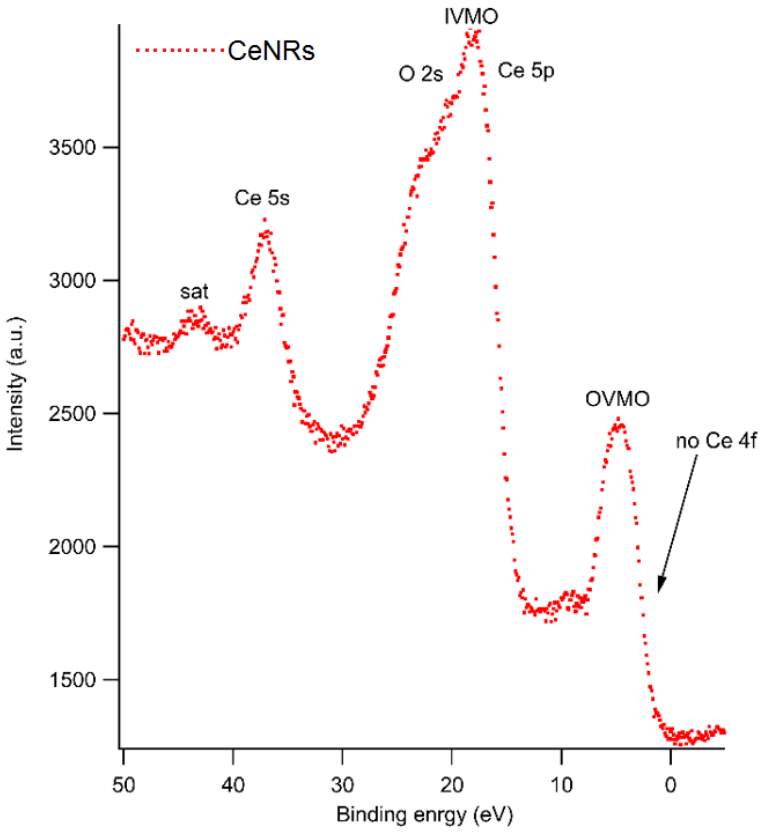

Fig. S3 Valence band XPS measurement of the CeNRs for the binding energy between 0 and 50 eV, displaying that there is no detectable Ce^{3+} abundance at the surface of the samples. In case of Ce^{3+}, this would have led to a shoulder at ~1.1 eV from unbound Ce 4f electrons as indicated by the arrow in the spectrum.

Section S5. CW-EPR measurement

In this study, 5-tert-butoxycarbonyl 5-methyl-1-pyrroline N-oxide (BMPO, high purity, Enzo Life Sciences GmbH) was used as trapping agent.[6] A continuous-wave electron paramagnetic resonance (CW-EPR) X-band spectrometer (EMXplus-10/12; Bruker Corporation) was used for measuring ·OH. Aqueous mixtures containing CeNPs and CeNRs were stirred with a vortex shaker (Heidolph Reax 1) for 10 min before EPR measurement. Then, approximately 20 µL of the suspension were immediately transferred into a micropipette for EPR analysis, which took <0.5 min. Thus, the reactants in each suspension sample totally reacted for 30±0.5 min at room temperature during our measurement. The concentration of BMPO in this study is 10 mM for all samples. The EPR spectra were recorded by setting the operating parameters as shown in Table S1. The spin-counting method embedded in the Bruker software, Xenon, was used to quantify BMPO-OH adducts. The spin-counting method was calibrated using the standard compound 4-hydroxy-2, 2, 6, 6-tetramethylpiperidin-1-oxyl (TEMPOL). EPR spectra were fitted and simulated using the Xenon software before quantification.[5]

Table S4. EPR settings used in this study.

Parameter	Value
Microwave frequency	9.84 Ghz
Microwave attenuation	20 dB
Microwave power	0.017 mW
Receiver gain	40 dB
Modulation amplitude	1 G
Scan number	50 scans
Center field	3509 G
Sweep width	100 G
Modulation frequency	100 kHz
Conversion time	11.05 ms
Time constant	10.24 ms

Table S5. BMPO-OH yield of aqueous mixtures of 1 mM $FeSO_4$, 10 mM H_2O_2, and varying loading of CeNPs (Ø 50 nm) in PBS with pH=4.7.

CeNP (Ø 50 nm) (mg/mL)	BMPO-OH (μM)
0	53.2±2.8
0.1±0.03	50.8±3.1
0.3±0.1	46.1±2.6
0.5±0.01	38.2±2.7
1.2±0.06	36.6±1.6
2.5±0.1	34.0±1.9
5.2±0.1	34.0±1.8
10.0±0.06	30.2±1.8
15.0±0.1	26.5±1.7
19.9±0.1	22.1±2.2
30.5±0.1	14.6±2.0

Table S6. BMPO-OH yield of aqueous mixtures of 1 mM $FeSO_4$, 10 mM H_2O_2, and varying loading of CeNPs (Ø 50 nm) in PBS with pH=7.4.

CeNP (Ø 50 nm) (mg/mL)	BMPO-OH (μM)
0	16.7±1.0
0.4±0.01	15.9±1.2
0.6±0.03	15.5±1.3
1.1±0.06	14.7±1.4
2.6±0.03	14.2±1.4
4.9±0.1	13.8±1.4
10.1±0.1	12.4±1.2
15.1±0.06	11.7±1.2
20.0±0.1	10.4±1.0
29.9±0.06	10.8±1.1

Table S7. BMPO-OH concentrations in aqueous mixtures of 1 mM $FeSO_4$, 10 mM H_2O_2, PBS, antioxidant, or SLF solutions with varying loadings of CeNPs or CeNRs.

PBS/Antioxidant/CeO_2	Fenton chemistry (μM)	Fenton+CeNPs (Ø 50 nm) (μM)	Fenton+CeNPs (Ø 25 nm) (μM)	Fenton+CeNRs (μM)
PBS	26.1±0.6			
SLF	16.4±2.6			
Citric acid	26.9±0.6			
Glutathione	24.0±7.1			
Uric Acid	19.9±7.2			
Ascorbate	15.8±2.9			
0.1		16.4±1.7	15.4±0.8	1.9±0.1
0.25		15.0±1.8	14.7±1.3	1.2±0.02
0.5		13.8±0.8	13.3±1.3	1.1±0.07
1.0		13.2±1.5	11.8±1.3	1.6±0.6
2.5		12.3±1.6	9.0±1.0	below LOD
5		10.3±1.1	1.2±1.1	below LOD
10		4.0±0.4	below LOD	below LOD
20		0.6±0.1	below LOD	

Notes and references

1. K. Korschelt, R. Schwidetzky, F. Pfitzner, J. Strugatchi, C. Schilling, M. von der Au, K. Kirchhoff, M. Panthofer, I. Lieberwirth, M. N. Tahir, C. Hess, B. Meermann and W. Tremel, *Nanoscale*, 2018, **10**, 13074-13082.
2. K. Herget, P. Hubach, S. Pusch, P. Deglmann, H. Gotz, T. E. Gorelik, I. A. Gural'skiy, F. Pfitzner, T. Link, S. Schenk, M. Panthofer, V. Ksenofontov, U. Kolb, T. Opatz, R. Andre and W. Tremel, *Adv. Mater.*, 2017, **29**, 1603823.
3. J. G. Charrier and C. Anastasio, *Atmos. Environ.*, 2011, **45**, 7555-7562.
4. K. I. Maslakov, Y. A. Teterin, A. J. Popel, A. Y. Teterin, K. E. Ivanov, S. N. Kalmykov, V. G. Petrov, P. K. Petrov and I. Farnan, *Appl. Surf. Sci.,* 2018, **448**, 154-162.
5. J. Haber, J. Stoch and L. Ungier, *J. Electron Spectrosc. Relat. Phenom.*, 1976, **9**, 459-467.
6. H. Tong, P. S. J. Lakey, A. M. Arangio, J. Socorro, F. Shen, K. Lucas, W. H. Brune, U. Poschl and M. Shiraiwa, *Environ. Sci. Technol.*, 2018, **52**, 11642-11651.

3.3 Oxidation Degree and its Influence on Radical Yield of Particulate Matter

This chapter is has been published in the scientific journal *Environmental science & technology*. As the third author of this paper I have contributed to the planning, conduction, and publication of this research project. More concretely, I have contributed a significant share of the spin-trapping EPR experiments in this study myself and supervised other coauthors including Ting Wang and Chenpei Li in conducting EPR studies and SOA formation. Furthermore, I contributed to discussions and editing of text and figures in the process of preparing the results for publication, particularly the EPR related work.

Radical formation by fine particulate matter associated with highly oxygenated molecules

Environmental Science & Technology, **53(21)**, 12506-12518, (2019)

Haijie Tong,[1] Yun Zhang,[2] Alexander Filippi,[1] Ting Wang,[1, 3] Chenpei Li,[1, 3] Fobang Liu,[1, 4] Denis Leppla,[2] Ivan Kourtchev,[5] Kai Wang,[2] Helmi-Marja Keskinen,[6] Janne T. Levula,[6] Andrea M. Arangio,[1, 7] Fangxia Shen,[8] Florian Ditas,[1] Scot T. Martin,[9, 10] Paulo Artaxo,[11] Ricardo H. M. Godoi,[12] Carlos I. Yamamoto,[13] Rodrigo A. F. de Souza,[14] Ru-Jin Huang,[15] Thomas Berkemeier,[1] Yueshe Wang,[3] Hang Su,[1] Yafang Cheng,[1] Francis D. Pope,[16] Pingqing Fu,[17] Maosheng Yao,[18] Christopher Pöhlker,[1] Tuukka Petäjä,[6] Markku Kulmala,[6] Meinrat O. Andreae,[1, 19] Manabu Shiraiwa,[20] Ulrich Pöschl,[1] Thorsten Hoffmann,[2] and Markus Kalberer.[5, 21]

[1] Multiphase Chemistry Department, Max Planck Institute for Chemistry, 55128 Mainz, Germany

[2] Institute of Inorganic and Analytical Chemistry, Johannes Gutenberg University, 55128 Mainz, Germany

[3] State Key Laboratory of Multiphase Flow in Power Engineering, Xi'an Jiaotong University, Xi'an 710049, China

[4] School of Chemical and Biomolecular Engineering, Georgia Institute of Technology, Atlanta, Georgia 30332, United States

[5] Centre for Atmospheric Science, Department of Chemistry, University of Cambridge, Cambridge CB2 1EW, United Kingdom

[6] Institute for Atmospheric and Earth System Research/Physics Faculty of Science, University of Helsinki, FI-00014 Helsinki, Finland

[7] École polytechnique fédérale de Lausanne, Lausanne 1015, Switzerland

[8] School of Space and Environment, Beihang University, Beijing 100191, China

[9] School of Engineering and Applied Sciences and [10] Department of Earth and Planetary Sciences, Harvard University, Cambridge, Massachusetts 02138, United States

[11] Physics Institute, University of São Paulo, São Paulo 05508-900, Brazil

[12] Environmental Engineering Department, Federal University of Paraná, Curitiba, Paraná 81531-980, Brazil

[13] Chemical Engineering Department, Federal University of Paraná, Curitiba, Paraná 81531-970, Brazil

[14] School of Technology, Amazonas State University, Manaus, Amazonas 69065-020, Brazil

[15] Key Laboratory of Aerosol Chemistry and Physics, State Key Laboratory of Loess and Quaternary Geology, Institute of Earth and Environment, Chinese Academy of Sciences, Xi'an, 710061, China

[16] School of Geography, Earth and Environmental Sciences, University of Birmingham, Birmingham B15 2TT, United Kingdom

[17] Institute of Surface-Earth System Science, Tianjin University, Tianjin 300072, China

[18] College of Environmental Sciences and Engineering, Peking University, Beijing 100871, China

[19] Scripps Institution of Oceanography, University of California San Diego, San Diego, California 92093, United States

[20] Department of Chemistry, University of California, Irvine, California 92697-2025, United States

[21] Department of Environmental Sciences, University of Basel, Klingelbergstrasse 27, 4056 Basel, Switzerland

Environmental Science & Technology

Article

Cite This: Environ. Sci. Technol. 2019, 53, 12506−12518

pubs.acs.org/est

Radical Formation by Fine Particulate Matter Associated with Highly Oxygenated Molecules

Haijie Tong,*[,1] Yun Zhang,[2] Alexander Filippi,[1] Ting Wang,[1,3] Chenpei Li,[1,3] Fobang Liu,[1,4] Denis Leppla,[2] Ivan Kourtchev,[5] Kai Wang,[2,†] Helmi-Marja Keskinen,[6] Janne T. Levula,[6] Andrea M. Arangio,[1,7] Fangxia Shen,[8] Florian Ditas,[1] Scot T. Martin,[9,10] Paulo Artaxo,[11] Ricardo H. M. Godoi,[12] Carlos I. Yamamoto,[13] Rodrigo A. F. de Souza,[14] Ru-Jin Huang,[15] Thomas Berkemeier,[1] Yueshe Wang,[3] Hang Su,[1] Yafang Cheng,[1] Francis D. Pope,[16] Pingqing Fu,[17] Maosheng Yao,[18] Christopher Pöhlker,[1] Tuukka Petäjä,[6] Markku Kulmala,[6] Meinrat O. Andreae,[1,19] Manabu Shiraiwa,[20] Ulrich Pöschl,[1] Thorsten Hoffmann,*[,2] and Markus Kalberer*[,5,21]

[1]Multiphase Chemistry Department, Max Planck Institute for Chemistry, 55128 Mainz, Germany

[2]Institute of Inorganic and Analytical Chemistry, Johannes Gutenberg University, 55128 Mainz, Germany

[3]State Key Laboratory of Multiphase Flow in Power Engineering, Xi'an Jiaotong University, Xi'an 710049, China

[4]School of Chemical and Biomolecular Engineering, Georgia Institute of Technology, Atlanta, Georgia 30332, United States

[5]Centre for Atmospheric Science, Department of Chemistry, University of Cambridge, Cambridge CB2 1EW, United Kingdom

[6]Institute for Atmospheric and Earth System Research/Physics Faculty of Science, University of Helsinki, FI-00014 Helsinki, Finland

[7]École polytechnique fédérale de Lausanne, Lausanne 1015, Switzerland

[8]School of Space and Environment, Beihang University, Beijing 100191, China

[9]School of Engineering and Applied Sciences and [10]Department of Earth and Planetary Sciences, Harvard University, Cambridge, Massachusetts 02138, United States

[11]Physics Institute, University of São Paulo, São Paulo 05508-900, Brazil

[12]Environmental Engineering Department, Federal University of Paraná, Curitiba, Paraná 81531-980, Brazil

[13]Chemical Engineering Department, Federal University of Paraná, Curitiba, Paraná 81531-970, Brazil

[14]School of Technology, Amazonas State University, Manaus, Amazonas 69065-020, Brazil

[15]Key Laboratory of Aerosol Chemistry and Physics, State Key Laboratory of Loess and Quaternary Geology, Institute of Earth and Environment, Chinese Academy of Sciences, Xi'an, 710061, China

[16]School of Geography, Earth and Environmental Sciences, University of Birmingham, Birmingham B15 2TT, United Kingdom

[17]Institute of Surface-Earth System Science, Tianjin University, Tianjin 300072, China

[18]College of Environmental Sciences and Engineering, Peking University, Beijing 100871, China

[19]Scripps Institution of Oceanography, University of California San Diego, San Diego, California 92093, United States

[20]Department of Chemistry, University of California, Irvine, California 92697-2025, United States

[21]Department of Environmental Sciences, University of Basel, Klingelbergstrasse 27, 4056 Basel, Switzerland

Supporting Information

ABSTRACT: Highly oxygenated molecules (HOMs) play an important role in the formation and evolution of secondary organic aerosols (SOA). However, the abundance of HOMs in different environments and their relation to the oxidative potential of fine particulate matter (PM) are largely unknown. Here, we investigated the relative HOM abundance and radical yield of laboratory-generated SOA and fine PM in ambient air ranging from remote forest areas to highly polluted megacities. By electron paramagnetic resonance and

continued...

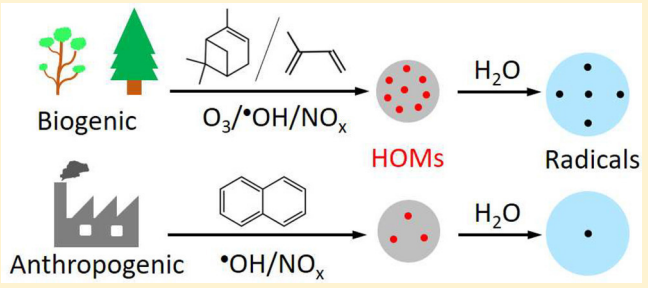

Received: August 26, 2019
Accepted: September 19, 2019
Published: September 19, 2019

DOI: 10.1021/acs.est.9b05149
Environ. Sci. Technol. 2019, 53, 12506−12518

mass spectrometric investigations, we found that the relative abundance of HOMs, especially the dimeric and low-volatility types, in ambient fine PM was positively correlated with the formation of radicals in aqueous PM extracts. SOA from photooxidation of isoprene, ozonolysis of α- and β-pinene, and fine PM from tropical (central Amazon) and boreal (Hyytiälä, Finland) forests exhibited a higher HOM abundance and radical yield than SOA from photooxidation of naphthalene and fine PM from urban sites (Beijing, Guangzhou, Mainz, Shanghai, and Xi'an), confirming that HOMs are important constituents of biogenic SOA to generate radicals. Our study provides new insights into the chemical relationship of HOM abundance, composition, and sources with the yield of radicals by laboratory and ambient aerosols, enabling better quantification of the component-specific contribution of source- or site-specific fine PM to its climate and health effects.

1. INTRODUCTION

Secondary organic aerosols (SOA) account for a major fraction of fine particulate matter ($PM_{2.5}$),[1] which plays a key role in climate change and public health.[2−7] Insights into the chemical and redox characteristics of SOA are important for properly understanding the role of fine PM at the atmosphere−biosphere interface.[8] SOA particles contain a large fraction of reactive substances such as peroxides and highly oxygenated molecules (HOMs).[9−12] The HOMs exist in the gas[12−15] and particle phases,[16−21] and they increase the oxidation state and initial growth of organic aerosols, as well as influencing the stability and reactivity of fine PM upon redox chemistry, including radical reactions.[12,20,22−24] Therefore, a comprehensive understanding of the physicochemical properties of HOMs and their relationship with the oxidative potential of fine PM is challenging but vital to unravel the climate and health effect of SOA.[24]

To date, a few studies have explored the formation mechanism, structure, and chemical aging processes of particle-phase HOMs. For instance, gas-phase oxidation of organic compounds including Criegee intermediates has been found to be an efficient formation pathway of HOMs.[13,16,20,25−27] Therein, SOA-bound HOMs were suggested to contain multiple functional groups including hydroperoxides and to have molecular formulas with high atom ratios of oxygen-to-carbon (>0.6 or 0.7).[11−13,16,28−30] To subdivide HOMs into different types, HOMs with carbon oxidation state[31] ($\overline{OS_C} \approx 2\frac{O}{C} - \frac{H}{C}$) $\geq$ 0 were assigned to be both highly oxygenated and highly oxidized compounds, while HOMs with $\overline{OS_C}$ < 0 were attributed to be highly oxygenated but less oxidized.[16] Furthermore, HOMs in fresh biogenic SOA were found to have formulas more closely resembling low-volatility oxygenated organic aerosols (LV-OOA) than HOMs in aged SOA.[16] Tröstl et al.[12] and Ehn et al.[13] found that HOMs in laboratory-generated α-pinene SOA fell into the following chemical composition range of $C_xH_yO_z$: monomers with x = 8−10, y = 12−16 and z = 6−12 and dimers with x = 17−20, y = 26−32, and z = 8−18.[12,32] Beyond this, it has been assumed that organic peroxides in α- and β-pinene SOA have molecular weights of <300 g mol^{-1},[33] falling in the typical molecular weight range of HOM monomers.[12] These peroxides are redox active[11] and can generate reactive species such as radicals through Fenton-like reactions[23,34] and photolytic or hydrolytic decomposition in water.[23,35−37] The reactive species are ubiquitous in atmospheric, environmental, and biological processes, exerting strong effects on climate change and public health.[38,39] In addition to organic peroxides, high-molecular-weight dimeric esters have been found as major products in aerosols from cyclohexene and α-pinene ozonolysis and boreal forest.[40−42] Therefore, HOMs have different sources, complicated composition, and various redox activities. Beyond these findings, the volatility, reactivity, and fate of different source HOMs remain unclear.[24] Insights into these uncertainties will enable a better assessment of aerosol climate and health effects.

In this study, HOMs from all laboratory and ambient samples were defined by molecular formulas matching the criteria from Tröstl et al.[12] and filtering out HOM monomers with O/C ratio <0.7.[16] On the basis of this criterion, we investigated the relative HOM abundance and radical yield of laboratory SOA formed in a chamber and ambient fine PM in the air ranging from remote forests to highly polluted megacities. The correlation of radical yield of fine PM in water with the relative fraction of HOMs (RF_{HOM}) among organic constituents was investigated. The RF_{HOM} was defined as the ratio of the number of HOM ions to all formulas identified in a spectrum. The molecular composition of organic aerosol components was determined using an ultrahigh-resolution mass spectrometer,[43,44] and the radicals in water were identified and quantified using continuous wave electron paramagnetic resonance spectrometry in combination with a spin-trapping technique.[36]

2. MATERIALS AND METHODS

2.1. Ambient Particle Sampling. Ambient particles were collected at seven different locations: central Amazon, Hyytiälä, Mainz, Beijing, Shanghai, Guangzhou, and Xi'an. Detailed information on sampling time and instrumentation can be found in Table S1.

The central Amazon fine PM was collected at two different stations. One set of samples was collected from the site "T3" of GoAmazon2014/5 located in a pasture area that was 70 km west and downwind of Manaus, Amazonas State, Brazil.[45] These samples were used for analyzing the RF_{HOM}. The other set of samples was collected at the Amazon Tall Tower Observatory (ATTO) station, which is located in a remote area of the central Amazon Basin, about 150 km northeast (upwind) of the city of Manaus.[46] At the T3 site, a Harvard impactor (Air Diagnostics, Harrison, ME, USA) and polycarbonate filters (Ø 47 mm, Nuclepore) were used for PM collection at an air flow of ∼10 L min^{-1}. Particles were collected in the dry and wet seasons in 2014 (Table S1). The collected particle samples were stored in −20 or −80 °C freezers until analysis. At the ATTO site, a micro-orifice uniform deposition impactor (MOUDI, Model 125R, MSP Corp., USA) was used to collect sample air from a 60 m high inlet at a 80 m tall tower with an air flow rate of ∼10 L min^{-1}. Afterward, the filters were transported from ATTO to Mainz in an icebox and then stored in a −80 °C freezer before analysis. Dry season ATTO PM samples were collected from October 20 to 21, 2017, and from October 25 to 31, 2018. These samples were used for analyzing the relationship between ion number and chromatographic peak area indicating the relative abundance of HOMs. Wet season samples were collected from March 27 to April 25, 2017. These samples were used for analyzing the radical yield of PM. More information about the ATTO tower and the typical characteristics of aerosol particles

DOI: 10.1021/acs.est.9b05149
Environ. Sci. Technol. 2019, 53, 12506−12518

in the upper troposphere over the Amazon Basin can be found in previous studies.[46,47]

The Hyytiälä fine PM samples were collected from the boreal forest site SMEAR II in Finland from July 7 to August 4, 2014 and from May 31 to July 19, 2017. Scots pine and Norway spruce are the dominant type of trees surrounding the station.[48] A three-stage Dekati PM_{10} impactor together with 47 mm diameter quartz fiber (Pallflex Tissuquartz 2500QAT-UP) and Teflon filters (PALL, Teflon) were used for particle sampling. The quartz filters were prebaked at 600 °C for half a day to remove organics. The air flow rate through the sampler was ∼35 L min^{-1}. After collection, all filter samples were stored at −20 °C (samples collected in 2014) or −80 °C (samples collected in 2017) before analysis.

The Mainz $PM_{2.5}$ samples were collected onto borosilicate glass fiber filters (Ø 70 mm, Pallflex T60A20, Pall Life Science, USA) using a $PM_{2.5}$ low volume air sampler in January 2015 at the campus site of Johannes Gutenberg University of Mainz. Additional fine MP samples were collected onto 47 mm diameter Teflon filters (100 nm pore size, Merck Chemicals GmbH) on the roof of the Max Planck Institute for Chemistry with a micro-orifice uniform deposition impactor (MOUDI, 110-R, MSP Corp.). The samplings were conducted from August to November 2017 and from March to April 2018. The air flow rate through both samplers was ∼30 L min^{-1}. The collected filter samples were stored in −20 °C (samples collected in 2015) or −80 °C (samples collected in 2017 and 2018) freezers before analysis. More information about the aerosol sampling and chemical characteristization can be found in our recent studies.[49,50]

$PM_{2.5}$ samples in urban sites of Beijing,[49] Shanghai, and Guangzhou were collected onto prebaked quartz-fiber filters (8 × 10 in.) in the period between January 1 and 23, 2014, using a high-volume air sampler (Tisch, Cleveland, OH, USA) at a flow rate of ∼1050 L min^{-1}. Additional $PM_{2.5}$ samples were collected at Peking University campus, central urban region of Beijing, onto 47 mm diameter Teflon filters (100 nm pore size, Merck Chemicals GmbH) in 2016 and 2017 with a TH-16 sampler (Tianhong company, China) at an air flow of ∼30 L min^{-1}. The samples collected in 2014 and 2018 were stored in −20 or −80 °C freezers before analysis.

The Xi'an fine PM samples were collected using a low-pressure cascade impactor (Tisch TE-20-800, USA) on the roof of Xi'an Jiaotong University in China. The cutoff aerodynamic diameters of the sampler are 0.43, 0.65, 1.1, 2.1, 3.3, 4.7, 5.8, and 9 μm. Particles were collected onto 90 mm diameter Teflon filters (100 nm pore size, Omnipore JVWP09025, Millipore). Each particle filter sample was collected for 48 h in the period between September 14 and 22, 2017. Before sampling, each filter was cleaned, dried, and weighed.[50] After sampling, filters were stored in a −80 °C freezer before analysis.

2.2. Laboratory SOA Formation and Collection. To compare the relative HOM abundances in anthropogenic and biogenic SOA, we measured the RF_{HOM} in SOA formed from the oxidation of naphthalene, isoprene, and α-pinene, which were used as SOA precursors representative for Beijing,[51] Amazon,[52] and Hyytiälä,[53] respectively. Laboratory SOA were generated in a 7 L quartz flow tube and a laboratory-scale reaction chamber (33 L).[23] α-Pinene SOA particles were generated through gas-phase ozonolysis. The isoprene and naphthalene SOA were generated through gas-phase photooxidation by •OH radicals. For the generation of SOA, the O_3 concentration was adjusted in the range of 600−1100 ppb to generate α-pinene SOA. The •OH concentrations were estimated to be $\sim 5.0 \times 10^{11}$ cm^{-3} for the formation of isoprene and naphthalene SOA.[36] On the basis of a calibration function measured by gas chromatography−mass spectrometry, the precursor concentration was estimated to be in the range of 1−2 ppm for α-pinene and 0.5−1 ppm for isoprene and naphthalene. A scanning mobility particle sizer (SMPS, GRIMM Aerosol Technik GmbH & Co. KG) was used to characterize the number and size distribution of SOA particles, which were collected onto 47 mm diameter Teflon filters (JVWP04700, Omnipore membrane filter) and extracted into water immediately after sampling. More information about the SOA formation, characterization, and collection are described in previous studies.[23,34,36]

2.3. Ultrahigh-Resolution Mass Spectrometer Measurements and Data Processing. The chemical composition of organics in the Amazon and Hyytiälä 2014 fine PM samples were identified using a negative ion mode electrospray ionization (ESI) LTQ Orbitrap mass spectrometer (Thermo Fisher Scientific, MA, USA) at the University of Cambridge. All other filter samples were analyzed at the Johannes Gutenberg University of Mainz, using a Q-Exactive Orbitrap MS instrument (Thermo Fisher Scientific, MA, USA) operated in both negative and positive ion mode ESI and coupled with an ultrahigh-performance liquid chromatography (UHPLC) system (Dionex UltiMate 3000, Thermo Scientific, Germany). A Hypersil Gold column (C18, 50 × 2.0 mm, 1.9 μm particle size, Thermo Fisher Scientific, MA, USA) was used for analyte separation. Eluent A (ultrapure water with 2% acetonitrile and 0.04% formic acid) and eluent B (acetonitrile with 2% ultrapure water) were used in gradient mode with a flow rate of 500 μL min^{-1}. Detailed information on the optimized gradient can be found in our recent study.[49] Both mass spectrometers were optimized, calibrated, and tuned using chemical standard kits. The filter extraction and data processing methods are the same as those which we used for organic aerosol composition analysis in previous studies.[49,54]

After obtaining the MS spectrum and UHPLC chromatogram of one sample, we processed the data through a nontarget screening approach by using the commercially available software SIEVE (Thermo Fisher Scientific, MA, USA).[49] Briefly, we searched the ions with peak abundance $>1 \times 10^5$ first and then subtracted the background signals and assigned molecular formulas. The numbers of C, H, O, N, S, and Cl atoms were constrained to be 1−39, 1−72, 0−20, 0−7, 0−4, and 0−2 with a tolerance of ±2 ppm. Furthermore, the atom ratio limits of H/C (0.3−3), O/C (0−3), N/C (0−1.3), S/C (0−0.8), and Cl/C (0−0.8) were used to eliminate chemically unreasonable formulas.

2.4. Continuous Wave Electron Paramagnetic Resonance Measurements. Continuous wave electron paramagnetic resonance (EMXplus-10/12, Bruker, Germany) spectrometry in combination with spin-trapping techniques was used to detect radicals. 5-*tert*-Butoxycarbonyl-5-methyl-1-pyrroline *N*-oxide (BMPO, high purity, Enzo Life Sciences GmbH) was used as the spin-trapping agent.[55] The concentration of BMPO in all extracts was 10 mM. The aqueous PM mass concentration in the extracts of ambient fine PM and laboratory SOA was in the range of 250−6300 μg mL^{-1}, with a higher concentration for ambient fine PM and a lower concentration for laboratory SOA. The aqueous PM mass concentration is defined here as the total PM mass on the filter cut divided by the volume of extraction solvent. The EPR parameters used in this study were the same as in our previous

DOI: 10.1021/acs.est.9b05149
Environ. Sci. Technol. 2019, 53, 12506−12518

studies:[23,34,50] a modulation frequency of 100 kHz, a modulation amplitude of 1.0 G, microwave power of 2.1 mW (20 dB), receiver gain of 40 dB, a time constant of 0.01 ms, a scan number of 50, and a magnetic field scan of 100 G. The spin-fitting and -counting methods embedded in the Bruker software Xenon were applied for quantification of radicals.[56]

3. RESULTS AND DISCUSSION

3.1. Spectral Fingerprint of HOMs. We distinguished HOMs from other organic components in ambient fine PM from Beijing, Amazon, Hyytiälä, and laboratory SOA from oxidation of α-pinene, isoprene, and naphthalene. We found that the ion number fraction of HOMs is in linear positive correlation with the fraction of chromatographic peak area of HOMs averaged from measured samples (Figure S1a; $y = 2.37 + 0.70x$, $R^2 = 0.88$), with the latter showing a positive exponential correlation with the radical yield of PM (Figure S1b; $y = 0.10 + 0.016 \exp(0.37x)$, $R^2 = 0.99$), indicating that RF_{HOM} may be an indicator of the relative abundance of particle-phase HOMs. Therefore, we showed the mass spectra as well as the RF values of HOMs in Figure 1 and Figure S2.

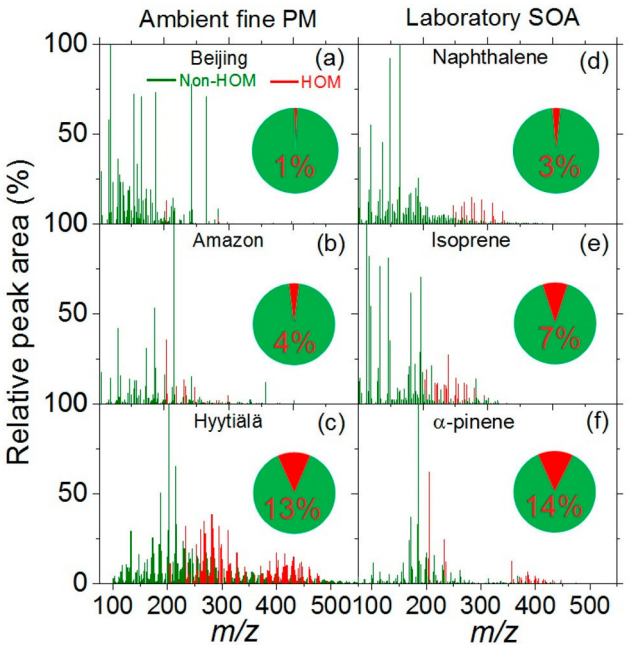

Figure 1. Spectral fingerprint and relative fraction of HOMs (red) and non-HOMs (green) in different types of particles. The mass spectra were measured using the LC-MS technique. The chromatographic peak areas were used to calculate relative fractions of HOMs for the pie charts. The relative peak area (%) of the spectra belonging to HOMs in ambient PM and laboratory SOA were multiplied by factors of 3 and 10, respectively. The pie charts and enclosed numbers indicate the ion number fraction of HOMs and non-HOMs. The spectra in (a)−(c) are for PM samples collected in November 2017, October 2018, and July and August 2014.

In ambient samples, most HOMs have been found in remote samples dominated by biogenic SOA, while almost no HOMs were found in fine PM in polluted urban sites. The lack of peaks meeting the HOM criteria in Figure 1a indicates that HOMs account for only a small fraction of the organic components in Beijing fine PM, with a relative fraction of ~1%. In contrast to Beijing fine PM, fine particles in remote forest air of the Amazon and Hyytiälä have much higher RF_{HOM} values of ~4% (Figure 1b) and ~13% (Figure 1c), respectively. This finding agrees well with previous studies, reporting that HOMs and high-molecular-weight dimeric esters are major components of fine PM from a measurement site in an agricultural pasture area in Germany (Melpitz, Leibniz Institute for Tropospheric Research (TROPOS)) and Hyytiälä, respectively.[20,41] Thus, ambient particle-phase HOMs are enriched in organic aerosols related to biogenic sources.

As shown in Figure 1d−f, naphthalene SOA has the lowest RF_{HOM} value of ~3% (Figure 1d). In contrast, relatively more HOM molecules were observed in isoprene (~7%, Figure 1e) and α-pinene SOA (~14%, Figure 1f). The higher RF_{HOM} value of α-pinene SOA in comparison to that of naphthalene SOA agrees with previous studies,[57,58] and the lower RF_{HOM} value of naphthalene SOA may be related to the lower molar yield of extremely low volatility organic compounds (ELVOC) or HOMs from oxidation of naphthalene (~1.8%) in comparison with α-pinene SOA (~3.4%).[19] In addition, it has been estimated that organic peroxides contributed up to 49%, 85%, 61%, and 28% of α-pinene, β-pinene, isoprene, and naphthalene SOA mass, respectively.[33,36,59,60] The consistently lower abundance of organic peroxides and HOMs in naphthalene SOA than in isoprene and α- and β-pinene SOA may reflect that organic peroxides are one type of HOM. Finally, the order of RF_{HOM} in the laboratory experiments with naphthalene, isoprene, and α-pinene SOA (Figure 1d−f) is consistent with ambient fine PM from Beijing, Amazon, and Hyytiälä (Figure 1a−c), confirming that oxidation of biogenic volatile organic compounds, including their autoxidation chemistry, is an efficient formation pathway of ambient particle-phase HOMs.[27] To demonstrate the source dependence of RF_{HOM}, it is useful to clarify the chemical composition and volatility of fine PM-bound HOMs in air ranging from clean background to heavily polluted areas.

3.2. Chemical Composition of Particle Phase HOMs. As shown in Figure 2a, HOM products only composed of carbon, hydrogen, and oxygen (CHO) were preferentially found in laboratory SOA, which was due to the extremely low concentration of NO_x during the experiments. In contrast, ambient fine PM contained relatively few pure CHO compounds as HOMs, increasing, however, with the decrease of air pollution levels from Beijing (~0.4%) to Hyytiälä (~5.1%). In addition to CHO, ambient fine PM also contained substantial fractions of CHON, CHOS, and CHONS forms of HOMs, with higher RF values in cleaner air. The RF values of CHOS and CHONS forms of HOMs in Amazon and Hyytiälä fine PM accounted for ~2% of totally assigned formula, which is comparable to previous findings of organosulfates contributing 4−30% of aerosol mass in central Amazonia,[61] Hungary, and the southeastern U.S.[47,62,63] Furthermore, we have observed a synchronous increase of the concentration of NO_x and nitrogen-containing organic compounds at Hyytiälä,[64] which might reflect the important role of NO_3-related multigenerational chemistry in organonitrate aerosol formation.[65,66] Beyond this, Table S2 shows that the RF value of the total CHOS subgroup in Shanghai fine PM was ~23%, while the HOMs only account for ~0.4% (Figure 2a). Such a result is in line with previous findings that the major CHOS compounds in Shanghai organic aerosols were organosulfates, which possess distinctive characteristics of long aliphatic carbon chains and a low degree of oxidation.[67,68]

In this study, all HOMs were assumed to have the same signal response when we compared their peak areas among different samples. However, different organic compounds might have

DOI: 10.1021/acs.est.9b05149
Environ. Sci. Technol. 2019, 53, 12506−12518

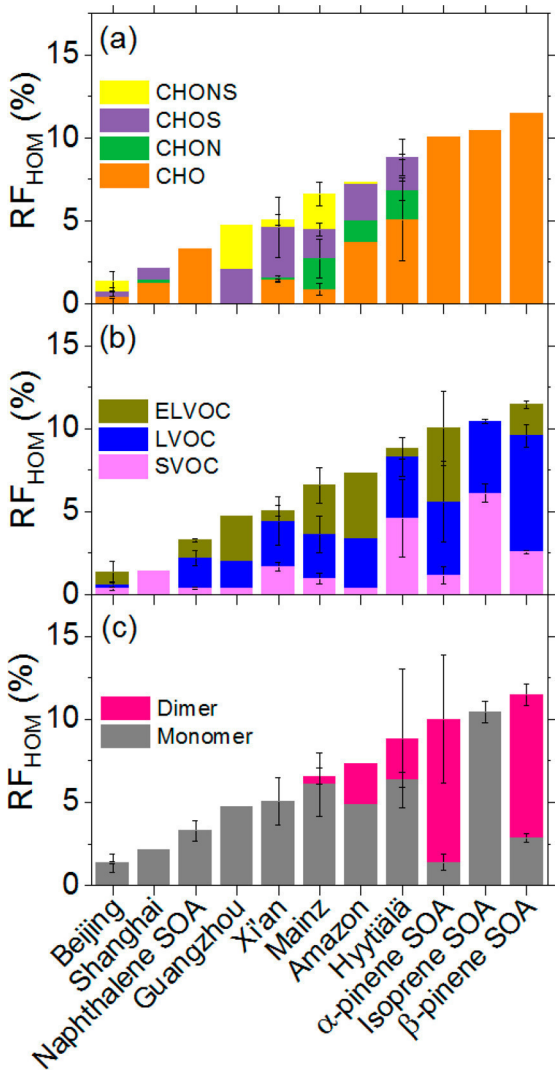

Figure 2. Chemical composition and volatility of HOMs in fine particles from different sources. (a) Chemical composition of HOMs. (b) Relative fractions of HOMs with different volatilities. (c) Relative fractions of HOM dimers and monomers. The error bars represent the standard deviations of measurements with more than three individual samples.

different sensitivities in the mass spectrometer in different ionization modes. Thus, uncertainties exist when the peak areas of HOMs in PM from different sources are compared. To investigate the effect of ion mode on the RF_{HOM} value, we compared the RF_{HOM} values of different types of PM measured in positive and negative ion modes, as shown in Table S3. It was found that 63−93% of particle-phase HOMs were detected in negative mode. This finding is in agreement with the study by Tu et al., which found many more HOMs in laboratory-generated limonene and α- and β-pinene SOA using a quadrupole-orbitrap mass spectrometer coupled with a negative ion mode ESI probe.[16] Thus, the HOMs detected in negative ESI mode dominate the total HOMs in PM. Furthermore, due to the complexity of the elemental composition of HOMs, more insights into their structural characteristics will enable a better understanding of the connection of different types of HOMs to the oxidative potential of organic aerosols.

3.3. Volatility of Particle-Phase HOMs. The volatility of HOMs in fine PM from different sources was estimated using a recently developed parametrization procedure for the volatility of organic compounds.[69] As shown by Figure 2b, laboratory biogenic SOA contained a higher RF value of highly oxygenated low volatility and extremely low volatility organic compounds (LVOC and ELVOC types of HOMs) in comparison to ambient fine PM, which contained fewer LVOC and ELVOC types of HOMs. In addition, the ELVOC type of HOMs was not found in isoprene SOA, which may correlate with the low SOA yield of isoprene and the remarkably low molar yield of gas-phase ELVOC.[57] Furthermore, both LVOC and ELVOC were not found in Shanghai particulate HOMs, an observation that agrees with a previous finding of semivolatile organic compounds and LVOC as the dominant component of the CHO subgroup in Shanghai winter fine PM.[68] The RF trend in the ambient samples of LVOC and ELVOC types of HOMs in Figure 2b resembles the CHO form of HOMs in Figure 2a, likely reflecting that particle-phase HOMs are mainly low-volatility CHO species. The generally higher RF values of LVOC and ELVOC types of HOMs in the CHOS and CHONS subgroups (Figure S3) indicate that the atmospheric nitrogen or sulfur chemistry of particulate HOMs may decrease the volatility and change the oxidative characteristics of organic aerosols.

3.4. HOM Monomers and Dimers in Fine PM. Figure 2c shows the RF values of HOM monomers and dimers in ambient fine PM and laboratory SOA. The HOM monomers were found in all analyzed particle samples, whereas HOM dimers were only found in fine PM from lightly polluted urban air (Mainz), remote forest air (Amazon and Hyytiälä), and laboratory SOA from α- and β-pinene. The absence of HOM dimers in isoprene-derived SOA may be due to the high volatility of products during the photochemical oxidation of isoprene precursors in the chamber.[57] The relative fraction of dimers in all PM samples increased in the order of polluted urban fine PM < remote forest fine PM < monoterpene SOA, which resembles the trend of RF_{HOM}. The HOMs in α- and β-pinene SOA were mainly composed of dimers, with RF values of ∼12% and ∼9%, supporting previous findings of high-molecular-weight dimeric esters as major products in aerosols from α-pinene ozonolysis and boreal forest.[40,41] Krapf et al. found that peroxide-containing HOMs have half-lives shorter than 1 h under dark conditions and are thermodynamically unstable.[11] Thus, the extremely low relative fraction of particle-phase HOM dimers in urban air may relate to the chemical aging and decomposition of HOMs in ambient fine PM. Furthermore, chemical aging of HOMs via redox chemistry of NO_x or sulfur oxides may change the composition and physicochemical properties of particle phase HOMs in urban fine PM. For example, recent studies have shown that atmospheric sulfur chemistry of HOMs[70] and reactive nitrogen chemistry in aerosol water[71] can be sources of organic and inorganic sulfates, respectively. Finally, it has been found that NO_x chemistry could alter the abundance of organic peroxides in laboratory SOA.[59,60] This might be a reason for the low abundance of HOM dimers in urban PM, because the HOMs always contain multiple peroxide functionalities.[17]

3.5. Oxidation State of HOMs. Both the O/C ratio and oxidation state of carbon ($\overline{OS_C}$) were used to describe the oxidation degree of HOMs,[31] where $\overline{OS_C} = -\sum_i OS_i \frac{n_i}{n_C}$, OS_i is the oxidation state associated with element i, and n_i/n_C is the molar ratio of element i to carbon. We found that Beijing HOM monomers (Figure 3a) had an O/C ratio of 0.89, which is lower than that for Amazon HOM monomers (0.95) but higher than that for Hyytiälä monomers (0.88). Such a trend is inconsistent

DOI: 10.1021/acs.est.9b05149
Environ. Sci. Technol. 2019, 53, 12506−12518

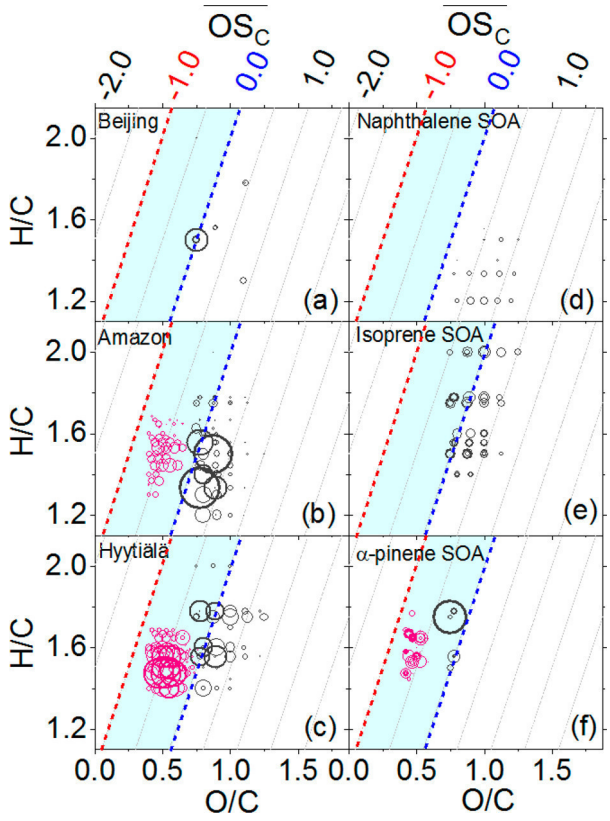

Figure 3. Van Krevelen and oxidation state diagrams for HOMs in fine PM from Beijing (a), Amazon (b), and Hyytiälä (c) as well as in SOA from oxidation of naphthalene (d), isoprene (e), and α-pinene (f). The red and blue dotted lines represent $\overline{OS_C}$ = −1.0 and 0.0, respectively. The cyan shaded areas represent oxidation states ranging from −1.0 to 0.0. Pink and dark gray data points represent HOM dimers and monomers, respectively. The size of the symbols reflects the relative peak intensities in the mass spectra. The scaling factor for Amazon and Hyytiälä monomers is 1, and for other data points it is 3. The results in (a)−(c) were based on selected fine PM samples collected in November 2017, June 2017, and March−October 2014, respectively.

with the RF values of HOMs and may not reflect the oxidation state of organic aerosols properly. Therefore, we plotted the O/C and H/C ratios of HOMs as well as $\overline{OS_C}$ for different values in Figure 3. To obtain $\overline{OS_C}$, we assumed the oxidation states of N and S to be +5 and +6 respectively. We found that the oxidation state of carbon in HOM monomers in fine PM from Beijing (−0.11, Figure 3a) is on average lower than that in the Amazon (−0.06, black circles in Figure 3b) and Hyytiälä (0.21, black circles in Figure 3c). This may be related to the stronger contribution of alkane derivatives from gasoline and lubrication oil vapors from anthropogenic emissions in Beijing.[72] Furthermore, Beijing fine PM contained amounts of HOM dimers below the detection limit (Figure 2c), whereas Amazon and Hyytiälä fine PM contained a large fraction of HOM dimers (pink circles in Figure 3b,c) exhibiting typical $\overline{OS_C}$ values between −1.0 (red dotted line) and 0.0 (blue dotted line), with average values of −0.64 and −0.59, respectively. Therefore, the oxidation states and RF values of HOMs (Figure 2c) in Beijing, Amazon, and Hyytiälä were observed in the same range, however with higher values for the cleaner sites.

To compare the oxidation state characteristics of HOMs in anthropogenic and biogenic SOA, Figure 3d−f shows the O/C and H/C ratios of laboratory-generated naphthalene, isoprene, and α-pinene SOA as well as the $\overline{OS_C}$ lines. We found that the HOM monomers in naphthalene SOA had a larger O/C ratio (1.06) in comparison to biogenic SOA (isoprene, 0.90; α-pinene, 0.78), and the $\overline{OS_C}$ of HOM monomers in naphthalene SOA (0.73) is also higher than in isoprene (0.14) and α-pinene SOA (−0.65), which is different from the lower $\overline{OS_C}$ values of HOM monomers in Beijing fine PM than in Amazon and Hyytiälä fine PM. This may be due to the different chemical aging processes of ambient fine PM from laboratory SOA: e.g., the absence of NO_x- and SO_2-related chemistry in our chamber experiments. Finally, ∼20%, ∼43%, and ∼62% of the HOMs in Beijing (Figure 3a), Amazon (Figure 3b), and Hyytiälä (Figure 3c) fine PM had an oxidation state between −1.0 and 0.0. Similarly, none, ∼19%, and ∼91% of the HOMs in naphthalene (Figure 3d), isoprene (Figure 3e), and α-pinene SOA (Figure 3f) had the same range of oxidation states, respectively. This consistency indicates that highly oxygenated but less oxidized HOMs should determine the oxidative potential of ambient fine PM and laboratory SOA.[16]

3.6. Yield and Formation Potential of Radicals by Ambient fine PM. To characterize the reactive species formation potential of ambient fine PM, we measured the radical yield and radical formation potential of fine PM from different sources in water. The results are shown in Figures 4 and 5 and Figure S4. Figure 4a displays the EPR spectra of BMPO-radical adducts formed in fine PM water extracts with BMPO.

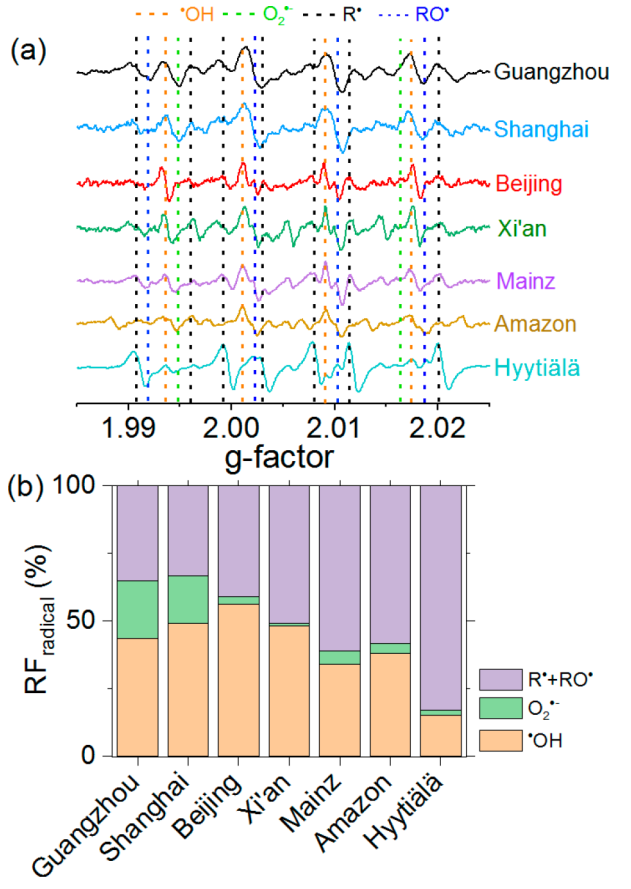

Figure 4. (a) EPR spectra and (b) relative fraction of radicals ($RF_{radical}$) formed by ambient fine particles. The yellow, green, black, and blue dashed lines in (a) indicate the peaks assigned to •OH, $O_2^{\bullet-}$, and C- and O-centered radicals, respectively.

DOI: 10.1021/acs.est.9b05149
Environ. Sci. Technol. 2019, 53, 12506−12518

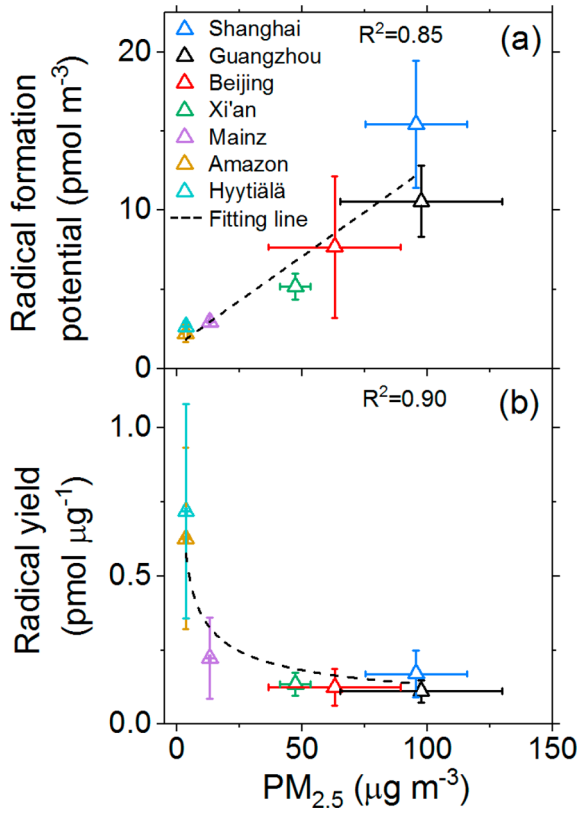

Figure 5. Correlation of air sample volume (a) and particle mass (b) normalized radical yields with $PM_{2.5}$ concentrations. The error bars represent the standard deviation of measurements with more than three individual samples.

The multiple peaks in the spectra indicate the formation of different radicals. Individual peaks were assigned to adducts of $^{\bullet}OH$, $O_2^{\bullet-}$, and C- and O-centered radicals, respectively. Figure 4b shows the relative fraction of formed radicals ($RF_{radical}$) and the amount of individual radicals quantified on the basis of spin-fitting and -counting techniques.[36] The fine PM from highly polluted megacities such as Shanghai, Guangzhou, and Beijing mainly generated $^{\bullet}OH$ and $O_2^{\bullet-}$ radicals, whereas the fine PM from less polluted urban and remote forest sites of Mainz, Amazon, and Hyytiälä dominantly yielded organic radicals. The higher yield of $^{\bullet}OH$ and $O_2^{\bullet-}$ by fine PM from highly polluted megacities may be related to the enhanced Fenton-like reactions associated with higher abundance of water-soluble transition metals.[73] The lower $^{\bullet}OH$ but higher organic radical yield of fine PM from the Amazon and Hyytiälä may be due to Fenton-like reactions initiated by transition metals and relatively stable organic hydroperoxides,[23,35,36] and also the interaction of $^{\bullet}OH$ with SOA material.[74]

Beyond the $RF_{radical}$ value, the radical yield from a given mass of particles or the formation potential in a given volume of air can also reflect radical formation of fine PM. Figure 5a shows that the sample volume normalized radical formation potential of ambient fine PM has a positive linear correlation with $PM_{2.5}$ concentration ($R^2 = 0.85$): $y = 1.47 + 0.11x$. Shanghai fine PM exhibited the highest formation potential of ~15 pmol m^{-3} radicals in ~96 $\mu g\ m^{-3}$ $PM_{2.5}$, whereas ~3.5 $\mu g\ m^{-3}$ Amazon $PM_{2.5}$ generated only ~3 pmol m^{-3} radicals. Thus, the radical formation potential of fine PM may become a metric reflecting the relative health risk of different concentrations of fine PM in air ranging from clean background to heavily polluted areas. As indicated in Figure 3, the oxidation state of HOMs in fine PM from remote forests (Amazon and Hyytiälä) and laboratory α-pinene SOA was mainly in the range of −1.0 to 1.0. Thus, we assume that radical formation by organic aerosols in water was mainly driven by highly oxygenated but less oxidized HOMs,[16] which had molecular formulas similar to those of low-volatility oxygenated organic aerosols.[16,75] Figure 5b shows the aerosol sample mass normalized total radical yield of ambient fine PM, which shows a negative power-law correlation with $PM_{2.5}$ concentrations ($R^2 = 0.90$): $y = x^{-0.43}$. Specifically, the Hyytiälä fine PM had the highest radical yield of ~0.7 pmol μg^{-1}, while the fine PM from Xi'an, Beijing, Guangzhou, and Shanghai generated only 0.1−0.2 pmol μg^{-1} radicals. The trend of higher radical yield from fine PM at remote forest sites in comparison to urban sites resembles the organic radical yields in Figure 4b and Figure S4 as well as the RF_{HOM} values in Figure 2, supporting the conclusion that HOMs represent an important source for radicals, especially organic radicals in water.

A previous study showed that, at −20 °C, the concentration of peroxides in α-pinene SOA decreased <20% in 1 week.[35] In this study, the laboratory SOA were collected immediately after their formation and analyzed within 4 h. Thus, the influence of aging effects on the relative HOM abundance and radical yield of laboratory SOA is negligible. Regarding the ambient PM samples, their RF_{HOM} values and radical yields were measured within a few days. Therefore, particle aging should not influence the relationship of RF_{HOM} and radical yield in Figure 6 significantly.

3.7. Association of RF_{HOM} with Radical Yield. As shown in Figure 6 and Figure S1b, both radical yields of ambient fine PM ($y = 0.071 + 0.015\ \exp(0.44x)$, $R^2 = 0.74$) and laboratory SOA ($y = 1.8 + 0.011\ \exp(0.52x)$, $R^2 = 0.92$) showed positive exponential correlations with the RF_{HOM} and chromatographic peak area fraction of HOMs, with the laboratory SOA showing a higher radical yield. This may reflect the different redox activities of HOMs in ambient fine PM and laboratory SOA. The larger deviations of radical yield and RF_{HOM} of Amazon and Hyytiälä fine PM than of urban fine PM may be due to the seasonal or year-to-year aerosol composition variations due to changing meteorological conditions.[43,64,76] In contrast to ambient fine PM, laboratory SOA had a much higher radical yield. Among laboratory SOA, β-pinene SOA had the highest RF_{HOM} value of ~11.5% and radical yield of ~5.9 pmol μg^{-1}, whereas naphthalene SOA had the lowest RF_{HOM} value of ~3.3% and radical yield of ~1.8 pmol μg^{-1}. Isoprene and α-pinene SOA exhibited similar RF_{HOM} values of ~10.4% and ~10.0% and radical yields of ~4.5 and ~3.4 pmol μg^{-1}, respectively. The higher radical yield of laboratory SOA may mainly be due to the higher relative fraction of CHO forms of HOMs in fresh laboratory SOA (Figure 3b). The consistent positive exponential correlations of RF_{HOM} and radical yield of ambient fine PM and laboratory SOA strongly indicate that HOMs are closely associated with the radical formation by PM in water.

To explore the influence of ionization mode during mass spectrometry analysis on the association of radical yield by PM with RF_{HOM}, we show the Spearman correlation coefficients (r) of radical yields (pmol μg^{-1}) with chemical groups analyzed in negative mode, positive mode, and their sum in Table S4. It can be seen that the radical yield has a close correlation with the RF value of total HOMs, HOM dimer, and LVOC type of HOMs identified in the different modes. Therefore, Tables S3 and S4 indicate that the RF_{HOM} value measured in negative mode resembles the distribution of total HOMs in fine PM.

DOI: 10.1021/acs.est.9b05149
Environ. Sci. Technol. 2019, 53, 12506−12518

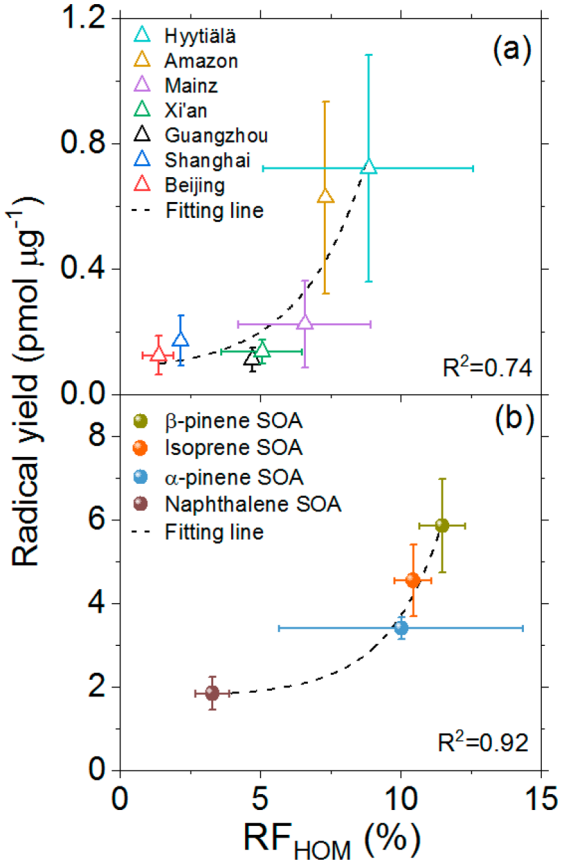

Figure 6. Correlation of particle mass normalized radical yield with relative ion number fraction of HOMs associated with ambient fine PM (a) and laboratory SOA (b). The error bars represent the standard deviation of measurement from replicates.

To explore the association of different types of HOMs with the radical yield, we calculated the Spearman correlation matrix[77] of total HOMs and individual chemical subgroups with the aerosol sample mass normalized radical yield (Figure 7 and Table S4; for the method see Supporting Information). As shown in Figure 7, blue colors and negative values indicate negative correlations, and red colors and positive values indicate positive correlations. When the Spearman r value is ≥ 0, a lighter color represents a weaker correlation and vice versa for a negative Spearman r value. The relative fraction of total HOMs showed one of the strongest correlations with the yield of total radicals (Spearman r = 0.92), confirming the important role of HOMs in generating radicals. Moreover, the CHO forms of HOMs showed a close positive correlation with the total radical yield (Spearman r = 0.91). In contrast, the CHON form of HOMs showed much weaker correlation with total radical yield (Spearman r = 0.13). Furthermore, both CHOS and CHONS forms of HOMs had negative correlations with the radical yield (Spearman r = −0.30 and −0.35). Therefore, the CHO forms of HOMs may play stronger roles in comparison to CHON, CHOS, and CHONS forms of HOMs in radical formation, and the atmospheric chemistry of nitrogen or sulfur should decrease the radical yield of organic aerosols in water. This can be explained by the decreased abundance of organic hydroperoxides upon formation of organic nitrates.[66,78,79] In addition to the CHO form of HOMs, the highly oxygenated SVOC and LVOC subgroups also showed close correlation with total radical yield (Spearman r = 0.56 and 0.95), which is in line with the lower RF value of ELVOCs in the CHO form of HOMs (Figure S3). Furthermore, the HOM dimers showed a closer correlation with the total radical yield of fine PM (Spearman r = 0.94), reflecting an important role of HOM dimers in generating radicals. This is consistent with previous findings of higher oxidation potential of oligomer-rich fractions of SOA from polycyclic aromatic hydrocarbons.[80] In contrast, the HOM monomers had weaker correlation with the radical yield (Spearman r = 0.23), indicating that HOM monomers may decompose and be lost more efficiently during particle aging. This hypothesis is supported by the finding of Krapf et al., which demonstrated that organic peroxides in α-pinene SOA are thermodynamically unstable with half-lives shorter than 1 h under dark conditions.[11] In addition, other studies also found that organic peroxides, including organic hydroperoxides, might be involved in the formation of organosulfates,[20] oligomers,[81] and radicals in water.[23,34−36] Therefore, organic peroxides may undergo heterogeneous chemical reactions during atmospheric aging processes. Given the presence of peroxide functional groups in HOMs, we speculate that the weak correlation of HOM monomers with the radical yield of fine PM from different sources may be due to aging processes of particle-phase HOMs. Furthermore, organic−metal interactions have shown synergistic effects in producing reactive oxygen species.[80,82] Thus, we suggest that the close correlation of RF_{HOM} with radical formation may also be related to redox chemistry involving metal ions. Finally, Table S4 and Figure S5 indicate that the radical yields of ambient fine PM and laboratory SOA have a weak negative correlation with the O/C ratio (Spearman r = −0.42) and oxidation state ($\overline{OS_C}$) (Spearman r = −0.3) of totally assigned compounds, supporting the conclusion of highly oxygenated but less oxidized HOMs as important radical precursors of fine PM in water.

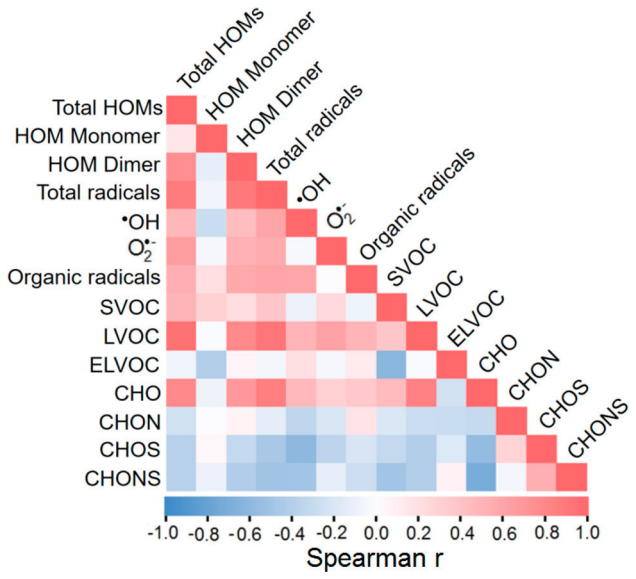

Figure 7. Spearman correlation matrix of HOM relative abundance and aerosol mass normalized radical yield.

In conclusion, we found that HOMs are closely associated with the radical formation by ambient fine PM and laboratory-generated SOA in water. The formed radicals may influence the formation and evolution of SOA through multigenerational chemical processes.[8,24,83−86] For example, aqueous-phase chemistry of HOMs has been suggested to be a major pathway

DOI: 10.1021/acs.est.9b05149
Environ. Sci. Technol. 2019, 53, 12506−12518

for the formation of organosulfates.[70,87] In addition, HOMs were suggested to contain at least one, and often multiple, hydroperoxide, peroxide, or peroxy acid groups.[24] These reactive functional groups may initiate redox chemistry, including Fenton-like reactions,[23,28,35,74,88−90] which may change the reactivity and role of fine PM during atmospheric processing. Beyond their climate effects, HOMs may exert adverse health effects due to the enrichment of organic peroxides and their ability to generate reactive species. For instance, exposure of lung epithelial cells to photochemically aged SOA showed increased toxic effects, which may be related to the elevated abundance of peroxides in aged SOA.[88] Thus, our findings may provide new insights in quantifying the contribution of specific components to the climate and health effects of fine PM from different sources.[91] Considering that HOMs widely exist in both biogenic and anthropogenic organic aerosols, the seasonality dependence and physicochemical properties of HOMs from different sources and their exact role in environmental and biological processes need to be investigated. Finally, during the ESI-MS measurement, ion suppression, ion enhancement, solvent interaction, adduct formation, etc. may influence the HOM detectability or the sensitivity of the method in distinguishing different type of HOMs, which warrants follow-up studies.

■ ASSOCIATED CONTENT

Supporting Information

The Supporting Information is available free of charge on the ACS Publications website at DOI: 10.1021/acs.est.9b05149.

Additional data as described in the text (PDF)

■ AUTHOR INFORMATION

Corresponding Authors

*H.T.: e-mail, h.tong@mpic.de; tel, +4961313057040.
*T.H.: e-mail, hoffmant@uni-mainz.de; tel, +4961313925716.
*M.K.: e-mail, markus.kalberer@unibas.ch; tel, +41612070701.

ORCID

Haijie Tong: 0000-0001-9887-7836
Fobang Liu: 0000-0002-9914-165X
Ricardo H. M. Godoi: 0000-0002-4774-4870
Ru-Jin Huang: 0000-0002-4907-9616
Thomas Berkemeier: 0000-0001-6390-6465
Pingqing Fu: 0000-0001-6249-2280
Maosheng Yao: 0000-0002-1442-8054
Christopher Pöhlker: 0000-0001-6958-425X
Meinrat O. Andreae: 0000-0003-1968-7925
Manabu Shiraiwa: 0000-0003-2532-5373
Ulrich Pöschl: 0000-0003-1412-3557

Present Address

†K.W.: Department of Chemistry, Aarhus University, Langelandsgade 140, DK-8000 Aarhus C, Denmark.

Notes

The authors declare no competing financial interest.

■ ACKNOWLEDGMENTS

This work was funded by the Max Planck Society, National Science Fund for Distinguished Young Scholars (41625014), Projects of International Cooperation and Exchanges NSFC (projects no. 41571130024 and 51576160), ACTRIS, ECAC, the Finnish Centre of Excellence under Academy of Finland (projects no. 307331 and 272041), German Federal Ministry of Education and Research (BMBF contracts 01LB1001A and 01LK1602B), Brazilian Ministério da Ciência, Tecnologia e Inovação (MCTI/FINEP contract 01.11.01248.00), China Scholarship Council, and Deutscher Akademischer Austauschdienst (DAAD). Technical staffs at the SMEARII station are acknowledged for logistical support during sample collection. For the operation of the ATTO site, we acknowledge support by the Amazon State University (UEA), FAPEAM, the Central Office of the Large Scale Biosphere Atmosphere Experiment in Amazonia (LBA), the National Institute of Amazonian Research (INPA), and SDS/CEUC/RDS-Uatumã. This paper contains results of research conducted under the Technical/Scientific Cooperation Agreement among the National Institute for Amazonian Research, the State University of Amazonas, and the Max-Planck-Gesellschaft eV; the opinions expressed are the entire responsibility of the authors and not of the participating institutions. For the operation of the T3 site, institutional support was provided by the Central Office of LBA, INPA, and UEA. We acknowledge support from the Atmospheric Radiation Measurement (ARM) Climate Research Facility, a user facility of the United States Department of Energy (DOE, DE-SC0006680), Office of Science, sponsored by the Office of Biological and Environmental Research. The research was conducted under scientific license 001030/2012-4 of the Brazilian National Council for Scientific and Technological Development (CNPq). M.S. acknowledges funding from the U.S. National Science Foundation (CHE-1808125). P.A. acknowledges funding from FAPESP project 2017/17047-0.

■ REFERENCES

(1) Hallquist, M.; Wenger, J.; Baltensperger, U.; Rudich, Y.; Simpson, D.; Claeys, M.; Dommen, J.; Donahue, N.; George, C.; Goldstein, A.; Hamilton, J. F.; Herrmann, H.; Hoffmann, T.; Iinuma, Y.; Jang, M.; Jenkin, M. E.; Jimenez, J. L.; Kiendler-Scharr, A.; Maenhaut, W.; McFiggans, G.; Mentel, T. F.; Monod, A.; Prévôt, A. S. H.; Seinfeld, J. H.; Surratt, J. D.; Szmigielski, R.; Wildt, J. The formation, properties and impact of secondary organic aerosol: current and emerging issues. *Atmos. Chem. Phys.* **2009**, *9* (14), 5155−5236.

(2) Shrivastava, M.; Cappa, C. D.; Fan, J.; Goldstein, A. H.; Guenther, A. B.; Jimenez, J. L.; Kuang, C.; Laskin, A.; Martin, S. T.; Ng, N. L.; Cappa, C. D.; Jimenez, J. L.; Seinfeld, J. H.; Volkamer, R.; Fan, J.; Smith, J. N.; Petaja, T.; Pierce, J. R.; Rasch, P. J.; Shilling, J.; Goldstein, A. H.; Kuang, C.; Laskin, A.; Thornton, J. A.; Wang, J.; Worsnop, D. R.; Zaveri, R. A.; Roldin, P.; Zelenyuk, A.; Zhang, Q. Recent advances in understanding secondary organic aerosol: Implications for global climate forcing. *Rev. Geophys.* **2017**, *55* (2), 509−559.

(3) West, J. J.; Cohen, A.; Dentener, F.; Brunekreef, B.; Zhu, T.; Armstrong, B.; Bell, M. L.; Brauer, M.; Carmichael, G.; Costa, D. L.; Dockery, D. W.; Kleeman, M.; Krzyzanowski, M.; Künzli, N.; Liousse, C.; Candice Lung, S.-C.; Martin, R. V.; Pöschl, U.; Pope, C. A.; Roberts, J. M.; Russell, A. G.; Wiedinmyer, C. What we breathe impacts our health: improving understanding of the link between air pollution and health. *Environ. Sci. Technol.* **2016**, *50*, 4895−4904.

(4) Shiraiwa, M.; Ueda, K.; Pozzer, A.; Lammel, G.; Kampf, C. J.; Fushimi, A.; Enami, S.; Arangio, A. M.; Fröhlich-Nowoisky, J.; Fujitani, Y.; Furuyama, A.; Furuyama, A.; Lakey, P. S. J.; Lelieveld, J.; Lucas, K.; Morino, Y.; Pöschl, U.; Takahama, S.; Takami, A.; Tong, H.; Weber, B.; Yoshino, A.; Sato, K. Aerosol health effects from molecular to global scales. *Environ. Sci. Technol.* **2017**, *51* (23), 13545−13567.

(5) Lelieveld, J.; Poschl, U. Chemists can help to solve the air-pollution health crisis. *Nature* **2017**, *551* (7680), 291−293.

(6) Lelieveld, J.; Klingmüller, K.; Pozzer, A.; Pöschl, U.; Fnais, M.; Daiber, A.; Münzel, T. Cardiovascular disease burden from ambient air pollution in Europe reassessed using novel hazard ratio functions. *Eur. Heart J.* **2019**, *40* (20), 1590−1596.

DOI: 10.1021/acs.est.9b05149
Environ. Sci. Technol. 2019, 53, 12506−12518

(7) Lelieveld, J.; Klingmüller, K.; Pozzer, A.; Burnett, R.; Haines, A.; Ramanathan, V. Effects of fossil fuel and total anthropogenic emission removal on public health and climate. *Proc. Natl. Acad. Sci. U. S. A.* **2019**, *116*, 7192−7197.
(8) Pöschl, U.; Shiraiwa, M. Multiphase chemistry at the atmosphere−biosphere interface influencing climate and public health in the anthropocene. *Chem. Rev.* **2015**, *115* (10), 4440−4475.
(9) Noziere, B.; Kalberer, M.; Claeys, M.; Allan, J.; D'Anna, B.; Decesari, S.; Finessi, E.; Glasius, M.; Grgic, I.; Hamilton, J. F.; Hoffmann, T.; Iinuma, Y.; Jaoui, M.; Kahnt, A.; Kampf, C. J.; Kourtchev, I.; Maenhaut, W.; Marsden, N.; Saarikoski, S.; Schnelle-Kreis, J. r.; Surratt, J. D.; Szidat, S. n.; Szmigielski, R.; Wisthaler, A. The molecular identification of organic compounds in the atmosphere: state of the art and challenges. *Chem. Rev.* **2015**, *115* (10), 3919−3983.
(10) Liu, P.; Li, Y. J.; Wang, Y.; Gilles, M. K.; Zaveri, R. A.; Bertram, A. K.; Martin, S. T. Lability of secondary organic particulate matter. *Proc. Natl. Acad. Sci. U. S. A.* **2016**, *113* (45), 12643−12648.
(11) Krapf, M.; El Haddad, I.; Bruns, E. A.; Molteni, U.; Daellenbach, K. R.; Prévôt, A. S.; Baltensperger, U.; Dommen, J. Labile peroxides in secondary organic aerosol. *Chem.* **2016**, *1* (4), 603−616.
(12) Tröstl, J.; Chuang, W. K.; Gordon, H.; Heinritzi, M.; Yan, C.; Molteni, U.; Ahlm, L.; Frege, C.; Bianchi, F.; Wagner, R.; Simon, M.; Lehtipalo, K.; Williamson, C.; Craven, J. S.; Duplissy, J.; Adamov, A.; Almeida, J.; Bernhammer, A.-K.; Breitenlechner, M.; Brilke, S.; Dias, A.; Ehrhart, S.; Flagan, R. C.; Franchin, A.; Fuchs, C.; Guida, R.; Gysel, M.; Hansel, A.; Hoyle, C. R.; Jokinen, T.; Junninen, H.; Kangasluoma, J.; Keskinen, H.; Kim, J.; Krapf, M.; Kürten, A.; Laaksonen, A.; Lawler, M.; Leiminger, M.; Mathot, S.; Möhler, O.; Nieminen, T.; Onnela, A.; Petäjä, T.; Piel, F. M.; Miettinen, P.; Rissanen, M. P.; Rondo, L.; Sarnela, N.; Schobesberger, S.; Sengupta, K.; Sipilä, M.; Smith, J. N.; Steiner, G.; Tomè, A.; Virtanen, A.; Wagner, A. C.; Weingartner, E.; Wimmer, D.; Winkler, P. M.; Ye, P.; Carslaw, K. S.; Curtius, J.; Dommen, J.; Kirkby, J.; Kulmala, M.; Riipinen, I.; Worsnop, D. R.; Donahue, N. M.; Baltensperger, U. The role of low-volatility organic compounds in initial particle growth in the atmosphere. *Nature* **2016**, *533* (7604), 527−531.
(13) Ehn, M.; Kleist, E.; Junninen, H.; Petäjä, T.; Lönn, G.; Schobesberger, S.; Maso, M. D.; Trimborn, A.; Kulmala, M.; Worsnop, D. R.; Wahner, A.; Wildt, J.; Mentel, T. F. Gas phase formation of extremely oxidized pinene reaction products in chamber and ambient air. *Atmos. Chem. Phys.* **2012**, *12* (11), 5113−5127.
(14) Bianchi, F.; Garmash, O.; He, X.; Yan, C.; Iyer, S.; Rosendahl, I.; Xu, Z.; Rissanen, M. P.; Riva, M.; Taipale, R.; Sarnela, N.; Petäjä, T.; Worsnop, D. R.; Kulmala, M.; Ehn, M.; Junninen, H. The role of highly oxygenated molecules (HOMs) in determining the composition of ambient ions in the boreal forest. *Atmos. Chem. Phys.* **2017**, *17* (22), 13819−13831.
(15) Wang, Z.; Popolan-Vaida, D. M.; Chen, B.; Moshammer, K.; Mohamed, S. Y.; Wang, H.; Sioud, S.; Raji, M. A.; Kohse-Höinghaus, K.; Hansen, N.; Dagaut, P.; Leone, S. R.; Sarathy, S. M. Unraveling the structure and chemical mechanisms of highly oxygenated intermediates in oxidation of organic compounds. *Proc. Natl. Acad. Sci. U. S. A.* **2017**, *114* (50), 13102−13107.
(16) Tu, P.; Hall, W. A., IV; Johnston, M. V. Characterization of highly oxidized molecules in fresh and aged biogenic secondary organic aerosol. *Anal. Chem.* **2016**, *88* (8), 4495−4501.
(17) Zhang, X.; Lambe, A. T.; Upshur, M. A.; Brooks, W. A.; Gray Bé, A.; Thomson, R. J.; Geiger, F. M.; Surratt, J. D.; Zhang, Z.; Gold, A.; Graf, S.; Cubison, M. J.; Groessl, M.; Jayne, J. T.; Worsnop, D. R.; Canagaratna, M. R. Highly oxygenated multifunctional compounds in α-pinene secondary organic aerosol. *Environ. Sci. Technol.* **2017**, *51* (11), 5932−5940.
(18) Lee, B. H.; Lopez-Hilfiker, F. D.; D'Ambro, E. L.; Zhou, P.; Boy, M.; Petäjä, T.; Hao, L.; Virtanen, A.; Thornton, J. A. Semi-volatile and highly oxygenated gaseous and particulate organic compounds observed above a boreal forest canopy. *Atmos. Chem. Phys.* **2018**, *18* (15), 11547−11562.
(19) Molteni, U.; Bianchi, F.; Klein, F.; Haddad, I. E.; Frege, C.; Rossi, M. J.; Dommen, J.; Baltensperger, U. Formation of highly oxygenated organic molecules from aromatic compounds. *Atmos. Chem. Phys.* **2018**, *18* (3), 1909−1921.
(20) Mutzel, A.; Poulain, L.; Berndt, T.; Iinuma, Y.; Rodigast, M.; Böge, O.; Richters, S.; Spindler, G.; Sipilä, M.; Jokinen, T.; Kulmala, M.; Herrmann, H. Highly oxidized multifunctional organic compounds observed in tropospheric particles: A field and laboratory study. *Environ. Sci. Technol.* **2015**, *49* (13), 7754−7761.
(21) Zhang, X.; McVay, R. C.; Huang, D. D.; Dalleska, N. F.; Aumont, B.; Flagan, R. C.; Seinfeld, J. H. Formation and evolution of molecular products in α-pinene secondary organic aerosol. *Proc. Natl. Acad. Sci. U. S. A.* **2015**, *112* (46), 14168−14173.
(22) Kirkby, J.; Duplissy, J.; Sengupta, K.; Frege, C.; Gordon, H.; Williamson, C.; Heinritzi, M.; Simon, M.; Yan, C.; Almeida, J.; Tröstl, J.; Nieminen, T.; Ortega, I. K.; Wagner, R.; Adamov, A.; Amorim, A.; Bernhammer, A.-K.; Bianchi, F.; Breitenlechner, M.; Brilke, S.; Chen, X.; Craven, J.; Dias, A.; Ehrhart, S.; Flagan, R. C.; Franchin, A.; Fuchs, C.; Guida, R.; Hakala, J.; Hoyle, C. R.; Jokinen, T.; Junninen, H.; Kangasluoma, J.; Kim, J.; Krapf, M.; Kürten, A.; Laaksonen, A.; Lehtipalo, K.; Makhmutov, V.; Mathot, S.; Molteni, U.; Onnela, A.; Peräkylä, O.; Piel, F.; Petäjä, T.; Praplan, A. P.; Pringle, K.; Rap, A.; Richards, N. A. D.; Riipinen, I.; Rissanen, M. P.; Rondo, L.; Sarnela, N.; Schobesberger, S.; Scott, C. E.; Seinfeld, J. H.; Sipilä, M.; Steiner, G.; Stozhkov, Y.; Stratmann, F.; Tomé, A.; Virtanen, A.; Vogel, A. L.; Wagner, A. C.; Wagner, P. E.; Weingartner, E.; Wimmer, D.; Winkler, P. M.; Ye, P.; Zhang, X.; Hansel, A.; Dommen, J.; Donahue, N. M.; Worsnop, D. R.; Baltensperger, U.; Kulmala, M.; Carslaw, K. S.; Curtius, J. Ion-induced nucleation of pure biogenic particles. *Nature* **2016**, *533*, 521−526.
(23) Tong, H.; Arangio, A. M.; Lakey, P. S.; Berkemeier, T.; Liu, F.; Kampf, C. J.; Brune, W. H.; Pöschl, U.; Shiraiwa, M. Hydroxyl radicals from secondary organic aerosol decomposition in water. *Atmos. Chem. Phys.* **2016**, *16* (3), 1761−1771.
(24) Bianchi, F.; Kurtén, T.; Riva, M.; Mohr, C.; Rissanen, M. P.; Roldin, P.; Berndt, T.; Crounse, J. D.; Wennberg, P. O.; Mentel, T. F.; Wildt, J.; Junninen, H.; Jokinen, T.; Kulmala, M.; Worsnop, D. R.; Thornton, J. A.; Donahue, N.; Kjaergaard, H. G.; Ehn, M. Highly Oxygenated Organic Molecules (HOM) from Gas-Phase Autoxidation Involving Peroxy Radicals: A Key Contributor to Atmospheric Aerosol. *Chem. Rev.* **2019**, *119*, 3472−3509.
(25) Crounse, J. D.; Nielsen, L. B.; Jørgensen, S.; Kjaergaard, H. G.; Wennberg, P. O. Autoxidation of organic compounds in the atmosphere. *J. Phys. Chem. Lett.* **2013**, *4* (20), 3513−3520.
(26) McGillen, M. R.; Curchod, B. F.; Chhantyal-Pun, R.; Beames, J. M.; Watson, N.; Khan, M. A. H.; McMahon, L.; Shallcross, D. E.; Orr-Ewing, A. J. Criegee Intermediate−Alcohol Reactions, A Potential Source of Functionalized Hydroperoxides in the Atmosphere. *ACS Earth Space Chem.* **2017**, *1* (10), 664−672.
(27) Praske, E.; Otkjær, R. V.; Crounse, J. D.; Hethcox, J. C.; Stoltz, B. M.; Kjaergaard, H. G.; Wennberg, P. O. Atmospheric autoxidation is increasingly important in urban and suburban North America. *Proc. Natl. Acad. Sci. U. S. A.* **2018**, *115* (1), 64−69.
(28) Riva, M. Multiphase chemistry of highly oxidized molecules: the case of organic hydroperoxides. *Chem.* **2016**, *1* (4), 526−528.
(29) Epstein, S. A.; Blair, S. L.; Nizkorodov, S. A. Direct photolysis of α-pinene ozonolysis secondary organic aerosol: effect on particle mass and peroxide content. *Environ. Sci. Technol.* **2014**, *48* (19), 11251−11258.
(30) Pagonis, D.; Ziemann, P. J. Chemistry of hydroperoxycarbonyls in secondary organic aerosol. *Aerosol Sci. Technol.* **2018**, *52* (10), 1178−1193.
(31) Kroll, J. H.; Donahue, N. M.; Jimenez, J. L.; Kessler, S. H.; Canagaratna, M. R.; Wilson, K. R.; Altieri, K. E.; Mazzoleni, L. R.; Wozniak, A. S.; Bluhm, H.; Mysak, E. R.; Smith, J. D.; Kolb, C. E.; Worsnop, D. R. Carbon oxidation state as a metric for describing the chemistry of atmospheric organic aerosol. *Nat. Chem.* **2011**, *3* (2), 133−139.
(32) Ehn, M.; Thornton, J. A.; Kleist, E.; Sipilä, M.; Junninen, H.; Pullinen, I.; Springer, M.; Rubach, F.; Tillmann, R.; Lee, B.; Lopez-Hilfiker, F.; Andres, S.; Acir, I.-H.; Rissanen, M.; Jokinen, T.;

DOI: 10.1021/acs.est.9b05149
Environ. Sci. Technol. 2019, 53, 12506−12518

Schobesberger, S.; Kangasluoma, J.; Kontkanen, J.; Nieminen, T.; Kurtén, T.; Nielsen, L. B.; Jørgensen, S.; Kjaergaard, H. G.; Canagaratna, M. R.; Maso, M. D.; Berndt, T.; Petäjä, T.; Wahner, A.; Kerminen, V.-M.; Kulmala, M.; Worsnop, D. R.; Wildt, J.; Mentel, T. F. A large source of low-volatility secondary organic aerosol. *Nature* **2014**, *506* (7489), 476−479.

(33) Docherty, K. S.; Wu, W.; Lim, Y. B.; Ziemann, P. J. Contributions of organic peroxides to secondary aerosol formed from reactions of monoterpenes with O3. *Environ. Sci. Technol.* **2005**, *39* (11), 4049−4059.

(34) Tong, H.; Lakey, P. S.; Arangio, A. M.; Socorro, J.; Kampf, C. J.; Berkemeier, T.; Brune, W. H.; Pöschl, U.; Shiraiwa, M. Reactive oxygen species formed in aqueous mixtures of secondary organic aerosols and mineral dust influencing cloud chemistry and public health in the Anthropocene. *Faraday Discuss.* **2017**, *200*, 251−270.

(35) Badali, K.; Zhou, S.; Aljawhary, D.; Antiñolo, M.; Chen, W.; Lok, A.; Mungall, E.; Wong, J.; Zhao, R.; Abbatt, J. Formation of hydroxyl radicals from photolysis of secondary organic aerosol material. *Atmos. Chem. Phys.* **2015**, *15* (14), 7831−7840.

(36) Tong, H.; Lakey, P. S.; Arangio, A. M.; Socorro, J.; Shen, F.; Lucas, K.; Brune, W. H.; Pöschl, U.; Shiraiwa, M. Reactive Oxygen Species Formed by Secondary Organic Aerosols in Water and Surrogate Lung Fluid. *Environ. Sci. Technol.* **2018**, *52* (20), 11642−11651.

(37) Zhao, R.; Aljawhary, D.; Lee, A. K.; Abbatt, J. P. Rapid aqueous-phase photooxidation of dimers in the α-pinene secondary organic aerosol. *Environ. Sci. Technol. Lett.* **2017**, *4* (6), 205−210.

(38) Gligorovski, S.; Strekowski, R.; Barbati, S.; Vione, D. Environmental implications of hydroxyl radicals ($^{\bullet}$OH). *Chem. Rev.* **2015**, *115* (24), 13051−13092.

(39) Anglada, J. M.; Martins-Costa, M.; Francisco, J. S.; Ruiz-Lopez, M. F. Interconnection of reactive oxygen species chemistry across the interfaces of atmospheric, environmental, and biological processes. *Acc. Chem. Res.* **2015**, *48* (3), 575−583.

(40) Müller, L.; Reinnig, M.-C.; Warnke, J.; Hoffmann, T. Unambiguous identification of esters as oligomers in secondary organic aerosol formed from cyclohexene and cyclohexene/α-pinene ozonolysis. *Atmos. Chem. Phys.* **2008**, *8* (5), 1423−1433.

(41) Kristensen, K.; Watne, Å. K.; Hammes, J.; Lutz, A.; Petäjä, T.; Hallquist, M.; Bilde, M.; Glasius, M. High-molecular weight dimer esters are major products in aerosols from α-pinene ozonolysis and the boreal forest. *Environ. Sci. Technol. Lett.* **2016**, *3* (8), 280−285.

(42) Kahnt, A.; Vermeylen, R.; Iinuma, Y.; Safi Shalamzari, M.; Maenhaut, W.; Claeys, M. High-molecular-weight esters in α-pinene ozonolysis secondary organic aerosol: structural characterization and mechanistic proposal for their formation from highly oxygenated molecules. *Atmos. Chem. Phys.* **2018**, *18* (11), 8453−8467.

(43) Kourtchev, I.; Godoi, R. H.; Connors, S.; Levine, J. G.; Archibald, A. T.; Godoi, A. F.; Paralovo, S. L.; Barbosa, C. G.; Souza, R. A.; Manzi, A. O.; Seco, R.; Sjostedt, S.; Park, J.-H.; Guenther, A.; Kim, S.; Smith, J.; Martin, S. T.; Kalberer, M. Molecular composition of organic aerosols in central Amazonia: an ultra-high-resolution mass spectrometry study. *Atmos. Chem. Phys.* **2016**, *16* (18), 11899−11913.

(44) Zielinski, A. T.; Kourtchev, I.; Bortolini, C.; Fuller, S. J.; Giorio, C.; Popoola, O. A.; Bogialli, S.; Tapparo, A.; Jones, R. L.; Kalberer, M. A new processing scheme for ultra-high resolution direct infusion mass spectrometry data. *Atmos. Environ.* **2018**, *178*, 129−139.

(45) Martin, S.; Artaxo, P.; Machado, L.; Manzi, A.; Souza, R.; Schumacher, C.; Wang, J.; Andreae, M.; Barbosa, H.; Fan, J.; Fisch, G.; Goldstein, A. H.; Guenther, A.; Jimenez, J. L.; Pöschl, U.; Silva Dias, M. A.; Smith, J. N.; Wendisch, M. Introduction: observations and modeling of the Green Ocean Amazon (GoAmazon2014/5). *Atmos. Chem. Phys.* **2016**, *16* (8), 4785−4797.

(46) Andreae, M.; Acevedo, O.; Araùjo, A.; Artaxo, P.; Barbosa, C.; Barbosa, H.; Brito, J.; Carbone, S.; Chi, X.; Cintra, B. B. L.; da Silva, N. F.; Dias, N. L.; Dias-Júnior, F.; Ditas, C. Q.; Ditz, R.; Godoi, A. F. L.; Godoi, R. H. M.; Heimann, M.; Hoffmann, T.; Kesselmeier, J.; Könemann, T.; Krüger, M. L.; Lavric, J. V.; Manzi, A. O.; Lopes, A. P.; Martins, D. L.; Mikhailov, E. F.; Moran-Zuloaga, D.; Nelson, B. W.; Nölscher, A. C.; Santos Nogueira, D.; Piedade, M. T. F.; Pöhlker, C.; Pöschl, U.; Quesada, C. A.; Rizzo, L. V.; Ro, C.-U.; Ruckteschler, N.; Sá, L. D. A.; de Oliveira Sá, M.; Sales, C. B.; dos Santos, R. M. N.; Saturno, J.; Schöngart, J.; Sörgel, M.; Souza, C. M. d.; de Souza, R. A. F.; Su, H.; Targhetta, N.; Tóta, J.; Trebs, I.; Trumbore, S.; van Eijck, A.; Walter, D.; Wang, Z.; Weber, B.; Williams, J.; Winderlich, J.; Wittmann, F.; Wolff, S.; Yáñez-Serrano, A. M. The Amazon Tall Tower Observatory (ATTO): overview of pilot measurements on ecosystem ecology, meteorology, trace gases, and aerosols. *Atmos. Chem. Phys.* **2015**, *15* (18), 10723−10776.

(47) Andreae, M. O.; Afchine, A.; Albrecht, R.; Holanda, B. A.; Artaxo, P.; Barbosa, H. M.; Borrmann, S.; Cecchini, M. A.; Costa, A.; Dollner, M.; Fütterer, D.; Järvinen, E.; Jurkat, T.; Klimach, T.; Konemann, T.; Knote, C.; Krämer, M.; Krisna, T.; Machado, L. A. T.; Mertes, S.; Minikin, A.; Pöhlker, C.; Pöhlker, M. L.; Pöschl, U.; Rosenfeld, D.; Sauer, D.; Schlager, H.; Schnaiter, M.; Schneider, J.; Schulz, C.; Spanu, A.; Sperling, V. B.; Voigt, C.; Walser, A.; Wang, J.; Weinzierl, B.; Wendisch, M.; Ziereis, H. Aerosol characteristics and particle production in the upper troposphere over the Amazon Basin. *Atmos. Chem. Phys.* **2018**, *18* (2), 921−961.

(48) Hari, P.; Kulmala, M. Station for measuring ecosystem-atmosphere relations: SMEAR. *Boreal Environ. Res.* **2005**, *10*, 315−322.

(49) Wang, K.; Zhang, Y.; Huang, R.-J.; Cao, J.; Hoffmann, T. UHPLC-Orbitrap mass spectrometric characterization of organic aerosol from a central European city (Mainz, Germany) and a Chinese megacity (Beijing). *Atmos. Environ.* **2018**, *189*, 22−29.

(50) Arangio, A. M.; Tong, H.; Socorro, J.; Pöschl, U.; Shiraiwa, M. Quantification of environmentally persistent free radicals and reactive oxygen species in atmospheric aerosol particles. *Atmos. Chem. Phys.* **2016**, *16* (20), 13105−13119.

(51) Huang, G.; Liu, Y.; Shao, M.; Li, Y.; Chen, Q.; Zheng, Y.; Wu, Z.; Liu, Y.; Wu, Y.; Hu, M.; Li, X.; Lu, S.; Wang, C.; Liu, J.; Zheng, M.; Zhu, T. Potentially Important Contribution of Gas-Phase Oxidation of Naphthalene and Methylnaphthalene to Secondary Organic Aerosol during Haze Events in Beijing. *Environ. Sci. Technol.* **2019**, *53* (3), 1235−1244.

(52) Liu, Y.; Brito, J.; Dorris, M. R.; Rivera-Rios, J. C.; Seco, R.; Bates, K. H.; Artaxo, P.; Duvoisin, S.; Keutsch, F. N.; Kim, S.; Goldstein, A. H.; Guenther, A. B.; Manzi, A. O.; Souza, R. A. F.; Springston, S. R.; Watson, T. B.; McKinney, K. A.; Martin, S. T. Isoprene photochemistry over the Amazon rainforest. *Proc. Natl. Acad. Sci. U. S. A.* **2016**, *113* (22), 6125−6130.

(53) Hakola, H.; Hellén, H.; Hemmilä, M.; Rinne, J.; Kulmala, M. In situ measurements of volatile organic compounds in a boreal forest. *Atmos. Chem. Phys.* **2012**, *12* (23), 11665−11678.

(54) Gallimore, P. J.; Mahon, B. M.; Wragg, F. P.; Fuller, S. J.; Giorio, C.; Kourtchev, I.; Kalberer, M. Multiphase composition changes and reactive oxygen species formation during limonene oxidation in the new Cambridge Atmospheric Simulation Chamber (CASC). *Atmos. Chem. Phys.* **2017**, *17* (16), 9853−9868.

(55) Zhao, H.; Joseph, J.; Zhang, H.; Karoui, H.; Kalyanaraman, B. Synthesis and biochemical applications of a solid cyclic nitrone spin trap: a relatively superior trap for detecting superoxide anions and glutathiyl radicals. *Free Radical Biol. Med.* **2001**, *31* (5), 599−606.

(56) Weber, R. T. *Xenon Data Processing Reference*; Bruker Instruments: Billerica, MA, 2012.

(57) Jokinen, T.; Berndt, T.; Makkonen, R.; Kerminen, V.-M.; Junninen, H.; Paasonen, P.; Stratmann, F.; Herrmann, H.; Guenther, A. B.; Worsnop, D. R.; Kulmala, M.; Ehn, M.; Sipilä, M. Production of extremely low volatile organic compounds from biogenic emissions: Measured yields and atmospheric implications. *Proc. Natl. Acad. Sci. U. S. A.* **2015**, *112* (23), 7123−7128.

(58) Gatzsche, K.; Iinuma, Y.; Tilgner, A.; Mutzel, A.; Berndt, T.; Wolke, R. Kinetic modeling studies of SOA formation from α-pinene ozonolysis. *Atmos. Chem. Phys.* **2017**, *17* (21), 13187−13211.

(59) Surratt, J. D.; Murphy, S. M.; Kroll, J. H.; Ng, N. L.; Hildebrandt, L.; Sorooshian, A.; Szmigielski, R.; Vermeylen, R.; Maenhaut, W.; Claeys, M.; Flagan, R. C.; Seinfeld, J. H. Chemical composition of secondary organic aerosol formed from the photooxidation of isoprene. *J. Phys. Chem. A* **2006**, *110* (31), 9665−9690.

DOI: 10.1021/acs.est.9b05149
Environ. Sci. Technol. 2019, 53, 12506−12518

(60) Kautzman, K.; Surratt, J.; Chan, M.; Chan, A.; Hersey, S.; Chhabra, P.; Dalleska, N.; Wennberg, P.; Flagan, R.; Seinfeld, J. Chemical composition of gas-and aerosol-phase products from the photooxidation of naphthalene. *J. Phys. Chem. A* **2010**, *114* (2), 913−934.
(61) Schulz, C.; Schneider, J.; Holanda, B. A.; Appel, O.; Costa, A.; de Sá, S. S.; Dreiling, V.; Fütterer, D.; Jurkat-Witschas, T.; Klimach, T.; Knote, C.; Krämer, M.; Martin, S. T.; Mertes, S.; Pöhlker, M. L.; Sauer, D.; Voigt, C.; Walser, A.; Weinzierl, B.; Ziereis, H.; Zöger, M.; Andreae, M. O.; Artaxo, P.; Machado, L. A. T.; Pöschl, U.; Wendisch, M.; Borrmann, S. Aircraft-based observations of isoprene-epoxydiol-derived secondary organic aerosol (IEPOX-SOA) in the tropical upper troposphere over the Amazon region. *Atmos. Chem. Phys.* **2018**, *18* (20), 14979−15001.
(62) Surratt, J. D.; Gómez-González, Y.; Chan, A. W.; Vermeylen, R.; Shahgholi, M.; Kleindienst, T. E.; Edney, E. O.; Offenberg, J. H.; Lewandowski, M.; Jaoui, M.; Maenhaut, W.; Claeys, M.; Flagan, R. C.; Seinfeld, J. H. Organosulfate formation in biogenic secondary organic aerosol. *J. Phys. Chem. A* **2008**, *112* (36), 8345−8378.
(63) Glasius, M.; Bering, M. S.; Yee, L. D.; de Sá, S. S.; Isaacman-VanWertz, G.; Wernis, R. A.; Barbosa, H. M.; Alexander, M. L.; Palm, B. B.; Hu, W.; Campuzano-Jost, P.; Day, D. A.; Jimenez, J. L.; Shrivastava, M.; Martin, S. T.; Goldstein, A. H. Organosulfates in aerosols downwind of an urban region in central Amazon. *Environ. Sci.: Processes Impacts* **2018**, *20* (11), 1546−1558.
(64) Kourtchev, I.; Fuller, S.; Aalto, J.; Ruuskanen, T. M.; McLeod, M. W.; Maenhaut, W.; Jones, R.; Kulmala, M.; Kalberer, M. Molecular composition of boreal forest aerosol from Hyytiala, Finland, using ultrahigh resolution mass spectrometry. *Environ. Sci. Technol.* **2013**, *47* (9), 4069−4079.
(65) Rollins, A. W.; Browne, E. C.; Min, K.-E.; Pusede, S. E.; Wooldridge, P. J.; Gentner, D. R.; Goldstein, A. H.; Liu, S.; Day, D. A.; Russell, L. M.; Cohen, R. C. Evidence for NOx control over nighttime SOA formation. *Science* **2012**, *337* (6099), 1210−1212.
(66) Berkemeier, T.; Ammann, M.; Mentel, T. F.; Pöschl, U.; Shiraiwa, M. Organic nitrate contribution to new particle formation and growth in secondary organic aerosols from α-pinene ozonolysis. *Environ. Sci. Technol.* **2016**, *50* (12), 6334−6342.
(67) Tao, S.; Lu, X.; Levac, N.; Bateman, A. P.; Nguyen, T. B.; Bones, D. L.; Nizkorodov, S. A.; Laskin, J.; Laskin, A.; Yang, X. Molecular characterization of organosulfates in organic aerosols from Shanghai and Los Angeles urban areas by nanospray-desorption electrospray ionization high-resolution mass spectrometry. *Environ. Sci. Technol.* **2014**, *48* (18), 10993−11001.
(68) Wang, X.; Hayeck, N.; Brüggemann, M.; Yao, L.; Chen, H.; Zhang, C.; Emmelin, C.; Chen, J.; George, C.; Wang, L. Chemical Characteristics of Organic Aerosols in Shanghai: A Study by Ultrahigh-Performance Liquid Chromatography Coupled With Orbitrap Mass Spectrometry. *J. Geophys. Res.* **2017**, *122*, 11703−11722.
(69) Li, Y.; Pöschl, U.; Shiraiwa, M. Molecular corridors and parameterizations of volatility in the chemical evolution of organic aerosols. *Atmos. Chem. Phys.* **2016**, *16* (5), 3327−3344.
(70) Hunt, S. W.; Laskin, A.; Nizkorodov, S. A. *Multiphase Environmental Chemistry in the Atmosphere*; American Chemical Society: Washington, DC, 2018; ACS Symposium Series.
(71) Cheng, Y.; Zheng, G.; Wei, C.; Mu, Q.; Zheng, B.; Wang, Z.; Gao, M.; Zhang, Q.; He, K.; Carmichael, G.; Pöschl, U.; Su, H. Reactive nitrogen chemistry in aerosol water as a source of sulfate during haze events in China. *Sci. Adv.* **2016**, *2* (12), No. e1601530.
(72) Tang, R.; Wu, Z.; Li, X.; Wang, Y.; Shang, D.; Xiao, Y.; Li, M.; Zeng, L.; Wu, Z.; Hallquist, M.; Hu, M.; Guo, S. Primary and secondary organic aerosols in summer 2016 in Beijing. *Atmos. Chem. Phys.* **2018**, *18* (6), 4055−4068.
(73) Lakey, P. S.; Berkemeier, T.; Tong, H.; Arangio, A. M.; Lucas, K.; Pöschl, U.; Shiraiwa, M. Chemical exposure-response relationship between air pollutants and reactive oxygen species in the human respiratory tract. *Sci. Rep.* **2016**, *6*, 32916.
(74) Hems, R. F.; Hsieh, J. S.; Slodki, M. A.; Zhou, S.; Abbatt, J. P. Suppression of OH generation from the Photo-Fenton reaction in the presence of α-Pinene secondary organic aerosol material. *Environ. Sci. Technol. Lett.* **2017**, *4* (10), 439−443.
(75) Jimenez, J. L.; Canagaratna, M.; Donahue, N.; Prevot, A.; Zhang, Q.; Kroll, J. H.; DeCarlo, P. F.; Allan, J. D.; Coe, H.; Ng, N. L.; Aiken, A. C.; Docherty, K. S.; Ulbrich, I. M.; Grieshop, A. P.; Robinson, A. L.; Duplissy, J.; Smith, J. D.; Wilson, K. R.; Lanz, V. A.; Hueglin, C.; Sun, Y. L.; Tian, J.; Laaksonen, A.; Raatikainen, T.; Rautiainen, J.; Vaattovaara, P.; Ehn, M.; Kulmala, M.; Tomlinson, J. M.; Collins, D. R.; Cubison, M. J.; Dunlea, E. J.; Huffman, J. A.; Onasch, T. B.; Alfarra, M. R.; Williams, P. I.; Bower, K.; Kondo, Y.; Drewnick, F.; Borrmann, S.; Weimer, S.; Demerjian, K.; Salcedo, D.; Cottrell, L.; Griffin, R.; Takami, A.; Miyoshi, T.; Hatakeyama, S.; Shimono, A.; Sun, J. Y.; Zhang, Y. M.; Dzepina, K.; Kimmel, J. R.; Sueper, D.; Jayne, J. T.; Herndon, S. C.; Trimborn, A. M.; Williams, L. R.; Wood, E. C.; Middlebrook, A. M.; Kolb, C. E.; Baltensperger, U.; Worsnop, D. R. Evolution of organic aerosols in the atmosphere. *Science* **2009**, *326* (5959), 1525−1529.
(76) Kourtchev, I.; Giorio, C.; Manninen, A.; Wilson, E.; Mahon, B.; Aalto, J.; Kajos, M.; Venables, D.; Ruuskanen, T.; Levula, J.; Loponen, M.; Connors, S.; Harris, N.; Zhao, D.; Kiendler-Scharr, A.; Mentel, T. F.; Rudich, Y.; Hallquist, M.; Doussin, J.-F.; Maenhaut, W.; Bäck, J.; Petäjä, T.; Wenger, J. C.; Kulmala, M.; Kalberer, M. Enhanced Volatile Organic Compounds emissions and organic aerosol mass increase the oligomer content of atmospheric aerosols. *Sci. Rep.* **2016**, *6*, 35038.
(77) Brehmer, C.; Lai, A. M.; Clark, S.; Shan, M.; Ni, K.; Ezzati, M.; Yang, X.; Baumgartner, J.; Schauer, J. J.; Carter, E. The Oxidative Potential of Personal and Household PM2. 5 in a Rural Setting in Southwestern China. *Environ. Sci. Technol.* **2019**, *53*, 2788−2798.
(78) Lee, B. H.; Mohr, C.; Lopez-Hilfiker, F. D.; Lutz, A.; Hallquist, M.; Lee, L.; Romer, P.; Cohen, R. C.; Iyer, S.; Kurten, T.; Hu, W.; Day, D. A.; Campuzano-Jost, P.; Jimenez, J. L.; Xu, L.; Ng, N. L.; Guo, H.; Weber, R. J.; Wild, R. J.; Brown, S. S.; Koss, A.; de Gouw, J.; Olson, K.; Goldstein, A. H.; Seco, R.; Kim, S.; McAvey, K.; Shepson, P. B.; Starn, T.; Baumann, K.; Edgerton, E. S.; Liu, J.; Shilling, J. E.; Miller, D. O.; Brune, W.; Schobesberger, S.; D'Ambro, E. L.; Thornton, J. A. Highly functionalized organic nitrates in the southeast United States: Contribution to secondary organic aerosol and reactive nitrogen budgets. *Proc. Natl. Acad. Sci. U. S. A.* **2016**, *113* (6), 1516−1521.
(79) Ng, N. L.; Brown, S. S.; Archibald, A. T.; Atlas, E.; Cohen, R. C.; Crowley, J. N.; Day, D. A.; Donahue, N. M.; Fry, J. L.; Fuchs, H.; Griffin, R. J.; Guzman, M. I.; Herrmann, H.; Hodzic, A.; Iinuma, Y.; Jimenez, J. L.; Kiendler-Scharr, A.; Lee, B. H.; Luecken, D. J.; Mao, J.; McLaren, R.; Mutzel, A.; Osthoff, H. D.; Ouyang, B.; Picquet-Varrault, B.; Platt, U.; Pye, H. O. T.; Rudich, Y.; Schwantes, R. H.; Shiraiwa, M.; Stutz, J.; Thornton, J. A.; Tilgner, A.; Williams, B. J.; Zaveri, R. A. Nitrate radicals and biogenic volatile organic compounds: oxidation, mechanisms, and organic aerosol. *Atmos. Chem. Phys.* **2017**, *17* (3), 2103−2162.
(80) Wang, S.; Ye, J.; Soong, R.; Wu, B.; Yu, L.; Simpson, A. J.; Chan, A. W. Relationship between chemical composition and oxidative potential of secondary organic aerosol from polycyclic aromatic hydrocarbons. *Atmos. Chem. Phys.* **2018**, *18* (6), 3987−4003.
(81) Riva, M.; Budisulistiorini, S. H.; Chen, Y.; Zhang, Z.; D'Ambro, E. L.; Zhang, X.; Gold, A.; Turpin, B. J.; Thornton, J. A.; Canagaratna, M. R.; Surratt, J. D. Chemical characterization of secondary organic aerosol from oxidation of isoprene hydroxyhydroperoxides. *Environ. Sci. Technol.* **2016**, *50* (18), 9889−9899.
(82) Wei, J.; Yu, H.; Wang, Y.; Verma, V. Complexation of Iron and Copper in Ambient Particulate Matter and Its Effect on the Oxidative Potential Measured in a Surrogate Lung Fluid. *Environ. Sci. Technol.* **2019**, *53* (3), 1661−1671.
(83) Ervens, B.; Turpin, B.; Weber, R. Secondary organic aerosol formation in cloud droplets and aqueous particles (aqSOA): a review of laboratory, field and model studies. *Atmos. Chem. Phys.* **2011**, *11* (21), 11069−11102.
(84) Herrmann, H.; Schaefer, T.; Tilgner, A.; Styler, S. A.; Weller, C.; Teich, M.; Otto, T. Tropospheric aqueous-phase chemistry: kinetics, mechanisms, and its coupling to a changing gas phase. *Chem. Rev.* **2015**, *115* (10), 4259−4334.
(85) Gilardoni, S.; Massoli, P.; Paglione, M.; Giulianelli, L.; Carbone, C.; Rinaldi, M.; Decesari, S.; Sandrini, S.; Costabile, F.; Gobbi, G. P.;

DOI: 10.1021/acs.est.9b05149
Environ. Sci. Technol. 2019, 53, 12506−12518

Pietrogrande, M. C.; Visentind, M.; Scottoe, F.; Fuzzia, S.; Facchinia, M. C. Direct observation of aqueous secondary organic aerosol from biomass-burning emissions. *Proc. Natl. Acad. Sci. U. S. A.* **2016**, *113* (36), 10013−10018.
(86) Riva, M.; Heikkinen, L.; Bell, D.; Peräkylä, O.; Zha, Q.; Schallhart, S.; Rissanen, M.; Imre, D.; Petäjä, T.; Thornton, J. A.; Zelenyuk, A.; Ehn, M. Chemical transformations in monoterpene-derived organic aerosol enhanced by inorganic composition. *npj Clim. Atmos. Sci.* **2019**, *2* (1), 2.
(87) Brüggemann, M.; Poulain, L.; Held, A.; Stelzer, T.; Zuth, C.; Richters, S.; Mutzel, A.; Pinxteren, D. v.; Iinuma, Y.; Katkevica, S.; Rabe, R.; Herrmann, H.; Hoffmann, T. Real-time detection of highly oxidized organosulfates and BSOA marker compounds during the F-BEACh 2014 field study. *Atmos. Chem. Phys.* **2017**, *17* (2), 1453−1469.
(88) Chowdhury, P. H.; He, Q.; Lasitza Male, T.; Brune, W. H.; Rudich, Y.; Pardo, M. Exposure of Lung Epithelial Cells to Photochemically-Aged Secondary Organic Aerosol Shows Increased Toxic Effects. *Environ. Sci. Technol. Lett.* **2018**, *5*, 424−430.
(89) Hua, W.; Chen, Z.; Jie, C.; Kondo, Y.; Hofzumahaus, A.; Takegawa, N.; Chang, C.; Lu, K.; Miyazaki, Y.; Kita, K.; Wang, H. L.; Zhang, Y. H.; Hu, M. Atmospheric hydrogen peroxide and organic hydroperoxides during PRIDE-PRD'06, China: their concentration, formation mechanism and contribution to secondary aerosols. *Atmos. Chem. Phys.* **2008**, *8* (22), 6755−6773.
(90) Li, X.; Chee, S.; Hao, J.; Abbatt, J. P.; Jiang, J.; Smith, J. N. Relative humidity effect on the formation of highly oxidized molecules and new particles during monoterpene oxidation. *Atmos. Chem. Phys.* **2019**, *19* (3), 1555−1570.
(91) Jin, L.; Xie, J.; Wong, C. K.-C.; Chan, S. K.; Abbaszade, G.; Schnelle-Kreis, J.; Zimmermann, R.; Li, J.; Zhang, G.; Fu, P.; Li, X. Contributions of city-specific PM2. 5 to differential in vitro oxidative stress and toxicity implications between Beijing and Guangzhou of China. *Environ. Sci. Technol.* **2019**, *53*, 2881−2891.

DOI: 10.1021/acs.est.9b05149
Environ. Sci. Technol. 2019, 53, 12506−12518

Supporting information for

Radical Formation by Fine Particulate Matter Associated with Highly Oxygenated Molecules

Haijie Tong,[*1] Yun Zhang,[2] Alexander Filippi,[1] Ting Wang,[1,3] Chenpei Li,[1,3] Fobang Liu,[1,4] Denis Leppla,[2] Ivan Kourtchev,[5] Kai Wang,[2,†] Helmi-Marja Keskinen,[6] Janne T. Levula,[6] Andrea M. Arangio,[1,7] Fangxia Shen,[8] Florian Ditas,[1] Scot T. Martin,[9,10] Paulo Artaxo [11] Ricardo H. M. Godoi,[12] Carlos I. Yamamoto,[13] Rodrigo A. F. de Souza,[14] Ru-Jin Huang,[15] Thomas Berkemeier,[1] Yueshe Wang,[3] Hang Su,[1] Yafang Cheng,[1] Francis D. Pope,[16] Pingqing Fu,[17] Maosheng Yao,[18] Christopher Pöhlker,[1] Tuukka Petäjä,[6] Markku Kulmala,[6] Meinrat O. Andreae,[1,19] Manabu Shiraiwa,[20] Ulrich Pöschl,[1] Thorsten Hoffmann,[*2] and Markus Kalberer[*5,21]

[1] Multiphase Chemistry Department, Max Planck Institute for Chemistry, 55128 Mainz, Germany

[2] Institute of Inorganic and Analytical Chemistry, Johannes Gutenberg University, 55128 Mainz, Germany

[3] State Key Laboratory of Multiphase Flow in Power Engineering, Xi'an Jiaotong University, Xi'an, 710049, China

[4] School of Chemical and Biomolecular Engineering, Georgia Institute of Technology, Atlanta, Georgia 30332, United States

[5] Centre for Atmospheric Science, Department of Chemistry, University of Cambridge, Cambridge CB2 1EW, United Kingdom

[6] Institute for Atmospheric and Earth System Research / Physics Faculty of Science, University of Helsinki FI-00014, Finland

[7] École polytechnique fédérale de Lausanne, Lausanne 1015, Switzerland

[8] School of Space and Environment, Beihang University, Beijing, 100191, China

[9] School of Engineering and Applied Sciences and [10] Department of Earth and Planetary Sciences, Harvard University, Cambridge, Massachusetts 02138, United State

[11] Physics Institute, University of São Paulo, São Paulo 05508-900, Brazil

[12] Environmental Engineering Department, Federal University of Paraná, Curitiba, Paraná 81531-980, Brazil

[13] Chemical Engineering Department, Federal University of Paraná, Curitiba, Paraná 81531-970, Brazil

[14] School of Technology, Amazonas State University, Manaus, Amazonas, 69065-020, Brazil

[15] Key Laboratory of Aerosol Chemistry and Physics, State Key Laboratory of Loess and Quaternary Geology, Institute of Earth and Environment, Chinese Academy of Sciences, Xi'an, 710061, China

[16] School of Geography, Earth and Environmental Sciences, University of Birmingham, Birmingham, B15 2TT, United Kingdom

[17] Institute of Surface-Earth System Science, Tianjin University, Tianjin 300072, China

[18] College of Environmental Sciences and Engineering, Peking University, Beijing, 100871, China

[19] Scripps Institution of Oceanography, University of California San Diego, CA 92093, United States

[20] Department of Chemistry, University of California, Irvine, California 92697-2025, United States

[21] Department of Environmental Sciences, University of Basel, Klingelbergstrasse 27, 4056 Basel, Switzerland

[†] now at: Department of Chemistry, Aarhus University, Langelandsgade 140, DK-8000 Aarhus C, Denmark

[*]Correspondence to:

Haijie Tong (h.tong@mpic.de)

Thorsten Hoffmann (hoffmant@uni-mainz.de)

Markus Kalberer (markus.kalberer@unibas.ch)

Tables:

Figures:

Section S1. Correlation coefficients and chemical groups included in Spearman correlation analysis.

Spearman correlation coefficients were calculated using the method in literatures:[1, 2] $r = 1 - (6 \cdot \frac{\sum d_i^2}{n \cdot (n^2 - 1)})$, where r is the correlation coefficient, d_i is the rank difference of two subgroups, and n is the sample size. The Spearmen correlation coefficient values for the included groups and species are listed in Table S3.

Table S1. Particle sampling information.

Site	Location	Air flow rate/L min^{-1}	Volume of air/m^3	Particle size	Sampler	Sampling time
Amazon	3.21◦N, 60.60◦E (T3)	10	14	$PM_{2.5}$	Harvard impactor (Air Diagnostics, Harrison, ME, USA)	05-06/03/2014
		10	14	$PM_{2.5}$		15-15/03/2014
		10	14	$PM_{2.5}$		15-16/03/2014
		10	14	$PM_{2.5}$		16-17/03/2014
		10	14	$PM_{2.5}$		18-19/03/2014
		10	14	$PM_{2.5}$		25-26/03/2014
		10	14	$PM_{2.5}$		07-09/09/2014
		10	14	$PM_{2.5}$		09-10/09/2014
		10	14	$PM_{2.5}$		12-13/09/2014
		10	14	$PM_{2.5}$		14-15/09/2014
		10	14	$PM_{2.5}$		15-16/09/2014
		10	14	$PM_{2.5}$		18-19/09/2014
		10	14	$PM_{2.5}$		23-24/09/2014
		10	14	$PM_{2.5}$		27-28/09/2014
		10	14	$PM_{2.5}$		03-04/10/2014
	3.21◦N, 60.60◦E (ATTO)	10	68	$PM_{1.8}$	MOUDI (125R, MSP corporation, USA)	27/03-01/04/2017
		10	101	$PM_{1.8}$		02-09/04/2017
		10	98	$PM_{1.8}$		09-16/04/2017
		10	126	$PM_{1.8}$		16-25/04/2017
		38	55	$PM_{2.5}$	Homemade $PM_{2.5}$ sampler	20/10/2017
		38	55	$PM_{2.5}$		21/10/2017
		38	55	$PM_{2.5}$		25/10/2018
		38	55	$PM_{2.5}$		29/10/2018
		38	55	$PM_{2.5}$		31/10/2018
Hyytiälä	61.85°N, 24.29°E	32	100-134	$PM_{2.5}$	Dekati PM_{10} impactor (Dekati Ltd., Tampere, Finland)	07/07-04/08/2014
			293	$PM_{2.5}$		02-05/06/2017
			202	$PM_{2.5}$		07-09/06/2017
			153	$PM_{2.5}$		09-12/06/2017
			100	$PM_{2.5}$		19-21/06/2017
			252	$PM_{2.5}$		21-26/06/2017
			100	$PM_{2.5}$		26-28/06/2017
			99	$PM_{2.5}$		28-30/06/2017
			153	$PM_{2.5}$		30/06-03/07/2017
			103	$PM_{2.5}$		03-05/07/2017
			155	$PM_{2.5}$		07-10/07/2017
			99	$PM_{2.5}$		10-12/07/2017
			98	$PM_{2.5}$		12-14/07/2017
			153	$PM_{2.5}$		14-17/07/2017
			102	$PM_{2.5}$		17-19/07/2017
Mainz		38	55	$PM_{2.5}$		25-26/01/2015

			55	$PM_{2.5}$	Homemade $PM_{2.5}$ sampler	26-27/01/2015
			55	$PM_{2.5}$		27-28/01/2015
		29	80	$PM_{1.8}$	MOUDI (122R, MSP corporation, USA)	22-24/08/2017
			80	$PM_{1.8}$		26-28/08/2017
			80	$PM_{1.8}$		28-30/08/2017
			80	$PM_{1.8}$		25-27/09/2017
	49.99°N, 8.23°E		80	$PM_{1.8}$		25-27/10/2017
			80	$PM_{1.8}$		14-16/11/2017
			80	$PM_{1.8}$		01-03/03/2018
			80	$PM_{1.8}$		14-16/03/2018
			80	$PM_{1.8}$		18-20/04/2018
			80	$PM_{1.8}$		18-20/04/2018
			80	$PM_{1.8}$		22-24/08/2018
Beijing	116.31°E, 39.99°N	30	43	$PM_{2.5}$	Tisch Environmental $PM_{2.5}$ sampler, Cleveland, OH, USA	06-07/11/2017
			43	$PM_{2.5}$		07-08/11/2017
			43	$PM_{2.5}$		08-09/11/2017
			43	$PM_{2.5}$		09-10/11/2017
			43	$PM_{2.5}$		20-21/11/2017
			43	$PM_{2.5}$		27-28/12/2017
			43	$PM_{2.5}$		28-29/12/2017
			43	$PM_{2.5}$		15-16/01/2018
Shanghai	121.43°E, 34.50°N	1000	1612	$PM_{2.5}$	Homemade $PM_{2.5}$ sampler	01-02/01/2014
			1585	$PM_{2.5}$		19-20/01/2014
			1620	$PM_{2.5}$		20-21/01/2014
			1628	$PM_{2.5}$		24-25/01/2014
			1614	$PM_{2.5}$		26-27/01/2014
			1612	$PM_{2.5}$		27-28/01/2014
Guangzhou	113.27°E, 23.13°N	1050	1690	$PM_{2.5}$	Tisch Environmental $PM_{2.5}$ sampler, USA	05-06/01/2014
			1599	$PM_{2.5}$		06-07/01/2014
			1596	$PM_{2.5}$		11-12/01/2014
			1601	$PM_{2.5}$		08-09/01/2014
			1616	$PM_{2.5}$		12-13/01/2014
			1646	$PM_{2.5}$		13-14/01/2014
Xi'an	108.95°E, 34.27°N	28.2	81	$PM_{2.1}$	Tisch TE-20-800, USA	14-16/09/2017
			81	$PM_{2.1}$		16-18/09/2017
			81	$PM_{2.1}$		18-20/09/2017
			81	$PM_{2.1}$		20-22/09/2017

Table S2. Total relative fraction of subgroups with different chemical composition and volatilities in fine PM.

Ambient fine PM/ laboratory SOA	CHO	CHON	CHOS	CHONS	VOC	IVOC	SVOC	LVOC	ELVOC
	Relative fraction (%)								
Guangzhou	40	33	18	9	0	29	47	13	11
Beijing	49±6	34±6	13±6	4±3	1±1	52±3	41±4	3±2	3±3
Shanghai	33	33	23	11	0	32	49	11	8
Xi'an	41±3	25±3	25±2	9±3	1±1	40±5	43±2	10±3	6±1
Mainz	35±5	30±3	17±2	18±3	1±1	21±5	36±5	21±4	21±6
Amazon	51±3	27±2	12±1	10±1	2±1	22±1	37±2	24±1	15±2
Hyytiälä	63±5	20±5	14±2	3±1	2±1	42±4	38±2	15±3	3±1
Naphthalene SOA	100	0	0	0	2	32	32	21	13
β-pinene SOA	100	0	0	0	5	31	31	28	5
Isoprene SOA	100	0	0	0	6	36	33	19	6
α-pinene SOA	100	0	0	0	5	25	31	29	10

Table S3. Relative fraction of HOMs measured in different ion mode.

Type of samples	RF_{HOM} (%)	
	negative	positive
Beijing	1.4	0.5
Shanghai	2.2	1.3
Guangzhou	4.7	1.9
Xi'an	5.1	0.4
Mainz	6.6	1.8
Amazon	7.3	2.0
Hyytiälä	8.8	1.7
α-pinene SOA	10.0	1.8
β-pinene SOA	11.5	1.6

Table S4. Spearman correlation coefficients (*r*) of radical yields (pmol μg^{-1}) and chemical groups that identified in negative mode, positive mode, and the sum of them.

Species	ion mode		
	negative	positive	sum
Total HOMs	0.92	0.36	0.86
HOM monomer	0.23	0.14	0.27
HOM dimer	0.94	0.93	0.94
SVOC	0.56	0.11	0.63
LVOC	0.95	0.62	0.88
ELVOC	0.24	0.42	0.59
CHO	0.91	0.80	0.90
CHON	0.13	-0.08	0.09
CHOS	-0.30	0.73	0.00
CHONS	-0.35	0.48	-0.03
O/C	-0.42	0.78	-
$\overline{OS_C}$	-0.30	0.66	-
$^{\bullet}OH$	0.73	0.73	0.73
$O_2^{\bullet-}$	0.69	0.71	0.71
Organic radicals	0.73	0.73	0.73

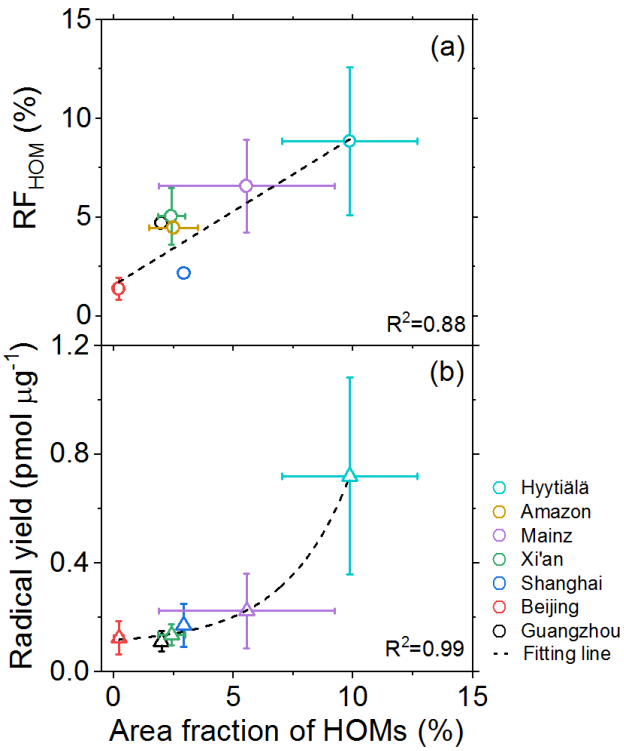

Figure S1. Relationship between relative abundance of HOMs and radical yield of fine PM. (a) Correlation of ion number fraction (RF_{HOM}) and chromatographic peak area fraction of HOMs. (b) Correlation of chromatographic peak area fraction of HOMs with radical yield of PM. The 'area fraction of HOMs' means sum chromatographic area of HOMs divided by the sum chromatographic area of all-assigned organic compounds. The Amazon PM samples used for panel (a) were collected in October 2018.

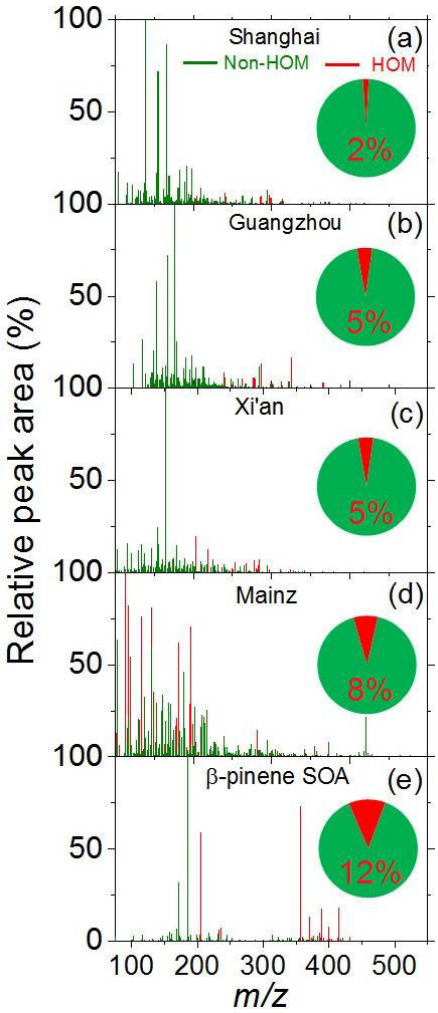

Figure S2. The spectral fingerprint and relative fraction of HOMs (red) and non-HOMs (green) in different type of particles. The peak area of each compound was obtained from LC-MS measurement. The relative peak area (%) of spectra belonging to HOMs were multiplied by a factor of 5. The red and green parts of the pie charts indicate the relative fraction of HOMs and non-HOMs, respectively.

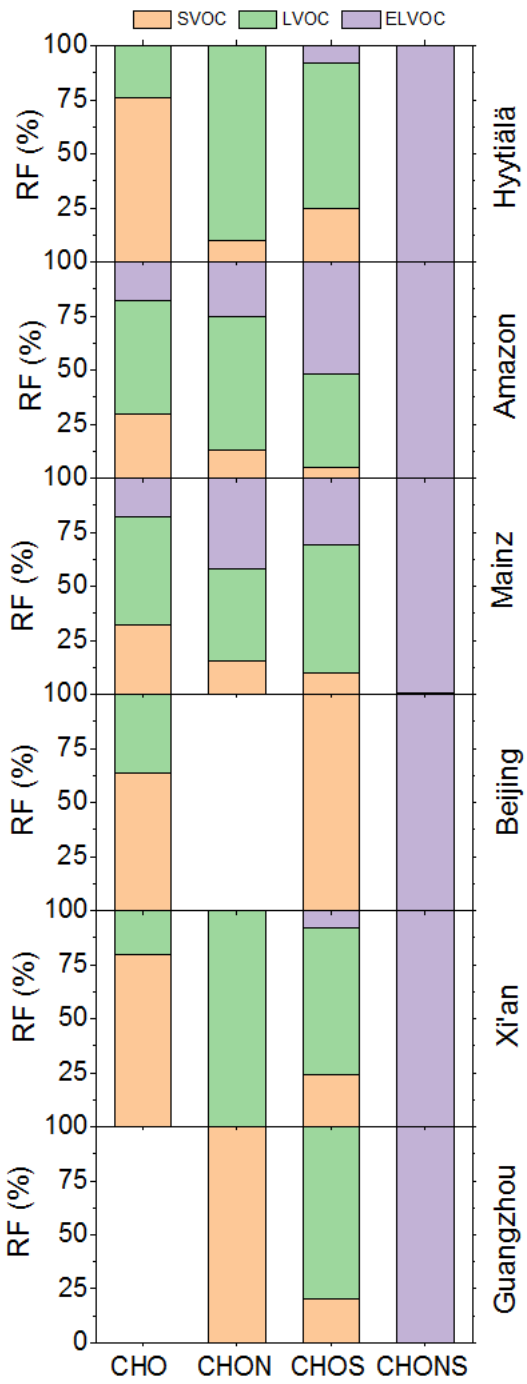

Figure S3. Relative fraction of highly oxygenated SVOC, LVOC, and ELVOC with different chemical composition.

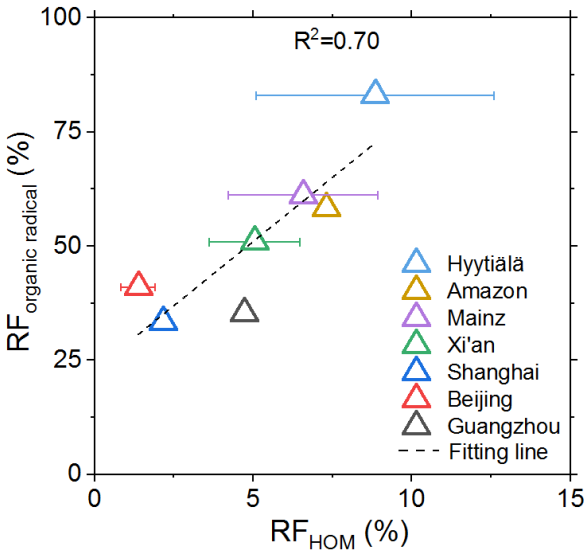

Figure S4. Relative fractions of HOMs and organic radicals formed by ambient fine PM in water. The $RF_{organic\ radical}$ is defined as the organic radical yield divided by total radical yield of particulate matter from different locations. The fitting equation is: y=22.9 + 5.6x.

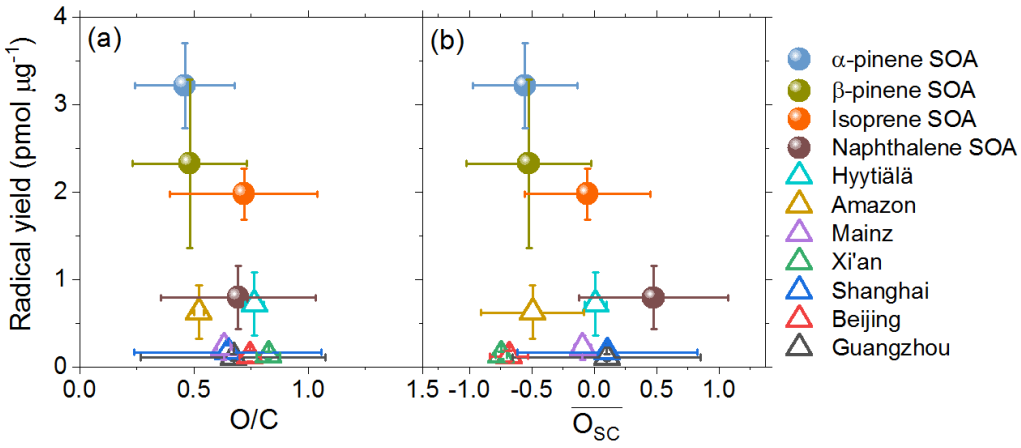

Figure S5. Correlation of particle mass normalized radical yield with *O/C* ratio (a) and oxidation state (b) of all assigned compounds in different type of PM.

REFERENCES

1. Myers, L.; Sirois, M. J. Spearman correlation coefficients, differences between. *Encyclopedia of statistical sciences;* **2006**.
2. Brehmer, C.; Lai, A. M.; Clark, S.; Shan, M.; Ni, K.; Ezzati, M.; Yang, X.; Baumgartner, J.; Schauer, J. J.; Carter, E. The Oxidative Potential of Personal and Household PM2. 5 in a Rural Setting in Southwestern China. *Environ. Sci. Technol.* **2019**, *53*, 2788−2798.

3.4 Reactive Species Yield of Particulate Matter from Clean and Polluted Environments

This chapter is currently under revision for publication on the preprint server *Atmospheric chemistry and physics discussions*. As third author of this manuscript I have been involved in planning, conducting, writing, and revising this manuscript. I have personally performed many of the EPR spin-trapping analyses of ambient PM for this study and shaped the interpretation of the results by contributing to writing and editing of the figures. In particular my contribution was focused on the analysis and presentation of the ambient PM samples.

Reactive species formed upon interaction of water with fine particulate matter from remote forest and polluted urban air

Atmospheric Chemistry and Physics Discussions, doi.org/10.5194/acp-2020-973, under review.

Haijie Tong,[1] Fobang Liu,[1, 2] Alexander Filippi,[1] Jake Wilson,[1] Andrea M. Arangio,[1, 3] Yun Zhang,[4] Siyao Yue,[5, 6, 7] Steven Lelieveld,[1] Fangxia Shen,[1, 8] Helmi-Marja K. Keskinen,[9, 10] Jing Li,[11] Haoxuan Chen,[11] Ting Zhang,[11] Thorsten Hoffmann,[4] Pingqing Fu,[7] William H. Brune,[12] Tuukka Petäjä,[9] Markku Kulmala,[9] Maosheng Yao,[11] Thomas Berkemeier,[1] Manabu Shiraiwa,[13] Ulrich Pöschl.[1]

[1] Multiphase Chemistry Department, Max Planck Institute for Chemistry, 55128 Mainz, Germany

[2] School of Chemical and Biomolecular Engineering, Georgia Institute of Technology, Atlanta, Georgia 10 30332, USA

[3] École polytechnique fédérale de Lausanne, Lausanne 1015, Switzerland

[4] Institute of Inorganic and Analytical Chemistry, Johannes Gutenberg University, 55128 Mainz, Germany

[5] State Key Laboratory of Atmospheric Boundary Layer Physics and Atmospheric Chemistry, Institute of Atmospheric Physics, Chinese Academy of Sciences, Beijing, 100029, China

[6] College of Earth and Planetary Sciences, University of Chinese Academy of Sciences, Beijing, 100049, China

[7] Institute of Surface-Earth System Science, Tianjin University, Tianjin, 300072, China

[8] School of Space and Environment, Beihang University, Beijing, 100191, China

[9] Institute for Atmospheric and Earth System Research / Physics, Faculty of Science, University of Helsinki, P.O. Box 64, FIN-00014, Helsinki, Finland

[10] Hyytiälä Forestry Field Station, Hyytiäläntie 124, FI-35500 Korkeakoski, Finland

[11] College of Environmental Sciences and Engineering, Peking University, Beijing, 100871, China

[12] Department of Meteorology, Pennsylvania State University, University Park, Pennsylvania 16802, United States

[13] Department of Chemistry, University of California, Irvine, California 92697-2025, USA

Reactive species formed upon interaction of water with fine particulate matter from remote forest and polluted urban air

Haijie Tong[1*], Fobang Liu[1,2], Alexander Filippi[1], Jake Wilson[1], Andrea M. Arangio[1,3], Yun Zhang[4], Siyao Yue[5,6,7], Steven Lelieveld[1], Fangxia Shen[1,8], Helmi-Marja K. Keskinen[9,10], Jing Li[11], Haoxuan Chen[11], Ting Zhang[11], Thorsten Hoffmann[4], Pingqing Fu[7], William H. Brune[12], Tuukka Petäjä[9], Markku Kulmala[9], Maosheng Yao[11], Thomas Berkemeier[1], Manabu Shiraiwa[13], Ulrich Pöschl[1]

[1] Multiphase Chemistry Department, Max Planck Institute for Chemistry, 55128 Mainz, Germany
[2] School of Chemical and Biomolecular Engineering, Georgia Institute of Technology, Atlanta, Georgia 30332, USA
[3] École polytechnique fédérale de Lausanne, Lausanne 1015, Switzerland
[4] Institute of Inorganic and Analytical Chemistry, Johannes Gutenberg University, 55128 Mainz, Germany
[5] State Key Laboratory of Atmospheric Boundary Layer Physics and Atmospheric Chemistry, Institute of Atmospheric Physics, Chinese Academy of Sciences, Beijing, 100029, China
[6] College of Earth and Planetary Sciences, University of Chinese Academy of Sciences, Beijing, 100049, China
[7] Institute of Surface-Earth System Science, Tianjin University, Tianjin, 300072, China
[8] School of Space and Environment, Beihang University, Beijing, 100191, China
[9] Institute for Atmospheric and Earth System Research / Physics, Faculty of Science, University of Helsinki, P.O. Box 64, FIN-00014, Helsinki, Finland
[10] Hyytiälä Forestry Field Station, Hyytiäläntie 124, FI-35500 Korkeakoski, Finland
[11] College of Environmental Sciences and Engineering, Peking University, Beijing, 100871, China
[12] Department of Meteorology, Pennsylvania State University, University Park, Pennsylvania 16802, United States
[13] Department of Chemistry, University of California, Irvine, California 92697-2025, USA

[*] *Correspondence to*: Haijie Tong (h.tong@mpic.de)

Abstract

Interaction of water with fine particulate matter leads to the formation of reactive species (RS) that may influence the aging, properties, and health effects of atmospheric aerosols. In this study, we explore the RS yields of fine PM from remote forest (Hyytiälä, Finland) and polluted urban air (Mainz, Germany and Beijing, China) and relate these yields to different chemical constituents and reaction mechanisms. Ultrahigh-resolution mass spectrometry was used to characterize organic aerosol composition, electron paramagnetic resonance (EPR) spectroscopy with a spin-trapping technique was used to determine the concentrations $^{\bullet}OH$, $O_2^{\bullet-}$, and carbon- or oxygen-centered organic radicals, and a fluorometric assay was used to quantify H_2O_2 concentration. The mass-specific yields of radicals were lower for sampling sites with higher concentration of ambient $PM_{2.5}$ (particles with a diameter < 2.5 μm), whereas the H_2O_2 yields exhibited no clear trend. The abundances of water-soluble transition metals and aromatics in ambient $PM_{2.5}$ were positively correlated with the relative fraction of $^{\bullet}OH$ to the totally detected radicals, but negatively correlated with the relative fraction of carbon-centered radicals. Moreover, we found that the relative fractions of different types of radicals formed by ambient $PM_{2.5}$ were comparable to the surrogate mixtures comprising transition metals, organic hydroperoxide, H_2O_2, and humic or fulvic acids. Therein humic and fulvic acids exhibited strong radical scavenging effect to substantially decrease the radical yield of mixtures comprising cumene hydroperoxide and Fe^{2+}. The interplay of transition metals (e.g., iron), highly oxidized compounds (e.g., organic hydroperoxides), and complexing agents (e.g., humic or fulvic acids), leads to non-linear concentration dependencies of production and yields of different types of RS. Our findings show that how the composition of $PM_{2.5}$ influences the amount and nature of RS produced upon interaction with water, which may explain differences in the chemical reactivity and health effects of particulate matter in clean and polluted air.

1 Introduction

Atmospheric fine particulate matter with a particle diameter < 2.5 µm ($PM_{2.5}$) forms reactive species (RS) upon interaction with water and respiratory antioxidants (Bates et al., 2015;Lakey et al., 2016;Park et al., 2018;Li et al., 2018;Tong et al., 2019). The umbrella term RS comprises reactive oxygen species (e.g., $^{\bullet}OH$, $O_2^{\bullet-}$, $^1O_2$, H_2O_2, and ROOH) as well as C- and O-centered organic radicals (Halliwell and Whiteman, 2004;Sies et al., 2017), which influence the chemical aging of atmospheric aerosols and their interaction with the biosphere (Pöschl and Shiraiwa, 2015;Reinmuth-Selzle et al., 2017;Shiraiwa et al., 2017). For example, Fenton-like reactions of hydroperoxides with transition metal ions contribute to the formation of aqueous-phase radicals including $^{\bullet}OH$ (Jacob, 2000;Enami et al., 2014;Anglada et al., 2015;Tong et al., 2016a), enhancing the conversion of organic precursors to secondary organic aerosols (SOA) (Donaldson and Valsaraj, 2010;Ervens et al., 2011;Gligorovski et al., 2015;Gilardoni et al., 2016). Moreover, $PM_{2.5}$ may generate excess concentrations of RS in human airways, causing antioxidant depletion, oxidative stress, and respiratory diseases (Nel, 2005;Cui et al., 2015;Lakey et al., 2016;Qu et al., 2017;Lelieveld and Pöschl, 2017;Rao et al., 2018).

The formation pathways and yields of RS from ambient PM and laboratory-generated SOA have been investigated in a wide range of studies (Valavanidis et al., 2005;Ohyama et al., 2007;Chen et al., 2010;Wang et al., 2011a;Wang et al., 2011b;Verma et al., 2014;Badali et al., 2015;Bates et al., 2015;Verma et al., 2015;Arangio et al., 2016;Tong et al., 2016a;Kuang et al., 2017;Tong et al., 2017;Zhou et al., 2018;Tong et al., 2019;Chowdhury et al., 2019;Fang et al., 2019;Liu et al., 2020). The mass, surface area, and chemical composition of PM were discussed as key factors influencing the reactivity of atmospheric aerosols (Møller et al., 2010;Fang et al., 2015;Jin et al., 2019). Among the substance groups associated with RS formation by PM in water are black carbon (Baumgartner et al., 2014), transition metals (Yu et al., 2018), oxidized aromatic compounds including quinones and environmentally persistent free radicals (Xia et al., 2004;Gehling et al., 2014;Charrier et al., 2014;Xiong et al., 2017), humic-like substances (Lin and Yu, 2011;Page et al., 2012;Fang et al., 2019), and peroxide-containing highly oxygenated organic molecules

(HOMs) (Chen et al., 2010;Wang et al., 2011b;Tong et al., 2016a;Tong et al., 2018;Tong et al., 2019;Fang et al., 2020;Qiu et al., 2020). Moreover, the humic-like substances and other multifunctional compounds containing carboxyl, carboxylate, phenolic, and quinoid groups may influence the redox activity of PM via chelating transition metals (Laglera and van den Berg, 2009;Kostić et al., 2011;Catrouillet et al., 2014;Gonzalez et al., 2017;Wang et al., 2018c;Win et al., 2018;Wei et al., 2019).

To assess the oxidative potential of ambient PM, the following cellular or acellular assays have been used: dichloro-dihydro-fluorescein diacetate (DCFH-DA), dithiothreitol (DTT), ascorbic acid (AA), macrophage, electron paramagnetic resonance (EPR), and surrogate lung fluids (SLF) (Landreman et al., 2008;Charrier and Anastasio, 2012;Kalyanaraman et al., 2012;Charrier et al., 2014;Charrier and Anastasio, 2015;Fang et al., 2016;Tong et al., 2018;Bates et al., 2019;Fang et al., 2019;Molina et al., 2020;Crobeddu et al., 2020). However, the interplay of different PM constituents often results in non-additive characteristics of the RS yields or oxidative potential of PM (Charrier et al., 2014;Lakey et al., 2016;Wang et al., 2018b). Thus, unraveling the adverse health effects of ambient PM requires systematic investigations of the RS formation and chemical reactivity of PM from different sources and environments (Shiraiwa et al., 2017).

The concentration of $PM_{2.5}$ and the composition of airborne organic matter vary considerably from clean forest to polluted urban environments. For example, the $PM_{2.5}$ concentrations at the Hyytiälä forest site are typically below 10 μg m^{-3}, with organic matter accounting for ~70% (Laakso et al., 2003;Maenhaut et al., 2011), whereas the $PM_{2.5}$ concentrations in Beijing during winter can reach and exceed daily average values of 150 μg m^{-3}, with organic matter accounting for ~40% (Huang et al., 2014). Moreover, anthropogenic emissions can enhance the formation of biogenic SOA and HOM as well as the levels of particulate transition metals, humic-like substances, and PM oxidative potential (Goldstein et al., 2009;Hoyle et al., 2011;Liu et al., 2014;Xu et al., 2015;Ma et al., 2018;Pye et al., 2019;Shrivastava et al., 2019).

In this study, we compared the RS yields of $PM_{2.5}$ in clean and polluted environments. We used three approaches to explore the RS formation by $PM_{2.5}$ from remote forest of Hyytiälä (Finland), intermediately polluted city of Mainz (Germany), and heavily polluted megacity of Beijing (China) (Figure 1). To quantify

the abundances of redox-active PM constituents related to RS formation, we collected ambient $PM_{2.5}$ and measured the chemical composition of organic matter, the abundance of water-soluble transition metals, and the yield of radicals and H_2O_2 in the liquid phase (Figure 1a). To assess the influence of anthropogenic-biogenic organic matter interactions on the RS formation by ambient $PM_{2.5}$, we analyzed the radical yield of SOA generated by oxidation of mixed anthropogenic and biogenic precursors in a laboratory chamber (Figure 1b). To get insights into the radical formation mechanism of ambient $PM_{2.5}$ in water, we differentiated the influence of transition metals, organic hydroperoxide (ROOH), water-soluble humic acid (HA) and fulvic acid (FA) on the radical formation by Fenton-like reactions (Figure 1c).

2 Materials and methods

2.1 Chemicals

The following chemicals were used as received without further purification: β-pinene (99%, Sigma-Aldrich), naphthalene (99.6%, Alfa Aesar GmbH&Co KG), cumene hydroperoxide (80%, Sigma-Aldrich), H_2O_2 (30%, Sigma-Aldrich), $FeSO_4•7H_2O$ (F7002, Sigma-Aldrich), $CuSO_4•5H_2O$ (209198, Sigma-Aldrich), $NiCl_2$ (98%, Sigma-Aldrich), $MnCl_2$ (≥99%, Sigma-Aldrich), VCl_2 (85%, Sigma-Aldrich), NaCl (443824T, VWR International GmbH), KH_2PO_4 (≥99%, Alfa Aesar GmbH&Co KG), Na_2HPO_4 (≥99.999%, Fluka), humic acid (53680, Sigma-Aldrich), fulvic acid (AG-CN2-0135-M005, Adipogen), 5-tert-Butoxycarbonyl-5-methyl-1-pyrroline-N-oxide (BMPO, high purity, Enzo Life Sciences, Inc.), H_2O_2 assay kit (MAK165, Sigma-Aldrich), ultra-pure water (14211-1L-F, Sigma-Aldrich), 47 mm diameter Teflon filters (JVWP04700, Omnipore membrane filter), and micropipettes (50 µL, Brand GmbH&Co KG). The used neutral saline (pH=7.4) consists of 10 mM phosphate buffer (2.2 mM KH_2PO_4 and 7.8 mM Na_2HPO_4) and 114 mM NaCl, which was used to simulate physiologically relevant condition.

2.2 Collection and extraction of ambient fine PM

Ambient fine particles were collected onto Teflon filters for all sites. The Hyytiälä $PM_{2.5}$ was collected using a three-stage cascade impactor (Dekati® PM10) at the Station for Measuring Forest Ecosystem-Atmosphere Relations station (SMEAR II station, Finland) during 31 May-19 July 2017 (Hari and Kulmala,

2005). The Mainz fine PM was collected using a micro-orifice uniform deposit impactor (MOUDI, 122-R, MSP Corporation) (Arangio et al., 2016) on the roof of Max Planck Institute for Chemistry during 22 August-17 November 2017 and 23-31 August 2018. The Beijing winter $PM_{2.5}$ was collected using a 4-channel $PM_{2.5}$ air sampler (TH-16, Wuhan Tianhong Instruments Co., Ltd.) in the campus of the Peking University, an urban site of Beijing, during 20 December-13 January 2016 and 6 November-17 January 2018 (Lin et al., 2015). The sampling time for a single filter sample in Hyytiälä, Mainz, and Beijing are 48-72, 25-54, and 5-24 h, respectively, depending on the local PM concentrations. More information about the sampling sites and instrumentation is shown in Table S1. After sampling, all filter samples were put in petri dishes and stored in a -80 ℃ freezer before analysis. To determine the mass of collected PM, each filter was weighed before and after the collection using a high sensitivity balance (±10 μg, Mettler Toledo XSE105DU). In Hyytiälä, the PM_1 and $PM_{1\text{-}2.5}$ were separately sampled, which were combined and extracted together to represent $PM_{2.5}$ samples. Mainz PM with cut-size range of 0.056-1.8 μm is taken as a proxy for $PM_{2.5}$. Particle concentrations in aqueous extracts were estimated to be in the range of 200-6000 μg mL^{-1} (Figure S1).

2.3 Formation, collection, and extraction of laboratory-generated SOA

To generate SOA from mixed anthropogenic and biogenic precursors, different concentrations of gas-phase naphthalene and β-pinene were mixed and oxidized in a potential aerosol mass (PAM) chamber, i.e., an oxidation flow reactor (OFR) (Kang et al., 2007;Tong et al., 2018). Naphthalene and β-pinene were used as representative SOA precursors in Beijing and Hyytiälä, respectively (Hakola et al., 2012;Huang et al., 2019). The concentrations of gas-phase O_3 and $^{\bullet}OH$ in the PAM chamber were ~1 ppm and ~5.0×10^{11} cm^{-3}, respectively. SOA was produced by adjusting the relative concentrations of naphthalene to the sum of it with β-pinene (i.e., [naphthalene]/([naphthalene] + [β-pinene])) to be ~9%, ~23%, and ~38%, respectively. The concentrations of naphthalene and β-pinene were 0.2-0.6 ppm and 1.0-2.5 ppm, respectively, which were determined on the basis of a calibration function measured by gas chromatography mass spectrometry (Tong et al., 2018). To investigate the influece of ozone/β-pinene ratios on redox property of SOA, we

measured the aqueous phase radical yields of SOA particles formed from oxidation of ~1 ppm and ~2.5 ppm β-pinene with the same concentration of ozone. With a similar purpose, we measured the radial yields of SOA formed from oxidation of ~0.2 ppm and ~0.6 ppm naphthalene by the same concenteation of gas-phase OH radical. The mean radical yields of β-pinene and naphthalene SOA formed at different concentrations of precursors are compared in Sect. 3.4. The number and size distributions of SOA particles were meaured using a scanning mobility particle sizer (SMPS, GRIMM Aerosol Technik GmbH&Co. KG). When the SOA concentration is stable, 47 mm diameter Teflon filters (JVWP04700, Omnipore membrane filter) were used to collect SOA particles, which were extracted into water solutions within 2 minutes after the sampling. More information about the SOA formation, characterization, collection, and extraction can be found in previous studies (Tong et al., 2016a;Tong et al., 2017;Tong et al., 2018;Tong et al., 2019).

2.4 Surrogate mixtures

Considering that cumene hydroperoxide (CHP), humic acid (HA), and fulvic acid (FA) have been used as model compounds mimicking the redox-active substances in biogenic and anthropogenic PM (Lin and Yu, 2011;Ma et al., 2018;Tong et al., 2019), we measured the relative fractions (RF) of different radicals formed by surrogate mixtures of CHP+Fe^{2+}+Cu^{2+}+HA+H_2O_2 to simulate the radical formation by fine PM from Hyytiälä, Mainz, and Beijing. The H_2O_2 was treated as a redox-active constituent preexisting in PM samples before extraction. The following method was used to make HA or FA solutions. First, 0-1000 μg mL^{-1} HA or FA water suspensions were made. Then, the suspensions were sonicated for 3 minutes to accelerate the dissolution of HA or FA. Afterwards, the sonicated suspensions were centrifuged at 6000 rpm (MiniStar, VWR International bvba) for 2 minutes. Finally, the supernatants were taken out from the centrifuge tubes with pipettes and stored in glass vials under 4-8 °C condition before analysis. The HA or FA solutions were prepared freshly day-to-day. To determine the concentrations of dissolved HA or FA, aliquots of the supernatants were dried with pure N_2 flow (1-2 bar) and weighted with a high sensitivity balance (± 0.01 mg, Mettler Toledo XSE105DU). The concentrations of Fe^{2+}, Cu^{2+}, HA, and H_2O_2 in the surrogate mixtures are 43 μM, 3 μM, 4 mg L^{-1}, and 7 μM, which are based on the measurement of ambient PM extracts (Fe^{2+} and Cu^{2+}, Section 2.8) or the estimated abundance in ambient PM (CHP, HA, FA, and H_2O_2, SI). To explore

the influence of HA/FA on Fenton-like reactions, the radical formation in the following aqueous mixtures was also analyzed: CHP+Fe^{2+}, CHP+Cu^{2+}, CHP+Cu^{2+}+HA, CHP+Cu^{2+}+FA. The concentrations of Fe^{2+}, Cu^{2+}, HA, FA, and H_2O_2 in these solutions are 15-300 μM, 15-300 μM, 0-180 μg mL^{-1}, 0-180 μg mL^{-1}, 0-300 μM, respectively.

2.5 Quantification of radicals by EPR

5-tert-Butoxycarbonyl-5-methyl-1-pyrroline-N-oxide (BMPO) was used as a spin-trapping agent for detecting different types of radicals formed in the extracts of PM. Ambient PM or laboratory-generated SOA were extracted from Teflon filters into 10 mM BMPO neutral saline or water solutions by vortex shaking for ~15 minutes (with Heidolph Reax 1). Around one fourth of each ambient PM filter or a whole SOA-loaded filter was used for extraction. It was assumed that during the extraction process, most of the short-lived radicals have reacted with BMPO to form stable adducts.

A continuous-wave electron paramagnetic resonance (CW-EPR) X-band spectrometer (EMXplus-10/12; Bruker Corporation) was applied for the identification and quantification of radical adducts (Tong et al., 2016a;Tong et al., 2017;Tong et al., 2018;Tong et al., 2019). In order to increase the signal to noise ratio of EPR spectra, some of the extracts were concentrated by a factor of 5 - 20 through 15 - 20 minutes drying under 1-2 bar pure N_2 flow. The EPR spectra of BMPO-radical adducts were recorded by setting the following operating parameters: a microwave frequency of 9.84 GHz, a microwave power of 0.017 mW (20 dB), a receiver gain of 40 dB, a modulation amplitude of 1 G, a scan number of 50, a sweep width of 100 G, a modulation frequency of 100 kHz, a conversion time of 11 ms, and a time constant of 10 ms.

To average EPR spectra of different $PM_{2.5}$ extracts for each site, the magnetic field values of each spectrum was transformed to g-values. Then we used the Bruker software, Xenon to do the averaging, irrespective of the concentrations of $PM_{2.5}$ in extracts. The spin-counting method embedded in Xenon was applied to quantify radical adducts. The spin-counting method was calibrated using the standard compound 4-hydroxy-2,2,6,6-tetramethylpiperidin-1-oxyl (TEMPOL). To obtain the relative yields of $^{\bullet}OH$, $O_2^{\bullet-}$, C- and O-centered organic radicals, EPR spectra were simulated and fitted using the Xenon software before

deconvolution (Arangio et al., 2016;Tong et al., 2018). The weight of assigned species accounts on average for more than 95% of totally observed radical adducts, which is characterized by the peak area ratios of corresponding species. EPR spectra with low signal-to-noise ratio introduce uncertainty into the parameters describing the lineshape of peaks representing radical adducts (Tseitlin et al., 2012), causing a total quantification uncertainty of 0-19% for the weight and total concentrations of different radical species. The hyperfine coupling constants used for spectrum fitting are shown in Table S2. More information on the hyperfine coupling constants of different types of BMPO radical adducts can be found in previous studies (Zhao et al., 2001;Arangio et al., 2016).

2.6 Measurement of H_2O_2 yields

We extracted ambient $PM_{2.5}$ from one fourth of each Teflon filter into 1 mL ultra-pure water or neutral saline by stirring it with a vortex shaker for ~15 minutes. Afterwards, the extracts were centrifuged at 9000 rpm (Eppendorf Minispin) for 3 minutes to remove the insoluble particles. Finally, the concentration of H_2O_2 in the supernatant was measured using the MAK165 assay kit (Yan et al., 2017;Tong et al., 2018). 50 µL of supernatant and 50 µL of a Master Mix solution containing horseradish peroxidase and Amplex Red substrate were mixed in a 96-well plate. The horseradish peroxidase catalyzed the oxidation of Amplex Red by H_2O_2 to form fluorescent resorufin (Wang et al., 2017), which was consequently quantified using a microplate reader (Synergy™ NEO, BioTek, excitation at 540 nm and emission at 590 nm) after 30 minutes of incubation. The concentration of H_2O_2 in aqueous PM extracts was determined using an H_2O_2 calibration curve based on standard H_2O_2 solutions and also corrected by blank measurements (Tong et al., 2018).

2.7 Mass spectrometry of organic compounds

By using a Q-Exactive Orbitrap mass spectrometer (Thermo Fisher Scientific, MA, USA) coupled with an ultra-high performance liquid chromatography (UHPLC) system (Dionex UltiMate 3000, Thermo Scientific, Germany) (Wang et al., 2018a;Wang et al., 2019;Tong et al., 2019), we characterized the HOMs and aromatic compounds in Hyytiälä, Mainz, and Beijing winter fine PM samples in negative ionization mode. We processed the MS spectrum and UHPLC chromatogram of measured samples through a non-

target screening approach by using the commercially available software SIEVE® (Thermo Fisher Scientific, MA, USA). Then, we blank-corrected the signals with peak intensity > 1×10^5. Afterwards, we used the following criteria to assign molecular formulae and filter out the irrational ones: (a) the number of atoms of C, H, O, N, S, and Cl should be in the range of 1-39, 1-72, 0-20, 0-7, 0-4, and 0-2. (b) Atomic ratios of H/C, O/C, N/C, S/C, and Cl/C should be in the range of 0.3-3, 0-3, 0-1.3, 0-0.8, and 0-0.8, respectively.

The HOMs are defined as formulae fell into the following chemical composition range of $C_xH_yO_z$: monomers with x = 8–10, y = 12–16, z = 6–12, and z/x > 0.7; dimers with x = 17–20, y = 26–32 and z = 8–18 (Ehn et al., 2014;Tröstl et al., 2016;Tong et al., 2019). Aromatics in this study are defined to be compounds with aromaticity index (AI) > 0.5 and aromaticity equivalent (X_c) > 2.5, with the parameters accounting for the fraction of oxygen and sulfur atoms involved in π-bond structures of a compound to be set as 1 (Koch and Dittmar, 2006;Yassine et al., 2014;Tong et al., 2016b). Beyond this, The relative abundance of HOMs or aromatic compounds is defined to be the sum chromatographic area of HOMs or aromatics divided by the sum chromatographic area of all assigned organic compounds, with < 30% of totally detected organic compounds not assigned (Wang et al., 2018a).

2.8 Determination of water-soluble transition metal concentrations

Based on the same extraction method as the H_2O_2 analysis in section 2.6, the concentration of five selected water-soluble transition metal species (Fe, Cu, Mn, Ni and V) in the supernatants of $PM_{2.5}$ extracts was quantified using an inductively coupled plasma mass spectrometer (ICP-MS, Agilent 7900). These five transition metal species were chosen for analysis due to their prominent concentrations and higher oxidative potential (Charrier and Anastasio, 2012). A calibration curve for the ICP-MS analysis was made by measuring standard multi-element stock solutions (Custom Grade, Inorganic Ventures). An aliquot of the supernatants was diluted and acidified using a mixture of nitric acid (5%) and hydrofluoric acid (1%), which was finalized to be 5 mL before analysis. The measured transition metal concentrations were blank-corrected and shown in corresponding figures. The detection limit of the ICP-MS analysis in this study was typically < 40 ng L^{-1}. The $PM_{2.5}$ samples collected on 2 June, 7 June, 9 June, 12 June in 2017 in Hyytiälä, on 22 August, 26 August, 28 August, 25 September, 25 October, 14 November in 2017 in Mainz, and all

the 12 $PM_{2.5}$ samples from Beijing winter were used for transition metal analysis. Temporal evolution of water-soluble transition metal concentrations in water extracts of Mainz $PM_{2.5}$ were also measured, and we found that the total ion concentration of Fe, Cu, Mn, Ni, and V showed a rapid rise during the first 15 min (Figure S2a), but at a much slower rate afterwards (Figure S2b).

3 Results and discussion

3.1 Relative yields of different types of radicals from ambient $PM_{2.5}$

Figure 2a shows the averaged EPR spectra of BMPO-radical adducts in neutral saline extracts of $PM_{2.5}$ samples from Hyytiälä, Mainz (cut-size range 0.056-1.8 μm PM as a proxy), and Beijing. Each spectrum is composed of multiple peaks attributable to different types of BMPO-radical adducts. The dotted vertical lines with different colors indicate the peaks attributable to adducts of BMPO with •OH (green), $O_2^{\bullet-}$ (orange), C- (blue) and O-centered organic radicals (purple) (Zhao et al., 2001;Arangio et al., 2016), respectively. The spectrum of Hyytiälä $PM_{2.5}$ is dominated by peaks attributable to C-centered radicals. In contrast, the spectrum of Mainz $PM_{2.5}$ comprises strong peaks attributable to •OH and C-centered radicals, with •OH exhibiting stronger signals. Finally, the spectrum of Beijing winter $PM_{2.5}$ is mainly composed of four peaks attributable to •OH.

Figure 2b shows the averaged relative fractions (RF) of •OH, $O_2^{\bullet-}$, C- and O-centered organic radicals generated by multiple PM samples from each site. In line with visual inspection of the spectra in Figure 2a, the $PM_{2.5}$ from clean forest site generates relatively more C- and O-centered organic radicals but less •OH, vice versa for the radical yield by $PM_{2.5}$ from polluted areas. Specifically, the mean RF of C- and O-centered organic radicals, ordered from highest to lowest are: Hyytiälä (66% and 11%) > Mainz (46% and 10%) > Beijing (39% and 5%). Note that, the significantly higher RF of C-centered radicals than O-centered organic radicals may be induced by the higher yield and stability of BMPO-C-centered radical adduct in the liquid phase (De Araujo et al., 2006). Moreover, the C- and O-centered organic radicals may comprise a series of radicals with different molecular structures, the yields of which are associated with aqueous redox chemistry of organic matter such as Fenton-like reactions (Arangio et al., 2016;Tong et al., 2018;Tong et

al., 2019). The mean RF of •OH, ordered from lowest to highest are: 21% (Hyytiälä) < 38% (Mainz) < 53% (Beijing). The presence of •OH is related to multiple formation pathways, such as Fenton-like reactions, thermal or hydrolytic decomposition of peroxide-containing HOMs, and redox chemistry of environmentally persistent free radicals or aromatic compounds-containing humic-like substances (Chevallier et al., 2004;Valavanidis et al., 2005;Li et al., 2008;Page et al., 2012;Gehling et al., 2014;Tong et al., 2016a;Tong et al., 2017;Tong et al., 2018;Tong et al., 2019;Qiu et al., 2020). The mean RF of $O_2^{\bullet-}$ only varies slightly in the range of 2-6%, showing no clear trend and within the range of standard errors in Figure 2b.

3.2 Mass-specific and air sample volume-specific yields of RS from ambient $PM_{2.5}$

Figure 3 shows the mass-specific and air sample volume-specific yields of reactive species (RS) including radicals, H_2O_2, and the sum of radicals and H_2O_2 by $PM_{2.5}$ from Hyytiälä, Mainz, and Beijing. The mass-specific yields of RS are shown in the unit of pmol μg^{-1} of $PM_{2.5}$, reflecting the redox activities of $PM_{2.5}$ irrespective of filter loadings. The air sample volume-specific yields of RS are shown in the unit of pmol m^{-3} of air, indicating that the redox activities of $PM_{2.5}$ scale with atmospheric concentration of $PM_{2.5}$. We note that, while the more polluted sampling sites led to higher mass loadings, the concentrations of PM in extracts were found to have a tiny impact on the radical yields (Figure S1c and S1d).

Figure 3a shows that the mass-specific radical yields are negatively correlated with $PM_{2.5}$ mass concentrations. The mean concentrations of $PM_{2.5}$ are lower to higher in the order of 5 (Hyytiälä) < 16 (Mainz) < 202 $\mu g\ m^{-3}$ (Beijing), whereas the radical yields are in a reverse order of 0.58 > 0.33 > 0.07 pmol μg^{-1}. The higher mass-specific radical yield of $PM_{2.5}$ from Hyytiälä may be associated with the higher abundance of particulate organic matter, which includes quinones and organic hydroperoxides that undergo thermal, photonic, or hydrolytical dissociation as well as redox chemistry such as Fenton-like reactions to produce radicals (Badali et al., 2015;Tong et al., 2016a;Tong et al., 2019). More than 70% of $PM_{2.5}$ in Hyytiälä forest is composed of organic matter (Jimenez et al., 2009;Maenhaut et al., 2011), whereas the abundances of organic matter in Mainz autumn and Beijing winter $PM_{2.5}$ are ~40% (Jimenez et al.,

2009;Huang et al., 2014), which might in part explain the lower radical yield of these samples. Figure 3a also shows that the mass-specific H_2O_2 yields of $PM_{2.5}$ from Hyytiälä (~2.2 pmol μg^{-1}), Mainz (~3.4 pmol μg^{-1}), and Beijing (~3.4 pmol μg^{-1}) exhibit a weak positive correlation with $PM_{2.5}$ mass concentrations, agreeing with previous measurements of the H_2O_2 formation by fine PM from different districts of Los Angeles (Arellanes et al., 2006;Wang et al., 2012) (Figure S4a). The higher H_2O_2 yield of urban fine PM may be associated with its higher abundance of transition metals and aromatic-containing organic matter (e.g., quinones and humic-like substances), which have been found as redox-active constituents to produce H_2O_2 upon dissolution of ambient PM or laboratory-generated SOA in water (Arellanes et al., 2006;Chung et al., 2006;Wang et al., 2010;Wang et al., 2012). The weak correlation of mass-specific H_2O_2 yields and $PM_{2.5}$ concentrations reflects the varying redox activity of $PM_{2.5}$ from different regions, which is driven by the PM source-dependent composition, abundance, and chemistry of redox active substances (e.g., transition metals and organic matter).

Figures 3b and S4b show that the air sample volume-specific yields of total RS (H_2O_2+radicals) increase as $PM_{2.5}$ concentrations increase, reflecting a higher RS formation in per cubic meter of polluted urban air. Specifically, the relative air sample volume-specific yields of H_2O_2 (i.e., $[H_2O_2]/([H_2O_2]+[radicals])$), ordered from lowest to highest are: 78% (Hyytiälä) > 91% (Mainz) > 97% (Beijing), whereas the relative air sample volume-specific radical yields (i.e., $[radicals]/([H_2O_2]+[radicals])$) are in the reverse order of 22% > 9% > 3%. The relatively stable H_2O_2 becomes increasingly important for the reactivity of ambient $PM_{2.5}$ compared to the more reactive radicals when transitioning from clean to polluted conditions. Due to its stability, H_2O_2 has been found previously to dominate the concentrations of RS formed by $PM_{2.5}$ in liquid phase with the presence of antioxidants but absence of spin traps (Lakey et al., 2016;Tong et al., 2018). This study shows a time integral concentration rather than the RS concentration taking into account the different lifetimes and evolution pathways of radicals and H_2O_2. H_2O_2 still constitutes the biggest fraction of RS detected. Of note, the EPR method may not detect all radicals produced but rather a fraction that is trapped with BMPO before undergoing other radical termination reactions. It is also notable that we measured the RS yields of PM from three different areas. Further measurements of PM from more locations

may shift the trend of the RS yields in Figure 3 by a certain degree, the extent of which warranty follow-up studies.

3.3 Correlation of radical yield with chemical composition of ambient $PM_{2.5}$

Figure 4 shows how the relative fractions (RF) of C-centered radicals and $^{\bullet}OH$ in aqueous extracts of ambient $PM_{2.5}$ are correlated with the abundance of HOMs, aromatic compounds, and water-soluble transition metals. Figure 4a shows that the relative abundance of HOMs exhibits a positive correlation with the RF of C-centered radicals, whereas a negative correlation with the RF of $^{\bullet}OH$. The relative abundance of HOMs, ordered from lowest to highest are: ~0.2% (Beijing) < ~6% (Mainz) < ~10% (Hyytiälä) (Tong et al., 2019), and the RF of C-centered radicals is in the same order of 39% < 46% < 66%, but the RF of $^{\bullet}OH$ are in the reverse order of 53% > 38% > 21%. The higher RF of C-centered radicals formed by $PM_{2.5}$ from less-polluted air is in the same trend as the total mass-specific radical yield of $PM_{2.5}$ from these sites (Figure 3a), confirming previous results that peroxide-containing HOMs may play an important role in organic radical formation (Tong et al., 2016a;Tong et al., 2019).

In contrast to HOMs, the relative abundance of aromatic compounds in $PM_{2.5}$ is higher in polluted urban air compared to clean forest: ~0.2% (Hyytiälä) < ~2% (Mainz) < ~16% (Beijing) (Figure 4b), causing a positive correlation with the RF of $^{\bullet}OH$, but a negative correlation with the RF of C-centered radicals. The higher relative abundance of particulate aromatics in Beijing compared to Hyytiälä can be attributed to the stronger anthropogenic emissions (e.g., from traffic) at the polluted urban site (Jimenez et al., 2009;Zhang and Tao, 2009;Elser et al., 2016;An et al., 2019). The chemistry of oxygenated aromatic-containing substances, such as quinones and semiquinones, may enhance the conversion of other RS (e.g., $O_2^{\bullet-}$) into $^{\bullet}OH$ due to redox cycling and interaction with water (Chung et al., 2006;Khachatryan et al., 2011;Fan et al., 2016).

Similar to the aromatics, the transition metal abundances exhibit a positive correlation with the RF of $^{\bullet}OH$, but a negative correlation with the RF of C-centered radicals (Figure 4c). The abundance of water-soluble transition metals in $PM_{2.5}$ from different locations, ordered from lowest to highest are: 13.4

(Hyytiälä) < 19.6 (Mainz) < 27.8 (Beijing) pmol μg^{-1}, and the RF of $^{\bullet}OH$ is in the same order of 21% < 38% < 53%, whereas the relative fraction of C-centered radicals is in the reverse order of 66% > 46% > 39%. The consistently higher abundance of water-soluble transition metals and RF of $^{\bullet}OH$ of urban $PM_{2.5}$ may reflect the importance of Fenton-like reactions in radical formation in polluted air, as H_2O_2 and hydroperoxides can be efficiently converted into $^{\bullet}OH$. Moreover, several studies have reported that metal-organic interactions may alter the oxidative potential and RS yield of PM under atmospheric and physiological conditions (Zuo and Hoigne, 1992;Singh and Gupta, 2016;Cheng et al., 2017;Wang et al., 2018b;Wei et al., 2019;Lin and Yu, 2020). Thus, investigations on the radical chemistry of transition metals strongly benefit from determination of organic aerosols to illuminate the mechanism of RS formation. Finally, additional measurements of $PM_{2.5}$ from more locations may shift the correlation of radical yields and abundances of transition metals and organic matter by a certain degree, the extent of which also warranty follow-up studies.

3.4 Radical yield of laboratory-generated SOA

To investigate the influence of biogenic-anthropogenic organic matter interaction on the formation of aqueous radicals, we measured the radical yield of SOA generated from oxidation of mixed naphthalene and β-pinene precursors. Figure 5a shows that the mass-specific radical yields of SOA decrease with increasing relative concentrations of naphthalene (i.e., [naphthalene]/([naphthalene]+[β-pinene])). As the relative concentration of naphthalene is increased from 0 to 9, 23, and 38%, the radical yields of SOA decrease in the order of ~8.4 > ~3.0 > ~2.3 > ~1.9 pmol μg^{-1}. This is because the naphthalene SOA has a lower radical yield than β-pinene SOA with the same mass concentration in water extracts (Tong et al., 2016a;Tong et al., 2017;Tong et al., 2018;Tong et al., 2019). Moreover, the mass-specific radical yield of β-pinene SOA in Figure 5a is the mean value of SOA from ~1 ppm and ~2.5 ppm of β-pinene (see Sect. 2.3). Therein the SOA from ~2.5 ppm β-pinene exhibits higher radical yield (11.5 pmol μg^{-1}) than the SOA generated from ~1 ppm β-pinene (4.5 pmol μg^{-1}), which may be associated with the increasing partition of oligomers into the particle phase with higher starting concentration of β-pinene (Kourtchev et al., 2016).

Some oligomers contain peroxide functional groups accounting for a major fraction of HOMs (Krapf et al., 2016). The radical yield of naphthalene SOA in Figure 5 is the average yields of SOA formed by the oxidation of ~0.2 ppm and ~0.6 ppm naphthalene (see section 2.3), respectively. Therein the radical yield of SOA from ~0.2 ppm naphthalene (1.1 pmol μg^{-1}) is slightly higher than the SOA from ~0.6 ppm naphthalene (0.8 pmol μg^{-1}), agreeing with the finding of enhanced oxidative potential of naphthalene SOA formed under higher oxidant/naphthalene ratio condition (Wang et al., 2018b).

Figure 5b shows that β-pinene SOA mainly generates $^{\bullet}OH$ (~86%), whereas the mixed precursor SOA and naphthalene SOA mainly generate $O_2^{\bullet-}$ (60-77%) and C-centered radicals (18-34%), which is in line with our previous findings (Tong et al., 2016a;Tong et al., 2018;Tong et al., 2019). The much lower RF of $^{\bullet}OH$ formed by mixed precursor SOA (< 10%) may mainly be due to its lower abundance of peroxide-containing HOMs. It is notable that $PM_{2.5}$ from polluted Beijing contains substantial amount of aromatics (Figure 4b), but mainly generates $^{\bullet}OH$ upon interaction with water, which seems to contradict our finding that naphthalene SOA generates $^{\bullet}OH$ only to a small extent. This may be related to the more complex composition of the ambient PM compared to laboratory-generated SOA. For example, conversion of $O_2^{\bullet-}$ to $^{\bullet}OH$, H_2O_2, and O_2 by transition metals or other redox-active PM constituents through Haber-Weiss reactions or other related redox chemistry (Kehrer, 2000;Tong et al., 2016a) is expected to occur in ambient samples, but would not be observed in laboratory-generated SOA that does not contain significant fractions of transition metals.

3.5 Radical yield of surrogate mixtures comprising transition metals, CHP, HA, FA and H_2O_2

Figure 6a shows the concentration of radicals formed in aqueous mixtures comprising 0-25 μM cumene hydroperoxide (CHP), 43 μM Fe^{2+}, 3 μM Cu^{2+}, 4 μg mL^{-1} humic acid (HA) and 7 μM H_2O_2, with mixtures containing 0, 5, and 25 μM CHP to be treated as surrogates of redox-active constituents in PM from Beijing, Mainz, and Hyytiälä. As the concentration of CHP is increased from 0 to 25 μM, the total concentration of detectable radicals increases from 0.4 to 2.8 μM, with the relative fractions (RF) of C-centered radicals increase from 1% to 30%, whereas the RF of $^{\bullet}OH$ and O-centered organic radicals decreases from 72% to

403 60% and from ~23% to ~8% (Figure 6b), respectively. The higher RF of C-centered radicals but lower RF
404 of •OH formed at higher concentration of CHP resembles the radical yield of ambient fine PM from cleaner
405 areas (Figure 2b), which contains a large fraction of HOMs (Tong et al., 2019). Moreover, Figure S5 shows
406 that adding 75, 100, 150, 200, and 300 μM H_2O_2 significantly and linearly (R^2=0.95) elevates the •OH
407 concentration in aqueous mixtures comprising CHP, Fe^{2+}, HA, and H_2O_2. Thus, the higher RF of •OH in
408 surrogate mixtures (Figure 6b) compared with ambient PM extracts (Figure 2b) may be due to the choice
409 of a slightly higher concentration of H_2O_2 in the surrogate mixture (7 μM, see SI).
410 To compare the Fenton-like reactions initiated by different transition metal ions related to ambient $PM_{2.5}$,
411 we measured the absolute and relative racial yields of aqueous mixtures containing CHP and different
412 transition metal species, such as Fe^{2+}, Cu^{2+}, Mn^{2+}, or Ni^{2+}. We found that Fe^{2+} is most efficient in initiating
413 Fenton-like reactions (Deguillaume et al., 2005) and the BMPO-radical adduct concentrations varied along
414 the reaction time (Figure S6). Of note, the abundance, chemical composition, and physicochemical
415 properties of the redox-active constituents in ambient PM (e.g., transition metals and organic matter) can
416 be different from the surrogate mixtures, causing partially different radical yields between surrogate
417 mixtures and ambient $PM_{2.5}$ (e.g., less comparable RF of •OH than the RF of C-centered radicals), which
418 warrants follow-up studies. To simplify the discussion, we only show the radical yields as mean values
419 within ~25 minutes of extraction and measurement.
420 To assess the influence of humic acid on Fenton-like reactions, we measured the radical yields of
421 mixtures comprising 100 μM CHP, 300 μM Fe^{2+}, and 0-180 μg mL^{-1} HA. As the concentration of HA is
422 increased from 0 to 36 μg mL^{-1}, the concentration of total formed radicals decreased by ~52% from 15.5 to
423 7.4 μM (Figure 6c). This may be associated with the following properties of HA. First, HA exhibits
424 pronounced iron binding capacity of 32 nmol Fe per milligram of HA, preferentially toward Fe^{3+} rather than
425 Fe^{2+} (Laglera and van den Berg, 2009;Scheinhardt et al., 2013). Thus, HA may interfere in the redox cycling
426 of Fe^{2+} and Fe^{3+} by chelating them. The lower concentration of free iron ions may prevent the formation
427 of radicals via Fenton-like reactions. Second, humic substances have been found to exhibit antioxidant

properties (Aeschbacher et al., 2012), thus the HA used for Figure 6c may act as an RS scavenger, therefore terminating radical processes and reducing the overall radical concentration. As the HA concentration is increased further from 36 to 180 μg mL^{-1}, the radical concentration is reduced slightly, by less than 20%. This plateau of radical concentration is accompanied by an increasing RF of C-centered radicals (Figure 6d), indicating that HA may also be involved in more complex radical chemistry with $O_2^{\bullet-}$, $^{\bullet}OH$, or oxygen-centered organic radicals enhancing carbon-centered radical formation (Shi et al., 2020). In fact, the RF of C-centered radicals steeply increases from ~19% to ~94% as the HA concentration is increased from 0 to 180 μg mL^{-1}, whereas the RF of $O_2^{\bullet-}$ and $^{\bullet}OH$ decreases from ~59% and ~21% to ~3%. The higher RF of C-centered radicals but lower RF of $O_2^{\bullet-}$ and $^{\bullet}OH$ at higher concentration of HA may be induced by the reactions of HA with $O_2^{\bullet-}$ and $^{\bullet}OH$. The RF of O-centered organic radicals does not exhibit a consistent trend and varies within the range of 5-20%. Moreover, we found that the reaction between HA and CHP (in the absence of Fe ions) produces only a negligible amount of radicals (not shown), which indicates that HA may mainly influence the radical formation upon interaction with iron ions or radicals formed by Fenton-like reactions, but does not form prominent amount of radicals by reactions with CHP or through the decomposition of CHP at the applied concentrations.

Fulvic acid (FA) is another kind of typical atmospheric humic-like substances exerting metal chelating activity (Graber and Rudich, 2006;Tang et al., 2014). Thus, we also measured the radical yields of the mixtures comprising CHP, transition metals, and FA. As shown in Figure 6e, the concentration of radicals formed by mixtures comprising 100 μM CHP, 300 μM Fe^{2+}, and FA decreases by ~10% as the concentration of FA is increased from 6 to 36 μg mL^{-1}. Therein the $O_2^{\bullet-}$ is the dominant radial species, accounting for > 59% of totally formed radicals (Figure 6f). The $O_2^{\bullet-}$ may be generated via multiple redox reaction pathways such as oxidation of Fe^{2+} or decomposition of organic peroxy radicals (Chevallier et al., 2004). Figure 6f also shows that RF of $^{\bullet}OH$, $O_2^{\bullet-}$, C- and O-centered organic radicals varies slightly, which is different from the decreasing radical yield by Fenton-like reaction system containing HA (Figure 6c), but agreeing with the lower capacity of FA (16.7±2.0 nmol mg^{-1}) than HA (32.0±2.2 nmol mg^{-1}) in binding

Fe(III) (Laglera and van den Berg, 2009). As the concentration of FA is increased further to 12 μg mL^{-1}, the observed radical concentration in aqueous mixtures of CHP+Fe^{2+}+FA decreases significantly to ~9.6 μM, which may mainly be associated with the formation of Fe-FA complexes and the radical scavenging effect of FA as discussed for HA above (Wang et al., 1996;Scheinhardt et al., 2013;Yang et al., 2017). During this process, the RF of C-centered radicals increases for 3-fold to be ~28%, indicating that FA may also be oxidized by different types of oxidants to form C-centered radicals (Gonzalez et al., 2017), similar to HA in Figure 6c. As the concentration of FA is increased further to 180 μg mL^{-1}, the concentration of totally formed radicals decreases further to 7.6 μM, the RF of C-centered radicals increases further to ~36%, whereas the RF of •OH and O-centered organic radicals decreases significantly to 4-5% and below the detecting limit, respectively (Figure 6f). Moreover, the Figure S7 indicates that the RF of different radicals formed by mixtures comprising CHP, Cu^{2+} and FA exhibited a different trend from the mixtures of CHP, Fe^{2+}, and FA, indicating that FA might influence the radical formation by Cu^{2+} initiated Fenton-like reactions in a efficiency different from the Fe^{2+} initiated Fenton-like reactions.

4 Conclusions and implications

In this study, we found that $PM_{2.5}$ levels exhibit a negative correlation with the mass-specific radical yields, but a weak positive correlation with the H_2O_2 yields. We also found that the mass-specific concentration of transition metals and relative abundance of aromatic compounds are higher in the urban air than the remote forest, in the order of Hyytiälä < Mainz < Beijing. The relative fractions (RF) of •OH formed by different source $PM_{2.5}$ in water is in the same order as the relative abundances of transition metals and aromatics, indicating that urban fine PM favors the formation of OH radicals upon redox chemistry of transition metals, aromatics, or transition metal-aromatic interactions in water. The relative abundance of highly oxygenated organic molecules (HOMs) exhibits a reverse trend compared to aromatics and transition metals, but is in a positive correlation with the RF of C-centered radicals, confirming the strong association of HOMs with organic radical formation by $PM_{2.5}$ in water (Tong et al., 2019).

We also measured the radical yield of laboratory-generated SOA from mixing the biogenic SOA precursor β-pinene and the anthropogenic SOA precursor naphthalene. We found that the relative fractions of naphthalene SOA of the totally formed SOA significantly influence the amount and types of radicals formed by the mixed precursor SOA in water with •OH radicals dominating pure β-pinene SOA, Carbon-centered radicals becoming increasingly dominant as the fraction of naphthalene increases. To get insights into the Fenton-like reactions in aqueous extracts of ambient $PM_{2.5}$, we investigated the radical formation by surrogate mixtures comprising cumene hydroperoxide, transition metals, water-soluble humic acid (HA) or fulvic acid (FA), and H_2O_2. We found that HA and FA exhibit different radical scavenging and antioxidant activity in suppressing the radical formation from Fenton-like reactions.

The synthetic application of ambient $PM_{2.5}$ characterization, chamber simulation, and surrogate mixture measurement in this study provides a novel approach to investigate the RS chemistry of atmospheric particles. The direct analysis of ambient $PM_{2.5}$ enables us to find and quantify the key component (e.g., HOMs, aromatics, or transition metals) of $PM_{2.5}$ that may influence its reactivity. The investigation of laboratory-generated SOA enables us to assess the influence of anthropogenic-biogenic organic component interactions on the radical formation by ambient PM. The measurement of surrogate or aqueous mixtures of model substances (transition metals, CHP, HA, FA, and H_2O_2) enables us to clarify the role of individual redox active compound as well as their interplays in the radical chemistry of PM, including Fenton-like reactions, transition metal-organic interactions, or subsequent chain reactions. Based on this systematic analysis, we quantitatively compared the RS formation mechanism of particulate matter from air ranging from clean to heavily polluted areas. The higher relative amount of detected radicals and H_2O_2 formed by urban $PM_{2.5}$ can be seen as a measure of higher potential oxidative damage caused by air pollutants in the epithelial lining fluid of the human respiratory tract. These newly achieved insights enable a better understanding of the influence of biogenic and anthropogenic emissions on atmospheric chemistry, air quality, and public health in the Anthropocene (Pöschl and Shiraiwa, 2015;Cheng et al., 2016;Shiraiwa et al., 2017). Finally, the composition and concentration of organic molecules have been found to influence its role in transition metal-initiated radical chemistry. For instance, carboxylic acids enhance the oxidative

potential of transition metals, whereas the imidazoles suppress it (Lin and Yu, 2020). Moreover, low concentration of oxalate forms mono-complexes with Fe^{2+}, but high concentration of oxalate scavenges OH radicals (Fang et al., 2020). Thus, the role of different humic-like substances component in Fenton-like reactions and its impact on aerosol reactivity have not been fully addressed, which warrants follow up studies.

References

Aeschbacher, M., Graf, C., Schwarzenbach, R. P., and Sander, M.: Antioxidant properties of humic substances, Environ. Sci. Technol. , 46, 4916-4925, 2012.

An, Z., Huang, R.-J., Zhang, R., Tie, X., Li, G., Cao, J., Zhou, W., Shi, Z., Han, Y., and Gu, Z.: Severe haze in Northern China: A synergy of anthropogenic emissions and atmospheric processes, P. Natl. Acad. Sci. USA, 116, 8657-8666, 2019.

Anglada, J. M., Martins-Costa, M., Francisco, J. S., and Ruiz-Lopez, M. F.: Interconnection of reactive oxygen species chemistry across the interfaces of atmospheric, environmental, and biological processes, Acc. Chem. Res. , 48, 575-583, 2015.

Arangio, A. M., Tong, H., Socorro, J., Pöschl, U., and Shiraiwa, M.: Quantification of environmentally persistent free radicals and reactive oxygen species in atmospheric aerosol particles, Atmos. Chem. Phys., 16, 13105-13119, 2016.

Arellanes, C., Paulson, S. E., Fine, P. M., and Sioutas, C.: Exceeding of Henry's law by hydrogen peroxide associated with urban aerosols, Environ. Sci. Technol., 40, 4859-4866, 2006.

Badali, K., Zhou, S., Aljawhary, D., Antiñolo, M., Chen, W., Lok, A., Mungall, E., Wong, J., Zhao, R., and Abbatt, J.: Formation of hydroxyl radicals from photolysis of secondary organic aerosol material, Atmos. Chem. Phys., 15, 7831-7840, 2015.

Bates, J. T., Weber, R. J., Abrams, J., Verma, V., Fang, T., Klein, M., Strickland, M. J., Sarnat, S. E., Chang, H. H., and Mulholland, J. A.: Reactive oxygen species generation linked to sources of atmospheric particulate matter and cardiorespiratory effects, Environ. Sci. Technol., 49, 13605-13612, 2015.

Bates, J. T., Fang, T., Verma, V., Zeng, L., Weber, R. J., Tolbert, P. E., Abrams, J. Y., Sarnat, S. E., Klein, M., Mulholland, J. A., and Russell, A. G.: Review of acellular assays of ambient particulate matter oxidative potential: Methods and relationships with composition, sources, and health effects, Environ. Sci. Technol. , 53, 4003-4019, 2019.

Baumgartner, J., Zhang, Y., Schauer, J. J., Huang, W., Wang, Y., and Ezzati, M.: Highway proximity and black carbon from cookstoves as a risk factor for higher blood pressure in rural China, P. Natl. Acad. Sci. USA, 111, 13229-13234, 2014.

Catrouillet, C., Davranche, M., Dia, A., Bouhnik-Le Coz, M., Marsac, R., Pourret, O., and Gruau, G.: Geochemical modeling of Fe (II) binding to humic and fulvic acids, Chem. Geol., 372, 109-118, 2014.

Charrier, J., and Anastasio, C.: On dithiothreitol (DTT) as a measure of oxidative potential for ambient particles: evidence for the importance of soluble transition metals, Atmos. Chem. Phys., 12, 9321–9333, 2012.

Charrier, J. G., McFall, A. S., Richards-Henderson, N. K., and Anastasio, C.: Hydrogen peroxide formation in a surrogate lung fluid by transition metals and quinones present in particulate matter, Environ. Sci. Technol., 48, 7010-7017, 2014.

Charrier, J. G., and Anastasio, C.: Rates of hydroxyl radical production from transition metals and quinones in a surrogate lung fluid, Environ. Sci. Technol., 49, 9317-9325, 2015.

Chen, X., Hopke, P. K., and Carter, W. P.: Secondary organic aerosol from ozonolysis of biogenic volatile organic compounds: chamber studies of particle and reactive oxygen species formation, Environ. Sci. Technol., 45, 276-282, 2010.

Cheng, C., Li, M., Chan, C. K., Tong, H., Chen, C., Chen, D., Wu, D., Li, L., Wu, C., and Cheng, P.: Mixing state of oxalic acid containing particles in the rural area of Pearl River Delta, China: implications for the formation mechanism of oxalic acid, Atmos. Chem. Phys., 17, 9519-9533, 2017.

Cheng, Y., Zheng, G., Wei, C., Mu, Q., Zheng, B., Wang, Z., Gao, M., Zhang, Q., He, K., and Carmichael, G.: Reactive nitrogen chemistry in aerosol water as a source of sulfate during haze events in China, Sci. Adv., 2, e1601530, 2016.

Chevallier, E., Jolibois, R. D., Meunier, N., Carlier, P., and Monod, A.: "Fenton-like" reactions of methylhydroperoxide and ethylhydroperoxide with Fe2+ in liquid aerosols under tropospheric conditions, Atmos. Environ., 38, 921-933, 2004.

Chowdhury, P. H., He, Q., Carmieli, R., Li, C., Rudich, Y., and Pardo, M.: Connecting the Oxidative Potential of Secondary Organic Aerosols with Reactive Oxygen Species in Exposed Lung Cells, Environ. Sci. Technol., 53, 13949-13958, 2019.

Chung, M. Y., Lazaro, R. A., Lim, D., Jackson, J., Lyon, J., Rendulic, D., and Hasson, A. S.: Aerosol-borne quinones and reactive oxygen species generation by particulate matter extracts, Environ. Sci. Technol. , 40, 4880-4886, 2006.

Crobeddu, B., Baudrimont, I., Deweirdt, J., Sciare, J., Badel, A., Camproux, A.-C., Bui, L. C., and Baeza-Squiban, A.: Lung Antioxidant Depletion: A Predictive Indicator of Cellular Stress Induced by Ambient Fine Particles, Environ. Sci. Technol. , 54, 2360-2369, 2020.

Cui, Y., Xie, X., Jia, F., He, J., Li, Z., Fu, M., Hao, H., Liu, Y., Liu, J. Z., and Cowan, P. J.: Ambient fine particulate matter induces apoptosis of endothelial progenitor cells through reactive oxygen species formation, Cell Physiol. Biochem., 35, 353-363, 2015.

De Araujo, M., De M. Carneiro, J., and Taranto, A.: Solvent effects on the relative stability of radicals derived from artemisinin: DFT study using the PCM/COSMO approach, Int. J. Quantum. Chem., 106, 2804-2810, 2006.

572 Deguillaume, L., Leriche, M., Desboeufs, K., Mailhot, G., George, C., and Chaumerliac, N.: Transition
573 metals in atmospheric liquid phases: Sources, reactivity, and sensitive parameters, Chem. Rev., 105, 3388-
574 3431, 2005.
575 Donaldson, D., and Valsaraj, K. T.: Adsorption and reaction of trace gas-phase organic compounds on
576 atmospheric water film surfaces: A critical review, Environ. Sci. Technol. , 44, 865-873, 2010.
577 Ehn, M., Thornton, J. A., Kleist, E., Sipilä, M., Junninen, H., Pullinen, I., Springer, M., Rubach, F.,
578 Tillmann, R., Lee, B., and Lopez-Hilfiker, F.: A large source of low-volatility secondary organic aerosol,
579 Nature, 506, 476, 2014.
580 Elser, M., Huang, R.-J., Wolf, R., Slowik, J. G., Wang, Q., Canonaco, F., Li, G., Bozzetti, C., Daellenbach,
581 K. R., and Huang, Y.: New insights into PM 2.5 chemical composition and sources in two major cities in
582 China during extreme haze events using aerosol mass spectrometry, Atmos. Chem. Phys., 16, 3207-3225,
583 2016.
584 Enami, S., Sakamoto, Y., and Colussi, A. J.: Fenton chemistry at aqueous interfaces, Proc. Natl. Acad. Sci.
585 U.S.A, 111, 623-628, 2014.
586 Ervens, B., Turpin, B., and Weber, R.: Secondary organic aerosol formation in cloud droplets and aqueous
587 particles (aqSOA): a review of laboratory, field and model studies, Atmos. Chem. Phys., 11, 11069-11102,
588 2011.
589 Fan, X., Wei, S., Zhu, M., Song, J., and Peng, P. a.: Comprehensive characterization of humic-like
590 substances in smoke PM 2.5 emitted from the combustion of biomass materials and fossil fuels, Atmos.
591 Chem. Phys., 16, 13321-13340, 2016.
592 Fang, T., Guo, H., Verma, V., Peltier, R., and Weber, R.: PM 2.5 water-soluble elements in the southeastern
593 United States: automated analytical method development, spatiotemporal distributions, source
594 apportionment, and implications for heath studies, Atmos. Chem. Phys., 15, 11667-11682, 2015.
595 Fang, T., Verma, V., Bates, J. T., Abrams, J., Klein, M., Strickland, M. J., Sarnat, S. E., Chang, H. H.,
596 Mulholland, J. A., and Tolbert, P. E.: Oxidative potential of ambient water-soluble PM 2.5 in the
597 southeastern United States: contrasts in sources and health associations between ascorbic acid (AA) and
598 dithiothreitol (DTT) assays, Atmos. Chem. Phys., 16, 3865-3879, 2016.
599 Fang, T., Lakey, P. S. J., Weber, R. J., and Shiraiwa, M.: Oxidative Potential of Particulate Matter and
600 Generation of Reactive Oxygen Species in Epithelial Lining Fluid, Environ. Sci. Technol., 53,
601 12784−12792, 2019.
602 Fang, T., Lakey, P. S. J., Rivera-Rios, J. C., Keutsch, F. N., and Shiraiwa, M.: Aqueous-Phase
603 Decomposition of Isoprene Hydroxy Hydroperoxide and Hydroxyl Radical Formation by Fenton-Like
604 Reactions with Iron Ions, J. Phys. Chem. A 124, 5230−5236, 2020.

Gehling, W., Khachatryan, L., and Dellinger, B.: Hydroxyl radical generation from environmentally persistent free radicals (EPFRs) in PM2. 5, Environ. Sci. Technol., 48, 4266-4272, 2014.

Gilardoni, S., Massoli, P., Paglione, M., Giulianelli, L., Carbone, C., Rinaldi, M., Decesari, S., Sandrini, S., Costabile, F., and Gobbi, G. P.: Direct observation of aqueous secondary organic aerosol from biomass-burning emissions, P. Natl. Acad. Sci. USA, 113, 10013-10018, 2016.

Gligorovski, S., Strekowski, R., Barbati, S., and Vione, D.: Environmental implications of hydroxyl radicals (• OH), Chem. Rev., 115, 13051-13092, 2015.

Goldstein, A. H., Koven, C. D., Heald, C. L., and Fung, I. Y.: Biogenic carbon and anthropogenic pollutants combine to form a cooling haze over the southeastern United States, P. Natl. Acad. Sci. USA, 106, 8835-8840, 2009.

Gonzalez, D. H., Cala, C. K., Peng, Q., and Paulson, S. E.: HULIS enhancement of hydroxyl radical formation from Fe (II): Kinetics of fulvic acid–Fe (II) complexes in the presence of lung antioxidants, Environ. Sci. Technol., 51, 7676-7685, 2017.

Graber, E., and Rudich, Y.: Atmospheric HULIS: How humic-like are they? A comprehensive and critical review, Atmos. Chem. Phys., 6, 729-753, 2006.

Hakola, H., Hellén, H., Hemmilä, M., Rinne, J., and Kulmala, M.: In situ measurements of volatile organic compounds in a boreal forest, Atmos. Chem. Phys., 12, 11665-11678, 2012.

Halliwell, B., and Whiteman, M.: Measuring reactive species and oxidative damage in vivo and in cell culture: how should you do it and what do the results mean?, Br. J. Pharmacol., 142, 231-255, 2004.

Hari, P., and Kulmala, M.: Station for Measuring EcosystemsAtmosphere Relations (SMEAR II), Boreal Env. Res., 10, 315-322, 2005.

Hoyle, C. R., Boy, M., Donahue, N. M., Fry, J. L., Glasius, M., Guenther, A., Hallar, A. G., Huff Hartz, K., Petters, M. D., and Petäjä, T.: A review of the anthropogenic influence on biogenic secondary organic aerosol, Atmos. Chem. Phys., 11, 321-343, 2011.

Huang, G., Liu, Y., Shao, M., Li, Y., Chen, Q., Zheng, Y., Wu, Z., Liu, Y., Wu, Y., Hu, M., Li, X., Lu, S., Wang, C., Liu, J., Zheng, M., and Zhu, T.: Potentially Important Contribution of Gas-Phase Oxidation of Naphthalene and Methylnaphthalene to Secondary Organic Aerosol during Haze Events in Beijing, Environ. Sci. Technol. , 53, 1235-1244, 2019.

Huang, R.-J., Zhang, Y., Bozzetti, C., Ho, K.-F., Cao, J.-J., Han, Y., Daellenbach, K. R., Slowik, J. G., Platt, S. M., and Canonaco, F.: High secondary aerosol contribution to particulate pollution during haze events in China, Nature, 514, 218, 2014.

Jacob, D. J.: Heterogeneous chemistry and tropospheric ozone, Atmos. Environ., 34, 2131-2159, 2000.

Jimenez, J. L., Canagaratna, M., Donahue, N., Prevot, A., Zhang, Q., Kroll, J. H., DeCarlo, P. F., Allan, J. D., Coe, H., and Ng, N.: Evolution of organic aerosols in the atmosphere, science, 326, 1525-1529, 2009.

Jin, L., Xie, J., Wong, C. K., Chan, S. K., Abbaszade, G. l., Schnelle-Kreis, J. r., Zimmermann, R., Li, J., Zhang, G., and Fu, P.: Contributions of city-specific fine particulate matter (PM2. 5) to differential in vitro oxidative stress and toxicity implications between Beijing and Guangzhou of China, Environ. Sci. Technol. , 53, 2881-2891, 2019.

Kalyanaraman, B., Darley-Usmar, V., Davies, K. J., Dennery, P. A., Forman, H. J., Grisham, M. B., Mann, G. E., Moore, K., Roberts II, L. J., and Ischiropoulos, H.: Measuring reactive oxygen and nitrogen species with fluorescent probes: challenges and limitations, Free Radic. Biol. Med., 52, 1-6, 2012.

Kang, E., Root, M., Toohey, D., and Brune, W. H.: Introducing the concept of potential aerosol mass (PAM), Atmos. Chem. Phys., 7, 5727-5744, 2007.

Kehrer, J. P.: The Haber–Weiss reaction and mechanisms of toxicity, Toxicology, 149, 43-50, 2000.

Khachatryan, L., Vejerano, E., Lomnicki, S., and Dellinger, B.: Environmentally persistent free radicals (EPFRs). 1. Generation of reactive oxygen species in aqueous solutions, Environ. Sci. Technol., 45, 8559-8566, 2011.

Koch, B., and Dittmar, T.: From mass to structure: An aromaticity index for high‐resolution mass data of natural organic matter, Rapid Commun. Mass Spectrom., 20, 926-932, 2006.

Kostić, I., Anđelković, T., Nikolić, R., Bojić, A., Purenović, M., Blagojević, S., and Anđelković, D.: Copper (II) and lead (II) complexation by humic acid and humic-like ligands, J. Serb. Chem. Soc., 76, 1325-1336, 2011.

Kourtchev, I., Giorio, C., Manninen, A., Wilson, E., Mahon, B., Aalto, J., Kajos, M., Venables, D., Ruuskanen, T., and Levula, J.: Enhanced volatile organic compounds emissions and organic aerosol mass increase the oligomer content of atmospheric aerosols, Sci. Rep., 6, 1-9, 2016.

Krapf, M., El Haddad, I., Bruns, E. A., Molteni, U., Daellenbach, K. R., Prévôt, A. S., Baltensperger, U., and Dommen, J.: Labile peroxides in secondary organic aerosol, Chem, 1, 603-616, 2016.

Kuang, X. M., Scott, J. A., da Rocha, G. O., Betha, R., Price, D. J., Russell, L. M., Cocker, D. R., and Paulson, S. E.: Hydroxyl radical formation and soluble trace metal content in particulate matter from renewable diesel and ultra low sulfur diesel in at-sea operations of a research vessel, Aerosol Sci. Technol., 51, 147-158, 2017.

Laakso, L., Hussein, T., Aarnio, P., Komppula, M., Hiltunen, V., Viisanen, Y., and Kulmala, M.: Diurnal and annual characteristics of particle mass and number concentrations in urban, rural and Arctic environments in Finland, Atmos. Environ., 37, 2629-2641, 2003.

Laglera, L. M., and van den Berg, C. M.: Evidence for geochemical control of iron by humic substances in seawater, Limnol. Oceanogr., 54, 610-619, 2009.

Lakey, P. S., Berkemeier, T., Tong, H., Arangio, A. M., Lucas, K., Pöschl, U., and Shiraiwa, M.: Chemical exposure-response relationship between air pollutants and reactive oxygen species in the human respiratory tract, Sci. Rep., 6, 32916, 2016.

Landreman, A. P., Shafer, M. M., Hemming, J. C., Hannigan, M. P., and Schauer, J. J.: A macrophage-based method for the assessment of the reactive oxygen species (ROS) activity of atmospheric particulate matter (PM) and application to routine (daily-24 h) aerosol monitoring studies, Aerosol Sci. Technol., 42, 946-957, 2008.

Lelieveld, J., and Pöschl, U.: Chemists can help to solve the air-pollution health crisis, Nature, 551, 291-293, 2017.

Li, N., Xia, T., and Nel, A. E.: The role of oxidative stress in ambient particulate matter-induced lung diseases and its implications in the toxicity of engineered nanoparticles, Free Radic. Biol. Med., 44, 1689-1699, 2008.

Li, X., Kuang, X. M., Yan, C., Ma, S., Paulson, S. E., Zhu, T., Zhang, Y., and Zheng, M.: Oxidative potential by PM2. 5 in the North China Plain: generation of hydroxyl radical, Environ. Sci. Technol. , 53, 512-520, 2018.

Lin, M., and Yu, J. Z.: Assessment of interactions between transition metals and atmospheric organics: Ascorbic Acid Depletion and Hydroxyl Radical Formation in Organic-metal Mixtures, Environ. Sci. Technol. , 54, 1431−1442, 2020.

Lin, P., and Yu, J. Z.: Generation of reactive oxygen species mediated by humic-like substances in atmospheric aerosols, Environ. Sci. Technol. , 45, 10362-10368, 2011.

Lin, Y., Ma, Y., Qiu, X., Li, R., Fang, Y., Wang, J., Zhu, Y., and Hu, D.: Sources, transformation, and health implications of PAHs and their nitrated, hydroxylated, and oxygenated derivatives in PM2. 5 in Beijing, J. Geophys. Res. Atmos., 120, 7219-7228, 2015.

Liu, F., Saavedra, M. G., Champion, J. A., Griendling, K. K., and Ng, N. L.: Prominent Contribution of Hydrogen Peroxide to Intracellular Reactive Oxygen Species Generated upon Exposure to Naphthalene Secondary Organic Aerosols, Environ. Sci. Technol. Lett., 7, 171-177, 2020.

Liu, Q., Baumgartner, J., Zhang, Y., Liu, Y., Sun, Y., and Zhang, M.: Oxidative potential and inflammatory impacts of source apportioned ambient air pollution in Beijing, Environ. Sci. Technol. , 48, 12920-12929, 2014.

Ma, Y., Cheng, Y., Qiu, X., Cao, G., Fang, Y., Wang, J., Zhu, T., Yu, J., and Hu, D.: Sources and oxidative potential of water-soluble humic-like substances (HULIS WS) in fine particulate matter (PM 2.5) in Beijing, Atmos. Chem. Phys., 18, 5607-5617, 2018.

Maenhaut, W., Nava, S., Lucarelli, F., Wang, W., Chi, X., and Kulmala, M.: Chemical composition, impact from biomass burning, and mass closure for PM2. 5 and PM10 aerosols at Hyytiälä, Finland, in summer 2007, X-Ray Spectrom., 40, 168-171, 2011.

Molina, C., Toro, R., Manzano, C., Canepari, S., Massimi, L., and Leiva-Guzmán, M. A.: Airborne aerosols and human health: Leapfrogging from mass concentration to oxidative potential, Atmosphere, 11, 917, 2020.

Møller, P., Jacobsen, N. R., Folkmann, J. K., Danielsen, P. H., Mikkelsen, L., Hemmingsen, J. G., Vesterdal, L. K., Forchhammer, L., Wallin, H., and Loft, S.: Role of oxidative damage in toxicity of particulates, Free Radic. Res., 44, 1-46, 2010.

Nel, A.: Air pollution-related illness: effects of particles, Science, 308, 804-806, 2005.

Ohyama, M., Otake, T., Adachi, S., Kobayashi, T., and Morinaga, K.: A comparison of the production of reactive oxygen species by suspended particulate matter and diesel exhaust particles with macrophages, Inhal. Toxicol., 19, 157-160, 2007.

Page, S. E., Sander, M., Arnold, W. A., and McNeill, K.: Hydroxyl radical formation upon oxidation of reduced humic acids by oxygen in the dark, Environ. Sci. Technol. , 46, 1590-1597, 2012.

Park, J., Park, E. H., Schauer, J. J., Yi, S.-M., and Heo, J.: Reactive oxygen species (ROS) activity of ambient fine particles (PM2. 5) measured in Seoul, Korea, Environ. Int., 117, 276-283, 2018.

Pöschl, U., and Shiraiwa, M.: Multiphase chemistry at the atmosphere–biosphere interface influencing climate and public health in the anthropocene, Chem. Rev., 115, 4440-4475, 2015.

Pye, H. O., D'Ambro, E. L., Lee, B. H., Schobesberger, S., Takeuchi, M., Zhao, Y., Lopez-Hilfiker, F., Liu, J., Shilling, J. E., and Xing, J.: Anthropogenic enhancements to production of highly oxygenated molecules from autoxidation, P. Natl. Acad. Sci. USA, 116, 6641-6646, 2019.

Qiu, J., Liang, Z., Tonokura, K., Colussi, A. J., and Enami, S.: Stability of Monoterpene-Derived α-Hydroxyalkyl-Hydroperoxides in Aqueous Organic Media: Relevance to the Fate of Hydroperoxides in Aerosol Particle Phases, Environ. Sci. Technol., 54, 3890-3899, 2020.

Qu, J., Li, Y., Zhong, W., Gao, P., and Hu, C.: Recent developments in the role of reactive oxygen species in allergic asthma, J. Thorac. Dis., 9, E32, 2017.

Rao, X., Zhong, J., Brook, R. D., and Rajagopalan, S.: Effect of particulate matter air pollution on cardiovascular oxidative stress pathways, Antioxid. Redox. Signal., 28, 797-818, 2018.

Reinmuth-Selzle, K., Kampf, C. J., Lucas, K., Lang-Yona, N., Fröhlich-Nowoisky, J., Shiraiwa, M., Lakey, P. S., Lai, S., Liu, F., and Kunert, A. T.: Air pollution and climate change effects on allergies in the anthropocene: abundance, interaction, and modification of allergens and adjuvants, Environ. Sci. Technol. , 51, 4119-4141, 2017.

Scheinhardt, S., Müller, K., Spindler, G., and Herrmann, H.: Complexation of trace metals in size-segregated aerosol particles at nine sites in Germany, Atmos. Environ., 74, 102-109, 2013.

Shi, Y., Dai, Y., Liu, Z., Nie, X., Zhao, S., Zhang, C., and Jia, H.: Light-induced variation in environmentally persistent free radicals and the generation of reactive radical species in humic substances, Front. Environ. Sci. Eng., 14, 1-10, 2020.

Shiraiwa, M., Ueda, K., Pozzer, A., Lammel, G., Kampf, C. J., Fushimi, A., Enami, S., Arangio, A. M., Fröhlich-Nowoisky, J., Fujitani, Y., Furuyama, A., Lakey, P. S. J., Lelieveld, J., Lucas, K., Morino, Y., Pöschl, U., Takahama, S., Takami, A., Tong, H., Weber, B., Yoshino, A., and Sato, K.: Aerosol health effects from molecular to global scales, Environ. Sci. Technol. , 51, 13545-13567, 2017.

Shrivastava, M., Andreae, M. O., Artaxo, P., Barbosa, H. M., Berg, L. K., Brito, J., Ching, J., Easter, R. C., Fan, J., and Fast, J. D.: Urban pollution greatly enhances formation of natural aerosols over the Amazon rainforest, Nat. Commun., 10, 1046, 2019.

Sies, H., Berndt, C., and Jones, D. P.: Oxidative stress, Annu. Rev. Biochem., 86, 715-748, 2017.

Singh, D. K., and Gupta, T.: Role of transition metals with water soluble organic carbon in the formation of secondary organic aerosol and metallo‐organics in PM1 sampled during post monsoon and pre-winter time, J. Aerosol Sci., 94, 56-69, 2016.

Tang, W.-W., Zeng, G.-M., Gong, J.-L., Liang, J., Xu, P., Zhang, C., and Huang, B.-B.: Impact of humic/fulvic acid on the removal of heavy metals from aqueous solutions using nanomaterials: a review, Sci. Total Environ., 468, 1014-1027, 2014.

Tong, H., Arangio, A. M., Lakey, P. S., Berkemeier, T., Liu, F., Kampf, C. J., Brune, W. H., Pöschl, U., and Shiraiwa, M.: Hydroxyl radicals from secondary organic aerosol decomposition in water, Atmos. Chem. Phys., 16, 1761-1771, 2016a.

Tong, H., Kourtchev, I., Pant, P., Keyte, I. J., O'Connor, I. P., Wenger, J. C., Pope, F. D., Harrison, R. M., and Kalberer, M.: Molecular composition of organic aerosols at urban background and road tunnel sites using ultra-high resolution mass spectrometry, Faraday Discuss., 189, 51-68, 2016b.

Tong, H., Lakey, P. S., Arangio, A. M., Socorro, J., Kampf, C. J., Berkemeier, T., Brune, W. H., Pöschl, U., and Shiraiwa, M.: Reactive oxygen species formed in aqueous mixtures of secondary organic aerosols and mineral dust influencing cloud chemistry and public health in the Anthropocene, Faraday Discuss., 200, 251-270, 2017.

Tong, H., Lakey, P. S., Arangio, A. M., Socorro, J., Shen, F., Lucas, K., Brune, W. H., Pöschl, U., and Shiraiwa, M.: Reactive oxygen species formed by secondary organic aerosols in water and surrogate lung fluid, Environ. Sci. Technol. , 52, 11642-11651, 2018.

Tong, H., Zhang, Y., Filippi, A., Wang, T., Li, C., Liu, F., Leppla, D., Kourtchev, I., Wang, K., Keskinen, H.-M., Levula, J. T., Arangio, A. M., Shen, F., Ditas, F., Martin, S. T., Artaxo, P., Godoi, R. H. M.,

Yamamoto, C. I., Souza, R. A. F. d., Huang, R.-J., Berkemeier, T., Wang, Y., Su, H., Cheng, Y., Pope, F. D., Fu, P., Yao, M., Pöhlker, C., Petäjä, T., Kulmala, M., Andreae, M. O., Shiraiwa, M., Pöschl, U., Hoffmann, T., and Kalberer, M.: Radical Formation by Fine Particulate Matter Associated with Highly Oxygenated Molecules, Environ. Sci. Technol. , 53, 12506−12518, 2019.

Tröstl, J., Chuang, W. K., Gordon, H., Heinritzi, M., Yan, C., Molteni, U., Ahlm, L., Frege, C., Bianchi, F., Wagner, R., and Simon, M.: The role of low-volatility organic compounds in initial particle growth in the atmosphere, Nature, 533, 527, 2016.

Tseitlin, M., Eaton, S. S., and Eaton, G. R.: Uncertainty analysis for absorption and first‐derivative electron paramagnetic resonance spectra, Concepts Magn. Reson., Part A, 40, 295-305, 2012.

Valavanidis, A., Fiotakis, K., Bakeas, E., and Vlahogianni, T.: Electron paramagnetic resonance study of the generation of reactive oxygen species catalysed by transition metals and quinoid redox cycling by inhalable ambient particulate matter, Redox. Rep., 10, 37-51, 2005.

Verma, V., Fang, T., Guo, H., King, L., Bates, J., Peltier, R., Edgerton, E., Russell, A., and Weber, R.: Reactive oxygen species associated with water-soluble PM 2.5 in the southeastern United States: spatiotemporal trends and source apportionment, Atmos. Chem. Phys., 14, 12915-12930, 2014.

Verma, V., Fang, T., Xu, L., Peltier, R. E., Russell, A. G., Ng, N. L., and Weber, R. J.: Organic aerosols associated with the generation of reactive oxygen species (ROS) by water-soluble PM2. 5, Environ. Sci. Technol., 49, 4646-4656, 2015.

Wang, C., Wang, Z., Peng, A., Hou, J., and Xin, W.: Interaction between fulvic acids of different origins and active oxygen radicals, Sci. China C Life Sci., 39, 267-275, 1996.

Wang, K., Zhang, Y., Huang, R.-J., Cao, J., and Hoffmann, T.: UHPLC-Orbitrap mass spectrometric characterization of organic aerosol from a central European city (Mainz, Germany) and a Chinese megacity (Beijing), Atmos. Environ., 189, 22-29, 2018a.

Wang, K., Zhang, Y., Huang, R.-J., Wang, M., Ni, H., Kampf, C. J., Cheng, Y., Bilde, M., Glasius, M., and Hoffmann, T.: Molecular characterization and source identification of atmospheric particulate organosulfates using ultrahigh resolution mass spectrometry, Environ. Sci. Technol. , 53, 6192−6202, 2019.

Wang, N., Miller, C. J., Wang, P., and Waite, T. D.: Quantitative determination of trace hydrogen peroxide in the presence of sulfide using the Amplex Red/horseradish peroxidase assay, Anal. Chim. Acta, 963, 61-67, 2017.

Wang, S., Ye, J., Soong, R., Wu, B., Yu, L., Simpson, A. J., and Chan, A. W.: Relationship between chemical composition and oxidative potential of secondary organic aerosol from polycyclic aromatic hydrocarbons, Atmos. Chem. Phys., 18, 3987-4003, 2018b.

Wang, Y., Arellanes, C., Curtis, D. B., and Paulson, S. E.: Probing the source of hydrogen peroxide associated with coarse mode aerosol particles in Southern California, Environ. Sci. Technol. , 44, 4070-4075, 2010.

Wang, Y., Hopke, P. K., Sun, L., Chalupa, D. C., and Utell, M. J.: Laboratory and field testing of an automated atmospheric particle-bound reactive oxygen species sampling-analysis system, J. Toxicol., 2011, 2011a.

Wang, Y., Kim, H., and Paulson, S. E.: Hydrogen peroxide generation from α-and β-pinene and toluene secondary organic aerosols, Atmos. Environ., 45, 3149-3156, 2011b.

Wang, Y., Arellanes, C., and Paulson, S. E.: Hydrogen peroxide associated with ambient fine-mode, diesel, and biodiesel aerosol particles in Southern California, Aerosol Sci. Technol., 46, 394-402, 2012.

Wang, Y., Hu, M., Guo, S., Wang, Y., Zheng, J., Yang, Y., Zhu, W., Tang, R., Li, X., and Liu, Y.: The secondary formation of organosulfates under interactions between biogenic emissions and anthropogenic pollutants in summer in Beijing, Atmos. Chem. Phys., 18, 10693-10713, 2018c.

Wei, J., Yu, H., Wang, Y., and Verma, V.: Complexation of Iron and Copper in Ambient Particulate Matter and Its Effect on the Oxidative Potential Measured in a Surrogate Lung Fluid, Environ. Sci. Technol., 53, 1661-1671, 2019.

Win, M. S., Tian, Z., Zhao, H., Xiao, K., Peng, J., Shang, Y., Wu, M., Xiu, G., Lu, S., and Yonemochi, S.: Atmospheric HULIS and its ability to mediate the reactive oxygen species (ROS): A review, J. Environ. Sci., 71, 13-31, 2018.

Xia, T., Korge, P., Weiss, J. N., Li, N., Venkatesen, M. I., Sioutas, C., and Nel, A.: Quinones and aromatic chemical compounds in particulate matter induce mitochondrial dysfunction: implications for ultrafine particle toxicity, Environ. Health Perspect., 112, 1347-1358, 2004.

Xiong, Q., Yu, H., Wang, R., Wei, J., and Verma, V.: Rethinking dithiothreitol-based particulate matter oxidative potential: measuring dithiothreitol consumption versus reactive oxygen species generation, Environ. Sci. Technol., 51, 6507-6514, 2017.

Xu, L., Guo, H., Boyd, C. M., Klein, M., Bougiatioti, A., Cerully, K. M., Hite, J. R., Isaacman-VanWertz, G., Kreisberg, N. M., and Knote, C.: Effects of anthropogenic emissions on aerosol formation from isoprene and monoterpenes in the southeastern United States, P. Natl. Acad. Sci. USA 112, 37-42, 2015.

Yan, D., Cui, H., Zhu, W., Talbot, A., Zhang, L. G., Sherman, J. H., and Keidar, M.: The strong cell-based hydrogen peroxide generation triggered by cold atmospheric plasma, Sci. Rep., 7, 1-9, 2017.

Yang, R., Su, H., Qu, S., and Wang, X.: Capacity of humic substances to complex with iron at different salinities in the Yangtze River estuary and East China Sea, Sci. Rep., 7, 1381, 2017.

Yassine, M. M., Harir, M., Dabek‐Zlotorzynska, E., and Schmitt‐Kopplin, P.: Structural characterization of organic aerosol using Fourier transform ion cyclotron resonance mass spectrometry: aromaticity equivalent approach, Rapid Commun. Mass Spectrom., 28, 2445-2454, 2014.

Yu, H., Wei, J., Cheng, Y., Subedi, K., and Verma, V.: Synergistic and antagonistic interactions among the particulate matter components in generating reactive oxygen species based on the dithiothreitol assay, Environ. Sci. Technol., 52, 2261-2270, 2018.

Zhang, Y., and Tao, S.: Global atmospheric emission inventory of polycyclic aromatic hydrocarbons (PAHs) for 2004, Atmos. Environ., 43, 812-819, 2009.

Zhao, H., Joseph, J., Zhang, H., Karoui, H., and Kalyanaraman, B.: Synthesis and biochemical applications of a solid cyclic nitrone spin trap: a relatively superior trap for detecting superoxide anions and glutathiyl radicals, Free Radic. Biol. Med., 31, 599-606, 2001.

Zhou, J., Zotter, P., Bruns, E. A., Stefenelli, G., Bhattu, D., Brown, S., Bertrand, A., Marchand, N., Lamkaddam, H., and Slowik, J. G.: Particle-bound reactive oxygen species (PB-ROS) emissions and formation pathways in residential wood smoke under different combustion and aging conditions, Atmos. Chem. Phys., 18, 6985-7000, 2018.

Zuo, Y., and Hoigne, J.: Formation of hydrogen peroxide and depletion of oxalic acid in atmospheric water by photolysis of iron (III)-oxalato complexes, Environ. Sci. Technol., 26, 1014-1022, 1992.

852 ***Data availability***

853 The dataset for this paper is available upon request from the corresponding author (h.tong@mpic.de).

854 ***Supporting Information***

855 Supporting material consists of seven figures and five tables.

856 ***Author contributions***

857 HT and UP designed the esperiment and wrote up the original draft together with FL. CX, SY, and HK
858 involved in the collection of ambient particles. HT, FL, AF, and YZ particpated in laboratory measurements
859 and data analysis. All other co-authors participated in results discussion and manuscript editing.

860 ***AUTHOR INFORMATION***

861 ***Corresponding Author***

862 *Haijie Tong*

863 Phone (+49) 6131-305-7040

864 E-mail: h.tong@mpic.de;

865 ***ORCID***:

866 Haijie Tong: 0000-0001-9887-7836

867 Maosheng Yao: 0000-0002-1442-8054

868 Thomas Berkemeier: 0000-0001-6390-6465

869 Manabu Shiraiwa: 0000-0003-2532-5373

870 Ulrich Pöschl: 0000-0003-1412-35570000-0001-9887-7836

871 ***Competing interests***

872 The authors declare no competing financial interest.

873 ***Acknowledgements***

874 This work was funded by the Max Planck Society, ACTRIS, ECAC, the Finnish Centre of Excellence under
875 Academy of Finland (projects no. 307331 and 272041). Siegfried Herrmann and Steve Galer from Climate
876 Geochemistry Department of Max Planck Institute for Chemistry are gratefully acknowledged for ICP-MS
877 analysis. Technical staffs at SMEARII station are acknowledged for the impactor maintenance. MS
878 acknowledges funding from the National Science Foundation (CHE-1808125) and the Japan Society for
879 the Promotion of Science (JSPS; No. 16K12582).

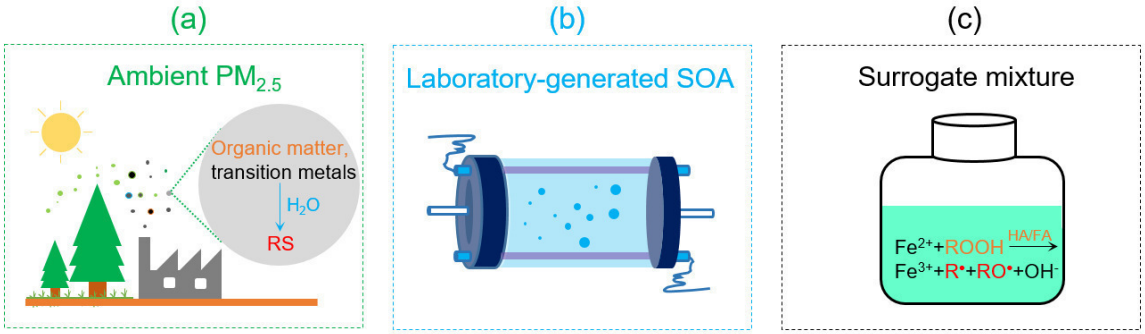

Figure 1. Schematic illustration of research approach and comparison of reactive species (RS) formed upon interaction of water with ambient fine particulate matter ($PM_{2.5}$), with laboratory generated secondary organic aerosols (SOA), and in surrogate mixtures. ROOH: organic hydroperoxide. HA: humic acid. FA: fulvic acid. $R^{\bullet}$ and $RO^{\bullet}$: C- and O-centered organic radicals, respectively.

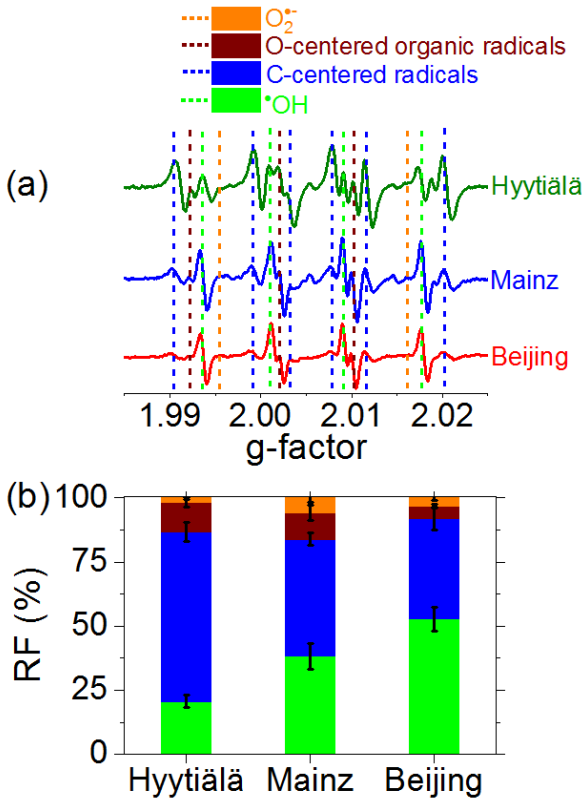

885

886 **Figure 2.** (a) EPR spectra and (b) relative fractions (RF) of different types of radicals formed in aqueous
887 extracts of ambient $PM_{2.5}$ from Hyytiälä, Mainz, and Beijing. Dotted vertical lines in (a) indicate peak
888 positions of different radical adducts. The spectra intensity in (a), RF values and error bars in (b) represent
889 arithmetic mean values and standard error (6-13 samples per location).

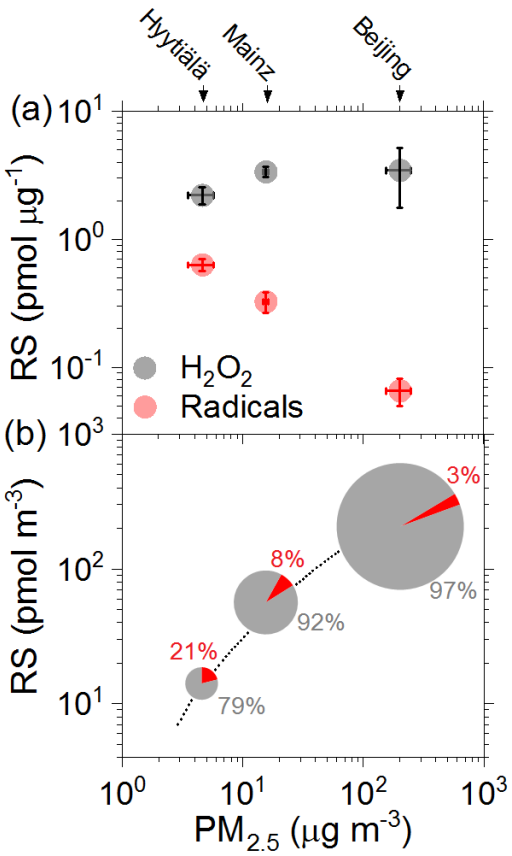

Figure 3. (a) Mass-specific yield and (b) air sample volume-specific yield of radicals (●) and H_2O_2 (●) observed upon water interaction of fine $PM_{2.5}$ from Hyytiälä, Mainz, and Beijing plotted against $PM_{2.5}$ concentration. The error bars represent standard errors of the mean (4-12 samples per location). The dotted line and pie charts are to guide the eye, reflecting the increase of total air sample volume-specific RS yield (not to scale) and the relative contributions of H_2O_2 and radicals.

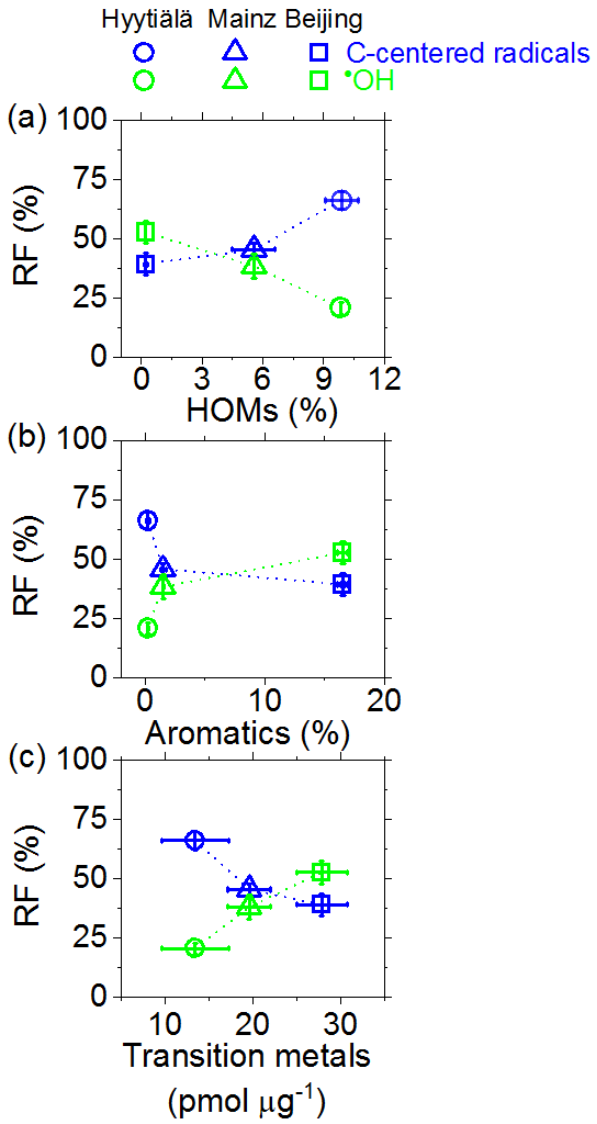

Figure 4. Correlation of (a) highly oxygenated organic molecules (HOMs), (b) aromatics, and (c) water-soluble transition metals in ambient $PM_{2.5}$ with relative fractions (RF) of $R^{\bullet}$ and $^{\bullet}OH$ observed upon interaction with water. The relative abundances of HOMs and aromatics in (a-b) represent the sum chromatographic area of HOMs or aromatics divided by the sum chromatographic area of all assigned organic compounds. The abundances of HOMs in (a) were adopted from a recent companion study (Tong et al., 2019). The error bars represent standard errors of the mean (4 to 12 samples per location). The dashed lines are to guide the eye.

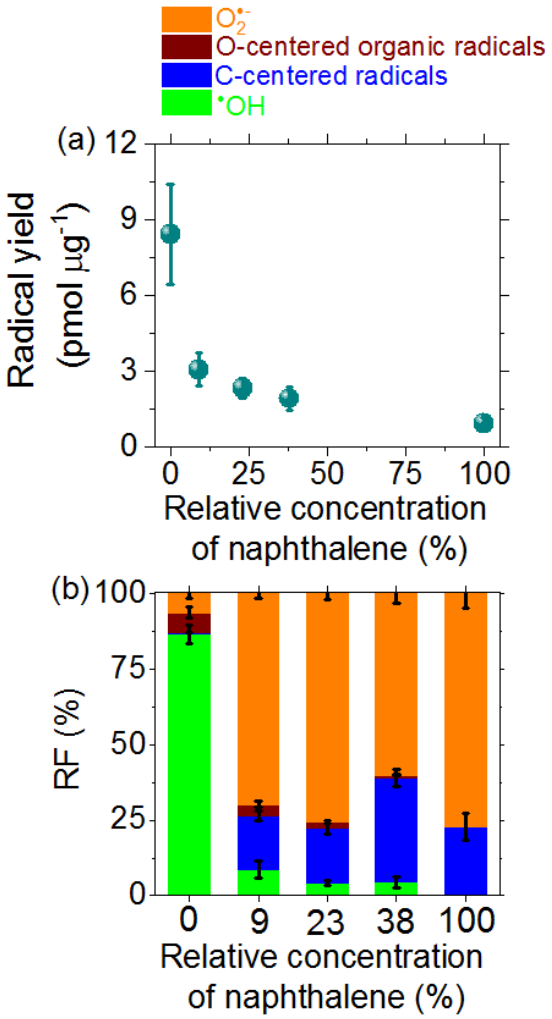

904

905 **Figure 5.** (a) Mass-specific yields and (b) relative fractions (RF) of radicals formed upon aqueous
906 extraction of laboratory-generated SOA from different precursors. The relative concentration of
907 naphthalene represents the relative molar fraction of gas-phase naphthalene to the mixture of naphthalene
908 and β-pinene. The error bars represent standard errors (4-6 samples per data point).

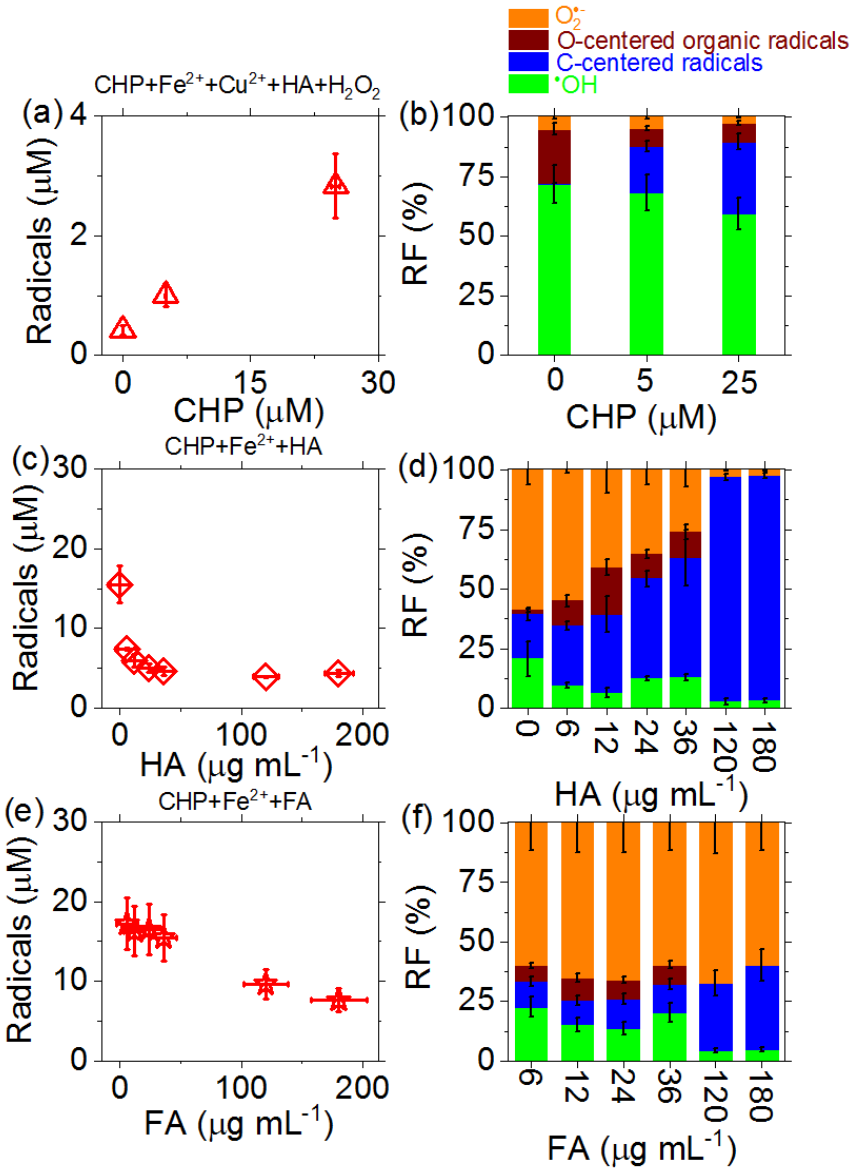

909

910 **Figure 6.** (a, c, e) Total radical yields and (b, d, f) relative fractions (RF) of different radical types observed
911 in aqueous surrogate mixtures of CHP, Fe^{2+}, Cu^{2+}, HA, FA, and H_2O_2. (a, b): 0-25 μM CHP, 43 μM Fe^{2+},
912 3 μM Cu^{2+}, 4 μg mL^{-1} HA, 7 μM H_2O_2 (CHP+Fe^{2+}+Cu^{2+}+HA+H_2O_2). (c, d): 100 μM CHP, 300 μM Fe^{2+},
913 0-180 μg mL^{-1} HA (CHP+Fe^{2+}+HA). (e, f): 100 μM CHP, 300 μM Fe^{2+}, 6-180 μg mL^{-1} FA (CHP+Fe^{2+}+FA).
914 The error bars represent uncertainties of signal integration of EPR spectra (for y-axis) or experimental
915 uncertainties of the solution concentration (for x-axis). CHP: cumene hydroperoxide. HA: humic acid. FA:
916 fulvic acid.

Supplementary of

Reactive species formed upon interaction of water with fine particulate matter from remote forest and polluted urban air

H. Tong *et al.*

Correspondence to: Haijie Tong (h.tong@mpic.de).

Influence of $PM_{2.5}$ extract concentration on the radical yield.

To assess the influence of the $PM_{2.5}$ extract concentrations on our results, we compared the mass-specific radical yields by different concentration of Beijing $PM_{2.5}$ extracts. We found the yield difference is on average for 37% among all extract samples. However, we did not see clear trend from low to high concentration of $PM_{2.5}$ extracts. Then we showed the $PM_{2.5}$ extract concentrations of each sample as well as the radical yields by different concentration of $PM_{2.5}$ extracts in Figure S1. Figures S1a-1c indicate that $PM_{2.5}$ extract concentrations of Hyytiälä and Mainz samples have narrower range distribution than Beijing samples. Figure S1d and 1e showed that radical yields by 500 μg mL^{-1} fine $PM_{2.5}$ overlapped the yields by 250-6400 μg mL^{-1} PM. Thus, the concentration of the $PM_{2.5}$ extracts has small impact on our results about RS yields. To evaluate the influence of $PM_{2.5}$ extract concentrations on the relative yields of different radicals, we measured the relative yields of different radicals by Beijing $PM_{2.5}$ (n=3) in 250, 500, and 1000 μg mL^{-1} $PM_{2.5}$ extracts. We found the relative yields of $^{\bullet}OH$, $O_2^{\bullet-}$, C- and O-centered organic radicals have standard deviations of ~10%, ~9%, ~2%, and ~2%, respectively.

Estimation of the abundance of organic hydroperoxides and humic-like substances in $PM_{2.5}$

Based on the compiled abundance of humic-like substances in $PM_{2.5}$ (Table S3), we obtained an averaged value of 7%, and we assumed that 15% of these $PM_{2.5}$-bound humic-like substances are extractable humic acid-like substances (Katsumi et al., 2019). Given that the concentration of $PM_{2.5}$ in aqueous extracts in this study ranged from 250 to 6500 μg mL^{-1}, thus the estimated concentration of humic acid-like substances typically ranged from 3 to 70 μg mL^{-1}. We assumed that 75% of the $PM_{2.5}$-bound humic-like substances are attributable to humic acid-like substances, thus the estimated concentration of extractable fulvic acid-like substances typically ranged from 15 to 350 μg mL^{-1}. To simulate the RS formation by Mainz and Beijing $PM_{2.5}$, we used 4 μg mL^{-1} humic acid standard. To investigate the influence of humic-like substances on the RS formation by Fenton-like reactions, we used 6-180 μg mL^{-1} humic or fulvic acid for surrogate mixture measurements.

To estimate the abundance of organic hydroperoxide in ambient $PM_{2.5}$, we assumed that the mass fractions of SOA in Hyytiälä, Mainz, and Beijing $PM_{2.5}$ were 60%, 25%, and 15%, respectively (Jimenez

et al., 2009). We also assumed that 2%, 2%, and 1% of Hyytiälä, Mainz, and Beijing SOA mass are attributable to organic hydroperoxides (Tong et al., 2018), which was assumed to have an averaged molecular weight of 300 g moL^{-1} (Docherty et al., 2005). In this case, the estimated concentration of organic hydroperoxides in the $PM_{2.5}$ extracts in this study was 5-35 μM. To simulate the RS formation by Hyytiälä, Mainz, and Beijing fine $PM_{2.5}$, we used 50, 25, and 0 μM cumene hydroperoxide (CHP), respectively. To investigate the RS yield of Fenton-like reactions, we used 50-100 μM CHP.

H_2O_2 yield of PM from other sources

The air sample volume-specific and mass-specific H_2O_2 yields as well as total RS yields of fine PM from other sites that different from Hyytiälä, Mainz, and Beijing are shown in Figure S4 and Table S5. Therein the H_2O_2 yields were measured using *p*-hydroxyphenylacetic acid (PHOPAA) as probe, and the total RS yields were measured using dichlorofluorescin (DCFH) assay as probe (Lazrus et al., 1985;Wang and Joseph, 1999;Kalyanaraman et al., 2012). Figure S4a shows that the air sample volume-specific H_2O_2 yields of fine PM from CRC-AES and different districts of UCLA exhibit a positive correlation with the concentration of $PM_{2.5}$ (R^2=0.60). In contrast, the mass-specific H_2O_2 yields exhibit no correlation with the $PM_{2.5}$ concentration (R^2=0.02, Figure S4b). Moreover, the DCFH-based total RS yields were overall higher than the H_2O_2 (Table S5), agreeing with this study.

Influence of H_2O_2 on the radical yield of Fenton-like reactions

We investigated the influence of H_2O_2 concentration on the radical yield of Fenton-like reactions initiated by mixtures comprising 100 μM CHP, 300 μM Fe^{2+}, 11 μg mL^{-1} HA, and 79 μg mL^{-1} FA. Figure S5a shows that as the concentration of H_2O_2 is increased from 0 to 300 μM, the concentration of total radicals increase from ~8.0 to ~18.4 μM, with the RF of $^{\bullet}OH$ and O-centered organic radicals increase from ~18 to ~69% and from ~7 to ~26% (Figure S5b), confirming the enhanced radical formation through Fenton-like reactions (Gligorovski et al., 2015). In contrast, the RF of C-centered radicals and $O_2^{\bullet-}$ decrease from ~25 to ~2% and from ~51 to ~3%, reflecting a plausible conversion of C-centered radicals to O-centered organic radicals via oxidation pathways (Chevallier et al., 2004;Tong et al., 2016). Thus, H_2O_2 can significantly

influence the total and relative yields of different types of radicals by Fenton-like reactions, and humic-like substances may co-mediate the radical formation.

Influence of HA and FA on the radical yields of Fenton-like reactions initiated by Cu^{2+}

Figure S7a shows that the concentration of radicals formed by Cu^{2+} and cumene hydroperoxide (CHP) mixtures exhibited a positive correlation with the concentration of Cu^{2+}. However, the Cu^{2+} played a less effective role than Fe^{2+} in initiating Fenton-like reactions via radical formation pathways, with 300 μM Cu^{2+} and 50 μM CHP produced ~1.8 μM radicals.

Figure S7b shows that as the concentration of Cu^{2+} increased from 15 to 75 μM, the RF of $^{\bullet}OH$ and $O_2^{\bullet-}$ decreased from ~44% to ~18% and from ~1.6% to ~0.1%. However, the RF of C- and O-centered organic radicals increased from~39% to ~61% and from ~15% to ~21%, respectively. As the concentration of Cu^{2+} is increased further to 150 and 300 μM, the RF of $^{\bullet}OH$, $O_2^{\bullet-}$, C- and O-centered organic radicals varied slightly, reflecting a low reactivity of Cu^{2+} with CHP.

Figure S7c shows that concentration of radicals formed by reactions of 100 μM CHP with 300 μM Cu^{2+} and HA decreased from ~2.3 to ~1.8 μM as the increasing of HA concentration from 0 to 180 μg mL^{-1}. This might mainly be associated with the low catalytic effect of Cu^{2+} in initiating Fenton-like reactions (Figure S5a). Beyond this, humic-like substances have been found to exhibit strong copper-binding ability (Kogut and Voelker, 2001), and 8-fold more Cu^{2+} than Fe^{2+} ions from Melpitz (Germany) PM were expected to be complexed by humic-like substances (Scheinhardt et al., 2013). We thus inferred that the Cu-HA complex might significantly influence the reactivity of Cu^{2+} in Fenton-like reactions. Finally, partial of the radical yield decay in Figure S7a might be caused by the antioxidant effect of HA (Aeschbacher et al., 2012). Figure S7d shows that as the concentration of HA increased from 6 to 180 μg mL^{-1}, the RF of $^{\bullet}OH$ and O-centered organic radicals increased from ~17 to ~44% and from ~16 to ~28%, respectively. The RF variation of $^{\bullet}OH$, C- and O-centered organic radicals in Figure S7d had a different trend from the results in Figure 6d, reflecting different impacts of HA on Cu and Fe initiated Fenton-like reactions. Compared to the

increasing RF of $^{\bullet}OH$ and O-centered organic radicals, the RF of C-centered radicals decreased from ~66 to ~28%, and the RF of $O_2^{\bullet-}$ only varied slightly between 0.8 and 1.5%.

Figure S7e shows that the radical yields of the mixtures consisting of 100 μM CHP, 300 μM Cu^{2+}, and FA only varied from ~0.9 to ~0.4 μM as the increasing FA concentration from 6 to 180 μg mL^{-1}, which may mainly be associated with the low catalytic effect of Cu^{2+} as well as the formation of Cu-FA complexes. Figure S7f indicates that as the concentration of FA increased from 0 to 180 μg mL^{-1}, the RF of C-centered radicals steeply increased from ~57 to ~89%, whereas the RF of O-centered organic radicals and $^{\bullet}OH$ exhibited overall decrease from ~25% and ~16% to ~3%.

Table S1. Sampling information.

City	Location	Sampler	Flow rate (L min^{-1})	Sampling time (h) [a]	Sampling period	Sample numbers
Hyytiälä	61.51°N, 24.17°E	Dekati® PM10 impactor (Finland)	30	48-72	31 May-19 July 2017	11
Mainz	49.99°N, 8.23°E	MOUDI (MSP corporation, USA) [b]	30	24-54	22 Aug.-17 Nov. 2017 23-31 Aug. 2018	11
Beijing	116.31°E, 39.99°N	$PM_{2.5}$ sampler (TH-16, Tianhong company, China)	30	5-24	20 Dec. 2016-13 Jan. 2017 6 Nov. 2017-17 Jan. 2018	20

[a] The sampling time is for one filter

[b] MOUDI: Micro-Orifice Uniform Deposition Impactor (122R)

92 **Table S2. The range of hyperfine coupling constants that used to fit the BMPO adducts.**

Spin adduct	Hyperfine coupling constant (G)		
	a_N	a_H^β	a_H^γ
BMPO-OH1	12-16	11-12	0.5-0.9
BMPO-OH2	14-15	13-14	0.6-0.7
BMPO-OOH1	13-14	8-10	—
BMPO-OOH2	13-14	11-13	—
BMPO-C-centered radicals	14-16	21-23	—
BMPO-O-centered organic radicals	14-16	17-18	—

93

Table S3. Compiled abundance of humic-like substances in ambient $PM_{2.5}$.

Location	Time/event	$PM_{2.5}$ ($\mu g\ m^{-3}$)	humic-like substances ($\mu g\ m^{-3}$)	humic-like substances /$PM_{2.5}$ (%)	Reference
Lanzhou	Winter	120.47	7.24	6.0	(Tan et al., 2016)
Lanzhou	Summer	34.12	2.15	6.3	(Tan et al., 2016)
Lanzhou	Annual	77.29	4.7	6.1	(Tan et al., 2016)
Lanzhou	Haze	182.08	10.06	5.5	(Tan et al., 2016)
Lanzhou	No-haze	51.65	3.49	6.8	(Tan et al., 2016)
Lanzhou	Snow	80.69	4.62	5.7	(Tan et al., 2016)
PRD[a]	Annual 2007-2008	49	4.9	10.0	(Lin et al., 2010)
Guangzhou	Annual 2009	56	4.8	8.6	(Kuang et al., 2015)
Beijing	Winter 2011	108	8.9	8.2	(Lang et al., 2017)
Beijing	Summer	98	5.5	5.9	(Li et al., 2019)
Beijing	Autumn	58	5.6	9.4	(Li et al., 2019)
Beijing	Winter	150	12.3	7.9	(Li et al., 2019)
Beijing	Spring	120	6.5	4.8	(Li et al., 2019)
Average		91.2	6.2	7.0	

PRD: Pearl River Delta Region in China

Table S4. The yields of different types of radicals and concentrations of different water-soluble transition metal species in $PM_{2.5}$ extracts.

Location	Radicals (pmol m^{-3})				Water-soluble transition metals (pmol m^{-3})				
	$^{\bullet}OH$	C-centered	O-centered organic	$O_2^{\bullet-}$	Fe	Mn	Cu	V	Ni
Hyytiälä	0.4 ± 0.2	2.2 ± 1.4	0.1 ± 0.1	0.02 ± 0.01	26.0 ± 16.0	4.9 ± 4.8	3.1 ± 1.2	2.5 ± 1.7	0.04 ± 0.01
Mainz	2.1 ± 1.3	1.8 ± 0.7	0.2 ± 2	0.1 ± 0.1	269.0 ± 113.0	28.0 ± 12.0	55.0 ± 17.0	2.9 ±0.8	1.2 ± 0.4
Beijing	3.6 ± 2.6	2.5 ± 1.7	0.3 ± 0.2	0.2 ± 0.3	(3300.0 ± 2300.0)	640.0 ± 531.0	452.0 ± 385.0	23.0 ± 23.0	51.0 ± 25.0
Location	Radicals (pmol μg^{-1})				Water-soluble transition metals (pmol μg^{-1})				
	$^{\bullet}OH$	C-centered	O-centered organic	$O_2^{\bullet-}$	Fe	Mn	Cu	V	Ni
Hyytiälä	0.08 ± 0.004	0.5 ± 0.2	0.03 ± 0.01	0.01 ± 0.01	5.5 ± 1.5	1.0 ± 0.5	0.7 ± 0.3	0.5 ± 0.2	0.01 ± 0.003
Mainz	0.2 ± 0.1	0.1 ± 0.07	0.02 ± 0.02	0.01 ± 0.01	18.0 ± 4.9	1.9 ± 0.7	3.9 ± 0.6	0.2 ± 0.03	0.08 ± 0.03
Beijing	0.04 ± 0.04	0.02 ± 0.02	0.003 ± 0.002	0.002 ± 0.002	20.0 ± 7.0	4.5 ± 2.6	2.3 ± 0.4	0.2 ± 0.2	0.5 ± 0.5

Table S5. Statistic of H_2O_2 or RS yields of ambient PM at different locations.

Sampling site	PM type	PM (μg m^{-3})	Sampling time	Method	Analyte	H_2O_2 or RS (pmol m^{-3})	H_2O_2 or RS (pmol μg^{-1})	Reference
Hyytiälä	$PM_{2.5}$	5 ± 2	Jun-Jul 2017	MAK165	H_2O_2	10 ± 8	1.9 ± 0.9	This study
UCLA Pacific coast	Fine	13 ± 10	May 2014-Jan 2015	PHOPAA+HRP	H_2O_2	12 ± 9	1.0 ± 0.9	(Arellanes et al., 2006)
MPI-C at Mainz	$PM_{1.8}$	16 ± 2	Aug-Sep 2017	MAK165	H_2O_2	47 ± 17	3.3 ± 1.1	This study
UCLA	$PM_{2.5}$	16 ± 7	2009-2010	PHOPAA+HRP	H_2O_2	47 ± 21	3.0 ± 2.0	(Wang et al., 2012)
CRC-AES, UC Riverside	$PM_{2.5}$	19 ± 6	Jun-Aug 2008	PHOPAA+HRP	H_2O_2	$(2.7 \pm 2.1) \times 10^2$	1.4 ± 1.6	(Wang et al., 2012)
UCLA freeway site	Fine	23 ± 8	Jan-May 2004	PHOPAA+HRP	H_2O_2	17 ± 90	0.7 ± 1.1	(Arellanes et al., 2006)
UCLA Pacific coast	Coarse	26 ± 15	Jul 2004	PHOPAA+HRP	H_2O_2	31 ± 9	1.2 ± 0.6	(Arellanes et al., 2006)
UCLA freeway site	Coarse	27 ± 33	Jul 2004	PHOPAA+HRP	H_2O_2	15 ± 9	0.6 ± 0.3	(Arellanes et al., 2006)
UC Riverside campus	$PM_{2.5}$	39 ± 22	Aug 2005	PHOPAA+HRP	H_2O_2	$(1.2 \pm 1.1) \times 10^3$	28.0 ± 20.0	(Wang et al., 2012)
UCLA campus	Coarse	46 ± 22	Aug 2005	PHOPAA+HRP	H_2O_2	$(5.0 \pm 2.4) \times 10^2$	14.1 ± 9.4	(Wang et al., 2010)
UCLA upwind Riverside	Coarse	97 ± 27	Jun-Aug 2008	PHOPAA+HRP	H_2O_2	$(1.0 \pm 0.4) \times 10^3$	10.9 ± 5.3	(Wang et al., 2010)
Beijing	$PM_{2.5}$	201 ± 160	Dec 2016- Jan 2017	MAK165	H_2O_2	190 ± 120	3.4 ± 5.6	This study
Taipei	Coarse	7.5± 2.8	Jul-Sep 2000	DCFH+HRP	RS	64 ± 33	8.5 ± 11.8	(Hung and Wang, 2001)
Bern	$PM_{2.5}$	10 ± 5	Nov 2014	DCFH+HRP	RS	$(4.9 \pm 2.9) \times 10^2$	50	(Zhou et al., 2018)

Atlanta	$PM_{2.5}$	10.5 ± 3.2	12-17 Jul 2012	DCFH+HRP	RS	$(1.6 \pm 0.2) \times 10^2$	14.8 ± 4.5	(King and Weber, 2013)
Atlanta	$PM_{2.5}$	11.5 ± 4.3	8-31 May 2012	DCFH+HRP	RS	$(2.6 \pm 0.1) \times 10^2$	22.6 ± 3.0	(King and Weber, 2013)
Atlanta	$PM_{2.5}$	13.2 ± 4.8	8-29 Jun 2012	DCFH+HRP	RS	$(1.4 \pm 0.1) \times 10^2$	10.6 ± 1.9	(King and Weber, 2013)
Atlanta	$PM_{2.5}$	13.2 ± 5.4	3-31 Jul 2012	DCFH+HRP	RS	$(2.4 \pm 0.1) \times 10^2$	18.2 ± 1.8	(King and Weber, 2013)
London	$PM_{2.5}$	5-28	not reported	DCFH+HRP	RS	$(0.4\text{-}2.4) \times 10^4$	not reported	(Wragg et al., 2016)
Singapore (campus)	$PM_{2.5}$	19 ± 2	Dec 2005	DCFH+HRP	RS	$(5.7 \pm 0.7) \times 10^3$	0.3	(See et al., 2007)
Taipei	$PM_{3.2}$	31 ± 15	Jul-Sep 2000	DCFH+HRP	RS	$(5.4 \pm 0.5) \times 10^2$	17.6 ± 29.2	(Hung and Wang, 2001)
Singapore (curbside)	$PM_{2.5}$	33 ± 6	Dec 2005	DCFH+HRP	RS	$(1.5 \pm 0.2) \times 10^4$	460	(See et al., 2007)
Milan (traffic site)	TSP	50 ± 7	July 2013	DCFH+HRP	RS	$(1.4 \pm 0.7) \times 10^2$	2.73 ± 1.29	(Perrone et al., 2016)
Milan (low emission zone)	TSP	52 ± 19	Oct 2013	DCFH+HRP	RS	$(2.0 \pm 1.1) \times 10^2$	3.74 ± 1.41	(Perrone et al., 2016)
Milan (traffic site)	TSP	57 ± 19	Oct 2013	DCFH+HRP	RS	$(2.4 \pm 1.3) \times 10^2$	4.02 ± 1.77	(Perrone et al., 2016)
Beijing	$PM_{2.5}$	5-110	Aug-Sep 2015	DCFH+HRP	RS	$(0.2\text{-}3.6) \times 10^4$	not reported	(Huang et al., 2018)
Beijing	$PM_{2.5}$	74 ± 58	Dec 2014	DCFH+HRP	RS	$(1.3 \pm 0.5) \times 10^4$	179.6 ± 87.8	(Huang et al., 2016)
Beijing	$PM_{2.5}$	79 ± 59	Apr 2015	DCFH+HRP	RS	$(5.8 \pm 2.6) \times 10^3$	73.6 ± 43.4	(Huang et al., 2016)
Milan (traffic site)	TSP	129± 60	Jan-Feb 2013	DCFH+HRP	RS	$(3.6 \pm 0.8) \times 10^2$	2..99 ± 1.52	(Perrone et al., 2016)
Rubidoux, CA	$PM_{2.5}$	not reported	Jul 2003	DCFH+HRP	RS	$(4.7 \pm 0.4) \times 10^3$	not reported	(Venkatachari et al., 2005)
Rochester, NY	$PM_{2.5}$	not reported	Aug 2009	DCFH+HRP	RS	$(8.3 \pm 2.2) \times 10^3$	not reported	(Wang et al., 2011)

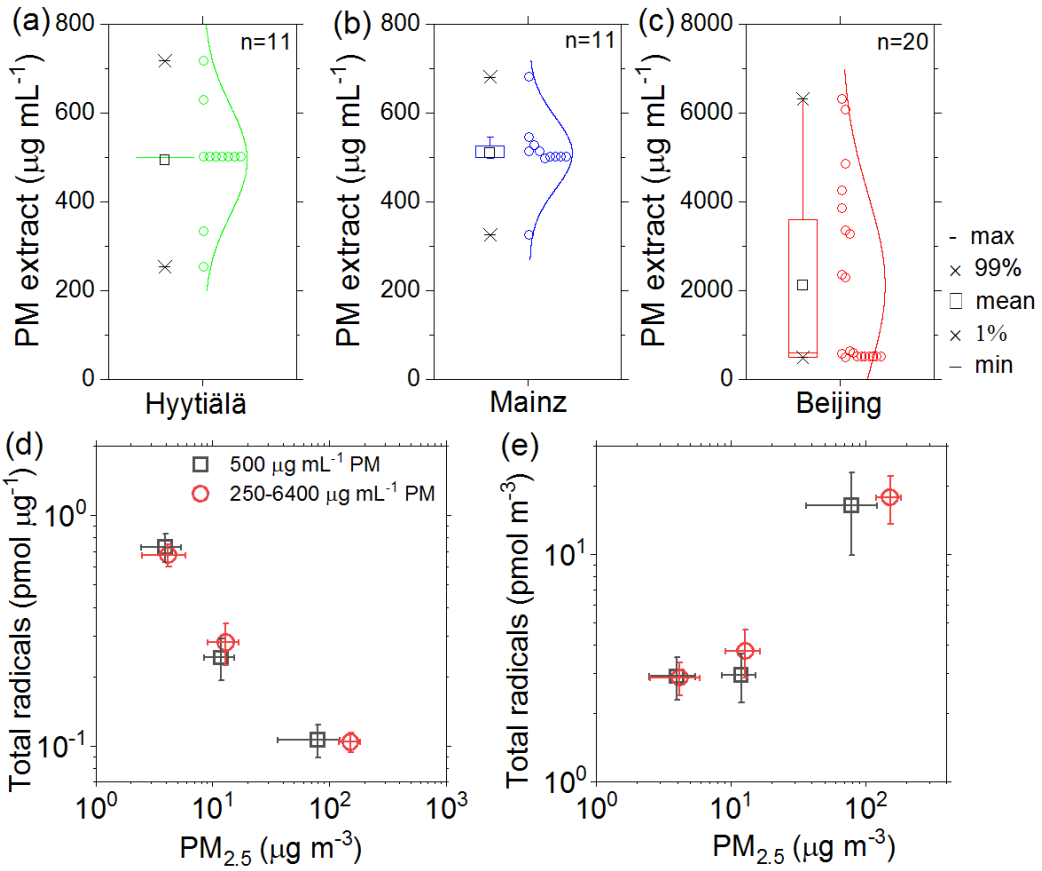

Figure S1. (a-c) Concentrations of $PM_{2.5}$ in aqueous extracts of each filter samples. (d) Mass-specific radical yields by different concentrations of $PM_{2.5}$ in water versus the concentration of ambient $PM_{2.5}$ in air. (e) Air sample volume-specific radical yields by different concentrations of PM versus the concentration of ambient $PM_{2.5}$. The error bars denote the standard errors (11-20 samples per location).

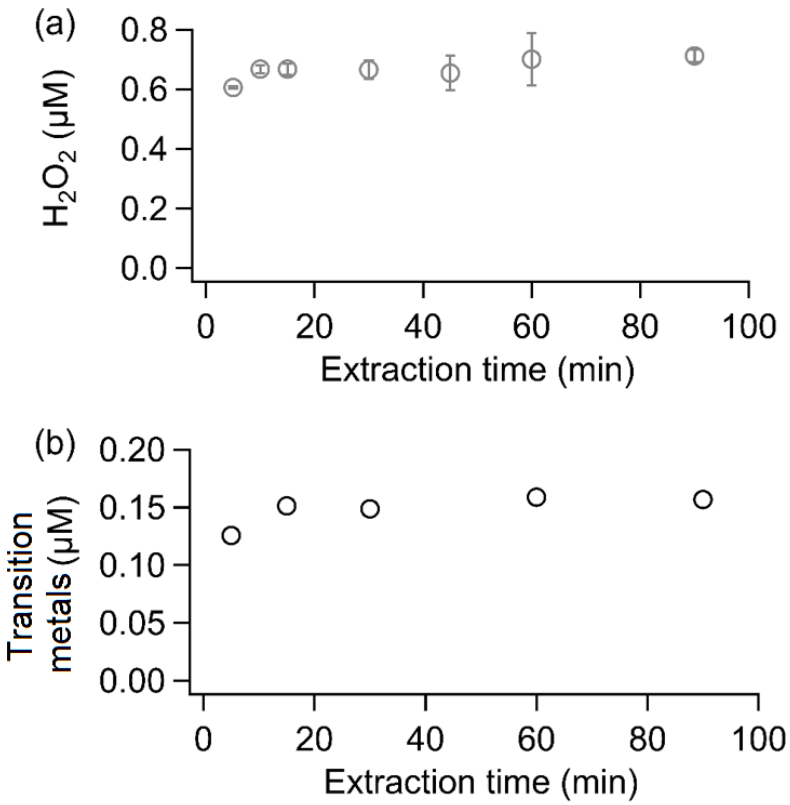

106

107 **Figure S2.** (a) Temporal evolution of H_2O_2 concentration in water extracts during the extraction process.
108 Error bars represent standard deviation of duplicate measurements. (b) Temporal evolution of water-soluble
109 transition metal concentration in water extracts during the extraction process. The H_2O_2 and transition metal
110 concentrations became constant after ~15 min's extraction. The filter used for these tests was collected at
111 Mainz from 25 to 27 Oct. 2017.

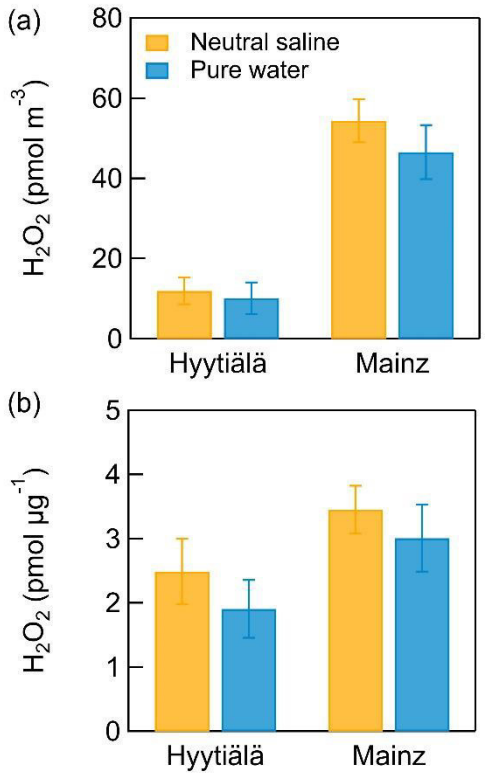

112

113 **Figure S3.** (a) Air sample volume-specific and (b) mass-specific H_2O_2 yield of Hyytiälä and Mainz fine

114 PM in neutral saline (yellow column) and pure water (blue column). The error bars represent standard

115 deviations of mean (11-12 samples per location).

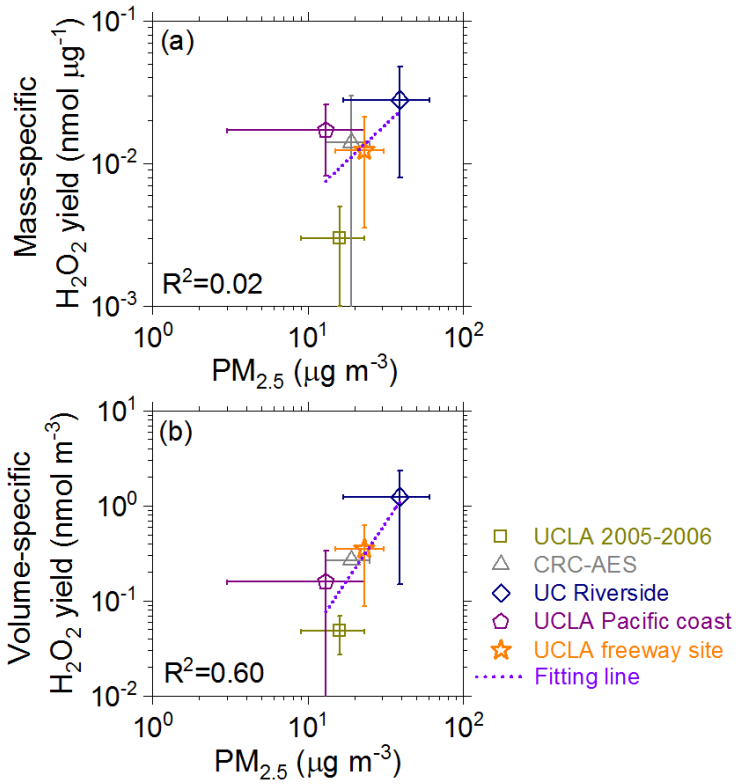

116

117 **Figure S4.** (a) Mass-specific and (b) air sample volume-specific H_2O_2 and RS yields of PM from different

118 sites. The error bars represent standard deviation.

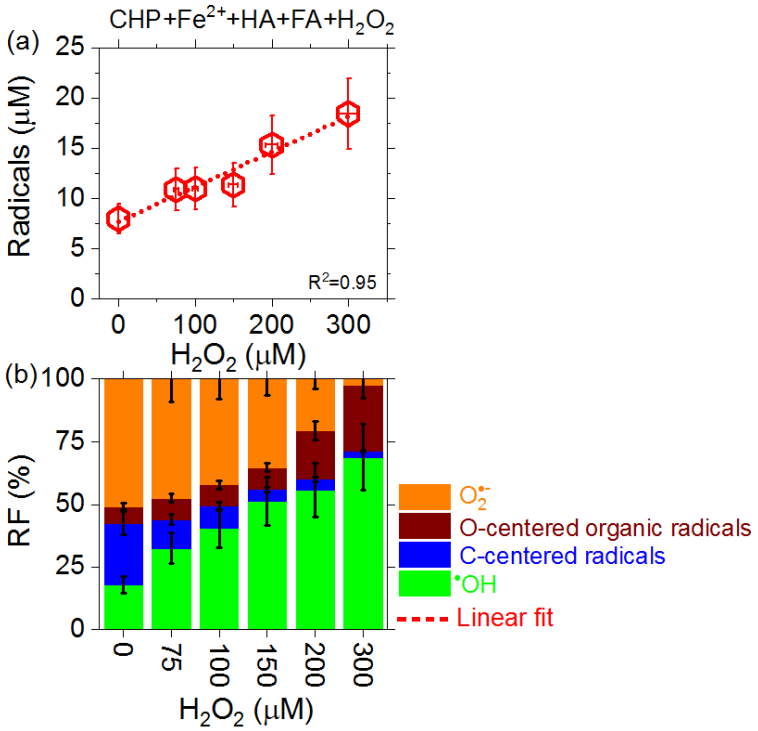

119

120 **Figure S5.** (a) Total radical yield and (b) relative fractions (RF) of individual radicals observed in aqueous

121 surrogate mixtures of CHP, Fe^{2+}, HA, FA, and H_2O_2. CHP: 100 μM. Fe^{2+}: 300 μM. HA: 100 μg mL^{-1}. FA:

122 80 μg mL^{-1}. H_2O_2: 0-300 μM. The error bars represent uncertainties of signal integration of EPR spectra

123 (for y-axis) or experimental uncertainties of the solution concentration (for x-axis).

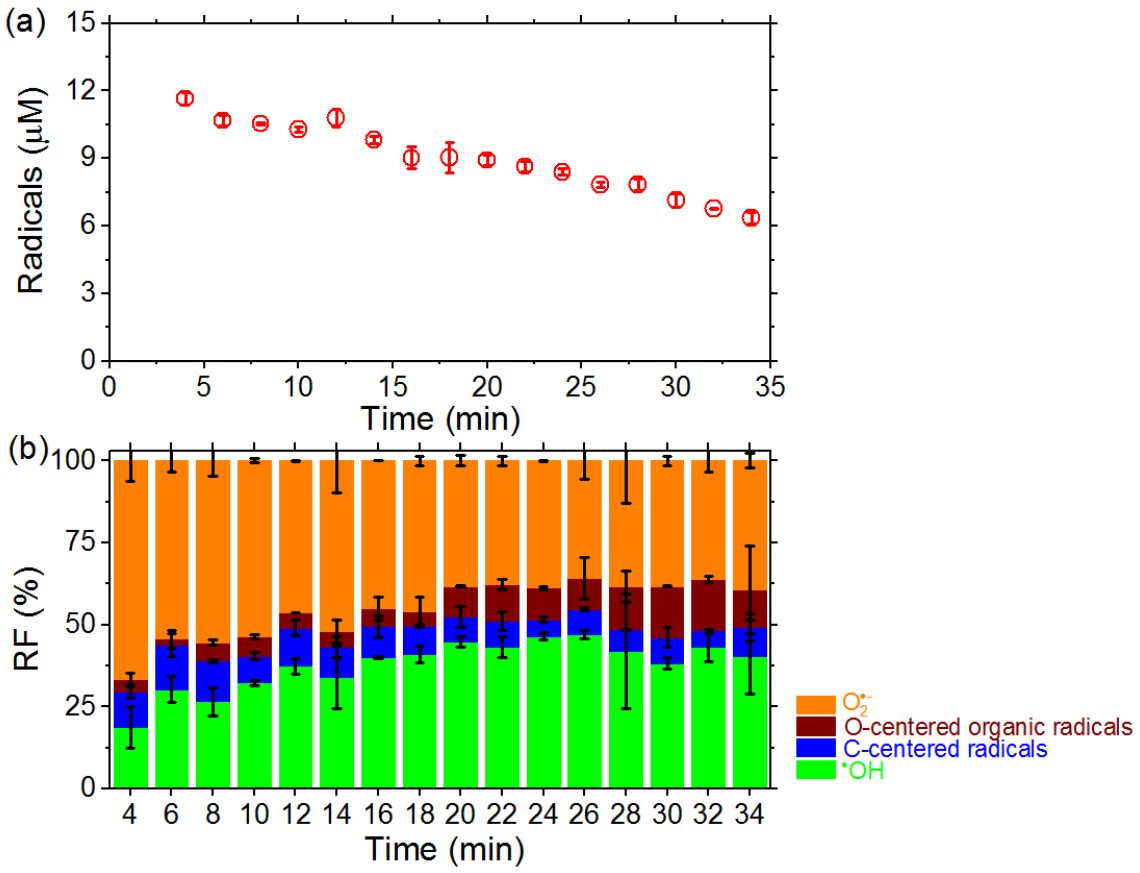

Figure S6. (a) Temporal evolution of total radical concentration and (b) relative fractions (RF) of individual radical species in aqueous mixtures of 100 μM CHP and 300 μM Fe^{2+}. Error bars represent standard deviation of duplicate measurements.

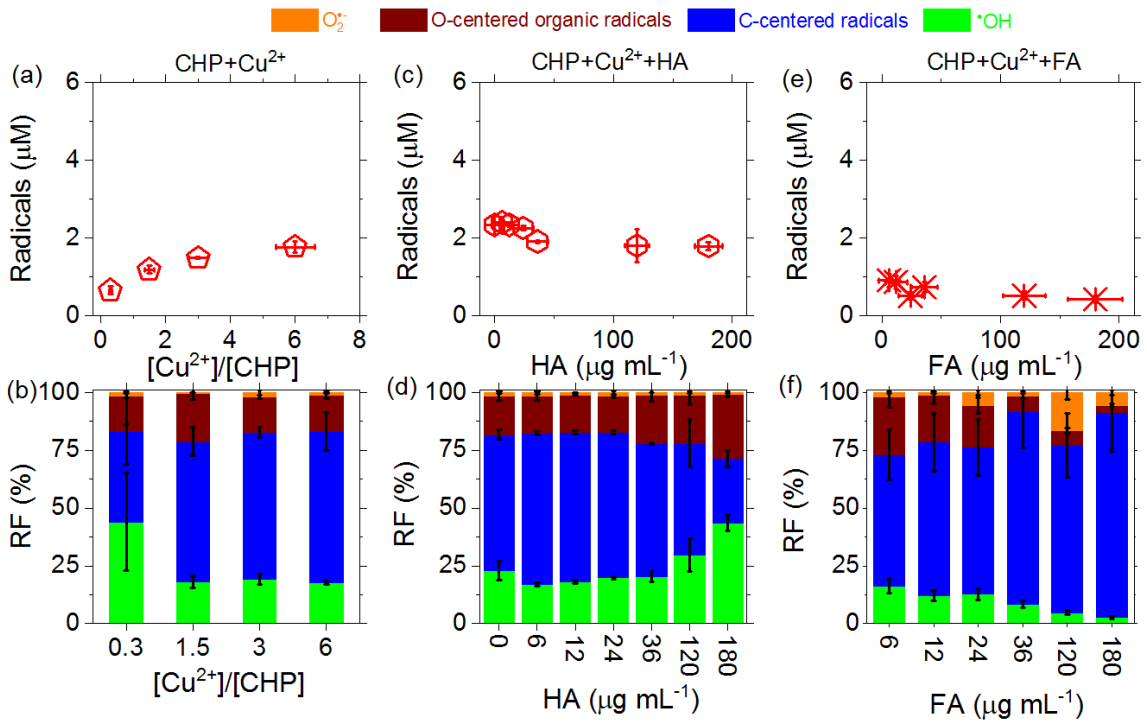

Figure S7. (a, c, e) Concentration of totally formed radicals and (b, d, f) RF of individual radicals in aqueous mixtures comprising CHP, Cu^{2+}, HA, or FA. The concentration of CHP in (a) and (b) is 50 μM. The concentrations of CHP and Cu^{2+} in (c-f) are 100 and 300 μM. The error bars in (a) to (d) represent standard errors of the mean (3 -5 samples per data point, a, b). The error bars for x- and y-axis in (e) and (f) represent experimental uncertainties of the solution concentration and signal integration of EPR spectra, respectively.

References

Aeschbacher, M., Graf, C., Schwarzenbach, R. P., and Sander, M.: Antioxidant properties of humic substances, Environ. Sci. Technol. , 46, 4916-4925, 2012.

Arellanes, C., Paulson, S. E., Fine, P. M., and Sioutas, C.: Exceeding of Henry's law by hydrogen peroxide associated with urban aerosols, Environ. Sci. Technol., 40, 4859-4866, 2006.

Chevallier, E., Jolibois, R. D., Meunier, N., Carlier, P., and Monod, A.: "Fenton-like" reactions of methylhydroperoxide and ethylhydroperoxide with Fe^{2+} in liquid aerosols under tropospheric conditions, Atmos. Environ., 38, 921-933, 2004.

Docherty, K. S., Wu, W., Lim, Y. B., and Ziemann, P. J.: Contributions of organic peroxides to secondary aerosol formed from reactions of monoterpenes with O3, Environ. Sci. Technol., 39, 4049-4059, 2005.

Gligorovski, S., Strekowski, R., Barbati, S., and Vione, D.: Environmental implications of hydroxyl radicals (•OH), Chem. Rev., 115, 13051-13092, 2015.

Huang, W., Zhang, Y., Zhang, Y., Zeng, L., Dong, H., Huo, P., Fang, D., and Schauer, J. J.: Development of an automated sampling-analysis system for simultaneous measurement of reactive oxygen species (ROS) in gas and particle phases: GAC-ROS, Atmos. Environ., 134, 18-26, 2016.

Huang, W., Fang, D., Shang, J., Li, Z., Zhang, Y., Huo, P., Liu, Z., Schauer, J. J., and Zhang, Y.: Relative impact of short-term emissions controls on gas and particle-phase oxidative potential during the 2015 China Victory Day Parade in Beijing, China, Atmos. Environ., 183, 49-56, 2018.

Hung, H.-F., and Wang, C.-S.: Experimental determination of reactive oxygen species in Taipei aerosols, J. Aerosol Sci., 32, 1201-1211, 2001.

Jimenez, J. L., Canagaratna, M., Donahue, N., Prevot, A., Zhang, Q., Kroll, J. H., DeCarlo, P. F., Allan, J. D., Coe, H., and Ng, N.: Evolution of organic aerosols in the atmosphere, science, 326, 1525-1529, 2009.

Kalyanaraman, B., Darley-Usmar, V., Davies, K. J., Dennery, P. A., Forman, H. J., Grisham, M. B., Mann, G. E., Moore, K., Roberts II, L. J., and Ischiropoulos, H.: Measuring reactive oxygen and nitrogen species with fluorescent probes: challenges and limitations, Free Radic. Biol. Med., 52, 1-6, 2012.

Katsumi, N., Miyake, S., Okochi, H., Minami, Y., Kobayashi, H., Kato, S., Wada, R., Takeuchi, M., Toda, K., and Miura, K.: Humic-like substances global levels and extraction methods in aerosols, Environ. Res. Lett., 17, 1023-1029, 2019.

King, L., and Weber, R.: Development and testing of an online method to measure ambient fine particulate reactive oxygen species (ROS) based on the 2', 7'-dichlorofluorescin (DCFH) assay, Atmos. Meas. Tech., 6, 1647-1658, 2013.

Kogut, M. B., and Voelker, B. M.: Strong copper-binding behavior of terrestrial humic substances in seawater, Environ. Sci. Technol. , 35, 1149-1156, 2001.

Kuang, B. Y., Lin, P., Huang, X., and Yu, J. Z.: Sources of humic-like substances in the Pearl River Delta, China: positive matrix factorization analysis of PM 2.5 major components and source markers, Atmos. Chem. Phys., 15, 1995-2008, 2015.

Lang, J., Zhang, Y., Zhou, Y., Cheng, S., Chen, D., Guo, X., Chen, S., Li, X., Xing, X., and Wang, H.: Trends of PM2. 5 and chemical composition in Beijing, 2000–2015, Aerosol Air Qual. Res., 17, 412-425, 2017.

Lazrus, A. L., Kok, G. L., Gitlin, S. N., Lind, J. A., and McLaren, S. E.: Automated fluorimetric method for hydrogen peroxide in atmospheric precipitation, Anal. Chem., 57, 917-922, 1985.

Li, X., Han, J., Hopke, P. K., Hu, J., Shu, Q., Chang, Q., and Ying, Q.: Quantifying primary and secondary humic-like substances in urban aerosol based on emission source characterization and a source-oriented air quality model, Atmos. Chem. Phys., 19, 2327-2341, 2019.

Lin, P., Engling, G., and Yu, J.: Humic-like substances in fresh emissions of rice straw burning and in ambient aerosols in the Pearl River Delta Region, China, Atmos. Chem. Phys., 10, 6487-6500, 2010.

Perrone, M. G., Zhou, J., Malandrino, M., Sangiorgi, G., Rizzi, C., Ferrero, L., Dommen, J., and Bolzacchini, E.: PM chemical composition and oxidative potential of the soluble fraction of particles at two sites in the urban area of Milan, Northern Italy, Atmos. Environ., 128, 104-113, 2016.

Scheinhardt, S., Müller, K., Spindler, G., and Herrmann, H.: Complexation of trace metals in size-segregated aerosol particles at nine sites in Germany, Atmos. Environ., 74, 102-109, 2013.

See, S., Wang, Y., and Balasubramanian, R.: Contrasting reactive oxygen species and transition metal concentrations in combustion aerosols, Environ. Res., 103, 317-324, 2007.

Tan, J., Xiang, P., Zhou, X., Duan, J., Ma, Y., He, K., Cheng, Y., Yu, J., and Querol, X.: Chemical characterization of humic-like substances (HULIS) in PM2. 5 in Lanzhou, China, Sci. Total Environ., 573, 1481-1490, 2016.

Tong, H., Arangio, A. M., Lakey, P. S., Berkemeier, T., Liu, F., Kampf, C. J., Brune, W. H., Pöschl, U., and Shiraiwa, M.: Hydroxyl radicals from secondary organic aerosol decomposition in water, Atmos. Chem. Phys., 16, 1761-1771, 2016.

Tong, H., Lakey, P. S., Arangio, A. M., Socorro, J., Shen, F., Lucas, K., Brune, W. H., Pöschl, U., and Shiraiwa, M.: Reactive oxygen species formed by secondary organic aerosols in water and surrogate lung fluid, Environ. Sci. Technol. , 52, 11642-11651, 2018.

Venkatachari, P., Hopke, P. K., Grover, B. D., and Eatough, D. J.: Measurement of particle-bound reactive oxygen species in Rubidoux aerosols, J. Atmos. Chem., 50, 49-58, 2005.

Wang, H., and Joseph, J. A.: Quantifying cellular oxidative stress by dichlorofluorescein assay using microplate reader, Free Radic. Biol. Med., 27, 612-616, 1999.

Wang, Y., Arellanes, C., Curtis, D. B., and Paulson, S. E.: Probing the source of hydrogen peroxide associated with coarse mode aerosol particles in Southern California, Environ. Sci. Technol. , 44, 4070-4075, 2010.

Wang, Y., Hopke, P. K., Sun, L., Chalupa, D. C., and Utell, M. J.: Laboratory and field testing of an automated atmospheric particle-bound reactive oxygen species sampling-analysis system, J. Toxicol, 2011, 1-9, 2011.

Wang, Y., Arellanes, C., and Paulson, S. E.: Hydrogen peroxide associated with ambient fine-mode, diesel, and biodiesel aerosol particles in Southern California, Aerosol Sci. Technol., 46, 394-402, 2012.

Wragg, F., Fuller, S. J., Freshwater, R., Green, D. C., Kelly, F. J., and Kalberer, M.: An automated online instrument to quantify aerosol-bound reactive oxygen species (ROS) for ambient measurement and health-relevant aerosol studies, Atmos. Meas. Tech., 9, 4891-4900, 2016.

Zhou, J., Bruns, E. A., Zotter, P., Stefenelli, G., Prévôt, A. S., Baltensperger, U., El-Haddad, I., and Dommen, J.: Development, characterization and first deployment of an improved online reactive oxygen species analyzer, Atmos. Meas. Tech., 11, 65-80, 2018.

3.5 Environmentally Persistent Free Radicals in Remote and Polluted Regions

This chapter represents the current state of a manuscript in preparation for submission as a research article to a peer reviewed scientific journal. I have done almost all the experimental work, which is relevant for this study. More concretely I planned and executed the sampling of PM in Mainz and analyzed all ambient PM samples except those from ATTO personally by EPR. Furthermore, I analyzed, processed, and visualized all data. Also the plotting of all figures and the first draft of text were prepared exclusively by me. However, the presented version takes into account a number of suggestions and comments by some of the coauthors, but these were all implemented and integrated under my coordination. I also did all modeling related to lung deposition presented in this chapter.

Size distributions and regional variations of environmentally persistent free radicals (EPFR) in air particulate matter

Alexander Filippi,[1] Fobang Liu,[2] Steven Lelieveld,[1] Florian Ditas,[1] Helmi-Marja Keskinen,[3] Markku Kulmala,[3] Senchao Lai,[4] Linjie Li,[5] Yao Meng,[4] Tuukka Petäjä,[3] Christopher Pöhlker,[1] Mira Pöhlker,[1] Hong Ren,[5] Fangxia Shen,[6] Siyao Yue,[5] Thomas Berkemeier,[1] Ulrich Pöschl,[1] Haijie Tong.[1]

[1] Multiphase Chemistry Department, Max Planck Institute for Chemistry, 55128 Mainz, Germany

[2] School of Chemical and Biomolecular Engineering, Georgia Institute of Technology, Atlanta, Georgia 30332, United States

[3] University of Helsinki, Department, of Physics, P.O. Box 64, FI-00014, Finland

[4] Guangdong Provincial Engineering and Technology Research Center for Environmental Risk Prevention and Emergency Disposal, School of Environment and Energy, South China University of Technology, Guangzhou, China

[5] LAPC, Institute of Atmospheric Physics, Chinese Academy of Sciences, Beijing 100029, China

[6] School of Space and Environment, Beihang University, Beijing, 100191, China

Abstract

Environmentally persistent free radicals (EPFR) are a class of pollutants that are associated with atmospheric aerosols and may contribute to the adverse health effects of air particulate matter (PM). The size distribution and regional variability of EPFR in atmospheric aerosols, however, is not well characterized. Here, we report size-resolved concentration measurements of EPFR in PM covering a particle diameter range from nanometers to micrometers for different environments ranging from remote tropical and boreal forests (Amazon Tall Tower Observatory/ATTO, Brazil; Hyytiälä, Finland) to moderately or heavily polluted urban areas (Mainz, Germany; Beijing and Guangzhou, China).

Across the investigated locations, we found a strong increase of EPFR, i.e., unpaired electrons or spins detected by electron paramagnetic resonance spectroscopy (EPR), with the mass concentration of particles with diameters up to 10 µm (PM_{10}). The observed average values of the total volumetric spin concentration ranged from well below 10^{12} m^{-3} in clear forest air to more than 10^{13} m^{-3} in heavily polluted urban air. The average mass-specific spin concentrations in PM_{10} ranged between 3×10^{10} μg^{-1} and 3×10^{11} μg^{-1}.

In urban air, the size-resolved EPFR distribution exhibited a pronounced maximum in the sub-micrometer size range (PM_1), and a similar pattern was observed in the boreal forest aerosols from Hyytiälä. In contrast, the ATTO rainforest aerosol exhibited very low EPFR concentrations in the submicron size range and a peak in the coarse mode at particle diameters around 4 µm. These EPFR exhibit higher g-values than samples from other sites, which could be an indication for a different source at the ATTO site. Preliminary experiments indicate that primary biological aerosol particles could play a role in this, also biomass burning aerosols from long range transport could contribute to this phenomenon.

For the moderately polluted urban air in Mainz, we found a pronounced maximum of EPFR in the accumulation mode at particle diameters around 0.1-0.5 µm and higher concentrations in autumn and winter compared to spring and summer, which may be due to anthropogenic combustion emissions (traffic and heating). Based on this high-resolved EPFR size distribution in Mainz, we estimated the airway deposition behavior and found that measurements based on PM_1 capture most of the depositing EPFR.

Introduction

Airborne particulate matter (PM) plays an important role in air quality, climate, and public health, but the chemical composition and reactivity of PM are not yet well characterized – especially with regard to organic constituents (Pöschl, 2005; Farmer et al., 2015; Poschl and Shiraiwa, 2015; Shiraiwa et al., 2017; Knopf et al., 2018; Heald and Kroll, 2020). Particularly little is known about environmentally persistent free radicals (EPFR), which are a class of substances that contain unpaired electrons (spins) (Vejerano et al., 2018). They can be detected by electron paramagnetic resonance (EPR) measurements and exhibit chemical lifetimes in the range of hours to months depending on oxidation state, ambient conditions, and chemical shielding in the bulk material of particles (Dellinger et al., 2001; Gehling and Dellinger, 2013; Chen et al., 2018a; Tong et al., 2016). Among the EPFR detected in ambient PM are resonance-stabilized polycyclic aromatic compounds such as semiquinones and phenoxy radicals, which may play a key role in oxidative stress and adverse health effects caused by fine particulate matter with a diameter smaller than 2.5 μm ($PM_{2.5}$) (Dellinger et al., 2007; Khachatryan et al., 2011; Mahne et al., 2012; Arangio et al., 2016; Lakey et al., 2016; Harmon et al., 2018). Among the potential sources of EPFR are direct emissions from combustion processes (Yang et al., 2017; Vejerano et al., 2018; Chen et al., 2019a; Jia et al., 2020; Zhao et al., 2019a) as well as chemical formation in the atmosphere involving multiphase chemical reactions of secondary organic aerosols, transition metal ions, and photo-oxidants like ozone, nitrogen oxides and hydroxyl radicals (Kiruri et al., 2013; Borrowman et al., 2016; Patterson et al., 2017; Tong et al., 2018; Chen et al., 2018b; Zhu et al., 2019; Zhao et al., 2019b; Pan et al., 2019; Jia et al., 2018; Li et al., 2020).

A number of studies have investigated the concentration of EPFR in urban areas with various influences from traffic, industrial, and residential emissions (**Table**), showing a diverse seasonal variations and size dependence (Squadrito et al., 2001; Shaltout et al., 2015; Arangio et al., 2016; Yang et al., 2017; Chen et al., 2019a; Chen et al., 2020). Some of the observed differences and variations, however, may be due to different sampling and measurement techniques applied in different studies as will be discussed below (Sect. 3). In this study, we apply a set of sampling and measurement techniques to determine the spin concentrations and size distributions of EPFR in samples from both urban and remote areas of the world.

To the best of our knowledge, this study will be the first to provide a comparison of size-resolved concentrations of EPFR in different environments from remote tropical and boreal forests (ATTO, Brazil; Hyytiälä, Finland) to moderately and heavily polluted urban areas (Mainz, Germany; Guangzhou and Beijing, China). Furthermore, we extend the understanding of size-resolved EPFR concentrations into the Aitken particle size range and also their seasonal variability in Mainz, Germany. Based on the measured size distribution of EPFR and PM, we estimated the deposition potential of EPFR and PM in different sections of the human respiratory tract by the multiple path particle dosimetry (MPPD) model.

Methods

Particle collection

Particulate matter samples in Guangzhou and Beijing were collected using the same Andersen type impactor (Model 20-800 ambient cascade impactor from Tisch Environmental, Incorporation). The sampling was conducted from November 1st to December 23rd 2017 in Guangzhou and from August 29th to September 7th 2017 in Beijing. The air flow rate was 15-17 L min^{-1}. Samples were collected for 24-120 h intervals. More sampling information and detailed results can be found in Tables S6, S10, and S11.

The sampling in Mainz, Germany, was conducted on the roof of the Max Planck Institute for Chemistry (49.9912° N, 8.2284° E) with a micro-orifice uniform deposition impactor (MOUDI) sampler (122R-126, MSP Corporation now TSI Inc.). The air flow rate used in the MOUDI system was 30 L min^{-1}. Each set of filter samples was collected for about 48 h. The 47 and 90 mm diameter Teflon filters (0.1 µm pore size, Merck Chemicals GmbH) were used to collect 0.056-18 and 0.01-0.056 µm particles, respectively. Immediately after the sampling, filter samples were weighted and subsequently stored at -80 °C until analysis. The sampling period ranges from August 2017 to February 2020, more sampling information and detailed results can be found in Table S2, S3, and S5.

A MOUDI sampler (II 125R, MSP Corporation now TSI Inc.) and 47 mm diameter Teflon filters (0.1 µm pore size, Merck Chemicals GmbH) were used to collect 0.01-18 µm particles at the remote Amazon Tall Tower Observatory (ATTO) in the Amazon basin in Brazil (2.1459° S, 59.0056° W). The air flow rate used in the MOUDI system was 10 L min^{-1}. Each set of filter samples was collected for 5-9 consecutive days, from March 27th to April 25th 2017. More sampling details and detailed results are shown in Table S3, and S7. More information about the station can be found elsewhere (Andreae et al., 2015).

The sampling at SMEARII station in Hyytiälä, Finland, (61.8439° N, 24.2883° E) (Hari and Kulmala, 2005) took place between 31st of May and 16th of July 2017. A Dekati PM_{10} impactor was used for the sampling and the working air flow rate in the pump is 30 L min^{-1} (Laakso et al., 2003; Heikkinen et al., 2020). More sampling information and detailed results can be found in Table S4, and S8.

After the particle collection, all filter samples from Amazon, Hyytiälä, Beijing and Guangzhou were kept at -20°C until shipping to Mainz, which occurred as fast as possible. Thereafter samples were stored at -80°C before analysis, which was typically within one week after arrival. More detailed discussion about sampling efficiencies and weighing of filters can be found in the supplementary information.

EPR measurements

We used a continuous wave electron paramagnetic resonance X-band spectrometer (EMXplus10/12, Bruker Corporation) for the EPFR measurements. Filter samples with particulate matter were folded and inserted into an EPR high purity quartz tube with an inner diameter of 4 mm as described in our earlier study (Arangio et al., 2016). The tube was then inserted into a high sensitivity cavity, which was continuously flushed with a gentle stream of dry N_2 gas. Instrument parameters were set as follows: modulation frequency of 100 kHz; microwave frequency of 9.84 GHz, microwave power of 2.149 mW (20 db), sweep width of 70 G, sweep time of 20.63 s, receiver gain of 30 db, time constant of 81.92 ms, conversion time of 15.48 ms, scan number of 15, and the modulation amplitude was adjusted between 1 and 3 G depending on sample properties. The spin-counting method embedded in the Bruker software, Xenon, was applied to quantify

EPFR number of the respective filter samples. The spin-counting method was calibrated using the reference compound 4-hydroxy-2, 2, 6, 6-tetramethylpiperidin-1oxyl (TEMPOL). The detection limit of this approach is ~ 10^{10} spins. The g-value of samples was manually retrieved from the baseline corrected EPR spectra, by estimating the center of the EPFR signal in the 2nd derivative of the spectrum with the cursor. Uncertainties including instrumental and processing errors of this approach amount to an error in g-value of approximately +/- 0.0005.

Particle deposition model

We used the Multiple-Path Particle Dosimetry Model (MPPD V3.01) to calculate the size-resolved deposition potential of EPFR and PM in Mainz in the human respiratory tract. More details on this model can be found in the literature (Asgharian et al., 2001). As model settings we used the following conditions: Airway Morphometry *PNNL symmetric*, particle size 0.01-10 µm in 12 fractions, breathing was simulated with a constant exposure at 12 breaths min^{-1}, a 625 mL tidal volume and a 50 mL head volume with oronasal-mouth breathing. More concretely we modelled EPFR deposition for a case study, represented by the average size distribution of PM and EPFR measured in this study. Based on this we estimated the airway deposition potential in three different compartments: the head region including mouth, nose, and throat, the tracheobronchial region being the distributing network of airways, and lastly the pulmonary region, including the alveoli (Figure 5). The resulting deposition fractions can be found in Table S12.

Results and discussion

Regional distribution of EPFR in ambient particles

We compared the concentrations of particulate matter smaller than 10 µm (PM_{10}) and EPFR in environments ranging from remote forests (ATTO and Hyytiälä) to intermediately polluted (Mainz) and heavily polluted (Guangzhou and Beijing) urban air. As shown in Figure 1, PM_{10} and EPFR exhibit a positive correlation at log-log scale (R^2=0.99; $C_{v(spins)} = 10 + 1.2 \times 10^{11} \times PM_{10}$). Therein the remote forests exhibit lower PM_{10} concentrations, with Hyytiälä having a smaller average PM_{10} concentration (6 µg m^{-3}) than ATTO (10 µg m^{-3}). These values are comparable to previously reported PM_{10} concentrations in the two areas (Hari and Kulmala, 2005; Moran-Zuloaga et al., 2018). The higher PM_{10} concentration at ATTO is largely due to a dust event that occurred during the sampling period (Figure S6), because the PM_{10} concentration during non-dust events is around 3-4 µg m^{-3}at ATTO (Moran-Zuloaga et al., 2018). Higher concentrations of PM_{10} were observed in intermediately and heavily polluted urban air: 16 µg m^{-3} in Mainz, 38 µg m^{-3} in Guangzhou, and 161 µg m^{-3} in Beijing, which correspond to previously reported PM concentrations in these areas (Drewnick et al., 2006; Zhang and Cao, 2015). Similar like the PM_{10} mass concentrations, the volumetric EPFR concentrations (spins per cubic meter of sampled air, i.e. spins m^{-3}) increase from remote forests to polluted urban areas: Hyytiälä (0.41×10^{12}) < ATTO (0.88×10^{12}) < Mainz (1.34×10^{12}) < Guangzhou (3.32×10^{12}) < Beijing (26.33×10^{12}). The positive correlation of EPFR and PM_{10} in Figure 1 is in line with the positive correlation of EPFR and $PM_{2.5}$ across different regions as well as at single sampling sites (Chen et al., 2018b; Chen et al., 2019a; Xu et al., 2020; Qian et al., 2020). Taken together this finding emphasizes the great contribution of anthropogenic emissions to the EPFR and PM pollution in metropolitan areas.

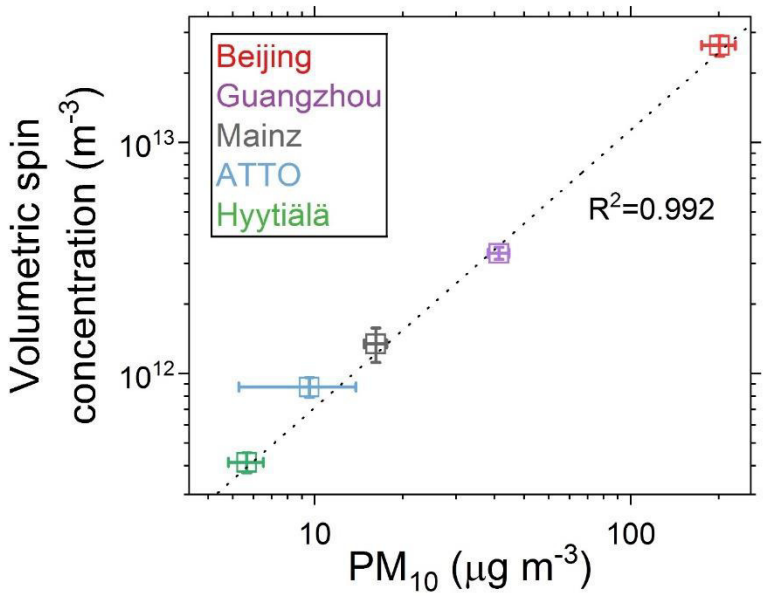

Figure 1: Total volumetric EPFR spin concentration (spin concentration per unit air volume, $C_{v(spins)}$) in PM_{10} sampled in different ambient areas plotted against the collected mass of particulate matter smaller than 10 µm (PM_{10}) at the respective site (Hyytiälä – 16 samples- , ATTO -4 samples-, Mainz - 40 samples-, Guangzhou - 8 samples, and Beijing - 5 samples). The black line is a linear fit of the indicated data points with a slope of 1.2 x 10^{12} spins μg^{-1}. The data points are arithmetic mean values and the error bars represent the standard error of the mean.

That this trend prevails also across different locations is not directly intuitive, because EPFR are believed to originate primarily from combustion sources and dust, with only minor contributions from other PM sources (Chen et al., 2018b; Vejerano et al., 2018). Accordingly by looking at different sampling sites with pronounced differences in PM source characteristics and varying influence from dust and combustion, a complicated relationship between PM mass and EPFR occurrence may be expected. Nevertheless our results show an almost linear correlation on a log-log scale from very remote places to large urban environments. However, for the data collected in Mainz only, this relationship is not so clear. These observations might be related to the different emission sources and meteorological conditions in Mainz, which did not induce a significant seasonality of PM mass concentrations (Table S14). Nevertheless it is know that PM sources are changing in different seasons in Mainz (Zhang et al., 2010), accordingly the temporal variability in the volumetric spin concentration may be closer connected to specific sources than to PM mass concentration considering only this site. Details about the mass-specific spin concentrations and it's correlation with PM mass can be found in Figure S7. Briefly all sites were found to have about ~10^{11} spins μg^{-1} of EPFR, only Beijing exhibited enhanced mass-specific concentrations in PM_{10}.

EPFR and PM concentrations in this study are compared with literature values in Table 1. Overall this table reinforce the findings in Figure 1: higher concentrations of EPFR in polluted urban air than in cleaner sites. Moreover, Table 1 shows the large variability of PM concentrations, EPFR concentrations, and EPFR characteristics across different studies. Therein the PM mass concentrations in Mainz, Guangzhou, and Beijing from this study cover the PM level range in literature studies that investigated EPFR abundance. The results for remote forest sites (ATTO and Hyytiälä) in this study are the first on EPFR in relative clean environments, indicated by their volumetric spin concentrations being lower than any other site. The EPFR concentrations in the intermediately polluted site in Mainz are comparable to recent data reported for a residential area in Denver (Colorado, USA) by Runberg et al. (2020) (1.04 - 1.07 x10^{12} m^{-3}). More literature results on EPFR concentrations in Chinese megacities are available for comparison with this study. For instance, Guo et al. (2020) observed 2.78 – 17.2 x10^{12} spins m^{-3} in Nanjing, where the $PM_{2.5}$ concentrations are up to 68 µg m^{-3}. This EPFR concentration is a bit higher than what we found in Guangzhou (2.68 x10^{12} m^{-3}), where we observed comparable mass concentrations of PM (42 µg m^{-3} for particles smaller 2.1 µm). Moreover, Chen et al. (2018b) found volumetric spin concentrations of 16-57 x10^{12} m^{-3} in $PM_{2.5}$ at three sampling sites in China (Erenhot, Zhangbei, Jinan), where the PM concentrations are between Guangzhou and Beijing. Finally, we found that the EPFR level in Guangzhou is lower and those for Beijing at a comparable level with that report (18 x10^{12} m^{-3} in PM smaller than 2.1 µm). Lastly, Chen et al. (2019a) found volumetric spin concentrations of 0.98 – 690 x10^{12} m^{-3} in Xi'an at $PM_{2.5}$ concentrations comparable to PM mass concentrations in Beijing and Guangzhou from this study. Therefore we conclude that under consideration of the varying site characteristics, our results complement and broaden the picture outlined by previous studies.

Size distribution of EPFR in ambient particulate matter

Beyond the content of EPFR in PM_{10} our data enable insights into the size distribution, therefore Figure 2 shows the size-resolved volumetric- (spins per sampled air volume, i.e. spins m^{-3}, left panels) and mass-specific concentrations (spins per microgram of collected PM, i.e., spins μg^{-1}, right panels) of EPFR in PM from different environments. We found that in Hyytiälä and urban areas (Beijing, Guangzhou, and Mainz), more EPFR were distributed in submicrometer particles (fine PM) than in supermicrometer particles (coarse PM). Whereas substantially more EPFR in coarse PM were observed at ATTO.

Table 1: Overview of characteristics and concentrations of EPFR and PM in different locations. Uncertainties of PM and EPFR concentrations in this study represent the standard error. *Size-resolved measurements for PM from different site. +Seasonality of EPFR for one constant sampling site.

site	site properties	g-value	PM size range	Mass-specific spin concentration ($x10^{11}$ μg^{-1})	Volumetric spin concentration ($x10^{12}$ m^{-3})	PM concentration (μg m^{-3})	study
Baton Rouge, USA	urban	2.0041	$PM_{2.5}$	0.28 ± 0.15	N/A	N/A	(Squadrito et al., 2001)
Durham, USA	urban	2.0036	$PM_{2.5}$	0.66 ± 0.32	N/A	N/A	
Phoenix, USA	urban	2.0032	$PM_{2.5}$	1.04 ± 0.46	N/A	N/A	
Philadelphia, USA	urban	2.0038	$PM_{2.5}$	0.64 ± 0.21	N/A	N/A	
Rubidoux, USA	urban	2.0039	$PM_{2.5}$	0.27 ± 0.11	N/A	N/A	
Baton Rouge, USA	urban	2.0035	$PM_{2.5}$	(0.20 – 34.8)	N/A	N/A	(Gehling and Dellinger, 2013)
Taif, Saudi Arabia	urban / suburban	2.0033-2.235	$PM_{2.5}$	(0.16-0.58)	N/A	48 ± 8	(Shaltout et al., 2015)
Mainz, Germany	suburban	2.003	0.056-10 µm*	2.00	N/A	N/A	(Arangio et al., 2016)*
Pune, India	rural	2.003	$PM_{2.5}$ / PM_{10}	(~ 1-10)	N/A	283 ± 185	(Roy et al., 2016)
	urban				N/A	176 ± 57	
Zhangbei, China	rural	2.0028-2.0033	$PM_{2.5}$	11.0	57.0	54 ± 26	(Chen et al., 2018b)
Jinan, China	urban	2.0026-2.0031	$PM_{2.5}$	4.60	46.0	103 ± 36	
Erenhot, China	urban	2.0030-2.0041	$PM_{2.5}$	3.70	16.0	56 ± 58	
Xuanwei, China	urban	2.0039-2.0046	TSP	(3.2 – 310)	N/A	N/A	(Wang et al., 2018)
Xi'an, China	urban	2.0029-2.0033	$PM_{2.5}$	(15.3 – 39.2)	(0.98 – 690)	(28-490)	(Chen et al., 2019a)+
Xi'an, China	urban	N/A	$PM_{2.5}$	(0.018 – 0.37)	(95 - 179)	(30-307)	(Wang et al., 2019)+
Beijing, China	urban	2.00339	$PM_{2.5}$	(2970 – 311000)	(6880 – 2950000)	N/A	(Xu et al., 2020)+
Wanzhou, China	urban	2.0032-2.0038	$PM_{2.5}$	(19.0 – 35.4)	70.0 ± 17	(23 – 43)	(Qian et al., 2020)
Linfen, China	urban	2.0031-2.0033	PM_{10}*	N/A	(252 – 570)	N/A	(Chen et al., 2020)*, +
Nanjing, China	urban	2.0029-2.0045	$PM_{2.5}$	(0.12 - 1.08)	(2.78 – 17.2)	(12-68)	(Guo et al., 2020)
Denver, USA	suburban	2.0016	$PM_{2.5}$	N/A	(1.04 - 1.07)	N/A	(Runberg et al., 2020)
Hyytiälä, Finland	remote	2.00299	PM_{10}*	0.80 ± 0.12	0.41 ± 0.07	6 ± 1	This study*
ATTO, Brazil	remote	2.00332	0.01-10 µm*	0.57 ± 0.17	0.88 ± 0.12	10 ± 8	
Mainz, Germany+	suburban	2.00282	0.01-10 µm*	0.94 ± 0.15	1.34 ± 0.23	16 ± 1	
Guangzhou, China	urban	2.00279	PM_{10}*	1.09 ± 0.13	3.32 ± 0.38	38 ± 2	
Beijing, China	urban	2.00271	PM_{10}*	1.22 ± 0.37	26.33 ± 2.70	191 ± 23	

More specifically, Beijing EPFR in particles smaller than 0.4 µm account for almost half of the detected spins (123 $x10^{11}$ m^{-3}), other fine particle fractions at this site contain relatively small amounts of EPFR. Among coarse particles in Beijing we found an increase towards larger particle size with the highest volumetric spin concentrations in 9-10 µm particles (30 $x10^{11}$ m^{-3}). Similar like Beijing, Guangzhou particles with diameter smaller than 0.4 µm also contain the highest concentration of EPFR (11 $x10^{11}$ m^{-3}), accounting for 1/3 of all detected EPFR species. In addition, 0.7-2.1 µm particles also contain 1/3 of EPFR, In Mainz fine PM also contain most EPFR, we observed on average most spins in particles with the biggest proportion in 0.056-0.560 µm particles (11 $x10^{11}$ m^{-3}) . Whereas, much lower concentrations of EPFR were found in coarse particles (<1 $x10^{11}$ m^{-3}). Interestingly, we also observed the enrichment of EPFR in ultrafine particles in Mainz (0.056-0.01 µm, 2 $x10^{11}$ m^{-3}), which is to the best of our knowledge the first report about EPFR in such small particles. Even though the lower MOUDI stages are particularly susceptible to bouncing of larger particles across several stages, we found consistently a significant amount of EPFR even in the smallest stage (0.01-0.018 µm), which is why we are confident about the occurrence of EPFR in ultrafine particles. Moreover at the remote forest site Hyytiälä, we also found most EPFR in fine particles (3.8 $x10^{11}$ m^{-3}) and coarse PM contains only a negligible amount of EPFR. The only area, where we found more EPFR in coarse particles (3.4 $x10^{11}$ m^{-3}) than in fine particles, is the ATTO site with 5.4 $x10^{11}$ spins m^{-3}.

Particulate matter at Atos composed of locally emitted primary biologic aerosols (PBA) and secondary organic aerosols (SOA) as well as long range transport of Saharan dust in combination with marine aerosols and biomass burning smoke from the Sahel region (Moran-Zuloaga et al., 2018). The generally low volumetric spin concentration of EPFR in ATTO is likely due the lack of local combustion particle emissions (Andreae et al., 2015). Even though dust storms have been established as source of EPFR in recent studies (Chen et al., 2018b; Wang et al., 2019), we found that mineral dust from long-range transport does not cause a strong increase of volumetric spin concentrations at ATTO (Figure S6, S13). This may be related to the long transport times of dust and the very high humidity at the site, which is known to reduce EPFR concentration in PM (Xu et al., 2020), especially as these samples were collected in the wet season of the Amazonian basin (Andreae et al., 2015; Moran-Zuloaga et al., 2018). Furthermore, Figure S13 shows, that the generally small concentrations of black carbon do not yield a conclusive correlation with the volumetric spin concentration. Therewith we assume that dust and combustion may have only a minor influence on EPFR in ATTO. Accordingly other sources could play a larger role in this remote environment e.g. secondary oxidation processes, such as photochemical formation from organic aerosols (Chen et al., 2019b; Wang et al., 2019; Li et al., 2020) and oxidation of PBA. In order to investigate the influence of photochemistry, we looked at the intensity of short-wave radiation in connection with the volumetric EPFR abundance, but the results are inconclusive. Nevertheless we found in preliminary experiments that different types of pollen contain EPFR (Figure S14) and also the large size of PBA could explain the higher EPFR content in coarse particles at ATTO (Huffman et al., 2012). Thereby processed primary biological particles may contribute to EPFR in particles larger 1 µm and influence the distinct EPFR size distribution at ATTO with most radicals in coarse particles.

Another indication for a different EPFR source at ATTO compared to the others sites is the g-value. The g-value is a qualitative information in EPR spectra, which enables clues about the chemical environment of the unpaired radical producing an EPR signal. For most organic radicals this value is close to the free electron signal (g_e = 2.0023), nevertheless the extent of deviation from this standard, yields hints on the structure also for organic radicals. We found that ATTO EPFR have the highest g-value of all sites in this study with g = 2.00332 (Table and Figure S3 and S10), which indicates a higher oxidation degree close to the radical center of the EPFR molecules (Segal et al., 1965). Also the EPFR we found in pollen (Figure

S14) exhibited a relatively large g-value of typically more than 2.004. Interestingly the other remote sampling site Hyytiälä exhibited the second highest value (g = 2.00299), which is still significantly higher than the samples from the suburban and urban sites with g = 2.00271-2.00282 (Table 1 and Figure S3). These observations could be indications that others sources than combustion, like photochemical EPFR formation involving highly oxygenated molecules or PBA, contribute a higher proportion or even most EPFR in remote environments like ATTO and Hyytiälä (Chen et al., 2019b; Li et al., 2020).

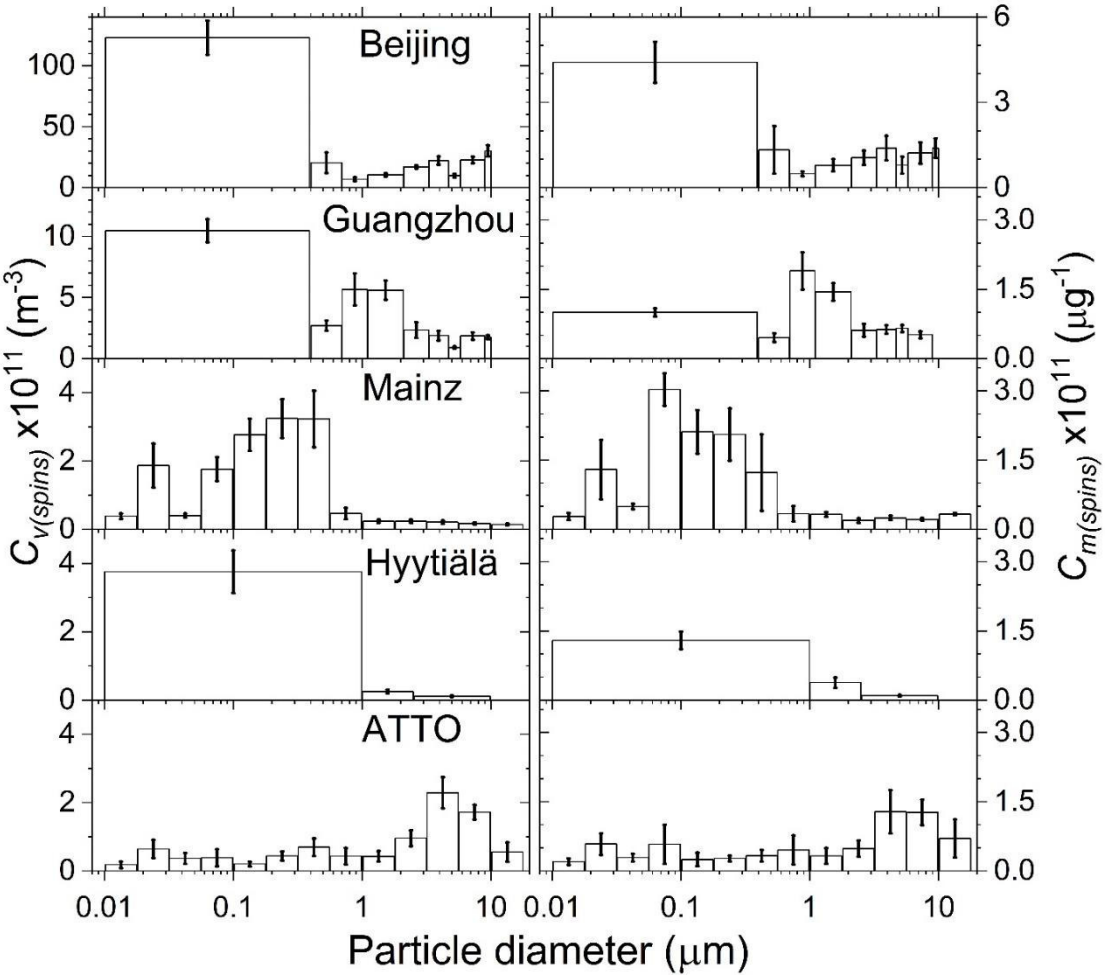

Figure 2: Panels on the left side show size resolved volumetric- and panels on the right side show mass-specific (spin concentration per unit mass of particulate matter, $C_{m(spins)}$) EPFR spin concentration in particulate matter from different locations. The width of the bars represents the respective sampled aerodynamic particle size interval. The height of the columns but not the area scales with the amount of spins in the respective size interval. Error bars represent the standard error of the mean.

The right panels in Figure 2 display the size-resolved mass-specific spin concentrations, which exhibit one order of magnitude variation. Overall the profile of the size-resolved mass-specific EPFR concentration in Beijing, Hyytiälä and ATTO PM resembles the volumetric EPFR concentrations at these sites (the left panels of Figure 2), whereas the highest Guangzhou and Mainz mass-specific EPFR concentrations were found in larger (0.7-1.1 µm) respectively smaller particles (0.056-0.1 µm) than the volumetric spin concentrations (< 0.4 µm for Guangzhou and 0.18-0.32 µm for Mainz). In Beijing, Hyytiälä and ATTO air, the highest mass-specific spin concentrations of EPFR were found in PM smaller 0.4 µm (4.4 x 10^{11} μg^{-1}),

smaller than 1 µm (1.3 x 10^{11} µg^{-1}), and 3.2-5.6 µm (4.4 x 10^{11} µg^{-1}), respectively. The lowest abundances of EPFR were found in PM between 0.7-1.1 µm (0.49 x 10^{11} µg^{-1}, Beijing), 2.5-10 µm (0.09 x 10^{11} µg^{-1}, Hyytiälä), and 0.01-0.018 µm (0.20 x 10^{11} µg^{-1}, ATTO), respectively. In contrast, the highest mass-specific spin concentrations in Guangzhou and Mainz were found in PM between 0.7-2.1 µm (1.4-1.6 x10^{11} µg^{-1}) and 0.054-1 µm (4.32 x10^{11} µg^{-1}), respectively. Furthermore, in Mainz PM the highest mass-specific spin concentrations (on average 4.32 x10^{11} µg^{-1}) were found to be one order of magnitude higher than EPFR concentrations in coarse PM (0.18-0.33 x 10^{11} µg^{-1}). Also in Hyytiälä we observed about one order of magnitude more EPFR in fine PM (1.30 x10^{11} µg^{-1}) than in coarse particles (0.09-0.38 x10^{11} µg^{-1}). To conclude it is noteworthy, that we found a high variety of size distributions of the mass-specific spin concentrations even though PM_{10} mass-specific EPFR concentration is relatively conserved across the sites in this study (Figure S7).

Among the sparse measurements of size-resolved EPFR concentrations, Chen et al. (2020) found higher EPFR concentrations in Linfen (China) (36-360 x10^{12} spins m^{-3} for different size fractions) than the urban and remote forest sites in this study. Furthermore, Chen and co-workers also found a major fraction (58%) of winter EPFR in particles smaller 2.1 µm, which is comparable to Guangzhou and Beijing PM in this study (74% for Guangzhou and 61% for Beijing). Moreover, the enrichment of EPFR in fine particles has also been observed by Yang et al. (2017), who found more than 70% of EPFR in $PM_{2.5}$ in Beijing covering a wide range of PM concentrations. However, a direct comparison of the absolute EPFR concentrations among different studies should be done with caution. For example, Yang and co-workers measured the extracted EPFR and not the sampled particle content directly. One reason for the small variations in between the cities could be differences in regional and local Pm sources as well as different oxidation states of the aerosol between these megacities (Tong et al., 2019). To conclude, most primary particles from combustion sources would typically exhibit a size below 1 µm (Cheng et al., 2012), which could be an explanation why we found most EPFR in cities to be in this size range. Nevertheless, differences in local PM sources and atmospheric chemistry are likely to have a substantial influence on the size distribution of EPFR.

Our previous study in Mainz found the highest mass-specific spin concentrations with 7 x10^{11} spins µg^{-1} for particles with 0.056-0.100 µm diameter (Arangio et al., 2016). This is in good agreement with the average concentration we found for particles of the same size fraction (5.88 x10^{11} spins µg^{-1}). The small deviation in between these studies may be attributed to different sample numbers, as variability of EPFR concentrations are pronounced (Figure S9). For instance we found that a strong storm in Mainz, resulted in a pronounced decrease not only of volumetric but also of mass-specific spin concentration (Table S1 and Figure S5). Other studies have investigated the effect of rain and changing humidity on EPFR concentration, which emphasizes the need for comprehensive studies covering a large range of meteorological conditions (Arangio et al., 2016; Xu et al., 2020). Nevertheless, we found a consistently high EPFR content for Mainz particles between 0.056 and 0.560 µm. This distribution reasonably corresponds to typical size distributions of combustion particles (Cheng et al., 2012), which are the most common EPFR sources (Vejerano et al., 2018). Combustion sources at this suburban site in Mainz are likely streets and highways in close proximity as well as residential heating in winter. With respect to the remote site in Hyytiälä, where we also found a high fraction of EPFR in particles smaller 1 µm, a large contribution of combustion to PM formation would be unexpected (Hari and Kulmala, 2005). In this environment, particle formation is typically dominated by secondary organic aerosols, these could produce persistent radicals upon photoexcitation (Chen et al., 2019b; Li et al., 2020) or during oxidation (Tong et al., 2018). This is supported by higher g-values in Hyytiälä than in the urban areas, as discussed above (Segal et al., 1965). Nonetheless, our findings indicate that this is resulting in less EPFR formation than combustion processes, indicated by the generally lower mass-specific concentrations found in this remote area. Accordingly, despite comparable EPFR size

distribution, the reasons for the relatively high mass-specific spin concentrations in fine particles may be different: while Mainz EPFR could be mainly linked to combustion, Hyytiälä EPFR could originate more from secondary photooxidation.

Hence, we found a high variability of size-resolved EPFR concentrations among the probed environments, which may be connected to differences in PM sources and meteorological conditions. Detailed lognormal size distributions of PM mass, as well as volumetric- and mass-specific spin concentrations of all sites can be found in the supplementary information (Table S2-5, Figure S1-S2). Generally combustion processes seem to play a dominating role in areas with pronounced anthropogenic influence, resulting in a high fraction of EPFR being associated to fine particulate matter. Conversely, in remote areas other (secondary) sources may contribute substantially to EPFR formation, resulting in a more complex distribution.

Seasonal variability of EPFR in different size PM from Mainz

Using the results from the long observation period in Mainz (>2 years) we analyzed the seasonal variability of the EPFR size distribution functions (Figure S4). We found that the mass-specific spin distribution exhibits similar patterns as the volumetric distribution. Moreover, based on a lognormal fitting, we also found that spring and summer EPFR exhibited a unimodal distribution, with the 0.18-0.32 µm particles containing most EPFR (accumulation mode). However, autumn and winter EPFR exhibited a bimodal distribution, with peak EPFR concentrations around 0.18-0.32 µm and 0.02-0.03 µm PM, respectively.

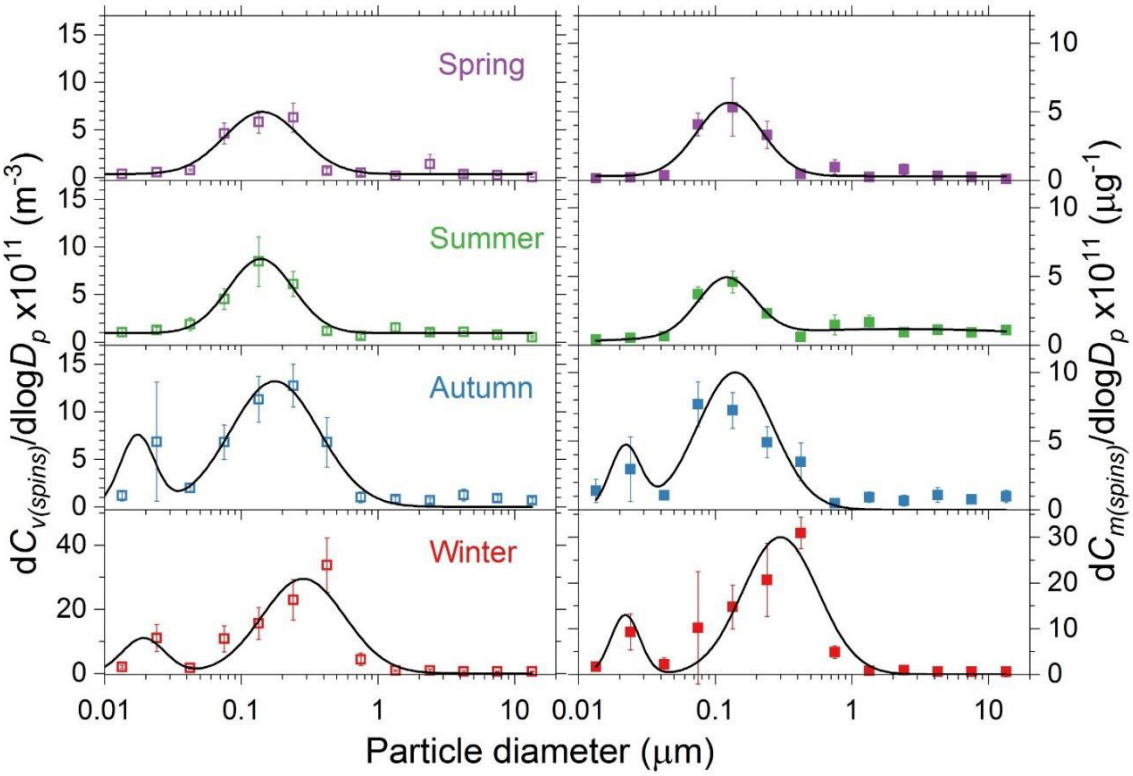

Figure 3: Size distribution of EPFR spin concentration in particulate matter from Mainz for different seasons. Panels on the left side show the size distribution function of the volumetric spin concentration, panels on right side show the size distribution function of the mass-specific spin concentration. Error bars represent uncertainties based on the standard error of the mean. Black lines represent lognormal fittings.

Panels on the left side in Figure 3 show that from summer to winter, the peak volumetric spin concentration based on the fitting is shifted to larger particles (summer: 7.6 x10^{11} m^{-3} at ~0.15 µm, winter: 33.8 x10^{11} m^{-3} at ~0.3 µm). Moreover we found an increase of EPFR in fine particles in autumn and winter compared to spring and summer, while simultaneously the average diameter of PM_{10} is increasing. More specifically, EPFR in autumn and winter occur in high volumetric spin concentrations in particles with 0.18-0.32 µm (~20 x10^{11} m^{-3}) as well as 0.018-0.032 µm diameter (~10 x10^{11} m^{-3}). This is substantially more than in summer and spring for 0.18-0.32 µm (~6 x10^{11} m^{-3}) and particles smaller 0.05 µm (<1 x10^{11} m^{-3}) respectively. The seasonal change in EPFR concentrations below 0.05 µm is reflected in the bimodal lognormal fitting of the size distribution function for autumn and winter (black lines). From now on we refer to this second mode as nucleation mode. In addition, we found increasing volumetric spin concentrations for the size fraction between 0.05 and 0.18 µm in the order spring, summer, autumn, and winter (5, 6, 9, 12 x10^{11} m^{-3}). We did not observe a significant seasonality for coarse particles, they were found to contain on average between 0.45 and 0.86 x10^{11} spin m^{-3} in the different seasons.

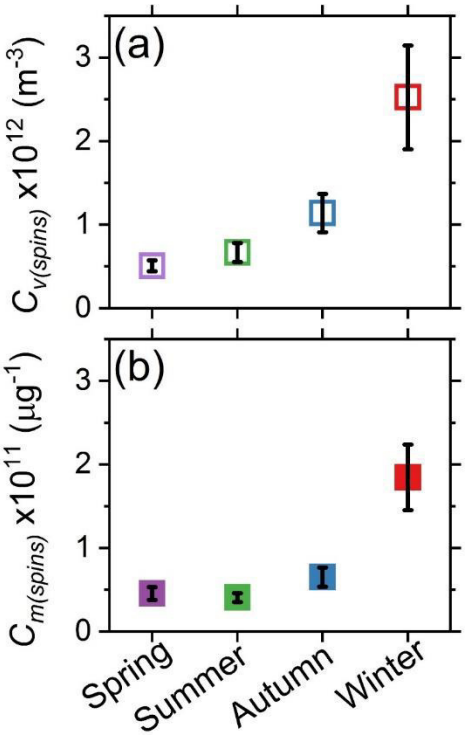

Figure 4: (a) Volumetric and (b) mass-specific EPFR spin concentrations in Mainz PM_{10} from different seasons. Error bars represent the standard error of the mean.

Right side panels in show that mass-specific EPFR spin distributions exhibited a similar pattern as the volumetric distributions. We found for all seasons an EPFR accumulation mode, which is centered on 0.15-0.30 µm and observed a nucleation mode in autumn and winter. The finding that both variables exhibit similar changes throughout the seasons indicates, that the seasonality of EPFR in Mainz could be driven by varying particle properties and therewith source characteristics. This is supported by the finding, that the PM mass distribution is very stable across the seasons in our study. More in detail, due the nucleation mode in autumn (2.4 x10^{11} µg^{-1}) and winter (7.1 x10^{11} µg^{-1}) EPFR concentrations in particles smaller 0.05 µm are much lower in spring and summer (~0.1 x10^{11} µg^{-1}). Moreover the mass-specific spin distribution function exhibits in all seasons a maximum in the fine particle range in the order spring<summer<autumn<winter (4.4, 6.4, 9.9, 23.3 x10^{11} µg^{-1}). This seasonality is less pronounced for coarse particles, therein summer,

autumn, and winter were found to have comparable EPFR concentrations (~1 $x10^{11}$ μg^{-1}), only the spring mass-specific spin concentration is significantly lower (~0.3 $x10^{11}$ μg^{-1}).

The lower EPFR abundance in fine particles in summer and spring could be explained by less heating activities in this suburban environment during warm periods (Birmili et al., 2001). A similar observation of volumetric spin concentrations in fine particulate matter increasing from summer to winter has been reported by Chen et al. (2020) for Linfen, which they attributed to varying local and regional sources of PM and EPFR across seasons (Zhang and Cao, 2015). For example, Chen et al. (2020) attributed the increase of wintertime fine EPFR in Linfen to residential coal heating, in Mainz other sources could play a larger role: Combustion processes in general (Dellinger et al., 2001) and more specifically motor vehicle emissions, dust, waste incineration, and industrial activities have been proposed as sources of EPFR (Chen et al., 2018b; Chen et al., 2019a; Wang et al., 2019). Moreover, the occurrence of a nucleation mode (0.02-0.03 µm) has been attributed to local sources before (Birmili et al., 2001), but not connecting these particles, combustion processes, and EPFR. If this finding is confirmed at other sites, nucleation size particles could serve as marker for changes in local combustion emissions. Especially as it can be expected, that the seasonality in EPFR size distribution may also appear at other sites than Mainz and Linfen, if these are studied over a longer period with size resolved particle collection. A particular finding in the seasonality of Mainz is, that we found pronounced changes in EPFR while PM concentrations and size distribution were relatively stable (Table S3). In other words there are only small variations in the quantity of PM in Mainz, but the sources may change considerably across seasons. As outlined above, enhanced combustion could be an explanation for the increase in wintertime EPFR, while sources of the spring and summertime PM with small spin content could be more similar to Hyytiälä and ATTO. Bioaerosols are an unlikely explanation due to the small amount of coarse particles collected. Other sources with increased emissions in spring and summer could be SOA or ammonia from agricultural activities or forests, which dominate the direct environment of the sampling site and could contribute to fine particle formation. Together, this emphasis the need for long-term measurements of size-resolved EPFR, which may yield insights into sources of EPFR in different.

Figure 4a shows the mean volumetric spin concentration in PM_{10} for different seasons in Mainz. Therein, we found for winter the highest EPFR concentrations (2.52 $x10^{12}$ m^{-3}), followed by autumn (1.14 $x10^{12}$ m^{-3}), summer (0.67 $x10^{12}$ m^{-3}), and spring (0.51 $x10^{12}$ m^{-3}). This seasonal variability of EPFR in PM_{10} may mainly be caused by changes of submicrometer PM composition as outlined in the paragraphs above, which is supported by the similar temporal EPFR distribution pattern between $PM_{2.5}$ and PM_1 (Figure S15) compared to Figure 4. Furthermore the contribution of coarse PM to the EPFR content decreases from 11% respectively 16% in spring and summer to only 4% in winter (8% in autumn). Another indicator for the central role of fine particles in the seasonality is, that changes of EPFR in coarse particles contribute less than 10% to the overall change from summer and spring to autumn and winter. As a result we conclude, that Mainz air in spring and summer contains less EPFR than in autumn and winter due to changes in submicron PM composition.

With respect to the mass–specific spin concentrations (Figure 4b), we found the same trend as for the volumetric concentration in Mainz: The winter EPFR concentration (1.85 $x10^{11}$ μg^{-1}) is substantially higher than autumn (0.65 $x10^{11}$ μg^{-1}), summer (0.41 $x10^{11}$ μg^{-1}), and spring (0.45 $x10^{11}$ μg^{-1}). As both volumetric and mass-specific EPFR revealed similar trends, the PM mass concentration should remain relatively constant. This is in fact, what our results in Mainz show: the average is comparatively stable (13-17.5 µg m^{-3}), with winter PM mass exhibiting the lowest concentrations. Accordingly, while varying sources and

outside temperatures may not have a strong impact on average PM levels across seasons in Mainz, the EPFR content of ambient PM increased especially in winter.

The described seasonality of the mass-specific spin concentration in Mainz can also be compared to investigations in Xi'an and Beijing (Xu et al., 2020; Chen et al., 2019a; Wang et al., 2019). Those three studies observed the highest mass normalized concentrations in $PM_{2.5}$ in spring, which is different from the pattern in Mainz (Figure 4b). This difference is reasonable because as outlined above, PM concentrations in Mainz do not increase in winter. To the contrary, cities like Beijing and Xi'an are known to experience increases in PM pollution in winter (Cheng et al., 2016; Shao et al., 2018; Shen et al., 2009). Consequently, combustion from heating in Mainz may be replacing other sources of PM and therewith increase the mass-specific spin concentration in winter as discussed above. In the same season in Beijing and Xi'an other sources like secondary nitrate and sulfate formation may result in increased ambient PM mass concentrations, therewith potentially diluting mass-specific spin concentrations. Another process, that might contribute to the lower mass-specific concentrations in Beijing and Xi'an in winter, is poisoning of trace metals by sulfate ions, which was found to prohibit EPFR formation (Feld-Cook et al., 2017). In other words, mass-specific EPFR concentrations in Mainz are highest in winter, which is different from Beijing and Xi'an due to varying sources of EPFR and PM.

Moreover Chen et al. (2019a) reported the following order of monthly resolved volumetric spin concentrations for $PM_{2.5}$ in the city of Xi'an in central China: winter (210×10^{12} m^{-3}) > spring > summer, autumn (70×10^{12} m^{-3}). Their trend across the different seasons is in reasonable agreement with our findings, thus wintertime air in urban environments seems to contain more EPFR than other seasons. This is also supported by other results for Xi'an (Wang et al., 2019) and Beijing (Xu et al., 2020), who reported a maximum in winter respectively a minimum in summer. In between these studies the degree of variation in between the seasons ranges from a factor 2 (Wang et al., 2019) to more than one order of magnitude (Xu et al., 2020). This may be a consequence of the varying degree to which other sources, like meteorology, dust intake, or biogenic emission can compensate the lower combustion emissions in warm seasons. Naturally, this is likely to be also dependent on the local extent and prevalent form of heating activities in winter. Taken together, with onset of the heating time in winter volumetric spin concentrations are increasing, which illustrates how combustion processes contribute to PM composition and therewith abundance of EPFR.

Airway deposition of EPFR

With the obtained detailed insights into EPFR size distribution in Mainz, we estimated the deposition potential in the lung upon inhalation (Figure 5). Using the Multiple-Path Particle Dosimetry Model (MPPD) (Asgharian et al., 2001), we differentiated the deposition potential into 3 compartments of the lung as shown in Figure 5a: head (green) representing mouth, nose, and throat, tracheobronchial (blue) being the distributing network, and lastly the pulmonary region (red) including the alveoli.

For the deposition potential of Mainz PM (Figure 5c), we found that submicrometer particles (PM_1) are the major fraction of Mainz PM_{10} mass that can be deposited in the airways. More specifically, PM_1 (fine particles) accounts for 74% of the total deposition potential of PM and still 54% of PM_{10} mass depositing in the airways are ultrafine particles (<0.1 µm). Moreover a small fraction of all particles in Mainz air is depositing in the head area (12%), which is about half the particle mass depositing in the tracheobronchial (22%) and pulmonary region (19%). There is an extensive body of literature describing the deposition behavior of PM in the airways (Kreyling et al., 2007; Rostami, 2009), which is why we do not go more into

these details. Overall our results agree well with the findings in those reports especially the outcome, that a majority of PM potentially depositing in the airways is smaller than 2.5 µm.

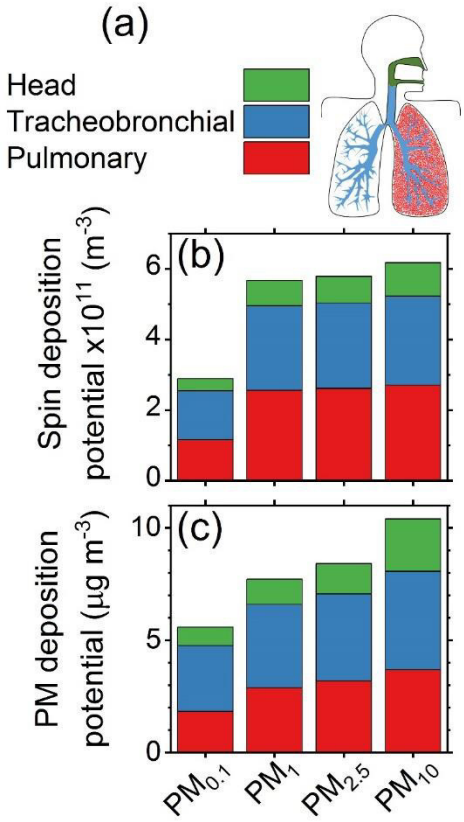

Figure 5: Estimated lung deposition potential of EPFR and PM for Mainz. (a) Schematic illustration of different sections of human airways with the following color code: green for head, blue for tracheobronchial tree, and red for pulmonary. (b) Deposition potential of EPFR in $PM_{0.1}$, PM_1, $PM_{2.5}$, and PM_{10}, in different regions of human airways. (c) Deposition potential of $PM_{0.1}$, PM_1, $PM_{2.5}$, and PM_{10} in different regions of human airways. The values for $PM_{2.5}$ are estimated taking all sampled stages for PM smaller than 1.8 µm and half of the stage covering 1.8-3.2 µm into account.

For the airway deposition potential of EPFR in Mainz PM (Figure 5b) we found that about 6 $x10^{11}$ spins per m^{-3} inhaled air are potentially depositing (43% of EPFR). More concretely, we found a very similar deposition potential as for PM: 92% of airway depositing EPFR in PM_{10} are associated to fine particles, with 47% being in ultrafine particles. Furthermore we found that the majority of potentially depositional EPFR in Mainz are reaching either the tracheobronchial (2.5 $x10^{11}$ m^{-3}) or pulmonary region (2.7 $x10^{11}$ m^{-3}), only 15% were found to deposit in the head region. This is particularly pronounced due to the small EPFR content in coarse particles (> 1 µm) in Mainz, which are more likely to deposit in the head region than smaller particles (Table S17). Accordingly, in environments with larger particles, their contribution might be substantially higher. Chen et al. (2020) have recently investigated the lung deposition of EPFR for such an environment with a higher proportion of EPFR in coarse particles namely Linfen in China. Consequently, they reported that about half of EPFR would be depositing in the upper airways. To our knowledge these are the only two studies to investigate lung deposition of EPFR. The differences in between Mainz and Linfen underline the importance of a more comprehensive understanding of EPFR size

distributions in different environments, to asses where these radicals are potentially depositing in the human airways and which role EPFR may play in the adverse health effects of particulate matter.

Conclusions

Within the scope of this study, we have analyzed the occurrence and size distribution of ambient EPFR from remote to urban environments. Furthermore we have investigated seasonal changes of EPFR in a suburban site in Mainz, Germany.

All studied sites had detectable concentrations of EPFR, even very remote sampling sites like the Amazon Tall Tower Observatory (ATTO), Brazil, or the SMEAR II station in Hyytiälä, Finland. Therein we found a positive correlation between volumetric EPFR spin concentration and PM mass concentration, in between the different sites.

The size resolved EPFR concentrations are highly variable in their distributions in different environments. In urban and suburban environments, most EPFR can be found in fine particles (<1 µm), but while Mainz shows a pronounced accumulation mode, Guangzhou PM has the highest concentrations in particles with about 1 µm diameter and also Beijing reveals a different pattern with high EPFR concentrations in particles larger 3 µm and smaller 1 µm. Among the remote environments with little anthropogenic influences, Hyytiälä PM also contains most EPFR in fine particles, while at the ATTO site coarse particles have the highest EPFR concentrations.

In these 2 remote places, there are almost no local combustion processes, which could contribute to the formation of fresh EPFR. Therewith in such environments other sources than combustion may be the dominating formation pathways of EPFRs. This could include secondary processing of secondary organic aerosols and primary biological aerosols (PBA) potentially involving photochemistry. Indications for this include a significant difference of the g-value between remote and urban environments, a case study of long range transported dust having little influence on ATTO EPFR concentrations, and preliminary experiments demonstrating the ability of PBA to contain EPFR.

A closer look at Mainz EPFR concentrations across seasons suggests, that there is a pronounced seasonality: Winter PM has a much higher mass-specific spin concentration than others seasons, while PM levels are largely unchanged. More concretely there is a pronounced increase in EPFR concentrations in accumulations size particles (<0.6 µm) and ultrafine particles (0.02-0.03 µm). This suggests changes in local sources of PM that have a pronounced impact on EPFR. These observation converge with increased heating activities in cold seasons (autumn and especially winter), which can be expected to have a substantial impact at the site. Lastly we estimated the airway deposition potential of EPFR and found a comparable distribution of airway deposition of EPFR and PM: A majority of radicals are likely to penetrate deep into the lung, particularly into the tracheobronchial tract, therein most EPFR potentially depositing are smaller than 2.5 µm.

Overall this study provides unprecedented insights into size-resolved EPFR abundance in different environments, revealing new clues about the variability of this emerging class of pollutants from remote sites to megacities. The data may help to improve the understanding about EPFR sources, its role in atmospheric processing as well as their relevance for the health effects of particulate matter.

Acknowledgments:

This work has been supported by the Max Planck Society (MPG) and the Max Planck Graduate Center with the Johannes Gutenberg University Mainz (MPGC). We would like to acknowledge the German Federal Ministry of Education and Research (BMBF contracts 01LB1001A and 01LK1602B) and the Max Planck Society, supporting this project as well as the construction and operation of the ATTO site. We also acknowledge the support of the Brazilian Ministério da Ciência, Tecnologia e Inovação (MCTI/FINEP contract 01.11.01248.00) as well as the Amazon State University (UEA), FAPEAM, LBA/INPA and SDS/CEUC/RDS-Uatumã for their support during construction and operation of the ATTO site. We thank INPA and all people involved in the operation of the ATTO site.

Author contribution:

HT, AF, FL, and SL designed and performed the experiments. HT, AF, conducted the experimental analysis with EPR spectroscopy. Weighing of samples was conducted by AF, FL, and SL.UP analyzed, interpreted and discussed the data. YM, SL collected and provided samples from Guangzhou; HR, SY, LL, and FS collected and provided samples from Beijing; FD and CP collected and provided samples from ATTO; TP and MK collected and provided samples from Finland; MP, CP, TB for further analysis/discussion of atmospheric aerosol perspectives. All authors contributed to the preparation and editing of the manuscript.

Competing interests: The authors declare that they have no conflict of interest.

References

Andreae, M., Acevedo, O., Araùjo, A., Artaxo, P., Barbosa, C., Barbosa, H., Brito, J., Carbone, S., Chi, X., and Cintra, B.: The Amazon Tall Tower Observatory (ATTO): overview of pilot measurements on ecosystem ecology, meteorology, trace gases, and aerosols, Atmospheric Chemistry and Physics, 15, 10723-10776, 2015.

Arangio, A. M., Tong, H., Socorro, J., Pöschl, U., and Shiraiwa, M.: Quantification of environmentally persistent free radicals and reactive oxygen species in atmospheric aerosol particles, Atmospheric Chemistry and Physics, 16, 13105-13119, 10.5194/acp-16-13105-2016, 2016.

Asgharian, B., Hofmann, W., and Bergmann, R.: Particle deposition in a multiple-path model of the human lung, Aerosol Science & Technology, 34, 332-339, 2001.

Birmili, W., Wiedensohler, A., Heintzenberg, J., and Lehmann, K.: Atmospheric particle number size distribution in central Europe: Statistical relations to air masses and meteorology, Journal of Geophysical Research: Atmospheres, 106, 32005-32018, 2001.

Borrowman, C. K., Zhou, S., Burrow, T. E., and Abbatt, J. P.: Formation of environmentally persistent free radicals from the heterogeneous reaction of ozone and polycyclic aromatic compounds, Phys Chem Chem Phys, 18, 205-212, 10.1039/c5cp05606c, 2016.

Chen, Q., Sun, H., Wang, M., Mu, Z., Wang, Y., Li, Y., Wang, Y., Zhang, L., and Zhang, Z.: Dominant Fraction of EPFRs from Nonsolvent-Extractable Organic Matter in Fine Particulates over Xi'an, China, Environmental science & technology, 52, 9646-9655, 2018a.

Chen, Q., Wang, M., Sun, H., Wang, X., Wang, Y., Li, Y., Zhang, L., and Mu, Z.: Enhanced health risks from exposure to environmentally persistent free radicals and the oxidative stress of PM2. 5 from Asian dust storms in Erenhot, Zhangbei and Jinan, China, Environment international, 121, 260-268, 2018b.

Chen, Q., Sun, H., Mu, Z., Wang, Y., Li, Y., Zhang, L., Wang, M., and Zhang, Z.: Characteristics of environmentally persistent free radicals in PM2. 5: Concentrations, species and sources in Xi'an, Northwestern China, Environmental Pollution, 247, 18-26, 2019a.

Chen, Q., Sun, H., Wang, M., Wang, Y., Zhang, L., and Han, Y.: Environmentally persistent free radical (EPFR) formation by visible-light illumination of the organic matter in atmospheric particles, Environ Sci Technol, 10.1021/acs.est.9b02327, 2019b.

Chen, Q., Sun, H., Song, W., Cao, F., Tian, C., and Zhang, Y. L.: Size-resolved exposure risk of persistent free radicals (PFRs) in atmospheric aerosols and their potential sources, Atmos. Chem. Phys. Discuss., 2020, 1-26, 10.5194/acp-2020-141, 2020.

Cheng, Y., Su, H., Rose, D., Gunthe, S., Berghof, M., Wehner, B., Achtert, P., Nowak, A., Takegawa, N., and Kondo, Y.: Size-resolved measurement of the mixing state of soot in the megacity Beijing, China: diurnal cycle, aging and parameterization, 2012.

Cheng, Y., Zheng, G., Wei, C., Mu, Q., Zheng, B., Wang, Z., Gao, M., Zhang, Q., He, K., and Carmichael, G.: Reactive nitrogen chemistry in aerosol water as a source of sulfate during haze events in China, Science Advances, 2, e1601530, 2016.

Dellinger, B., Pryor, W. A., Cueto, R., Squadrito, G. L., Hegde, V., and Deutsch, W. A.: Role of Free Radicals in the Toxicity of Airborne Fine Particulate Matter, Chemical Research in Toxicology, 14, 1371-1377, 2001.

Dellinger, B., Lomnicki, S., Khachatryan, L., Maskos, Z., Hall, R. W., Adounkpe, J., McFerrin, C., and Truong, H.: Formation and stabilization of persistent free radicals, Proceedings of the Combustion Institute, 31, 521-528, 2007.

Drewnick, F., Hings, S. S., Curtius, J., Eerdekens, G., and Williams, J.: Measurement of fine particulate and gas-phase species during the New Year's fireworks 2005 in Mainz, Germany, Atmospheric Environment, 40, 4316-4327, 2006.

Farmer, D. K., Cappa, C. D., and Kreidenweis, S. M.: Atmospheric processes and their controlling influence on cloud condensation nuclei activity, Chemical reviews, 115, 4199-4217, 2015.

Feld-Cook, E. E., Bovenkamp-Langlois, L., and Lomnicki, S. M.: Effect of Particulate Matter Mineral Composition on Environmentally Persistent Free Radical (EPFR) Formation, Environ Sci Technol, 51, 10396-10402, 10.1021/acs.est.7b01521, 2017.

Gehling, W., and Dellinger, B.: Environmentally persistent free radicals and their lifetimes in PM2.5, Environ Sci Technol, 47, 8172-8178, 10.1021/es401767m, 2013.

Guo, X., Zhang, N., Hu, X., Huang, Y., Ding, Z., Chen, Y., and Lian, H.-z.: Characteristics and potential inhalation exposure risks of PM2. 5–bound environmental persistent free radicals in Nanjing, a mega–city in China, Atmospheric Environment, 224, 117355, 2020.

Hari, P., and Kulmala, M.: Station for measuring ecosystem-atmosphere relations (SMEAR II), Boreal. Env. Res., 10, 315-322, 2005.

Harmon, A. C., Hebert, V. Y., Cormier, S. A., Subramanian, B., Reed, J. R., Backes, W. L., and Dugas, T. R.: Particulate matter containing environmentally persistent free radicals induces AhR-dependent cytokine and reactive oxygen species production in human bronchial epithelial cells, PLoS One, 13, e0205412, 10.1371/journal.pone.0205412, 2018.

Heald, C. L., and Kroll, J.: The fuel of atmospheric chemistry: Toward a complete description of reactive organic carbon, Science advances, 6, eaay8967, 2020.

Heikkinen, L., Äijälä, M., Riva, M., Luoma, K., Dällenbach, K., Aalto, J., Aalto, P., Aliaga, D., Aurela, M., Keskinen, H., Makkonen, U., Rantala, P., Kulmala, M., Petäjä, T., Worsnop, D., and Ehn, M.: Long-term sub-micrometer aerosol chemical composition in the boreal forest: inter- and intra-annual variability, Atmos. Chem. Phys., 20, 3151-3180, 10.5194/acp-20-3151-2020, 2020.

Huffman, J., Sinha, B., Garland, R., Snee-Pollmann, A., Gunthe, S., Artaxo, P., Martin, S., Andreae, M., and Pöschl, U.: Biological aerosol particle concentrations and size distributions measured in pristine tropical rainforest air during AMAZE-08, Atmos. Chem. Phys, 12, 11997-12019, 2012.

Jia, H., Zhao, S., Shi, Y., Zhu, L., Wang, C., and Sharma, V. K.: Transformation of Polycyclic Aromatic Hydrocarbons and Formation of Environmentally Persistent Free Radicals on Modified Montmorillonite: The Role of Surface Metal Ions and Polycyclic Aromatic Hydrocarbon Molecular Properties, Environ Sci Technol, 52, 5725-5733, 10.1021/acs.est.8b00425, 2018.

Jia, H., Li, S., Wu, L., Li, S., Sharma, V. K., and Yan, B.: Cytotoxic free radicals on air-borne soot particles generated by burning wood or low-maturity coals, Environmental Science & Technology, 2020.

Khachatryan, L., Vejerano, E., Lomnicki, S., and Dellinger, B.: Environmentally persistent free radicals (EPFRs). 1. Generation of reactive oxygen species in aqueous solutions, Environmental science & technology, 45, 8559-8566, 2011.

Kiruri, L. W., Dellinger, B., and Lomnicki, S.: Tar balls from Deep Water Horizon oil spill: environmentally persistent free radicals (EPFR) formation during crude weathering, Environmental science & technology, 47, 4220-4226, 2013.

Knopf, D. A., Alpert, P. A., and Wang, B.: The role of organic aerosol in atmospheric ice nucleation: a review, ACS Earth and Space Chemistry, 2, 168-202, 2018.

Kreyling, W. G., Möller, W., Semmler-Behnke, M., Oberdörster, G., Donaldson, K., and Borm, P.: Particle dosimetry: deposition and clearance from the respiratory tract and translocation towards extrapulmonary sites, Particle toxicology, 2007, 2007.

Laakso, L., Hussein, T., Aarnio, P., Komppula, M., Hiltunen, V., Viisanen, Y., and Kulmala, M.: Diurnal and annual characteristics of particle mass and number concentrations in urban, rural and Arctic environments in Finland, Atmos. Environ., 37, 2629-2641, 2003.

Lakey, P. S., Berkemeier, T., Tong, H., Arangio, A. M., Lucas, K., Poschl, U., and Shiraiwa, M.: Chemical exposure-response relationship between air pollutants and reactive oxygen species in the human respiratory tract, Sci Rep, 6, 32916, 10.1038/srep32916, 2016.

Li, X., Shen, C., Zhao, H., Jiang, J., Ban, Z., Chen, Z., and Qu, B.: Photoformation of persistent free radicals on a montmorillonite-humic acid complex simulated as particulate organic matter in an aqueous solution, Environmental Science: Processes & Impacts, 2020.

Mahne, S., Chuang, G. C., Pankey, E., Kiruri, L., Kadowitz, P. J., Dellinger, B., and Varner, K. J.: Environmentally persistent free radicals decrease cardiac function and increase pulmonary artery pressure, American Journal of Physiology-Heart and Circulatory Physiology, 303, H1135-H1142, 2012.

Moran-Zuloaga, D., Ditas, F., Walter, D., Saturno, J., Brito, J., Carbone, S., Chi, X., de Angelis, I. H., Baars, H., and Godoi, R. H.: Long-term study on coarse mode aerosols in the Amazon rain forest with the frequent intrusion of Saharan dust plumes, Atmospheric Chemistry and Physics, 18, 10055-10088, 2018.

Pan, B., Li, H., Lang, D., and Xing, B.: Environmentally persistent free radicals: Occurrence, formation mechanisms and implications, Environmental Pollution, 2019.

Patterson, M. C., DiTusa, M. F., McFerrin, C. A., Kurtz, R. L., Hall, R. W., Poliakoff, E. D., and Sprunger, P. T.: Formation of environmentally persistent free radicals (EPFRs) on ZnO at room temperature: Implications for the fundamental model of EPFR generation, Chem Phys Lett, 670, 5-10, 10.1016/j.cplett.2016.12.061, 2017.

Poschl, U., and Shiraiwa, M.: Multiphase chemistry at the atmosphere-biosphere interface influencing climate and public health in the anthropocene, Chem Rev, 115, 4440-4475, 10.1021/cr500487s, 2015.

Pöschl, U.: Atmospheric aerosols: composition, transformation, climate and health effects, Angewandte Chemie International Edition, 44, 7520-7540, 2005.

Qian, R., Zhang, S., Peng, C., Zhang, L., Yang, F., Tian, M., Huang, R., Wang, Q., Chen, Q., and Yao, X.: Characteristics and Potential Exposure Risks of Environmentally Persistent Free Radicals in PM2. 5 in the Three Gorges Reservoir Area, Southwestern China, Chemosphere, 126425, 2020.

Rostami, A. A.: Computational Modeling of Aerosol Deposition in Respiratory Tract: A Review, Inhalation Toxicology, 21, 262-290, 10.1080/08958370802448987, 2009.

Roy, R., Jan, R., Yadav, S., Vasave, M. H., and Satsangi, P. G.: Study of metals in radical-mediated toxicity of particulate matter in indoor environments of Pune, India, Air Quality, Atmosphere & Health, 9, 669-680, 2016.

Runberg, H. L., Mitchell, D. G., Eaton, S. S., Eaton, G. R., and Majestic, B. J.: Stability of environmentally persistent free radicals (EPFR) in atmospheric particulate matter and combustion particles, Atmospheric Environment, 117809, 2020.

Segal, B. G., Kaplan, M., and Fraenkel, G. K.: Measurement of g values in the electron spin resonance spectra of free radicals, The Journal of Chemical Physics, 43, 4191-4200, 1965.

Shaltout, A. A., Boman, J., Shehadeh, Z. F., Dhaif-allah, R., Hemeda, O., and Morsy, M. M.: Spectroscopic investigation of PM2. 5 collected at industrial, residential and traffic sites in Taif, Saudi Arabia, Journal of Aerosol Science, 79, 97-108, 2015.

Shao, P., Tian, H., Sun, Y., Liu, H., Wu, B., Liu, S., Liu, X., Wu, Y., Liang, W., and Wang, Y.: Characterizing remarkable changes of severe haze events and chemical compositions in multi-size airborne particles (PM1, PM2. 5 and PM10) from January 2013 to 2016–2017 winter in Beijing, China, Atmospheric Environment, 189, 133-144, 2018.

Shen, Z., Cao, J., Arimoto, R., Han, Z., Zhang, R., Han, Y., Liu, S., Okuda, T., Nakao, S., and Tanaka, S.: Ionic composition of TSP and PM2. 5 during dust storms and air pollution episodes at Xi'an, China, Atmospheric Environment, 43, 2911-2918, 2009.

Shiraiwa, M., Li, Y., Tsimpidi, A. P., Karydis, V. A., Berkemeier, T., Pandis, S. N., Lelieveld, J., Koop, T., and Poschl, U.: Global distribution of particle phase state in atmospheric secondary organic aerosols, Nat Commun, 8, 15002, 10.1038/ncomms15002, 2017.

Squadrito, G. L., Cueto, R., Dellinger, B., and Pryor, W. A.: Quinoid redox cycling as a mechanism for sustained free radical generation by inhaled airborne particulate matter, Free Radical Biology and Medicine, 31, 1132-1138, 2001.

Tong, H., Arangio, A. M., Lakey, P. S. J., Berkemeier, T., Liu, F., Kampf, C. J., Brune, W. H., Pöschl, U., and Shiraiwa, M.: Hydroxyl radicals from secondary organic aerosol decomposition in water, Atmospheric Chemistry and Physics, 16, 1761-1771, 10.5194/acp-16-1761-2016, 2016.

Tong, H., Lakey, P. S. J., Arangio, A. M., Socorro, J., Shen, F., Lucas, K., Brune, W. H., Poschl, U., and Shiraiwa, M.: Reactive Oxygen Species Formed by Secondary Organic Aerosols in Water and Surrogate Lung Fluid, Environ Sci Technol, 10.1021/acs.est.8b03695, 2018.

Tong, H., Zhang, Y., Filippi, A., Wang, T., Li, C., Liu, F., Leppla, D., Kourtchev, I., Wang, K., and Keskinen, H.-M.: Radical formation by fine particulate matter associated with highly oxygenated molecules, Environmental science & technology, 53, 12506-12518, 2019.

Vejerano, E. P., Rao, G., Khachatryan, L., Cormier, S. A., and Lomnicki, S.: Environmentally persistent free radicals: insights on a new class of pollutants, Environmental science & technology, 52, 2468-2481, 2018.

Wang, P., Pan, B., Li, H., Huang, Y., Dong, X., Ai, F., Liu, L., Wu, M., and Xing, B.: The overlooked occurrence of environmentally persistent free radicals in an area with low-rank coal burning, Xuanwei, China, Environmental science & technology, 52, 1054-1061, 2018.

Wang, Y., Li, S., Wang, M., Sun, H., Mu, Z., Zhang, L., Li, Y., and Chen, Q.: Source apportionment of environmentally persistent free radicals (EPFRs) in PM2. 5 over Xi'an, China, Science of The Total Environment, 689, 193-202, 2019.

Xu, Y., Yang, L., Wang, X., Zheng, M., Li, C., Zhang, A., Fu, J., Yang, Y., Qin, L., and Liu, X.: Risk evaluation of environmentally persistent free radicals in airborne particulate matter and influence of atmospheric factors, Ecotoxicology and Environmental Safety, 196, 110571, 2020.

Yang, L., Liu, G., Zheng, M., Jin, R., Zhu, Q., Zhao, Y., Wu, X., and Xu, Y.: Highly elevated levels and particle-size distributions of environmentally persistent free radicals in haze-associated atmosphere, Environmental science & technology, 51, 7936-7944, 2017.

Zhang, Y.-L., and Cao, F.: Fine particulate matter (PM 2.5) in China at a city level, Scientific reports, 5, 14884, 2015.

Zhang, Y., Müller, L., Winterhalter, R., Moortgat, G., Hoffmann, T., and Pöschl, U.: Seasonal cycle and temperature dependence of pinene oxidation products, dicarboxylic acids and nitrophenols in fine and coarse air particulate matter, Atmospheric Chemistry and Physics, 10, 7859-7873, 2010.

Zhao, S., Gao, P., Miao, D., Wu, L., Qian, Y., Chen, S., Sharma, V. K., and Jia, H.: Formation and Evolution of Solvent-Extracted and Non-Extractable Environmentally Persistent Free Radicals in Fly Ash of Municipal Solid Waste Incinerators, Environmental science & technology, 2019a.

Zhao, S., Miao, D., Zhu, K., Tao, K., Wang, C., Sharma, V. K., and Jia, H.: Interaction of benzo [a] pyrene with Cu (II)-montmorillonite: Generation and toxicity of environmentally persistent free radicals and reactive oxygen species, Environment international, 129, 154-163, 2019b.

Zhu, K., Jia, H., Zhao, S., Xia, T., Guo, X., Wang, T., and Zhu, L.: Formation of Environmentally Persistent Free Radicals on Microplastics under Light Irradiation, Environmental Science & Technology, 2019.

Supplementary information for

Size distribution and regional variations of environmentally persistent free radicals (EPFR) in air particulate matter

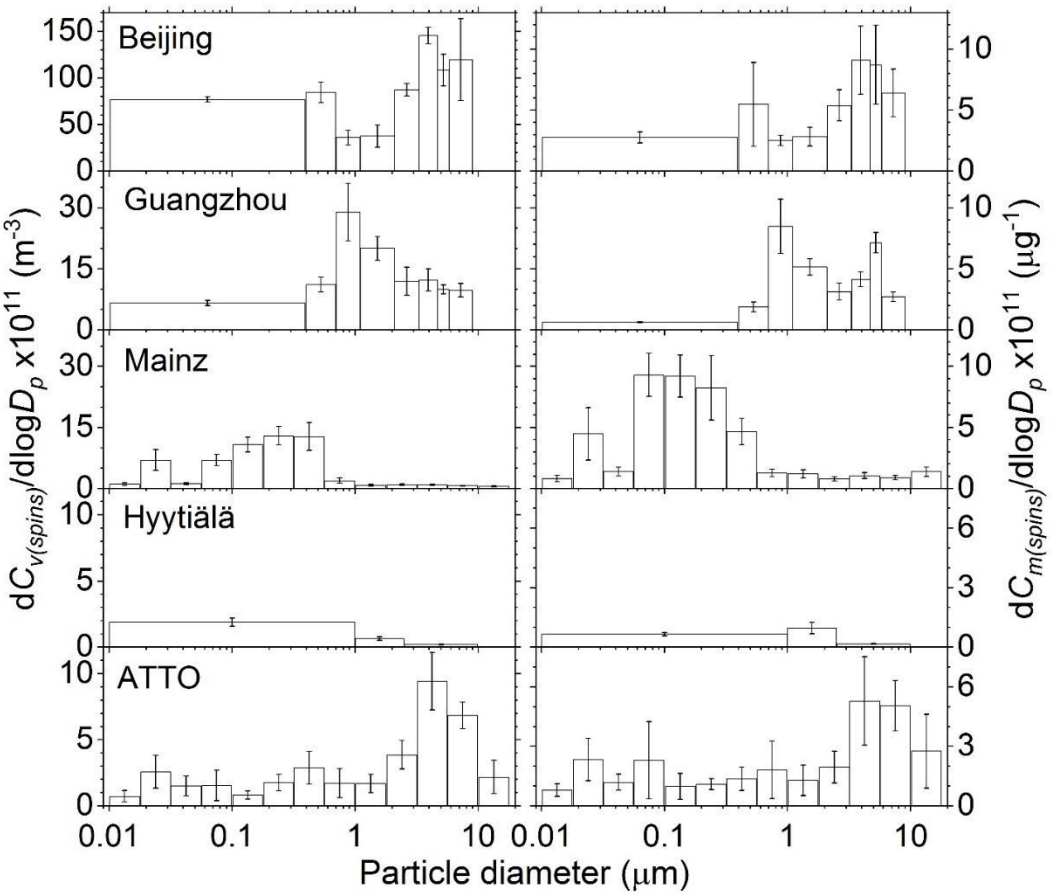

Figure S1: Log-normalized size distribution of EPFR spin concentration in particulate matter from remote tropical and boreal forests (ATTO, Brazil; Hyytiälä, Finland) to moderately and heavily polluted urban areas (Mainz, Germany; Beijing/Guangzhou, Beijing/China). Panels on the left show the size distribution per unit air volume (volumetric concentration, $C_{v(spins)}$), panels on the right show the size distribution per unit mass of particulate matter (mass specific concentration, $C_{m(spins)}$). All values are normalized by the size of the respective sampled particle diameter range (logDp). Therewith the area of the columns scales directly with the amount of EPFR. Error bars represent uncertainties based on the standard error of the mean.

Lognormal EPFR Size-Distribution

Figure S1 shows the size distribution of EPFR normalized by the range of sampled particle sizes ($logD_p$). Panels on the left side show volumetric - ($C_{v(spins)}$, spins per sampled air volume, i.e. spins m^{-3}) and panels in the right side mass-specific ($C_{m(spins)}$, spins per sampled particle mass, i.e. spins μg^{-1}) spin concentrations

in PM from different environments. Results will be discussed in two groups, sorted by the available size resolution for submicrometer particles: Beijing, Guangzhou, and Hyytiälä are group 1, Mainz and ATTO are group 2 details about the different samplers can be found in the methods section.

For group 1 we have only limited information about the distribution within the fractions captured by back-up filters (<1 µm for Hyytiälä and < 0.4 µm for Beijing and Guangzhou). Nevertheless, we found that in Hyytiälä submicrometer particles (fine PM) contain most EPFR (1.9 x 10^{11} m^{-3}), followed by 1-2.5 µm particles (0.6 x 10^{11} m^{-3}), and particles larger 2.5 µm containing only 0.2 x 10^{11} spins m^{-3}. This is true for the volumetric distribution, accordingly most EPFR in Hyytiälä are in fine PM (see also Figure S8). Furthermore Figure S1 shows, that with regard to the mass-specific spin concentrations, particles between 1 and 2.5 µm have the highest EPFR concentration (1.0 x 10^{11} μg^{-1}). Compared to the other 2 sites in this group Hyytiälä PM contains in all size ranges substantially less EPFR than Beijing and Guangzhou.

Even though these 2 sites are both located in large Chinese cities, we found that the EPFR distribution exhibits pronounced differences. More concretely in Beijing we found that particle fractions larger than 2.1 µm contain constantly high volumetric spin concentrations (87-145 x 10^{11} m^{-3}). Furthermore, around 1 µm we found a minimum in volumetric spin concentration (36 x 10^{11} m^{-3}), while PM smaller 0.7 µm exhibited again higher EPFR concentrations 77-84 x 10^{11} m^{-3}. Different from this, the size distribution for Guangzhou samples shows a steady increase in the lognormal spin abundance towards particle diameters 0.7-1.1 µm (29 x 10^{11} m^{-3}). In the particle fraction smaller than 0.4 µm (7 x 10^{11} m^{-3}) and in particles with 5.8-9 µm diameter (10 x 10^{11} m^{-3}) we found the smallest volumetric spin concentrations. Nonetheless due to the wide particle range covered in the < 0.4 µm PM fraction, about 1/3 of all EPFR is found in this fraction in Guangzhou, which is roughly the same as in particles between 0.7 and 2.1 µm (49 x 10^{11} m^{-3}). Therewith also in the two cities in this group a majority of 57% of EPFR were found in particles smaller 1 µm (Figure S8).

With respect to the mass-specific spin concentration, we found comparable size distributions to the volumetric measure: Beijing particles contain high spin concentrations in PM larger 2.1 µm and with 0.4-0.7 µm (5.4 -9.1 x 10^{11} μg^{-1}), while Guangzhou PM displays a maximum around 0.7-1.1 µm (8.5 x 10^{11} μg^{-1}). Interestingly we found that the values of $dC_{m(spins)}/d\log D_p$ do not vary strongly in between Beijing and Guangzhou, only the smallest size fraction shows a much higher EPFR content in Beijing (0.6 x 10^{11} μg^{-1} in Guangzhou and 2.8 x 10^{11} μg^{-1} in Beijing). This similarity in the mass specific spin concentration in Guangzhou and Beijing is surprising, because the two sites have pronounced differences in PM sources and local atmospheric chemistry (Zhang et al., 2015). An explanation for that observation could be competing effects, which balance each other out in this particular case: stronger relative contributions from combustion and heating activities may increase the EPFR concentration per particle mass (Vejerano et al., 2018), on the other hand different PM constituents like SO_4^{2-} could quench some of these radicals (Feld-Cook et al., 2017).

Moreover the results from Hyytiälä suggest, that in such a remote environment the shortage of combustion sources (Hari et al., 2005) may results in decreased mass-specific spin concentration. Nevertheless we found a significant amount of EPFR even at this boreal site, where typically secondary organic aerosols (SOA) are the dominating PM source. Therewith in such remote places, SOA could contribute significantly in producing persistent radicals upon photoexcitation (Chen et al., 2019b; Li et al., 2020) or during oxidation (Tong et al., 2018). The observed higher volumetric spin concentrations in fine particles at Hyytiälä could be another argument for this EPFR formation pathway from SOA. On the other hand the EPFR in fine PM in Beijing and Guangzhou (Figure S8) could originate predominantly from local combustion sources

(Wang et al., 2019). Therewith the complex interplay of different EPFR and PM sources may be the explanation for the variations in spin concentration as well as their size distribution.

The size resolutions of EPFR in Mainz and ATTO in Figure S1 enable more insights into variations of spin concentrations in fine particles due to their resolution down to 10 nm. Therein we found for the volumetric spin distribution in Mainz that coarse particles contain 0.53-0.94 x 10^{11} spins m^{-3} (PM larger 1 µm), while most EPFR are in 0.056-0.560 µm particles (7.0-12.9 m^{-3} x 10^{11} m^{-3}). Interestingly, we found EPFR also in ultrafine particles (<0.05 µm) in Mainz, which is to the best of our knowledge the first report about EPFR in such small particles (0.010-0.056: 1.0-7.0 x 10^{11} m^{-3}). These very small particles are particularly susceptible to particle bouncing from higher stages, but we found consistently a significant amount of EPFR even in the smallest stage (10-18 nm), which is why we are confident about the occurrence of EPFR in ultrafine particles. On the contrary in ATTO PM, we found the highest EPFR concentrations in 3.2-10 µm particles (6.8-9.4 x 10^{11} m^{-3}) and together with 1.0-3.2 µm particles (1.7-3.8 x 10^{11} m^{-3}) coarse PM contains 62% of EPFR at this remote site. We found that fine particles contain 0.7-2.9 x 10^{11} spins m^{-3} and do not show a pronounced variability in between the fractions.

Panels on the right side in Figure S1show for the Mainz mass-specific spin distribution in 1-10 µm particles 0.7-1.1 x 10^{11} spins μg^{-1}, in 0.056-0.560 µm particles 4.5-12.2 x 10^{11} spins μg^{-1}, and in 0.010-0.056 µm particles 0.7-4.2 x 10^{11} spins μg^{-1}. For the ATTO side we found in 1-10 µm particles 1.3-5.3 x 10^{11} spins μg^{-1} and in fine particles 0.8-2.3 x 10^{11} spins μg^{-1}. Therewith ATTO and Mainz show for the mass-specific just like in the volumetric spin distribution an opposing trend.

Variability of EPFR Abundance

As opposed to the size distribution pattern, total concentrations show a pronounced variability as can be seen for the Mainz dataset (Figure S9). These data cover a timeframe of 31 months, during which we have sampled in varying reoccurrences. But independently whether we collected on consecutive dates or with several weeks offset, concentrations scatter over one order of magnitude. Nevertheless, the coarse particle fraction consistently has a significantly lower concentration of EPFRs than fine particles. Whereby the more pronounced variability of the coarse mode concentration is attributable to higher measurement uncertainties approaching the limit of detection for a number of the respective samples. Comparing the variation based on mass and volume normalization, the former is substantially more conserved. Accordingly it seems, that the variations in number concentration may have a dominating influence on the day to day variations in EPFRs concentration.

Sampling Efficiencies at Different Locations

To note, at different sampling locations, we used different aerosol samplers, which may have resulted in varying collections efficiencies for particles with the same size. Especially for submicron particles, the MOUDI used in Mainz and ATTO can be expected to have different collection characteristics than the back-up filter in the sampling devices used in Hyytiälä, Beijing, and Guangzhou. For our analysis we assume that the back-up filter are efficiently collecting down to 10 nm. Another factor that may have influenced the sampling efficiency across the different locations are the varying sampling times. Longer sampling may have an effect on particle bouncing between stages or retention of collected particles on filter stages (Bateman et al., 2014). In order to capture these influences, we compared the collected particle masses for different sites with data from scanning mobility particle sizers (SMPS), which were not permanently available for all sites (TSI model 3080 in ATTO, Grimm model 5.416 in Mainz) and optical

particle sizer (OPS, model 3330, TSI Inc. Shoreview, MN, USA in ATTO). The SMPS data have been processed using the TSI software (aerosol instrument manager - AIM). These controls revealed a reasonable agreement between particle distributions obtained by online SMPS measurements and differential weighing of the filters before and after sampling (Figure S12). Only for the ATTO site differential weighing resulted in substantial discrepancies to the SMPS data, which may be related to the very low sampled PM mass per filter during the clean Amazonian wet season and the especially high humidity at this location. That is why, for ATTO we decided to rely on the SMPS data for mass normalizations to PM_{10} and $PM_{2.5}$. Furthermore, the losses of very small and very large particles in the sampling line are biggest due to diffusion respectively impaction losses. Based on the different sampler designs at the locations we performed estimations of sampling losses, which did not reveal substantial differences in between the sites. An exemplified output for Mainz can be found in Figure S11 a representative estimation for ATTO can be found in Moran-Zuloaga et al. (2018).

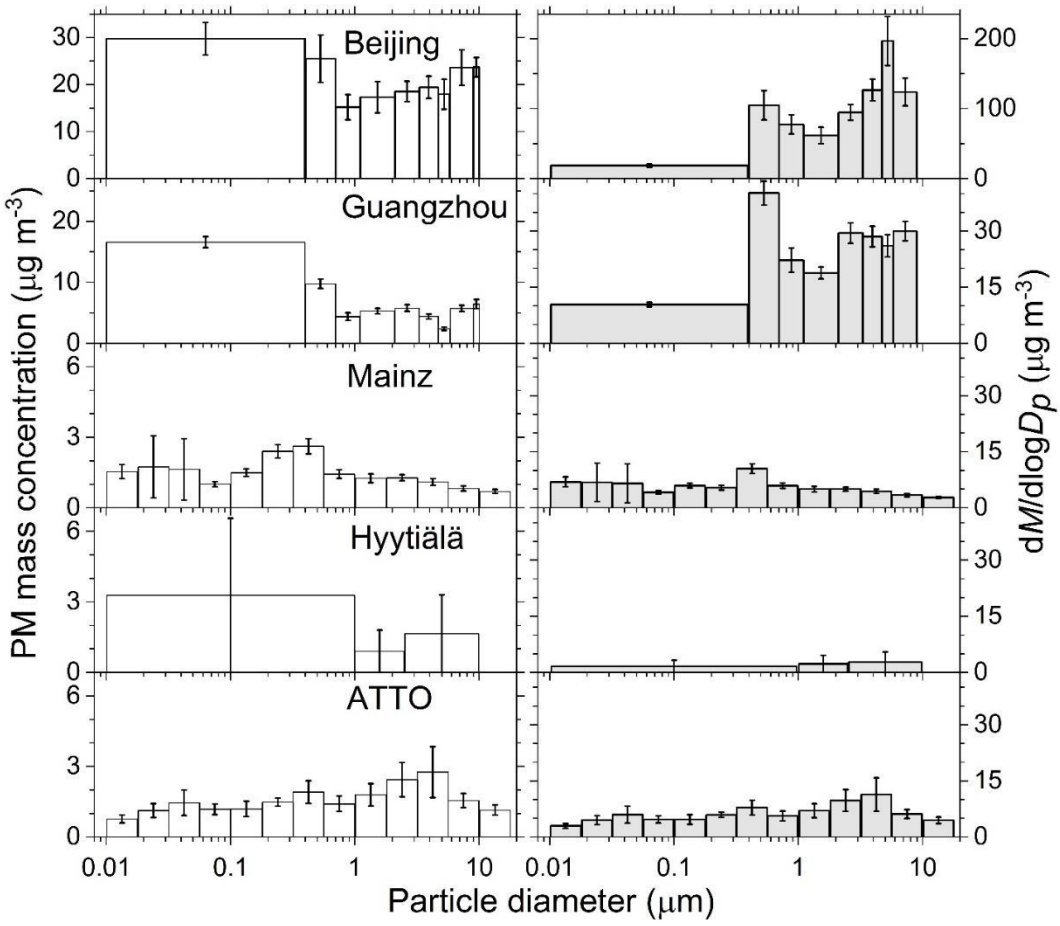

Figure S2: Panels on the left show the mass concentration of particulate matter per unit air mass at the different sites in this study. Values are based on differential weighing of filters as described in the experimental section. Panels of the right side show the lognormalized mass size distribution functions for the different sites in this study ($dM/\log D_p$). The area of the columns in right side panels scales directly with the mass of particulate matter, as opposed to panels on the left side, where the width only indicates the range of the sampled particle sizes and not with PM mass concentration. Error bars represent the standard error of the mean.

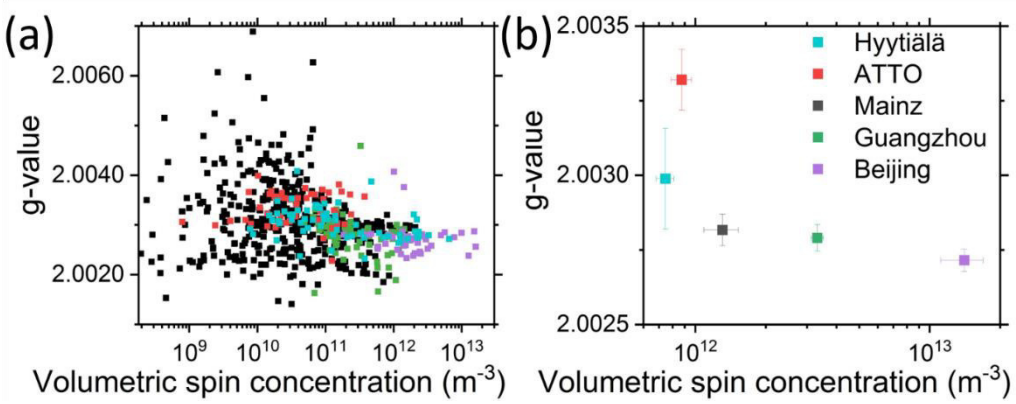

Figure S3: (a) Scatter of the g-value of all analyzed samples plotted against the volumetric spin concentration; (b) Average g-value of the EPFR collected at the different sampling sites plotted against the average volumetric spin concentration. The error bars represent the standard error of the mean.

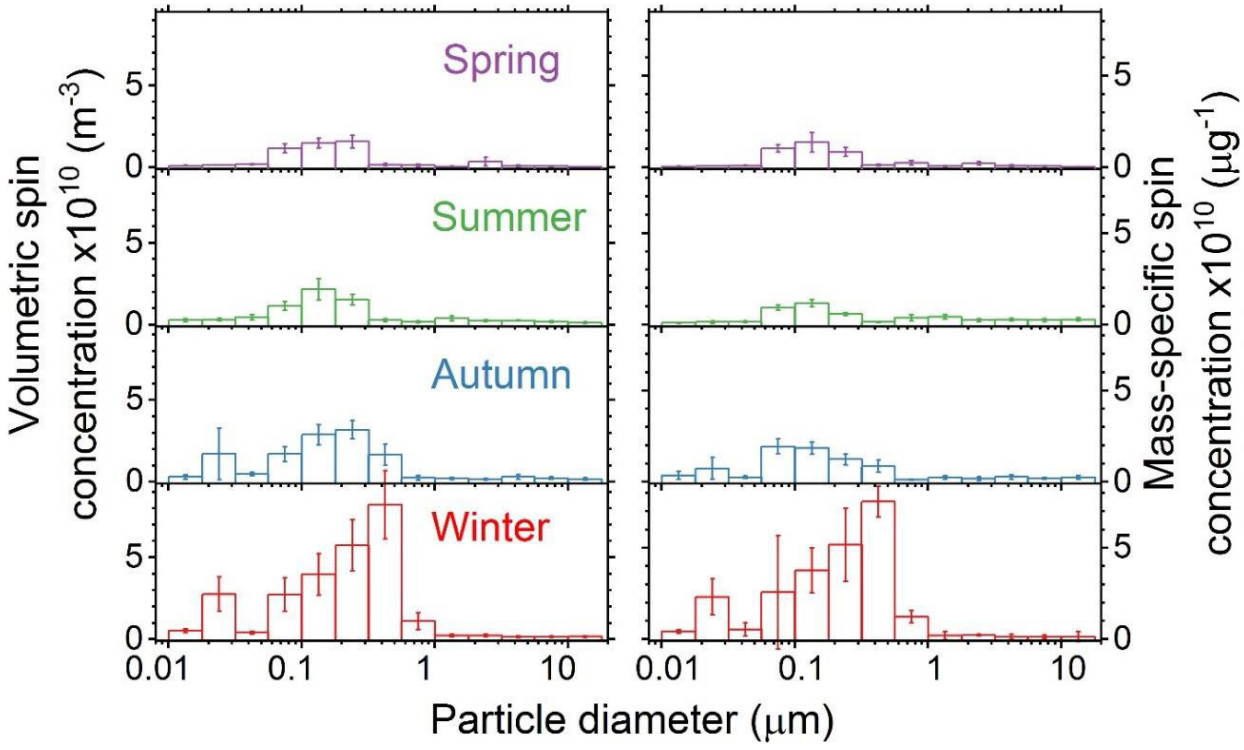

Figure S42: Size distribution of EPR in particulate matter from Mainz for different seasons. Panels on the left side show volumetric- ($C_{v(spins)}$) and panels in the right side mass-specific spin ($C_{m(spins)}$) concentration in different seasons in Mainz PM_{10}. Column width represents the sampled particle size range. Error bars represent the standard error of the mean.

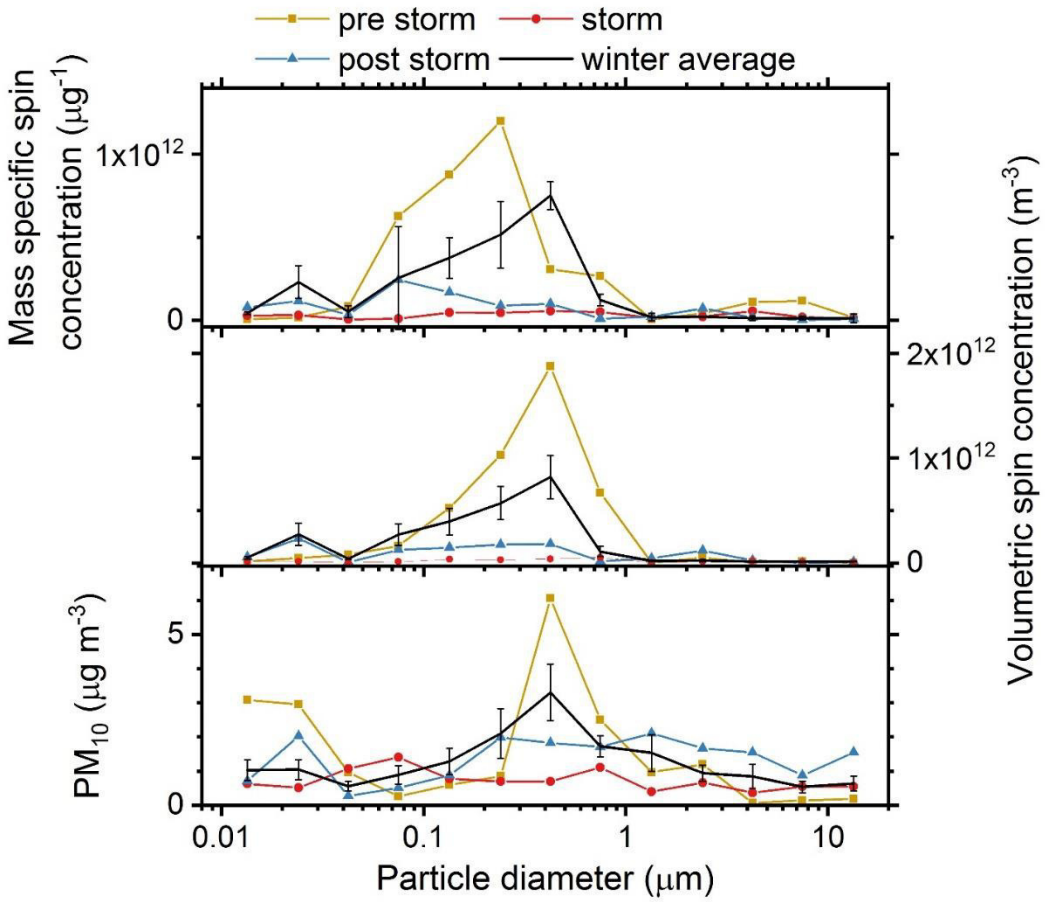

Figure S53: Case study on a storm in Mainz during February 2020. Mass-specific (a) and volumetric spin concentration (b), as well as the PM concentration (c). Whereby the black line is reference line representing the average winter concentrations. Each sample is collected for 2 consecutive days.

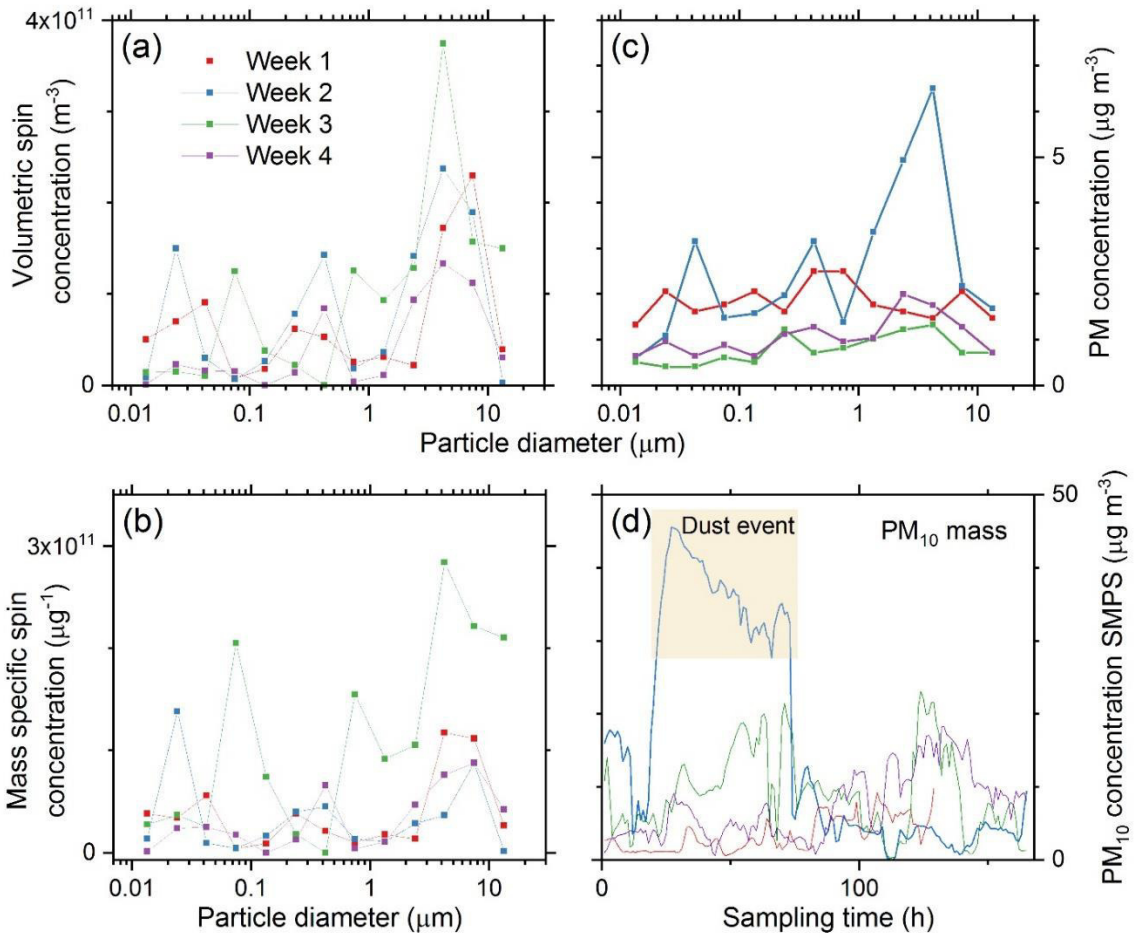

Figure S64: (a) Volumetric - and (b) mass specific spin concentration as well as (c) PM concentration of all individual ATTO samples. During the sampling period of sample *Week 2* a dust event occurred at the sampling site, which was accompanied by a rise in PM_{10} concentrations from around 10 µg m^{-3} to more than 30 µg m^{-3} for about 2 days. This can be seen in panel (d), which shows the PM_{10} concentration over the sampling time of Week 2 as it was measured by an OPS system, which is part of the permanent instrumentation at the sampling site.

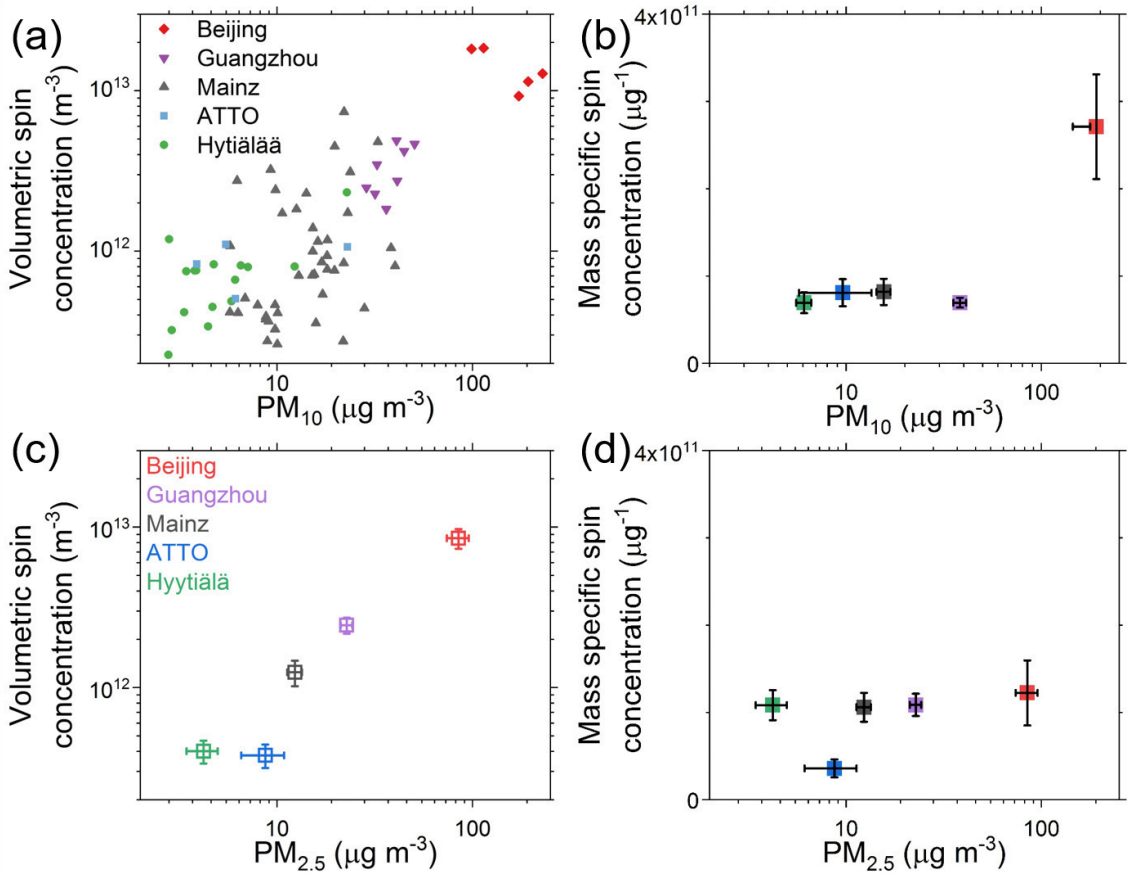

Figure S7: Spin concentrations of PM_{10} plotted against PM_{10} (a+b) respectively $PM_{2.5}$ (c+d) mass concentration for different ambient areas (Hyytiälä, ATTO, Mainz, Guangzhou, and Beijing air). (a) Each data point represents the volumetric spins concentration of a single sample; (b) average mass specific spin concentration in PM_{10}; (c) average volumetric spin concentration in $PM_{2.5}$; (d) average mass specific spin concentration in $PM_{2.5}$.

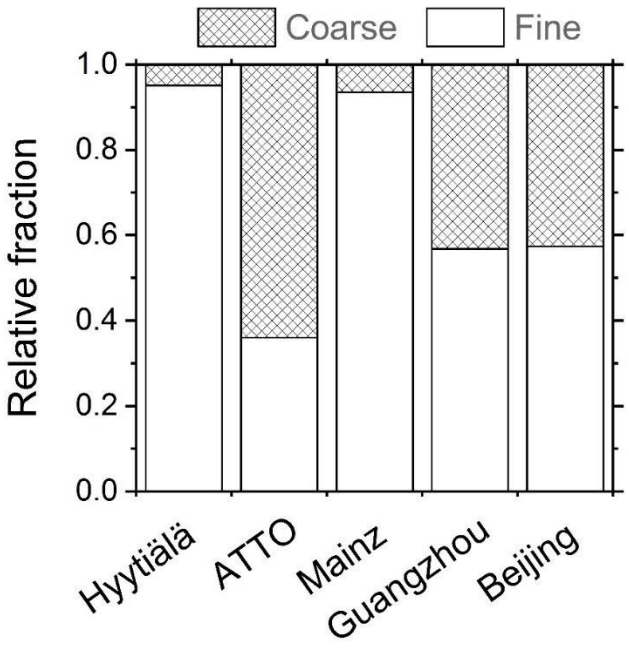

Figure S8: Non-filled and filled columns indicate the relative fractions of EPFR distributed in fine and coarse PM, respectively (coarse particles are PM_{10}-PM_1 and fine particles PM_1).

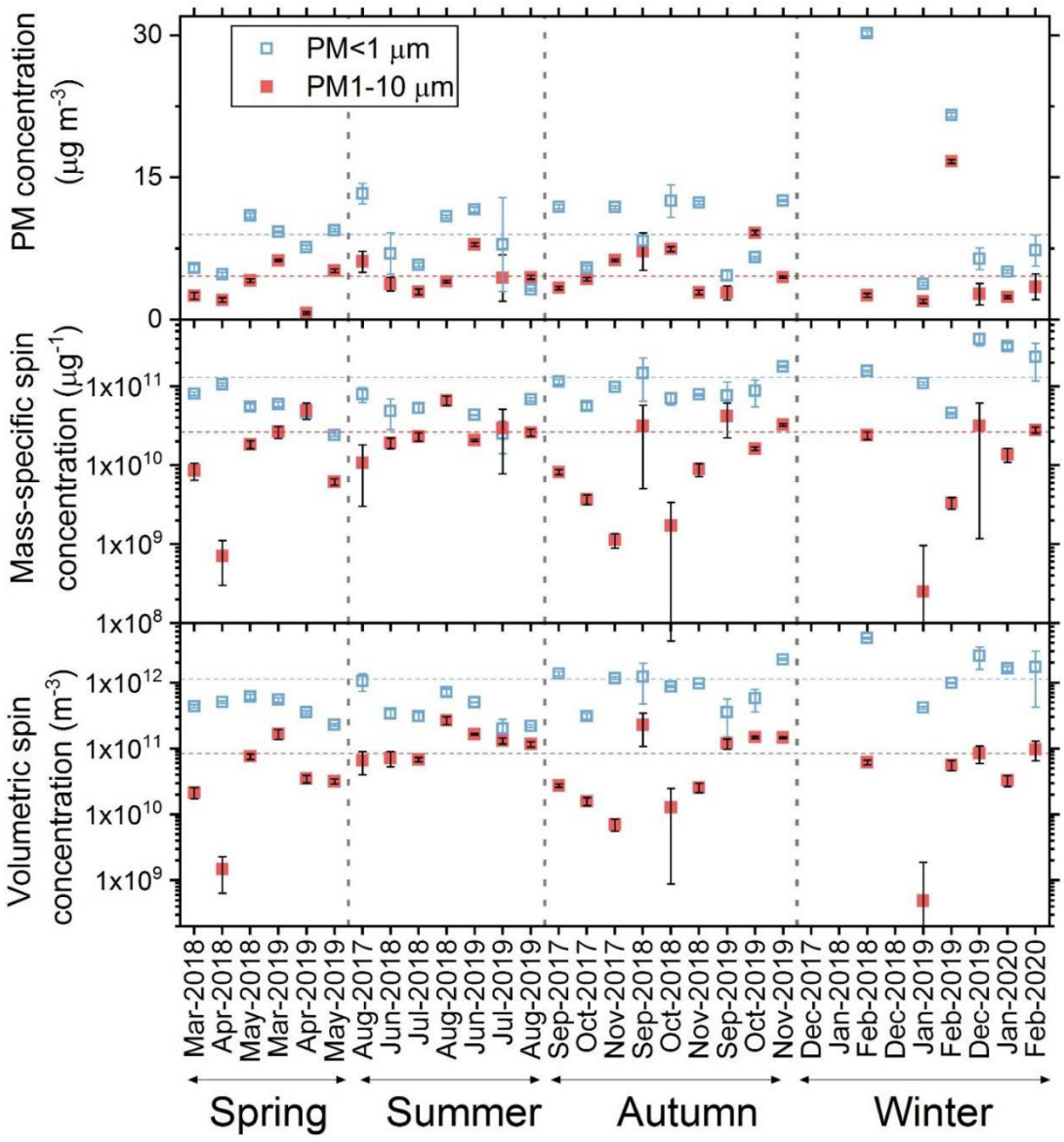

Figure S9: Inter sample variation of PM1 collected with an Impactor in Mainz, over the whole sampling period. Seasons are separated by grey, vertical, dashed lines. Filled red squares represent fine particles with a diameter smaller than 1 µm; open blue squares represent coarse particles with a size in between 1 and 10 µm. Whenever we have multiple samples for one month, the squares represent an average – corresponding months are marked with *. The horizontal red and blue line represent the average spin concentration of the respective particle fraction.

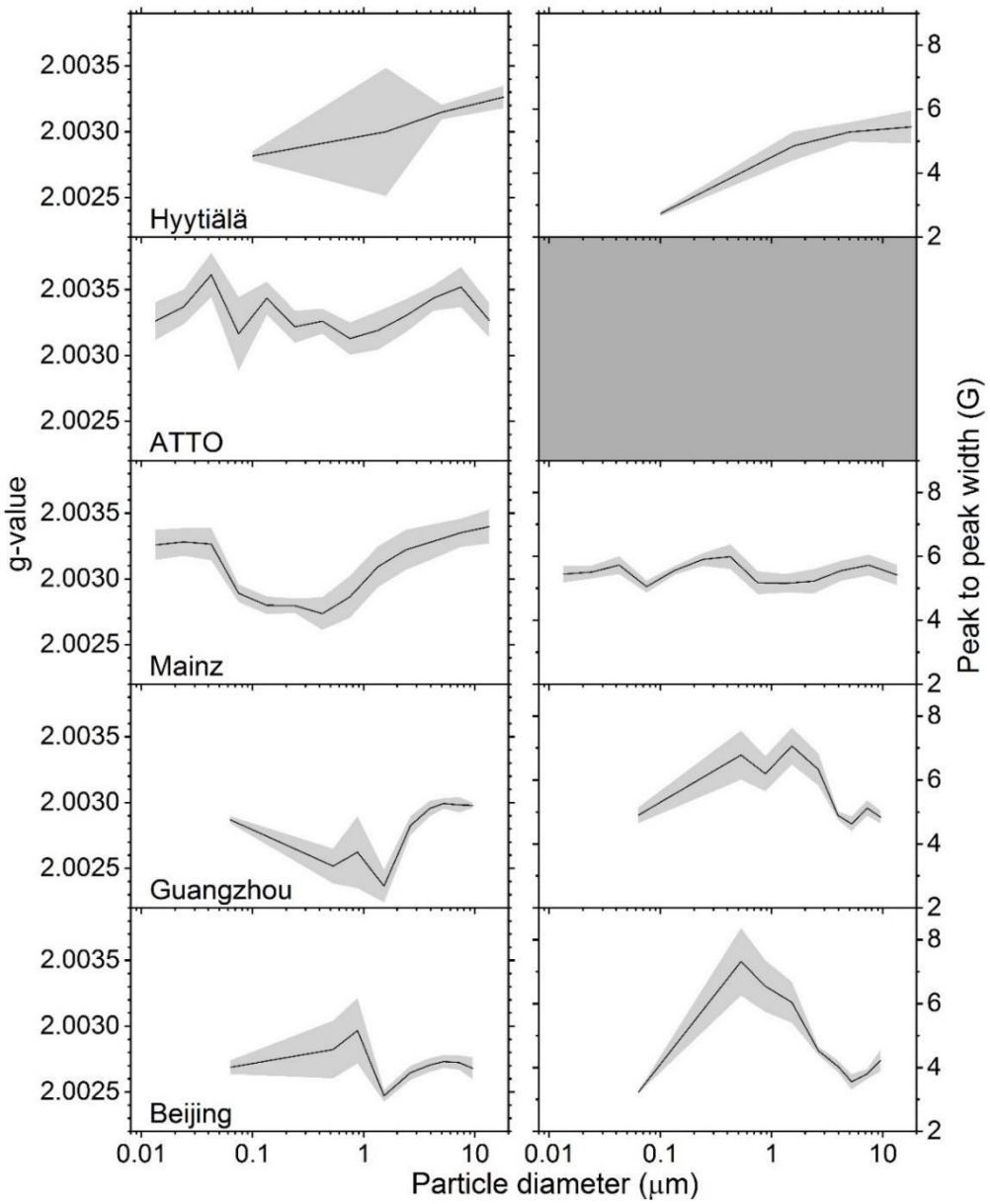

Figure S10: Size distribution of EPR spectral properties of radicals in PM from different sites: (a-e) average g-value of the quantified EPFR signal; (f-i) average peak to peak width of the EPFR signal. Grey shaded areas indicate the standard error of the mean.

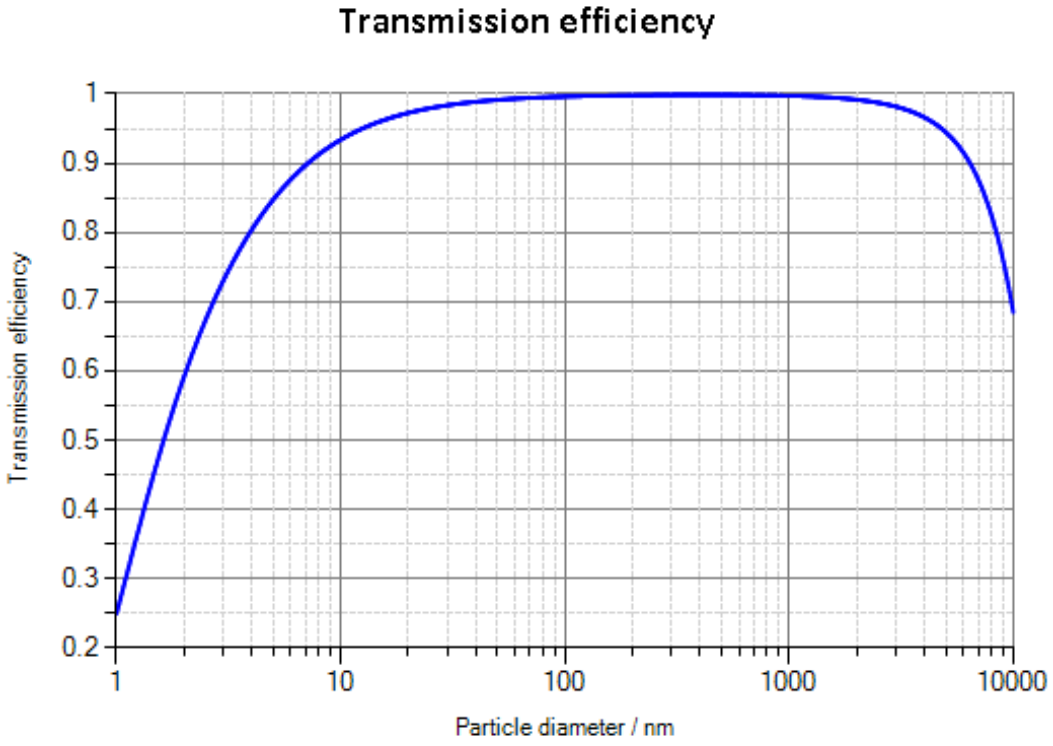

Figure S11: Particle loss during sampling with the assembled inlet line and dryer for the sampling site in Mainz with the described MOUDI. Calculated by the particle loss calculator 2.0 (Van der Weiden et al., 2009). Assuming a flow rate of 30L/min, considering diffusion and sedimentation losses as well.

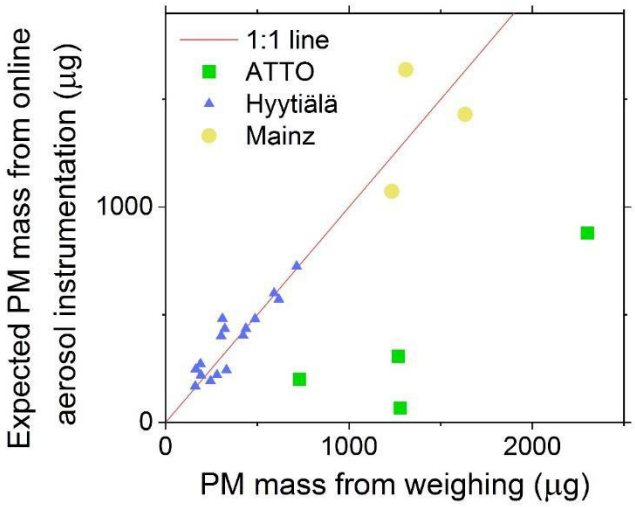

Figure S12: Intercomparison of the expected mass collected on filters estimated based on results from online aerosol instrumentation (SMPS respectively OPS as described in the experimental section) compared to the PM mass obtained by differential weighing of the empty and loaded filter for selected samples.

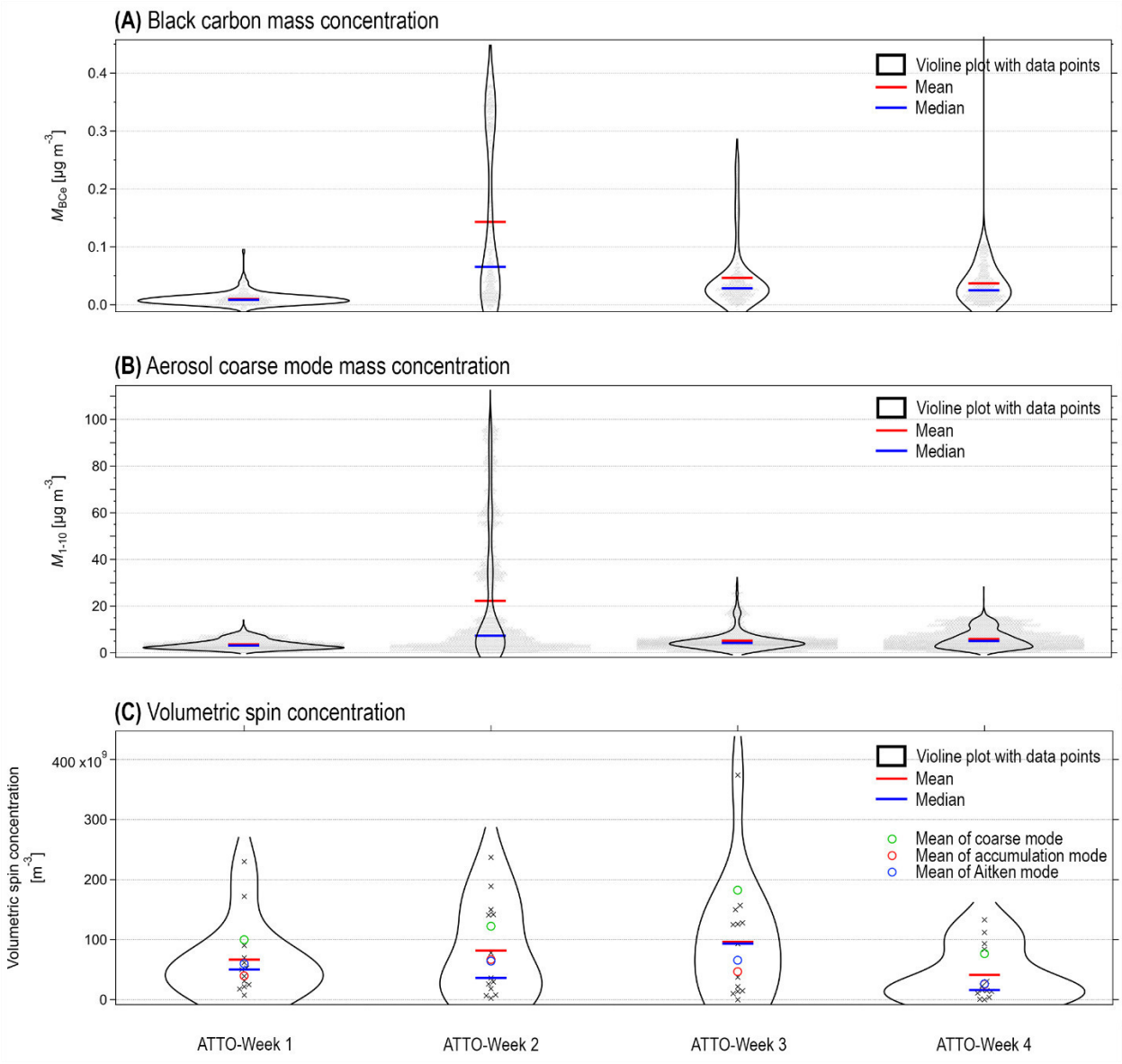

Figure S13: Variability of (A) black carbon mass concentration, (B) $PM_{1\text{-}10}$ mass concentration, and (C) Volumetric spin concentration at the ATTO site during the 4 sampling periods used for this study.

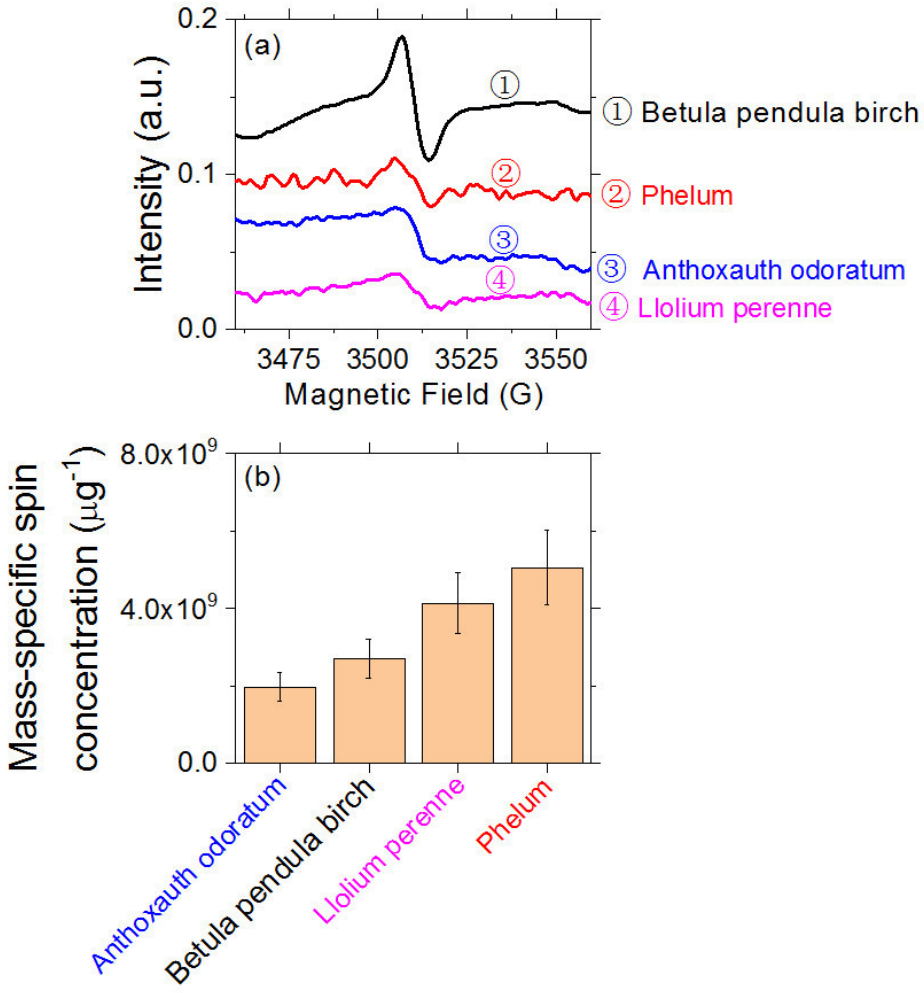

Figure S14: (a) EPR spectra of different pollen species after baseline correction; (b) mass-specific spin concentration of EPFR in different untreated pollen.

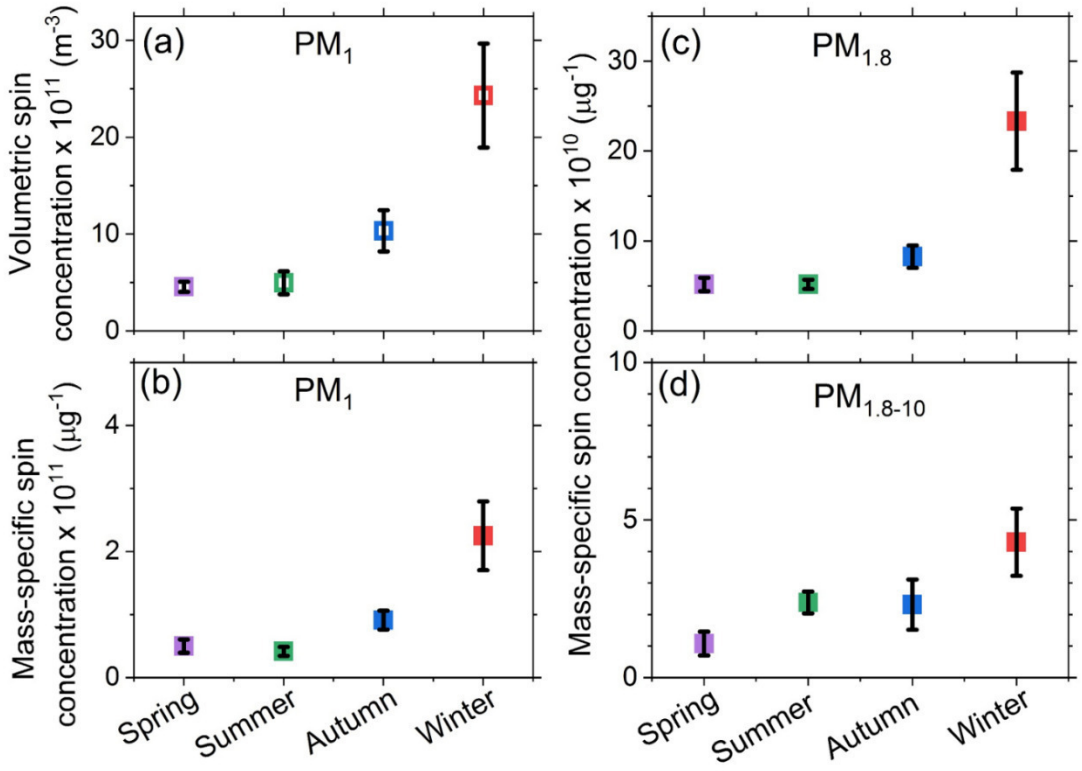

Figure S15: Average spin concentrations in different size fractions of Mainz PM shown for all seasons. (a) Volumetric and (b) mass-specific spin concentrations of EPFR in Mainz PM_1 (particles smaller 1 µm) from different seasons. (c) $PM_{1.8}$ (particles smaller 1.8 µm) and (d) $PM_{1.8\text{-}10}$ (particles between 1.8 and 10 µm) mass-specific spin concentrations for Mainz seasons. Error bars represent the standard error of the mean.

Table S1: Meteorological conditions during the storm in Mainz described in Figure S53.

Conditions	Feb-20_1 (pre storm)	Feb-20_2 (storm)	Feb-20_3 (post storm)
Wind speed (km/h)	5.8	33.1	18.6
Temperature (K)	277	280	277
Air pressure (mbar)	1022	1007	1012
Precipitation (L m^{-2})	2.77	3.73	1.93

Table S2: Average volume-specific spin concentration of EPFRs in Mainz. Values are sorted by the lower cut off diameter of the respective stage of the sampler. Before the first stage, a preseperator filtered all particles larger than 18 µm away.

Cut off (µm)	Mainz volumetric spin concentration (×10^{10} spins m^{-3})				
	Average	Spring	Summer	Autumn	Winter
10	1.36	0.13	1.33	1.72	1.65
5.6	1.65	0.65	1.98	2.31	1.48
3.2	2.11	0.86	2.61	3.02	1.50
1.8	2.36	3.53	2.58	1.66	2.37
1	2.01	0.48	3.85	2.06	2.26
0.560	4.74	1.26	1.60	2.51	11.1
0.320	31.0	1.71	2.85	16.5	82.1
0.180	32.2	15.7	15.3	31.8	57.3
0.100	27.6	14.9	21.6	28.9	39.7
0.056	17.6	11.7	11.4	17.1	27.2
0.032	2.81	1.92	4.59	4.79	4.13
0.018	17.5	1.39	3.17	17.1	27.5
0.010	2.65	0.96	2.70	3.01	5.21

Table S3: Average volume-specific spin concentration of EPFRs and PM mass concentration in ATTO. Values are sorted by the lower cut off diameter of the respective stage of the sampler. Before the first stage, a preseperator filtered all particles larger than 18 µm away.

Cut off (µm)	Volumetric spin concentration (×10^{10} spins m^{-3})	PM mass (µg m^{-3})
10	5.54	1.14
5.6	17.2	1.55
3.2	22.9	2.76
1.8	9.62	2.44
1	4.28	1.79
0.560	4.33	1.41
0.320	6.98	1.91
0.180	4.39	1.48
0.100	2.04	1.19
0.056	3.85	1.18
0.032	3.66	1.45
0.018	6.43	1.13
0.010	1.83	0.76

Table S4: Volume-specific spin concentration of EPFRs and particulate matter in Hyytiälä. Values are sorted by the upper cut off diameter of the respective stage of the sampler.

Cut off (µm)	Volumetric EPFR spin concentration ($\times 10^{10}$ spins m^{-3})	PM mass concentration (µg m^{-3})
10	2.11	3.35
2.5	1.17	1.88
1	2.53	0.96
0.01*	37.6	3.25

Table S5: Average PM mass concentration in Mainz and in the ATTO. Values are sorted by the lower cut off diameter of the respective stage of the sampler. Before the first stage, a preseperator filtered all particles larger than 18 µm away.

Cut off (µm)	Mainz PM mass concentration (µg m^{-3})				
	Average	Spring	Summer	Autumn	Winter
10	0.69	0.65	0.71	0.85	0.64
5.6	0.83	0.61	1.15	1.10	0.54
3.2	1.10	0.87	1.23	1.33	0.85
1.8	1.28	1.24	1.33	1.68	0.94
1	1.26	0.85	1.37	1.42	1.54
0.560	1.44	1.02	1.13	1.53	1.73
0.320	2.62	2.15	1.78	2.78	3.31
0.180	2.41	2.27	2.63	2.57	2.11
0.100	1.49	1.46	1.86	1.44	1.29
0.056	1.01	1.11	1.23	0.87	0.89
0.032	1.63	2.20	2.68	2.31	0.57
0.018	1.74	2.52	3.49	1.43	1.05
0.010	1.54	2.49	2.90	1.08	1.03

Table S6: Average volume-specific spin concentration of EPFRs and Particulate matter in Guangzhou and Beijing. Values are sorted by the lower cut off diameter of the respective stage of the sampler. Before the first stage a preseperator removed particles larger than 10 µm.

Cut off (µm)	Guangzhou		Beijing	
	EPFR ($\times 10^{10}$ spins m^{-3})	PM (µg m^{-3})	EPFR ($\times 10^{10}$ spins m^{-3})	PM (µg m^{-3})
9	17.5	6.43	302	23.71
5.8	18.5	5.72	228	23.63
4.7	9.06	2.38	98.8	17.94
3.3	18.8	4.38	223	19.44
2.1	23.3	5.78	171	18.55
1.1	56.	5.28	105	17.33
0.7	56.7	4.36	70.3	15.20
0.4	26.9	9.76	205	25.50
0.01*	105	16.59	1230	29.75

Table S7: ATTO sampling parameters, collection times, and volumes. Details about the location of the sampling site and the used instrumentation can be found in the method section.

Sample ID	Sampling date	Sampling time (h)	Flow rate (L min^{-1})	Sampling volume (m^3)
ATTO-Week 1	27.03.17, 19:15 – 01.04.17, 15:37	116.37	9.76	68.14
ATTO-Week 2	02.04.17, 18:30 - 09.04.17, 14:04	172.43	9.81	101.44
ATTO-Week 3	09.04.17, 14:55 - 16.04.17, 14:09	167.23	9.82	98.48
ATTO-Week 4	16.04.17, 15:08 - 25.04.17, 12:03	212.92	9.83	125.51

Table S8: Hyytiälä sampling parameters, collection times, and volumes. Details about the location of the sampling site and the used instrumentation can be found in the method section.

Sample ID	Sampling date	Sampling time (h)	Flow rate (L min^{-1})	Sampling volume (m^3)
Hyy-01	31.05.17, 8:37 – 02.06.17, 9:28	48.85	30	87.93
Hyy-02	02.06.17, 9:28 – 05.06.17, 8:09	70.81	30	127.46
Hyy-03	07.06.17, 8:41 – 09.06.17, 7:32	22.85	30	41.13
Hyy-04	09.06.17, 7:32 – 12.06.17, 8:31	73.17	30	131.71
Hyy-05	12.06.17, 8:31 – 14.06.17, 8:14	47.72	30	85.90
Hyy-06	19.06.17, 8:13 – 21.06.17, 7:48	23.58	30	42.44
Hyy-07	21.06.17, 7:48 – 26.06.17, 7:47	119.98	30	215.96
Hyy-08	26.06.17, 7:47 – 28.06.17, 7:49	48.32	30	86.98
Hyy-09	28.06.17, 7:49 – 30.06.17, 6:48	22.98	30	41.36
Hyy-10	30.06.17, 6:48 – 03.07.17, 7:48	73.00	30	131.40
Hyy-11	03.07.17, 7:48 – 05.07.17, 8:48	49.00	30	88.20
Hyy-12	07.07.17, 7:05 – 10.07.17, 9:02	73.95	30	133.11
Hyy-13	10.07.17, 9:02 – 12.07.17, 8:11	47.78	30	86.00
Hyy-14	12.07.17, 8:11 – 14.07.17, 6:59	46.8	30	84.24
Hyy-15	14.07.17, 6:59 – 17.07.17, 7:50	72.85	30	131.13
Hyy-16	17.07.17, 7:50 – 19.07.17, 7:59	48.15	30	86.67

Table S9: Mainz sampling parameters, collection times, and volumes. Details about the location of the sampling site and the used instrumentation can be found in the method section.

Sample ID	Sampling date	Sampling time (h)	Flow rate (L min^{-1})	Sampling volume (m^3)
Aug-17_1	22.08.17, 17:15 – 24.08.17, 14:55	45.67	30	82.21
Aug-17_2	26.08.17, 11:30 – 28.08.17, 11:15	47.75	30	85.95
Aug-17_3	28.08.17, 11:45 – 30.08.17, 10:50	47.09	30	84.76
Sep-17	25.09.17, 14:50 – 27.09.17, 17:15	50.25	30	90.45
Oct-17	25.10.17, 11:30 – 27.10.17, 17:30	54.00	30	97.20
Nov-17	14.11.17, 11:00 – 16.11.17, 7:21	44.35	30	79.83
Feb-18	01.03.18, 14:30 – 03.03.18, 17:30	51.00	30	91.80
Mar-18	14.03.18, 9:40 – 15.03.18, 18:00	32.33	30	58.19
Apr-18	29.03.18, 16:30 – 31.03.18, 16:30	48.00	30	86.40
May-18	25.05.18, 10:00 – 27.05.18, 16:40	54.70	30	98.46
Jun-18_1	05.06.18, 10:00 - 07.06.18, 9:20	47.30	30	85.14
Jun-18_2	19.06.18, 12:50 – 21.06.18, 9:20	44.50	30	80.10
Jun-18_3	27.06.18, 12:10 – 29.06.18, 11:00	46.84	30	84.31
Jul-18	16.07.18, 11:00 – 18.07.18, 11:30	48.50	30	87.30
Aug-18	23.07.18, 12:10 – 25.07.18, 13:50	49.67	30	89.41
Sep-18_1	17.09.18, 11:53 – 19.09.18, 15:45	51.78	30	93.20
Sep-18_2	19.09.18, 15:50 – 21.09.18, 14:42	46.87	30	84.37
Oct-18_1	18.10.18, 14:00 – 20.10.18, 13:00	47.00	30	84.60
Oct-18_2	31.10.18, 11:20 – 02.11.18, 11:20	48.00	30	86.40
Nov-18	21.11.18, 14:30 – 23.11.18, 15:15	48.72	30	87.70
Jan-19	15.01.19, 11:20 – 17.01.19, 12:40	49.33	30	88.79
Feb-19	13.02.19, 9:00 – 15.02.19, 12:15	51.25	30	92.25
Mar-19	18.03.19, 17:59 – 21.03.19, 10:00	63.98	30	115.16
Apr-19	23.04.19, 11:49 – 25.04.19, 14:14	50.42	30	90.76
May-19	24.05.19, 18:30 – 27.05.19, 9:40	63.17	30	113.71
Jun-19	17.06.19, 16:17 – 19.06.19, 15:00	46.72	30	84.10
Jul-19_1	01.07.19, 18:11 – 03.07.19, 15:44	45.55	30	81.99
Jul-19_2	15.07.19, 12:14 – 17.07.19, 15:57	51.72	30	93.10
Aug-19	12.08.19, 10:49 – 14.08.19, 15:00	52.82	30	95.08
Sep-19_1	02.09.19, 14:54 – 04.09.19, 17:54	51.00	30	91.80
Sep-19_2	11.09.19, 18:08 – 13.09.19, 17:10	47.03	30	84.65
Oct-19	10.10.19, 15:40 – 12.10.19, 11:54	44.23	30	79.61
Nov-19	20.11.19, 11:00 – 11.11.19, 15:00	52.00	30	93.60

Dec-19_1	02.12.19, 14:18 – 04.12.19, 13:25	47.12	30	84.82
Dec-19_2	04.12.19, 13:55 – 06.12.19, 15:01	50.10	30	90.18
Dec-19_3	09.12.19, 11:25 – 11.12.19, 13:45	50.33	30	90.59
Dec-19_4	11.12.19, 14:00 – 13.12.19, 16:30	50.50	30	90.90
Dec-19_5	16.12.19, 14:40 – 18.12.19, 15:10	48.50	30	87.30
Dec-19_6	18.12.19, 15:30 – 20.12.19, 15:30	48.00	30	86.40
Jan-20	14.01.20, 11:20 – 16.01.20, 14:25	51.16	30	92.09
Feb-20_1	07.02.20, 13:49 – 09.02.20, 15:16	49.45	30	89.01
Feb-20_2	09.02.20, 15:32 – 11.02.20, 17:30	49.97	30	89.95
Feb-20_3	11.02.20, 17:45 – 13.02.20, 16:15	46.50	30	83.70

Table S10: Guangzhou sampling parameters, collection times, and volumes. Details about the location of the sampling site and the used instrumentation can be found in the method section.

Sample ID	Sampling date	Sampling time (h)	Flow rate (L min^{-1})	Sampling volume (m^3)
Guang-01	01.11-06.11.2017	48.85	26	187.28
Guang -02	06.11-11.11.2017	70.81	26	187.36
Guang -03	21.11-26.11.2017	22.85	26	189.28
Guang -04	26.11-01.12.2017	73.17	26	186.86
Guang -05	03.12-08.12.2017	47.72	26	189.77
Guang -06	08.12-13.12.2017	23.58	26	172.33
Guang -07	13.12-18.12.2017	119.98	26	185.67
Guang -08	18.12-23.12.2017	48.32	26	188.01

Table S11: Beijing sampling parameters, collection times, and volumes. Details about the location of the sampling site and the used instrumentation can be found in the method section.

Sample ID	Sampling date	Sampling time (h)	Flow rate (L min^{-1})	Sampling volume (m^3)
Beijing-01	29.08.17, 9:01 – 30.08.17, 9:01	24	15-17	23.04
Beijing-02	30.08.17, 9:30 – 31.08.17, 8:41	23.18	15-17	22.25
Beijing-03	03.09.17, 8:40 – 04.09.17, 8:34	23.90	15-17	22.94
Beijing-04	04.09.17, 8:56 – 05.09.17, 8:14	23.30	15-17	22.37
Beijing-05	06.09.17, 8:31 – 07.09.17, 8:44	24.22	15-17	23.25

Table S12: Lung deposition fractions: Output from MPPD Model, with the conditions described in the method section. Cut off diameters are indicative of the lower threshold of particle sizes modelled in the respective interval.

Cut off (µm)	Total deposition	Head deposition	Tracheobronchial deposition	Pulmonary deposition
10	99%	77%	21%	0%
5.623	95%	58%	30%	8%
3.162	81%	36%	19%	26%
1.778	52%	19%	11%	22%
1.000	29%	8%	8%	13%
0.562	21%	4%	7%	9%
0.316	21%	3%	8%	10%
0.178	28%	4%	10%	14%
0.100	40%	5%	14%	21%
0.056	55%	4%	21%	30%
0.032	71%	7%	30%	34%
0.018	81%	11%	43%	28%
0.010	87%	19%	56%	13%

References

1. Zhang, Y.-L.; Cao, F., Fine particulate matter (PM 2.5) in China at a city level. *Scientific reports* **2015,** *5*, 14884.

2. Vejerano, E. P.; Rao, G.; Khachatryan, L.; Cormier, S. A.; Lomnicki, S., Environmentally persistent free radicals: insights on a new class of pollutants. *Environmental science & technology* **2018,** *52*, (5), 2468-2481.

3. Feld-Cook, E. E.; Bovenkamp-Langlois, L.; Lomnicki, S. M., Effect of Particulate Matter Mineral Composition on Environmentally Persistent Free Radical (EPFR) Formation. *Environ Sci Technol* **2017,** *51*, (18), 10396-10402.

4. Hari, P.; Kulmala, M., Station for measuring ecosystem-atmosphere relations (SMEAR II). *Boreal. Env. Res.* **2005,** *10*, 315-322.

5. Chen, Q.; Sun, H.; Wang, M.; Wang, Y.; Zhang, L.; Han, Y., Environmentally persistent free radical (EPFR) formation by visible-light illumination of the organic matter in atmospheric particles. *Environ Sci Technol* **2019**.

6. Li, X.; Shen, C.; Zhao, H.; Jiang, J.; Ban, Z.; Chen, Z.; Qu, B., Photoformation of persistent free radicals on a montmorillonite-humic acid complex simulated as particulate organic matter in an aqueous solution. *Environmental Science: Processes & Impacts* **2020**.

7. Tong, H.; Lakey, P. S. J.; Arangio, A. M.; Socorro, J.; Shen, F.; Lucas, K.; Brune, W. H.; Poschl, U.; Shiraiwa, M., Reactive Oxygen Species Formed by Secondary Organic Aerosols in Water and Surrogate Lung Fluid. *Environ Sci Technol* **2018**.

8. Wang, Y.; Li, S.; Wang, M.; Sun, H.; Mu, Z.; Zhang, L.; Li, Y.; Chen, Q., Source apportionment of environmentally persistent free radicals (EPFRs) in PM2. 5 over Xi'an, China. *Science of The Total Environment* **2019,** *689*, 193-202.

9. Bateman, A. P.; Belassein, H.; Martin, S. T., Impactor apparatus for the study of particle rebound: Relative humidity and capillary forces. *Aerosol Science and Technology* **2014,** *48*, (1), 42-52.

10. Moran-Zuloaga, D.; Ditas, F.; Walter, D.; Saturno, J.; Brito, J.; Carbone, S.; Chi, X.; de Angelis, I. H.; Baars, H.; Godoi, R. H., Long-term study on coarse mode aerosols in the Amazon rain forest with the frequent intrusion of Saharan dust plumes. *Atmospheric Chemistry and Physics* **2018,** *18*, (3), 10055-10088.

11. Von der Weiden, S.; Drewnick, F.; Borrmann, S., Particle Loss Calculator–a new software tool for the assessment of the performance of aerosol inlet systems. *Atmos. Meas. Tech* **2009,** *2*, (2), 479-494.

3.6 The Role of Environmentally Persistent Free Radicals Indoors

This chapter represents the current draft of a manuscript in preparation for submission as a letter article in a peer reviewed journal. I have planned in exchange with the coauthors the sampling of PM conducted in this study. Furthermore, I personally did the sampling of outdoor PM and analysis of all samples by EPR spectroscopy including all exposure experiments. Moreover, I analyzed all data, prepared all figures, and coordinated the discussion of all people involved about the results. The presented version of the text is largely my initial draft, describing the results and implications of the findings. Also I integrated the literature about indoor environments together with the literature about EPFR, which is the basis for this study.

Environmentally persistent free radicals in indoor air, dust, and on surfaces

Alexander Filippi,[1] Roger Sheu,[2] Ulrich Poschl,[1] Thomas Berkemeier,[1] Haijie Tong,[1] Drew Gentner.[2]

[1] Multiphase Chemistry Department, Max Planck Institute for Chemistry, 55128 Mainz, Germany

[2] Department of Chemical and Environmental Engineering, Yale University, New Haven, CT, USA.

Abstract

Environmentally persistent free radicals (EPFR) are an emerging class of constituents in particulate matter (PM), which play a role in PM toxicity and multiphase chemistry. Their abundance has been investigated in a number of laboratory studies and outdoor locations globally, but their prevalence indoors remains unstudied. Here we show EPFR are present in similar concentrations in indoor and outdoor PM, as well as on indoor surfaces and dust in a case study home, with the highest surface loadings observed on windows. These radical reservoirs are likely rapidly cycling and are shown to evolve with typical indoor summertime ozone exposure. We show that at the observed concentrations, the indoor PM, surfaces, and dust are reservoirs of reactivity in multiphase systems due to their EPFR content as their radical concentration exceeds that of typical indoor radical sources. These results warrant further consideration of EPFR reservoirs in indoor chemistry studies and models with implications for inaccessible or unseen spaces within the building envelope that will accumulate larger organic coatings and dust over time.

Introduction

With humans spending 90% of their time in enclosed spaces,[1] indoor multiphase chemistry is a key consideration for human health and well-being. The indoor environment has an abundance of reservoirs and surfaces for multiphase chemistry (e.g. condensed and aqueous phases) with greater overall organic loadings than outdoors, which thus play a larger role in physical-chemical processes.[2–4] Films comprised of organic and inorganic compounds accumulate on airborne particles, surfaces, and dust in all occupied spaces and air handling systems (e.g. ducts), and include primary and secondary organic compounds, soot, and transition metals (esp. in dust) that originate from a mix of outdoor and indoor sources.[4–6]

These accumulated layers on surfaces, particles, and dust are a key part of the indoor multiphase system with close interactions with the gas phase—both near-surface and beyond. Organic chemistry at the surfaces of aerosols is known to be important, but the role of other surfaces in the built environment is largely unstudied. However, surfaces are known to be important sources of emissions and sinks for deposition of aerosols and gases, and studies on inorganic HONO chemistry at the interface of surfaces has been shown to be important for urban HONO chemistry.[7,8] Reactive surfaces in rooms or air handling systems (esp. filters) have been identified and studied as indoor sources of reactive oxidized species (e.g. carbonyls) following ozonation.[7,9–11]

These organic and aqueous layers also represent potential, un-studied reservoirs for. Radicals and oxidants are essential for initiating and propagating chemistry across all three phases in the atmosphere. Organic oxidation chemistry is known to regenerate radicals (e.g. OH, HO2) that can lead to further oxidation of other molecules, therein photochemistry is often an important source of radicals.[12,13] More recently, oxidized organic compounds generated as byproducts of oxidation (i.e. reactive oxygen intermediates (ROI)) have been shown to survive in the aerosol phase as environmental persistent free radicals (EPFRs).[14–19] The lifetimes of these EPFRs (~days-years) have the ability to retain and transport chemistry-initiating radicals beyond the initial time and location of oxidation.[12,15] These present major concerns for human health since they can penetrate deep into lungs and even blood, causing oxidative stress,[20,21] but also in the atmosphere as reservoirs of reactivity.[22–25] Radicals previously observed in outdoor samples include oxygen-centered organic radicals (e.g. CnHmOp•), carbon-centered organic radicals (e.g. •CnHmOp), HOX (OH+HO2), and superoxide (O2-).[22,26,27] The formation is known to be very dependent on oxidation conditions, metal

content, and precursor types. The molecular identities of the oxidized organics that lead to this radical production are largely unknown, with the exception of quinones, semi-quinones and organic peroxides.[14,28]

While radical transport via EPFRs and ROS/RNS-generating species has been shown to be important for in-lung chemistry and climate-related cloud chemistry,[16,22–25,28–30,] their importance as reservoirs of relatively stable oxidation-initiating compounds is likely to translate to indoor environments, both airborne and as they accumulate on surfaces and in dust. Yet, the abundance of indoor multiphase radicals is unknown, even as smog chamber surfaces exposed to chemistry are now known non-permanent sinks, but temporary reservoirs for radicals and reactivity.

The overarching objective of this paper is an exploratory investigation of the presence and potential implications of EPFR in suspended PM and on surfaces within a typical indoor environment. Specifically, we (a) collect 20 indoor PM samples during Fall 2019 with concurrent outdoor samples from a background site, and examine their EPFR content via electron paramagnetic resonance spectroscopy (EPR); (b) compare airborne PM to surface and dust samples from the same environment; (c) expose a subset of samples to typical indoor ozone and nitrogendioxide concentrations; and (d) examine the importance of indoor EPFR on PM radical content and multiphase chemistry compared to common radical concentrations in PM.

Materials and Methods

Sampling of total suspended particles (TSP) was conducted at two locations in the city of Mainz, Germany: one indoor in an apartment kitchen, the other one outside on the roof of the Max Planck Institute for Chemistry. Details about the sampling sites and setup are available in the supporting material and in our previous work.[22] The TSP collection was done in parallel at both sites with sampling times ranging from 1-7 days, see Figure S1 and Tables S1-S2 for details. Furthermore, we collected indoor surface samples from the same apartment as the TSP samples (Table S3). For this purpose the respective surface was slightly wetted with acetone and afterwards wiped with a filter. After collection all samples were stored in a refrigerator at -20°C or -80°C until analysis.

To determine the collected particle mass we weighted the filter before and after collection with a high accuracy balance (+/- 0.01 mg). For the analysis of our samples, we used a Bruker EMXplus X-Band electron paramagnetic resonance spectrometer (EPR). Before measuring the filter we incubated them for more than 1 hour in a dry N_2 atmosphere in a desiccator, to obtain consistent lattice conditions and prevent humidity induced spin-lattice relaxation. After this conditioning step, the samples were cut out of their frame with a scalpel, wrapped, and packed into a 2 mm ID quartz EPR tube. Afterwards the sample was fixed in the EPR cavity, which was continuously flushed with a gentle N_2-Stream. The following instrument parameter were used for the measurements: 100 kHz modulation frequency, 9.84 GHz microwave frequency, 2.149mW (20 db) microwave power, 30 db receiver gain, 81.92 ms time constant, 15.48 ms conversion time, 3 G Modulation Amplitude, 10 scans, 80-300 G sweep width. Following these steps the quantification of spins was performed with the Xenon software (Bruker) by double integration of baseline corrected spectra.

Exposure of the collected particles to Ozone and NO_2 was performed online in the EPR by channeling the respective gas mixture through a piece of filter. A detailed description is given in the supplementary information, together with a sketch of the setup.

Results and Discussion

EPFRs observed in indoor PM, dust, and surface samples

Particulate matter (PM) collected inside a residential apartment was found to contain similar concentrations of environmentally persistent free radicals (EPFR) (Figure 1a) as at a reference outdoor site in the same city (Mainz, Germany). In most cases, slightly higher volumetric concentrations were observed at the outdoor sampling site, though they were not co-located. Nevertheless, some dates revealed more pronounced divergence in between the two locations with either indoor or outdoor EPFR levels exceeding the other environment. More in depth analysis showed that in the indoor site uninhabited periods may result in lower volumetric spin concentrations than inhabited periods, but the difference is not very pronounced (Figure S2b). This effect may be either connected to increased indoor activities that could contribute to EPFR formation like cooking and heating or be induced by more regular ventilation resulting in more EPFR intake from outdoor. However variations in indoor activities did not result in significant changes of EPFR concentrations on the timescales analyzed in this study (Table S1). Furthermore Figure 1a shows that this volumetric concentration of EPFR varied by more than one order of magnitude during the observation period covering about 2 months of consecutive sampling (0.4-13.2 $x10^{12}$ spins m^{-3}). Taken together we found that indoor and outdoor PM EPFR concentrations are closely linked, with outdoor concentrations often exceeding indoor levels (Figure S2a).

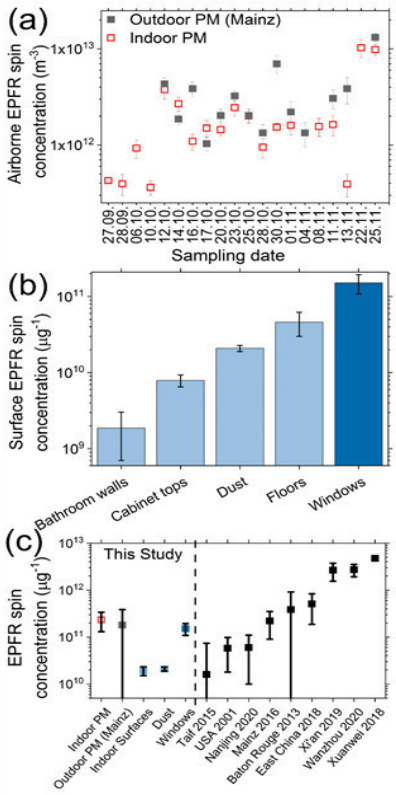

Figure 1: Concentrations of environmentally persistent free radicals in a home apartment compared to outdoor air and other locations. (A) Volumetric EPFR spin concentrations in total suspended particulate matter (PM) inside an apartment compared to an outdoor sampling site in Mainz, Germany. (B) Mass-normalized EPFR spin concentrations in surface films inside the apartment ($N_{Bathroom\ walls}$=2; $N_{Cabinet\ tops}$=4; N_{Dust}=2; $N_{Floor\ surfaces}$=2; $N_{Windows}$=2). (C) Comparison of observed spin concentrations to prior outdoor studies on $PM_{2.5}$.

Surfaces, which comprise an outsize fraction of organic loading in indoor environments,[31] had significant EPFR concentrations and varied between surface types (Figure 1b). Mass specific EPFR concentrations (per unit mass) were greatest on windows (15.14 $x10^{10}$ spins μg^{-1}) followed by floors (4.59 $x10^{10}$ spins μg^{-1}), the tops of cabinets (0.79 $x10^{10}$ spins μg^{-1}), and then tiled bathroom walls (0.19 $x10^{10}$ spins μg^{-1}). The high concentrations on windows could be explained by the increased efficiency of photochemistry-producing EPFR on these surfaces.[12,32]

Dust samples collected from the home, including loose dust from under furniture, also displayed substantial EPFR content (2.01 $x10^{10}$ spins μg^{-1}) that was in the middle of the range observed on surfaces. While accumulated dust may have been incorporated as part of the horizontal surface sample (e.g. floors, cabinet tops), it would have made minor contributions to vertical surfaces (e.g. windows or bathroom tiles). The EPFR content in dust may be particularly relevant, because its constitutions is characterized by a high surface to volume ratio, making it an efficient condensational sink and accessible interface for multiphase processes. However the pronounced difference in mass specific EPFR concentrations of PM (2.40 x1011 spins µg-1) and dust may be an indication timescales for equilibrium between PM and dust may be insufficiently long compared to ventilation. Another explanation for the observed difference could be, that the mass of dust is significantly influenced by large objects (e.g. fabric debris or hair), which dilute the EPFR concentration without contribution to reactivity.

The EPFR concentrations measured in this study fall within the range of outdoor $PM_{2.5}$ EPFR observed in prior studies (Figure 1c). Therein we found, that our results are well in accordance with our previous measurements of EPFR in Mainz [22] and also comparable to spin concentrations found in Baton Rouge[15] and three different sites in east China.[33] However other studies found substantially higher[34–36] or lower[37–39] concentrations of EPFR in $PM_{2.5}$, which points out the high variability of this new class of pollutants in different environments. As previous studies have demonstrated, this variability may be explained by different PM sources as well as changing concentrations of PM2.5.[34,40,41] Interestingly we found that the mass-specific EPFR spin concentrations on window surfaces are very similar to the concentration we measured in PM samples indoor as well as outdoors in Mainz, while the average of all other surfaces is about one order of magnitude smaller. This could be an indication for substantial differences in composition and chemistry of surfaces on windows compared to other indoor surfaces, which are less exposed to radiation.[42,43]

Reactivity of Surface samples upon O_3/NO_2 exposure

The different indoor samples showed significant differences in EPFR composition based on their EPR spectra (Figure 2a-c). This is an indication for the occurrence of different organic species with unpaired electrons. In all samples, we found a single broad peak around 2.002-2.004 G, which corresponds to the frequently described EPFR signal (Type 1) associated with combustion processes.[15] Additionally, we found on some surfaces (Figure 2b) and to a smaller extent in dust (Figure 2c) a signal constituting a triplet with 1:2:1 intensity distribution (44 G splitting) and centered around 1.9951 G (Type 2). Such a pattern may be explained by two equivalent hydrogen atoms in close proximity to the unpaired electron and strong influences of heteroatoms inducing a shift of the signal in the magnetic field.[44,45] To conclude we observed 2 distinct molecules with long-lived unpaired electrons on surfaces indoors (more spectra can be found in the Figure S4 and S5).

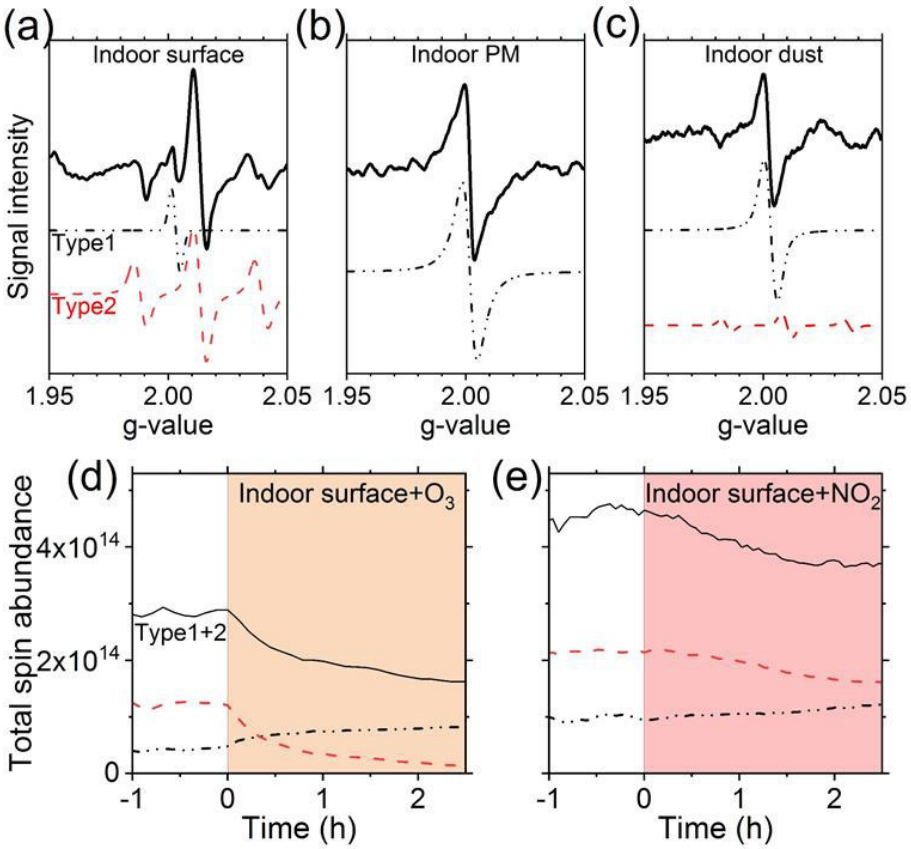

Figure 2: Electron paramagnetic resonance spectra for EPFRs in PM, dust, and surfaces and their reactivity with ozone and nitrogen dioxide. (a-c) EPR spectra for indoor surface (cabinet top), dust, and PM samples, shown with the total spectra in black and Type 1 and Type 2 radicals obtained by peak-fitting of the observed spectra. (d-e) Changes in indoor surface sample EPFR abundances for total observed radicals and each type upon exposure to (d) Ozone (Surface-01) and (e) NO_2 (Surface-03) (at t=0 after being flushed with dry N_2 gas). (See notes on spectra fitting and the specific samples shown here in the text and SI)

In order to better understand their characteristics, we exposed surface samples to reactive gas mixtures containing either ozone (d) or nitrogen dioxide (e); both oxidants induced a pronounced change in the EPR signal after prior equilibration under dry nitrogen gas. A related experiment exposing polycyclic aromatic compounds to ozone also showed the formation of EPFR.[14] More concretely we found the Type 1 EPFR signal increased in intensity, while the Type 2 signal significantly decreased and also the total spin concentration decreased upon exposure to a reactive gas. This could be an indication that we observed two distinct molecular species, which showed variations in their response to reactive gases. The increase in Type 1 EPFR may be explained by the mechanism described by Borrowman et al.. Interestingly, we found a significantly higher g-value for this Type 1 EPFR from surfaces compared to the PM samples in mind. As this value enables insights into the atoms adjacent to the radical center, this difference may be an indication for higher oxygen content in the close proximity to the C-centered radicals and accordingly a higher oxidation degree of the organic phase. A potential explanation for the more pronounced response of Type 2 EPFR could be that they are more easily accessible or that these are less persistent species, but rather transient intermediary products of slow reactions in surface films. Examples for such substances could be aliphatic radicals containing double bonds or even crigee intermediates resonance stabilized by transition metals. Such structures could explain the much lower g-value of Type 2 EPFR.

Taken together, these changes of EPFR signals upon exposure with reactive gases could be indications that EPFR occurrence may be linked to condensed phase reactivity. These EPFRs may act as a source of oxidation chemistry-initiating radicals in indoor environments and may provide a reservoir in reactive multiphase systems and surfaces (aqueous and particle). Accordingly EPFR may participate in heterogeneous chemistry and influence equilibrium partitioning of oxidized gas-phase organics in the VOC/IVOC/SVOC range.

Implications of EPFR reservoirs for indoor reactivity and multiphase chemistry

As we have shown in the previous sections, EPFR are interacting with other reactive species in multiphase processes. Accordingly it is worthwhile to consider how many radicals there are in a given environment and how the abundance of different species compares (Figure 3). If we consider only the condensed phase of PM in a typical indoor compartment (Figure 3a) we found that EPFR have a much higher abundance than other reactive species. The reason for this is the very long lifetime in the condensed phase of EPFR compared to species like ozone or nitrogendioxide, but as we have seen some of the more short lived species may induce the formation of more EPFR. Furthermore we know from previous studies, that there are different kinds of EPFR with varying lifetimes and some of them having half-life times in the range of hours.[15,34] Based on these observations we hypothesize, that EPFR could be a reservoir of reactivity in the condensed phase, and therewith enable more radical reactions than would be possible by the uptake of reactive gases alone. Other indications for such a mechanism could be recent findings of some stable oxidized organics produced in SOA being sources of radicals when dissolved into aqueous systems (i.e. water-soluble redox activity).[25,28,30,46] Along with metals, these long-lived organic compounds are critical for ROS generation and lung damage,[24] and are an understudied, but potentially major reservoir of radicals in indoor multiphase systems.

If we want to understand how the amount of EPFR in an entire indoor room, not only the suspended PM, compares to other radical species, we need to consider the gas phase, surfaces, and dust as well (Figure 3b). Doing this exercise we found reactive species like O_3 or NO_2 are likely more abundant than EPFR. Nevertheless especially the amount of EPFR in surface films (1.71×10^{-2} μmol m^{-3}), contributes substantially to the total radical budget in an indoor environment, and has outlined above may even be the dominating source of radicals in the condensed phase. Moreover we found that dust (9.47×10^{-3} μmol m^{-3}) and PM (5.39×10^{-6} μmol m^{-3}) contribute less to the total amount of EPFR indoors, but due to their more favorable surface to volume ratio they may nevertheless be relevant for multiphase processes. Particularly under the consideration that dust may be easily resuspended by activities like vacuum cleaning, therewith becoming relevant for inhalation and adverse health effects again. Taken together there has been compelling evidence about the loss of radicals to surfaces indoors, with this study we have demonstrated that they may have a longer life cycle than expected with EPFR being a reservoir in the condensed phase contributing significantly to the total radical budget indoors.

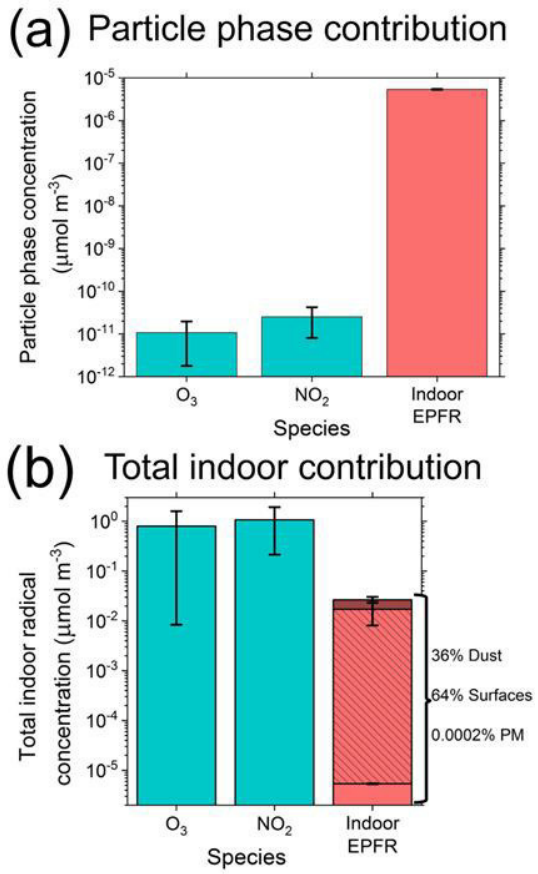

Figure 3: Comparison of EPFR contributions to indoor reactivity for PM, surfaces, and dust to common reactive species indoors. Comparison of (a) contributions to particle-phase radical concentrations for indoor suspended PM shown as their volumetric concentrations in air; (b) total gas- (blue bars) and particle-phase radical concentrations (red bar) including contributions with typical indoor prevalence of surfaces (striped) and dust (dark red). Details about the underlying room geometry and the assumed air composition (0.2-39 ppb O_3, 5-45 ppb NO_2,) can be found in the supplementary information.

Key areas for future exploration include the relevance of outdoor surfaces for multiphase processes, there is already evidence for EPFR abundance in soil, biochar, and microplastics. Accordingly integrating these budgets and constraining the frequency of interaction with other radicals may help to improve radical reactions in the condensed phase. Similarly, the results of this study emphasize the importance of incorporating these EPFR reservoirs into indoor (and potentially outdoor) chemistry models.

References

(1) Szalai, S. *The Use of Time: Daily Activities of Urban and Suburban Populations in Twelve Countries*; Mouton De Gruyter, 1973.

(2) Abbatt, J. P. D.; Wang, C. The Atmospheric Chemistry of Indoor Environments. *Environ. Sci. Process. Impacts* **2020**, *22* (1), 25–48.

(3) Eichler, C. M. A.; Cao, J.; Isaacman-VanWertz, G.; Little, J. C. Modeling the Formation and Growth of Organic Films on Indoor Surfaces. *Indoor Air* **2019**, *29* (1), 17–29.

(4) Weschler, C. J.; Nazaroff, W. W. Growth of Organic Films on Indoor Surfaces. *Indoor Air* **2017**, *27* (6), 1101–1112.

(5) Or, V. W.; Wade, M.; Patel, S.; Alves, M. R.; Kim, D.; Schwab, S.; Przelomski, H.; O'Brien, R.; Rim, D.; Corsi, R. L.; Vance, M. E.; Farmer, D. K.; Grassian, V. H. Glass Surface Evolution Following Gas Adsorption and Particle Deposition from Indoor Cooking Events as Probed by Microspectroscopic Analysis. *Environ. Sci. Process. Impacts* **2020**, *22* (8), 1698–1709.

(6) Lim, C. Y.; Abbatt, J. P. Chemical Composition, Spatial Homogeneity, and Growth of Indoor Surface Films. *Environ. Sci. Technol.* **2020**, *54* (22), 14372–14379.

(7) Weschler, C. J.; Nazaroff, W. W. Semivolatile Organic Compounds in Indoor Environments. *Atmospheric Environment*. 2008, pp 9018–9040. https://doi.org/10.1016/j.atmosenv.2008.09.052.

(8) Stutz, J.; Alicke, B.; Ackermann, R.; Geyer, A.; Wang, S.; White, A. B.; Williams, E. J.; Spicer, C. W.; Fast, J. D. Relative Humidity Dependence of HONO Chemistry in Urban Areas. *Journal of Geophysical Research: Atmospheres*. 2004. https://doi.org/10.1029/2003jd004135.

(9) Poppendieck, D. G.; Hubbard, H. F.; Weschler, C. J.; Corsi, R. L. Formation and Emissions of Carbonyls during and Following Gas-Phase Ozonation of Indoor Materials. *Atmospheric Environment*. 2007, pp 7614–7626. https://doi.org/10.1016/j.atmosenv.2007.05.049.

(10) Morrison, G. C.; Nazaroff, W. W. Ozone Interactions with Carpet: Secondary Emissions of Aldehydes. *Environ. Sci. Technol.* **2002**, *36* (10), 2185–2192.

(11) Pagonis, D.; Price, D. J.; Algrim, L. B.; Day, D. A.; Handschy, A. V.; Stark, H.; Miller, S. L.; de Gouw, J.; Jimenez, J. L.; Ziemann, P. J. Time-Resolved Measurements of Indoor Chemical Emissions, Deposition, and Reactions in a University Art Museum. *Environmental Science & Technology*. 2019, pp 4794–4802. https://doi.org/10.1021/acs.est.9b00276.

(12) Chen, Q.; Sun, H.; Wang, M.; Wang, Y.; Zhang, L.; Han, Y. Environmentally Persistent Free Radical (EPFR) Formation by Visible-Light Illumination of the Organic Matter in Atmospheric Particles. *Environ. Sci. Technol.* **2019**, *53* (17), 10053–10061.

(13) Seinfeld, J. H.; Pandis, S. N. *Atmospheric Chemistry and Physics: From Air Pollution to Climate Change*; John Wiley & Sons, 2012.

(14) Borrowman, C. K.; Zhou, S.; Burrow, T. E.; Abbatt, J. P. D. Formation of Environmentally Persistent Free Radicals from the Heterogeneous Reaction of Ozone and Polycyclic Aromatic Compounds. *Phys. Chem. Chem. Phys.* **2016**, *18* (1), 205–212.

(15) Gehling, W.; Dellinger, B. Environmentally Persistent Free Radicals and Their Lifetimes in PM2.5. *Environ. Sci. Technol.* **2013**, *47* (15), 8172–8178.

(16) Pöschl, U.; Shiraiwa, M. Multiphase Chemistry at the Atmosphere-Biosphere Interface Influencing Climate and Public Health in the Anthropocene. *Chem. Rev.* **2015**, *115* (10), 4440–4475.

(17) Shiraiwa, M.; Ammann, M.; Koop, T.; Pöschl, U. Gas Uptake and Chemical Aging of Semisolid Organic Aerosol Particles. *Proc. Natl. Acad. Sci. U. S. A.* **2011**, *108* (27), 11003–11008.

(18) Jia, H.; Zhao, S.; Shi, Y.; Zhu, L.; Wang, C.; Sharma, V. K. Transformation of Polycyclic Aromatic Hydrocarbons and Formation of Environmentally Persistent Free Radicals on Modified Montmorillonite: The Role of Surface Metal Ions and Polycyclic Aromatic Hydrocarbon Molecular

Properties. *Environ. Sci. Technol.* **2018**, *52* (10), 5725–5733.

(19) Roy, R.; Jan, R.; Yadav, S.; Vasave, M. H.; Gursumeeran Satsangi, P. Study of Metals in Radical-Mediated Toxicity of Particulate Matter in Indoor Environments of Pune, India. *Air Quality, Atmosphere & Health*. 2016, pp 669–680. https://doi.org/10.1007/s11869-015-0376-x.

(20) Reed, J. R.; Cawley, G. F.; Ardoin, T. G.; Dellinger, B.; Lomnicki, S. M.; Hasan, F.; Kiruri, L. W.; Backes, W. L. Environmentally Persistent Free Radicals Inhibit Cytochrome P450 Activity in Rat Liver Microsomes. *Toxicol. Appl. Pharmacol.* **2014**, *277* (2), 200–209.

(21) Harmon, A. C.; Hebert, V. Y.; Cormier, S. A.; Subramanian, B.; Reed, J. R.; Backes, W. L.; Dugas, T. R. Particulate Matter Containing Environmentally Persistent Free Radicals Induces AhR-Dependent Cytokine and Reactive Oxygen Species Production in Human Bronchial Epithelial Cells. *PLoS One* **2018**, *13* (10), e0205412.

(22) Arangio, A. M.; Tong, H.; Socorro, J.; Pöschl, U.; Shiraiwa, M. Quantification of Environmentally Persistent Free Radicals and Reactive Oxygen Species in Atmospheric Aerosol Particles. *Atmospheric Chemistry and Physics*. 2016, pp 13105–13119. https://doi.org/10.5194/acp-16-13105-2016.

(23) Gehling, W.; Khachatryan, L.; Dellinger, B. Hydroxyl Radical Generation from Environmentally Persistent Free Radicals (EPFRs) in PM2.5. *Environ. Sci. Technol.* **2014**, *48* (8), 4266–4272.

(24) Lakey, P. S. J.; Berkemeier, T.; Tong, H.; Arangio, A. M.; Lucas, K.; Pöschl, U.; Shiraiwa, M. Chemical Exposure-Response Relationship between Air Pollutants and Reactive Oxygen Species in the Human Respiratory Tract. *Sci. Rep.* **2016**, *6*, 32916.

(25) Tong, H.; Arangio, A. M.; Lakey, P. S. J.; Berkemeier, T.; Liu, F.; Kampf, C. J.; Brune, W. H.; Pöschl, U.; Shiraiwa, M. Hydroxyl Radicals from Secondary Organic Aerosol Decomposition in Water, 2016. https://doi.org/10.5194/acp-16-1761-2016.

(26) Khachatryan, L.; Vejerano, E.; Lomnicki, S.; Dellinger, B. Environmentally Persistent Free Radicals (EPFRs). 1. Generation of Reactive Oxygen Species in Aqueous Solutions. *Environ. Sci. Technol.* **2011**, *45* (19), 8559–8566.

(27) Khachatryan, L.; Dellinger, B. Environmentally Persistent Free Radicals (EPFRs)-2. Are Free Hydroxyl Radicals Generated in Aqueous Solutions? *Environ. Sci. Technol.* **2011**, *45* (21), 9232–9239.

(28) McWhinney, R. D.; Zhou, S.; Abbatt, J. P. D. Naphthalene SOA: Redox Activity and Naphthoquinone Gas–particle Partitioning. *Atmospheric Chemistry and Physics*. 2013, pp 9731–9744. https://doi.org/10.5194/acp-13-9731-2013.

(29) Shafer, M. M.; Hemming, J. D. C.; Antkiewicz, D. S.; Schauer, J. J. Oxidative Potential of Size-Fractionated Atmospheric Aerosol in Urban and Rural Sites across Europe. *Faraday Discussions*. 2016, pp 381–405. https://doi.org/10.1039/c5fd00196j.

(30) McWhinney, R. D.; Badali, K.; Liggio, J.; Li, S.-M.; Abbatt, J. P. D. Filterable Redox Cycling Activity: A Comparison between Diesel Exhaust Particles and Secondary Organic Aerosol Constituents. *Environ. Sci. Technol.* **2013**, *47* (7), 3362–3369.

(31) Ault, A. P.; Grassian, V. H.; Carslaw, N.; Collins, D. B.; Destaillats, H.; Donaldson, D. J.; Farmer, D. K.; Jimenez, J. L.; McNeill, V. F.; Morrison, G. C.; O'Brien, R. E.; Shiraiwa, M.; Vance, M. E.; Wells, J. R.; Xiong, W. Indoor Surface Chemistry: Developing a Molecular Picture of Reactions on Indoor Interfaces. *Chem* **2020**. https://doi.org/10.1016/j.chempr.2020.08.023.

(32) Zhu, K.; Jia, H.; Zhao, S.; Xia, T.; Guo, X.; Wang, T.; Zhu, L. Formation of Environmentally Persistent Free Radicals on Microplastics under Light Irradiation. *Environ. Sci. Technol.* **2019**, *53* (14), 8177–8186.

(33) Chen, Q.; Wang, M.; Sun, H.; Wang, X.; Wang, Y.; Li, Y.; Zhang, L.; Mu, Z. Enhanced Health Risks

from Exposure to Environmentally Persistent Free Radicals and the Oxidative Stress of PM from Asian Dust Storms in Erenhot, Zhangbei and Jinan, China. *Environ. Int.* **2018**, *121* (Pt 1), 260–268.

(34) Chen, Q.; Sun, H.; Mu, Z.; Wang, Y.; Li, Y.; Zhang, L.; Wang, M.; Zhang, Z. Characteristics of Environmentally Persistent Free Radicals in PM2.5: Concentrations, Species and Sources in Xi'an, Northwestern China. *Environmental Pollution*. 2019, pp 18–26. https://doi.org/10.1016/j.envpol.2019.01.015.

(35) Qian, R.; Zhang, S.; Peng, C.; Zhang, L.; Yang, F.; Tian, M.; Huang, R.; Wang, Q.; Chen, Q.; Yao, X.; Chen, Y. Characteristics and Potential Exposure Risks of Environmentally Persistent Free Radicals in PM in the Three Gorges Reservoir Area, Southwestern China. *Chemosphere* **2020**, *252*, 126425.

(36) Wang, P.; Pan, B.; Li, H.; Huang, Y.; Dong, X.; Ai, F.; Liu, L.; Wu, M.; Xing, B. The Overlooked Occurrence of Environmentally Persistent Free Radicals in an Area with Low-Rank Coal Burning, Xuanwei, China. *Environmental Science & Technology*. 2018, pp 1054–1061. https://doi.org/10.1021/acs.est.7b05453.

(37) Squadrito, G. L.; Cueto, R.; Dellinger, B.; Pryor, W. A. Quinoid Redox Cycling as a Mechanism for Sustained Free Radical Generation by Inhaled Airborne Particulate Matter. *Free Radic. Biol. Med.* **2001**, *31* (9), 1132–1138.

(38) Shaltout, A. A.; Boman, J.; Shehadeh, Z. F.; Al-Malawi, D.-A. R.; Hemeda, O. M.; Morsy, M. M. Spectroscopic Investigation of PM2.5 Collected at Industrial, Residential and Traffic Sites in Taif, Saudi Arabia. *J. Aerosol Sci.* **2015**, *79*, 97–108.

(39) Guo, X.; Zhang, N.; Hu, X.; Huang, Y.; Ding, Z.; Chen, Y.; Lian, H.-Z. Characteristics and Potential Inhalation Exposure Risks of PM2.5–bound Environmental Persistent Free Radicals in Nanjing, a Mega–city in China. *Atmospheric Environment*. 2020, p 117355. https://doi.org/10.1016/j.atmosenv.2020.117355.

(40) Chen, Q.; Sun, H.; Song, W.; Cao, F.; Tian, C.; Zhang, Y.-L. Size-Resolved Exposure Risk of Persistent Free Radicals (PFRs) in Atmospheric Aerosols and Their Potential Sources. https://doi.org/10.5194/acp-2020-141.

(41) Wang, Y.; Li, S.; Wang, M.; Sun, H.; Mu, Z.; Zhang, L.; Li, Y.; Chen, Q. Source Apportionment of Environmentally Persistent Free Radicals (EPFRs) in PM2.5 over Xi'an, China. *Science of The Total Environment*. 2019, pp 193–202. https://doi.org/10.1016/j.scitotenv.2019.06.424.

(42) Liu, Q.-T.; Diamond, M. L.; Gingrich, S. E.; Ondov, J. M.; Maciejczyk, P.; Stern, G. A. Accumulation of Metals, Trace Elements and Semi-Volatile Organic Compounds on Exterior Window Surfaces in Baltimore. *Environ. Pollut.* **2003**, *122* (1), 51–61.

(43) Robinson, A. L.; Donahue, N. M.; Shrivastava, M. K.; Weitkamp, E. A.; Sage, A. M.; Grieshop, A. P.; Lane, T. E.; Pierce, J. R.; Pandis, S. N. Rethinking Organic Aerosols: Semivolatile Emissions and Photochemical Aging. *Science* **2007**, *315* (5816), 1259–1262.

(44) Davies, M. J. Detection and Characterisation of Radicals Using Electron Paramagnetic Resonance (EPR) Spin Trapping and Related Methods. *Methods* **2016**, *109*, 21–30.

(45) Bertrand, P. *Electron Paramagnetic Resonance Spectroscopy: Fundamentals*; Springer Nature, 2020.

(46) Tong, H.; Lakey, P. S. J.; Arangio, A. M.; Socorro, J.; Kampf, C. J.; Berkemeier, T.; Brune, W. H.; Pöschl, U.; Shiraiwa, M. Reactive Oxygen Species Formed in Aqueous Mixtures of Secondary Organic Aerosols and Mineral Dust Influencing Cloud Chemistry and Public Health in the Anthropocene. *Faraday Discuss.* **2017**, *200*, 251–270.

Supplementary Information for:

Environmentally persistent free radicals in indoor air, dust, and on surfaces

Methods

The samplers for collection of particulate matter consisted of a vacuum pump, a mass flow controller (Mass Stream < 70 L min-1, M+W instruments), and a 47 mm single stage filter assembly (Savillex Corp.) in vertical orientation 47 mm PTFE membrane disc filter with support ring (46 µm thick, Pall Corporation), all connected by ¼ inch Teflon tubing. At the indoor location, the sampling rate controlled by the mass flow controller was set to 16 L min-1, the sampler outside was operated at 17 L min-1. Surface samples were collected using 47 mm Teflon membrane filter (0.1 µm pore size, Omnipore, Merck Millipore). A representative blank sample using the surface sampling technique described in the main text on cleaned aluminum foil is shown in Figure S5. All samples were stored in Analyslide Petri Dishes (Pall Corporation) and wrapped in aluminum foil immediately after collection.

For exposure of samples to NO_2 and O_3 a part of the filter was wrapped around the end of a quartz EPR tube (outer diameter 4 mm) and fixed with Teflon tape. This tube was inserted into a 1 cm quartz tube and on the other end connected to ¼ inch Teflon tubing. Via this tubing we flushed the respective gas mixture through the filter into the 1 cm EPR tube. You may find a sketch of the experimental set up in Figure S6.

The prevalence of dust and indoor surfaces were estimated for a typical residential room (volume = 40 m^3, surface area = 120 m^2; see SI for details) and EPFR abundance is based on this study. Occurrence of other species are based on typical literature values for indoor gas phase oxidants (Table S4). Furthermore we took into consideration data about ambient concentrations of NO_2 and O_3 from public monitoring stations in Mainz. More in detail these results showed for October 2019 the following results: average daily mean NO_2 concentration 11-21 ppb (maximum daily mean value 33 ppb) and an average daily mean concentration O_3 of 12 ppb (maximum daily mean value 24 ppb). For Ozone the uncertainty indicated in the Figure 3 is based on the indoor outdoor ratio reported in the literature(Abbatt and Wang, 2020) (0.1 - 0.8) taking the average daily mean value from the observations as a basis. As NO_2 concentrations vary on much smaller scales, the lower threshold in Figure 3 is given by the lowest reported indoor concentration reported in Table S4 (4 ppb) and the upper threshold is given by the highest daily mean value measured outdoors. Particle-phase concentrations of NO_2 and O_3 were estimated via Henry's law using constants reported in the literature.(Sander, 2015)

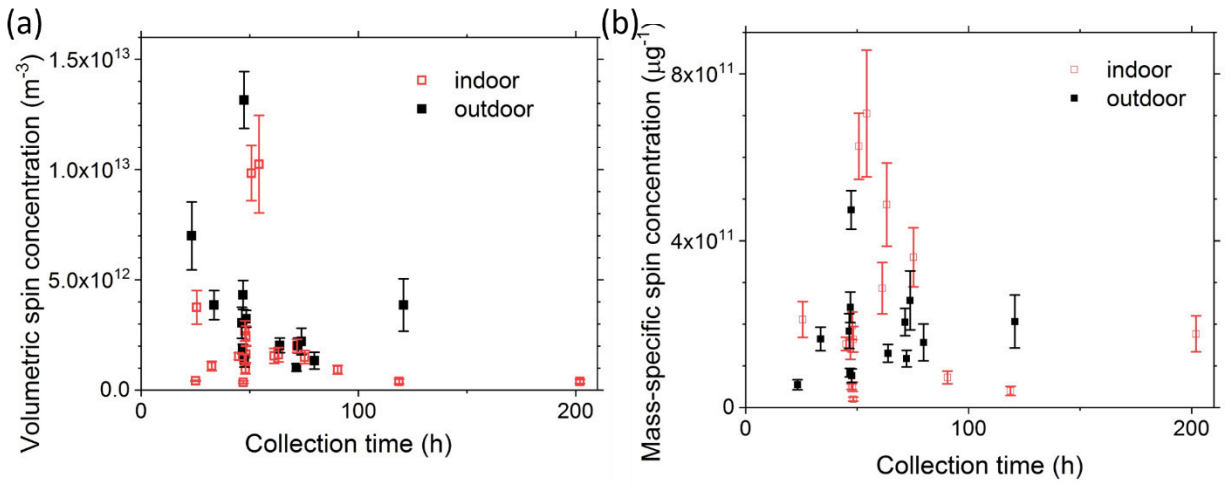

Figure S1: EPFR concentrations in particulate matter (PM) by collection time of the respective sample. (a) Volumetric spin concentration per volume of sampled air (spins m^{-3}); (b) Mass-specific EPFR spin concentration per mass of collected particulate matter (spins μg^{-1}).

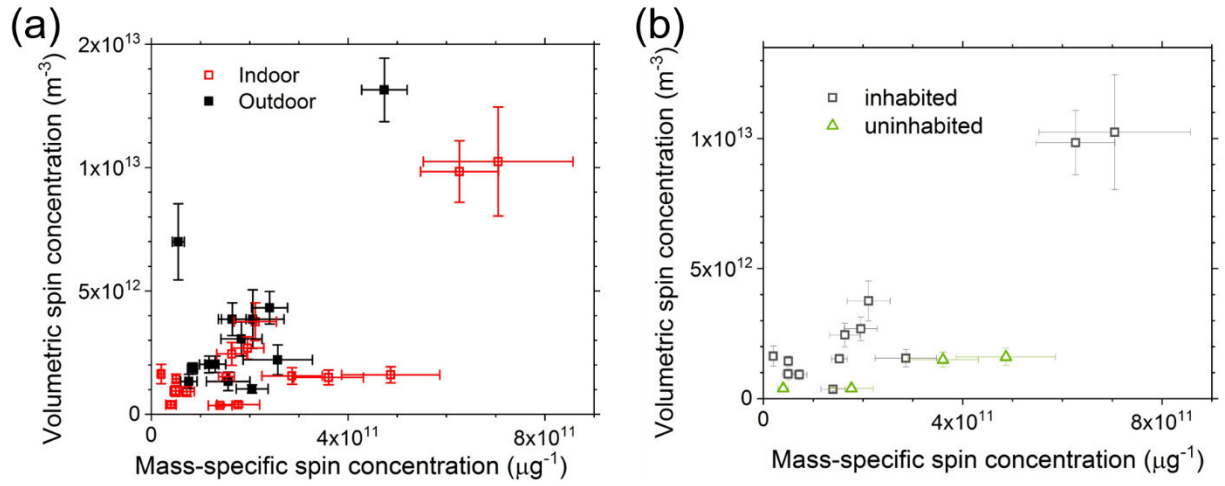

Figure S2: Correlation of volumetric and mass-specific EPFR spin concentrations in PM. (a) EPFR concentrations for indoor (empty red squares) and outdoor samples (solid black squares). (b) EPFR concentrations in indoor air differentiated by inhabited (grey squares) and uninhabited periods (light green triangles).

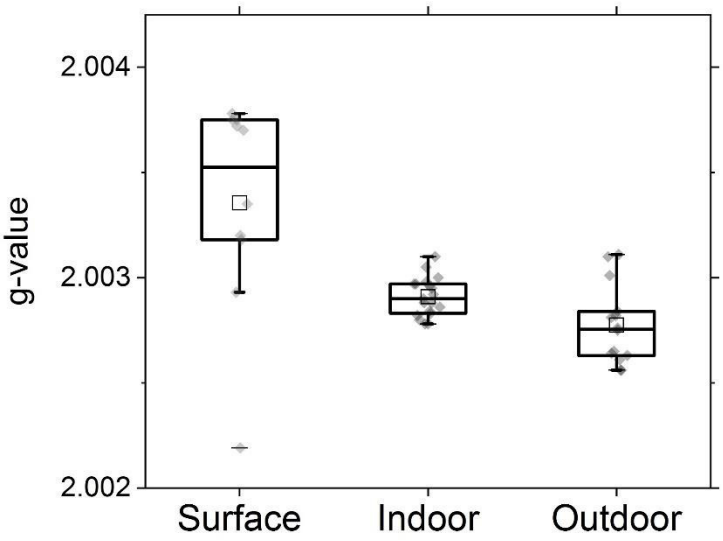

Figure S3: G-value of EPFR from indoor surfaces, indoor PM, and outdoor PM.

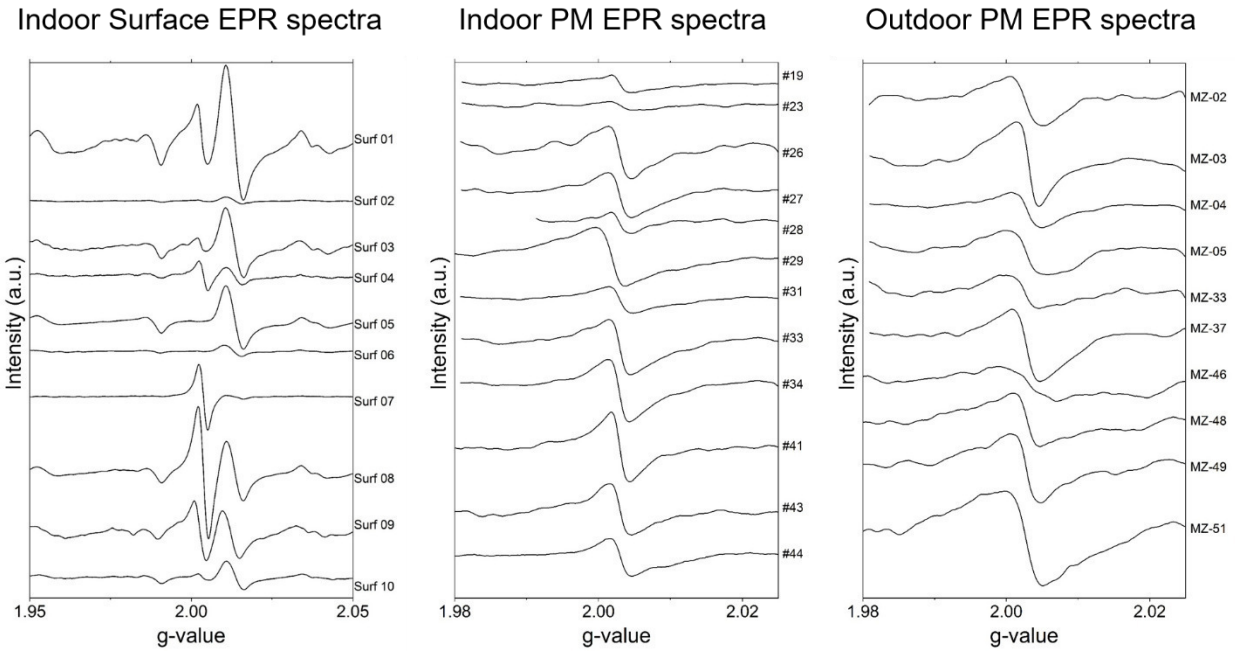

Figure S4: Baseline corrected EPR spectra of all samples collected. Panels on the left side show indoor surface spectra (specifications can be found in Table S1-3), panels in the center show indoor PM spectra, and panels on the rights side outdoor PM. The y-Axis dimensions are conserved within the respective panels.

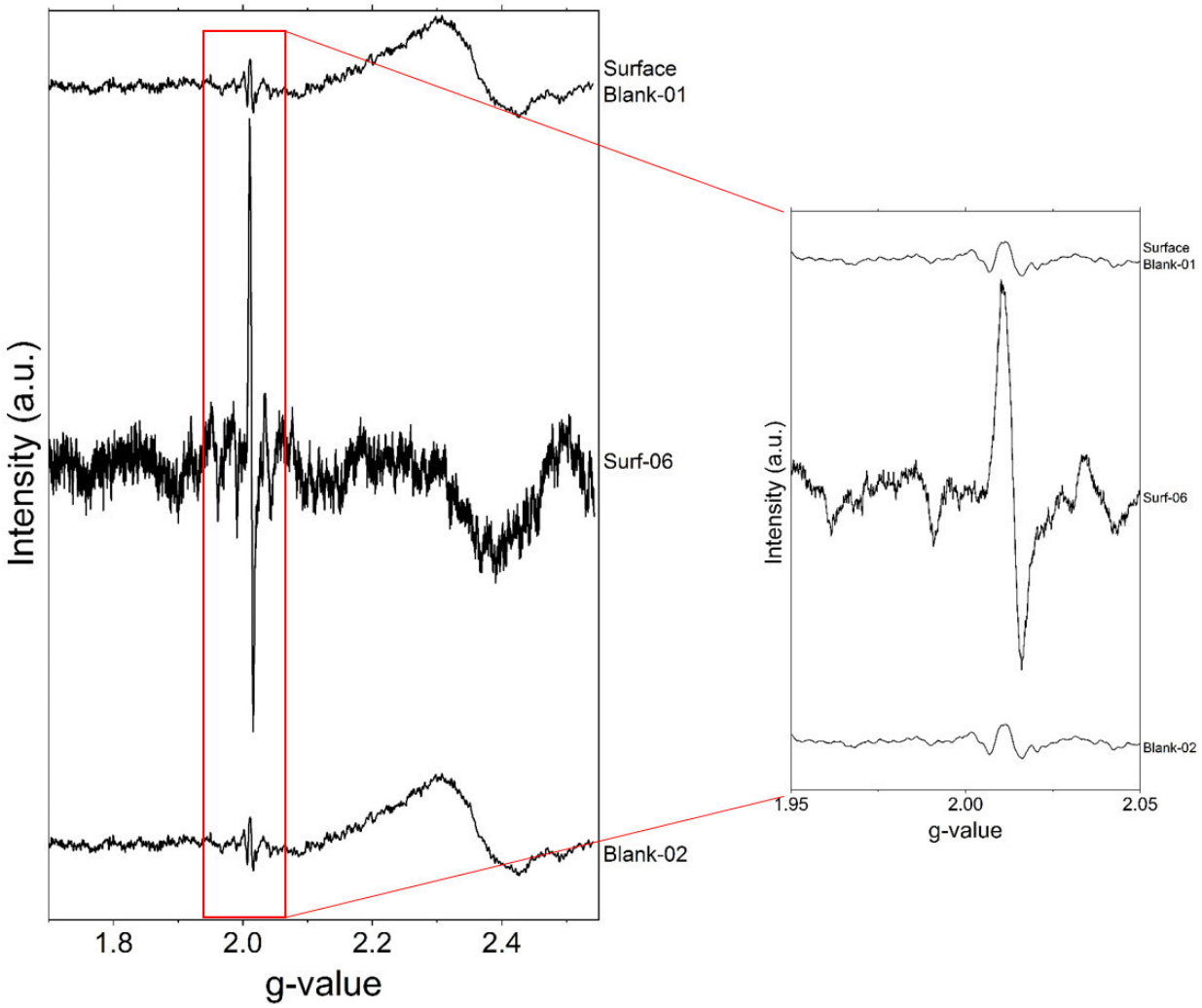

Figure S5: Surface Blank EPR spectra in comparison to a representative surface sample. The panel on the left side shows an EPR spectra recorded over a wide magnetic field range, on the right side only the g-value range displayed in Figure S4 is shown.

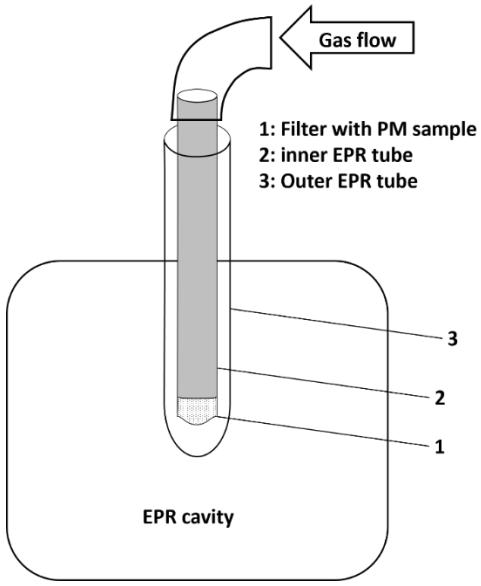

Figure S6: Sketch of the experimental setup used for exposure of samples to reactive gas mixtures.

Table S1: Sampling details of indoor PM samples, including the total sampled air volume, PM mass, and EPFR number.

Sample ID	Collection date (mm/dd/yy)	Sampling details	Sampled air volume (m^3)	PM mass (mg)	EPFR spin number (spins)
#23	09/27/19 - 09/28/19	several cooking events	24.08	not available	1.03E+13
#26	09/28/19 - 10/06/19	uninhabited except for cleaning visit	193.92	0.43	7.66E+13
#27	10/06/19 – 10/10/19	inhabited	86.88	1.11	8.03E+13
#28	10/10/19 – 10/12/19	inhabited	45.12	0.12	1.63E+13
#29	10/12/19 – 10/14/19	Increased ventilation, limited cooking	24.56	0.44	9.22E+13
#30	10/14/19 – 10/16/19	cooking and cleaning	45.92	0.63	1.23E+14
#19	10/16/19 – 10/17/19	cooking	31.20	not available	3.41E+13
#33	10/17/19 – 10/20/19	uninhabited with lots of outdoor rain	72.24	0.30	1.08E+14
#32	10/21/19 – 10/23/19	cleaning, oven usage and cooking	45.60	1.31	6.57E+13
#34	10/23/19 – 10/25/19	some cooking, pan-fried chicken	46.32	0.69	1.13E+14
#35	10/25/19 – 10/28/19	less cooking this weekend	68.88	not available	1.38E+14
#36	10/28/19 – 10/30/19	some cooking	46.08	0.88	4.37E+13
#40	10/30/19 – 11/01/19	cooking	43.20	0.43	6.61E+13
#41	11/01/19 – 11/03/19	uninhabited	60.72	0.20	9.73E+13
#43	11/08/19 – 11/11/19	water leak, higher humidity	58.80	0.32	9.16E+13
#44	11/11/19 – 11/13/19	smoke from burnt food in oven	46.32	3.76	7.56E+13
#50	11/13/19 – 11/18/19	partially uninhabited	114.00	1.12	4.47E+13
#52	11/18/19 – 11/25/19	active mold in the apartment	52.08	0.76	5.34E+14
#53	11/25/19 – 11/27/19	active mold in the apartment	48.72	0.77	4.79E+14

Table S2: Sampling details of outdoor PM samples, including the total sampled air volume, PM mass, and EPFR number.

Sample ID	Collection date (mm/dd/yy)	Sampled air volume (m^3)	PM mass (mg)	EPFR spin number (spins)
MZ-01	10/12/19 – 10/14/19	47.86	0.86	2.07E+14
MZ-02	10/14/19 – 10/16/19	47.69	1.06	8.87E+13
MZ-03	10/16/19 – 10/17/19	34.25	*0.80333*	1.32E+14
MZ-04	10/17/19 – 10/20/19	72.93	*0.36667*	7.51E+13
MZ-05	10/20/19 – 10/23/19	65.10	1.016667	1.32E+14
MZ-37	10/23/19 – 10/25/19	49.30	not available	1.59E+14
MZ-38	10/25/19 – 10/28/19	73.61	1.27	1.49E+14
MZ-39	10/28/19 – 10/30/19	48.53	0.85	6.49E+13
MZ-45	10/30/19 – 11/01/19	23.72	3.03	1.66E+14
MZ-49	11/01/19 – 11/04/19	75.23	0.65	1.66E+14
MZ-46	11/04/19 – 11/07/19	81.35	0.70	1.09E+14
MZ-48	11/11/19 – 11/13/19	47.35	0.79	1.45E+14
MZ-51	11/13/19 – 11/18/19	123.17	2.30	4.75E+14
MZ-58	11/25/19 – 11/27/19	48.28	1.34	6.35E+14

Table S3: Sampling details and results of the collected surface samples within the studied apartment.

Sample ID	Collection place	PM mass (mg)	Total EPFR Type-1 spin number (spins)	Total EPFR Type-2 spin number (spins)
Surface-01	Kitchen cabinet above oven (horizontal)	21.54	1.66E+14	2.26E+14
Surface-02	Above main room cabinet (horizontal)	0.76	2.94E+12	4.03E+12
Surface-03	on top of bathroom cabinet (horizontal)	3.39	1.82E+13	3.14E+13
Surface-04	Window #1 main room (vertical)	1.01	4.91E+13	9.24E+13
Surface-05	Wall in main bathroom (tile)	1.84	Not available	4.51E+12
Surface-06	Wall in 2nd bathroom (tile outside shower)	0.69	Not available	8.82E+11
Surface-07	Window #2 main room (vertical)	0.90	1.23E+14	1.91E+14
Surface-08	Floor corner main room (horizontal)	8.83	2.92E+14	4.70E+14
Surface-09	Floor corner entry way (horizontal)	15.07	2.06E+14	5.81E+14
Surface-10	Same spot as sample Surface-01	2.57	9.92E+12	1.67E+13
House dust-1	Under the couch	3.05	5.91E+13	Not available
House dust-2	Under the couch	1.56	3.49E+13	Not available

Table S4: Literature reports about Ozone and Nitrogendioxide concentrations indoor.

Ozone (ppb)			Nitrogendioxide (ppb)		
Reference	Mean	Range	Reference	Mean	Range
Lee et al. (2002)	14.9	0.6 - 67.8	Lee et al. (2002)	28.0	4.3 - 52.0
(Zhang and Lioy, 1994)	28	1-181	(Zhou et al., 2018)	3.7	20 other studies: 4.8 - 46.5
(Zhang et al., 1994)		30-60	(Weschler, 2000)	30	
(Hwang and Park, 2020)	11.4		(Hwang and Park, 2020)	13.9	
(Zhou et al., 2019)	0.62 (residence) 21.5 (lab) 22.5 (office)		(Zhou et al., 2019)	8.4 (residence) 9.1 (lab) 11.3 (office)	
(Abbatt and Wang, 2020)	< 5	0.1 - 0.8 of outdoor air			

References

1. Abbatt, J. P.; Wang, C., The atmospheric chemistry of indoor environments. *Environmental Science: Processes & Impacts* **2020,** *22*, (1), 25-48.
2. Sander, R., Compilation of Henry's law constants (version 4.0) for water as solvent. *Atmos Chem Phys* **2015**.
3. Lee, K.; Xue, J.; Geyh, A. S.; Ozkaynak, H.; Leaderer, B. P.; Weschler, C. J.; Spengler, J. D., Nitrous acid, nitrogen dioxide, and ozone concentrations in residential environments. *Environmental health perspectives* **2002,** *110*, (2), 145-150.
4. Zhang, J.; Lioy, P. J., Ozone in residential air: concentrations, I/O ratios, indoor chemistry, and exposures. *Indoor Air* **1994,** *4*, (2), 95-105.
5. Zhou, S.; Young, C. J.; VandenBoer, T. C.; Kowal, S. F.; Kahan, T. F., Time-Resolved Measurements of Nitric Oxide, Nitrogen Dioxide, and Nitrous Acid in an Occupied New York Home. *Environmental Science & Technology* **2018,** *52*, (15), 8355-8364.
6. Zhang, J.; Lioy, P. J.; He, Q., Characteristics of aldehydes: concentrations, sources, and exposures for indoor and outdoor residential microenvironments. *Environmental Science & Technology* **1994,** *28*, (1), 146-152.
7. Weschler, C. J., Ozone in indoor environments: concentration and chemistry. *Indoor air* **2000,** *10*, (4), 269-288.
8. Hwang, S. H.; Park, W. M., Indoor air concentrations of carbon dioxide (CO2), nitrogen dioxide (NO2), and ozone (O3) in multiple healthcare facilities. *Environmental Geochemistry and Health* **2020,** *42*, (5), 1487-1496.
9. Zhou, S.; Young, C. J.; VandenBoer, T. C.; Kahan, T. F., Role of location, season, occupant activity, and chemistry in indoor ozone and nitrogen oxide mixing ratios. *Environmental Science: Processes & Impacts* **2019,** *21*, (8), 1374-1383.

4. Summary and Conclusions

4.1 Individual Studies

Hydroxyl Radical Scavenging by Cerium Dioxide Nanoparticles

The effectiveness of hydroxyl radicals (•OH) scavenging by cerium oxide nanoparticles (CeNPs) was explored experimentally in comparison to their ability to produce •OH. The effect of CeNPs on this particularly damaging reactive species was tested in EPR spin trapping measurements of •OH in aqueous solutions. The activity of CeNPs on •OH shows a pronounced dependence on the surface to volume ratio as well as the surface composition of the nanomaterial. Under physiologically relevant conditions in surrogate lung fluid, CeNPs showed a predominate •OH scavenging activity, which could be an indication that they act as antioxidants under such conditions. For details see chapter 3.2.

Oxidation Degree and its Influence on Radical Yield of Particulate Matter

Ambient particulate matter (PM) from remote and urban environments was analyzed alongside laboratory generated secondary organic aerosols (SOA) for their content of highly oxygenated molecules (HOMs) and radical yield upon suspension in water. Structural information about the oxidation degree of organic molecules from mass spectrometry was combined with radical yields estimated with EPR spin-trapping and subsequently insights into the chemical relationship between these two variables were tested. In fact, a correlation between HOMs abundance and radical yield could be found by comparing the ambient samples. Also, different SOA followed this trend, therewith suggesting that HOMs may play a significant role in the radical production of PM in solutions. The results further indicated that PM from remote forests, which typically has a high content of organic molecules from biogenic sources, has a higher mass-specific radical yield than urban PM. For details see chapter 3.3.

Reactive Species Yield of Particulate Matter from Clean and Polluted Environments

The reactive species (RS) formation upon suspension in water was compared for PM from a remote forest site (Hyytiälä), Mainz, and Beijing using EPR spin-trapping and a fluorimetric H_2O_2 assay. Furthermore, these insights were complemented with the chemical characterization of molecular composition and transition metal content. Lastly RS yields of ambient PM samples were experimentally modeled using surrogate molecules. With mixtures of transition metals, organic hydroperoxide, H_2O_2, humic- and fulvic acids we achieved comparable results for RS formation ratios as observed for Hyytiälä, Mainz, and Beijing PM. Results suggested that transition metals may contribute to a preferential formation of •OH over organic radicals. However, the interplay of different organic and inorganic constituents even in these relatively simple mixtures caused a complex formation of different RS. For details see chapter 3.4.

Environmentally Persistent Free Radicals in Remote and Polluted Regions

Particulate matter from remote and urban environments was investigated for its content and size distribution of environmentally persistent free radicals (EPFR). By resolving the distribution of this emerging class of pollutants for particles ranging from 10 nm to 10 µm, new perspectives on sources and formation pathways of EPFR were enabled. It is shown that EPFR concentrations positively correlated with PM abundance across the studied sites and that even in remote environments substantial amounts of EPFR occurred. More

concretely the results indicated that the majority of EPFR in most environments are in particles smaller than 1 µm. However, the results suggested that there is a pronounced influence of local PM sources on EPFR abundance and size distribution. This finding likely explained the pronounced seasonality of EPFR concentrations, which we observed in a case study for Mainz. The results of this study shall soon be published, see chapter 3.5.

The Role of Environmentally Persistent Free Radicals Indoors

In the framework of a coordinated campaign, an apartment in Mainz (Germany) was sampled for its content of EPFR and compared to an outdoor reference site. By sampling PM, surfaces, and house dust, we were able to assess the potential role of EPFR in multiphase chemistry indoors. The results are the first to confirm the presence of EPFR indoors, which we find is oftentimes closely linked to outdoor EPFR concentrations. Based on the abundance in PM, dust, and on surfaces we show that most EPFR indoors are in surface films and that the total amount of this substance class in a typical apartment may contribute significantly to the budget of radicals. We estimated that in the condensed phase EPFR concentrations exceed the abundance of O_3 and NO_2 by orders of magnitude and could be a reservoir for radical reactions. The results of this campaign shall soon be published, see chapter 3.6.

4.2 Conclusions

In the scope of this PhD project, EPR spectroscopy has been applied to tackle questions motivated by the adverse health effects of ambient PM. Using this technique, samples of ambient particles were analyzed for their radical content and suspensions of PM in aqueous solution were investigated for RS formation, especially short-lived radicals.

The role of insoluble PM constituents was targeted by immersion of synthetic CeNPs into a surrogate lung fluid containing moderate RS levels. The results indicate that poorly soluble, redox-active molecules may exhibit a substantial influence on the RS budget in physiologic environments by multiphase processes. The studies on SOA and ambient PM demonstrate differences in RS production between particle types, particularly the influence of varying oxidation degree of organic molecules. With these insights, the contribution of organic molecules to the RS yield of PM may be better described in models. Beyond this, the finding that remote aerosols have a higher mass-specific RS yield than urban PM, emphasizes the importance of organic molecules in contributing to radical production. On the topic of RS generation by PM in solution, future studies could employ EPR spectroscopy to further constrain which types of RS are produced at which reaction rates by specific PM constituents.

For the first time, EPFR concentrations were compared across different continents and types of environments; the size distribution and abundance of this substance class were comprehensively assessed. The occurrence of EPFR in remote and polluted environments as well as indoors was confirmed. With the new data on this emerging class of pollutants, a more detailed analysis of their role in atmospheric processing and the health effects of PM is enabled. Nevertheless, it remains unclear how readily EPFR participate in radical reactions in the particles phase or upon dissolution. Also what their fate during long-range atmospheric transport is and the exact EPFR sources in remote places should be further explored.

All of these studies demonstrate that it is worthwhile to pursue further research on redox reactions and radical abundance in particulate matter because there is a large potential to improve the description of multiphase chemistry and the effect of PM on human health.

5. Bibliography

Abbatt, J. P., and Wang, C.: The atmospheric chemistry of indoor environments, Environmental Science: Processes & Impacts, 22, 25-48, 2020.

Alfadda, A. A., and Sallam, R. M.: Reactive oxygen species in health and disease, J Biomed Biotechnol, 2012, 936486, 2012.

Andreae, M., and Gelencsér, A.: Black carbon or brown carbon? The nature of light-absorbing carbonaceous aerosols, 2006.

Arangio, A. M., Slade, J. H., Berkemeier, T., Pöschl, U., Knopf, D. A., and Shiraiwa, M.: Multiphase chemical kinetics of OH radical uptake by molecular organic markers of biomass burning aerosols: humidity and temperature dependence, surface reaction, and bulk diffusion, The Journal of Physical Chemistry A, 119, 4533-4544, 2015.

Araujo, J. A., Barajas, B., Kleinman, M., Wang, X., Bennett, B. J., Gong, K. W., Navab, M., Harkema, J., Sioutas, C., and Lusis, A. J.: Ambient particulate pollutants in the ultrafine range promote early atherosclerosis and systemic oxidative stress, Circulation research, 102, 589-596, 2008.

Balakrishna, S., Lomnicki, S., McAvey, K. M., Cole, R. B., Dellinger, B., and Cormier, S. A.: Environmentally persistent free radicals amplify ultrafine particle mediated cellular oxidative stress and cytotoxicity, Particle and fibre toxicology, 6, 11, 2009.

Bates, J. T., Fang, T., Verma, V., Zeng, L., Weber, R. J., Tolbert, P. E., Abrams, J., Sarnat, S. E., Klein, M., and Mulholland, J. A.: Review of acellular assays of ambient particulate matter oxidative potential: methods and relationships with composition, sources, and health effects, Environmental Science & Technology, 2019.

Borrowman, C. K., Zhou, S., Burrow, T. E., and Abbatt, J. P.: Formation of environmentally persistent free radicals from the heterogeneous reaction of ozone and polycyclic aromatic compounds, Phys Chem Chem Phys, 18, 205-212, 2016.

Calas, A., Uzu, G., Kelly, F. J., Houdier, S., Martins, J. M. F., Thomas, F., Molton, F., Charron, A., Dunster, C., Oliete, A., Jacob, V., Besombes, J.-L., Chevrier, F., and Jaffrezo, J.-L.: Comparison between five acellular oxidative potential measurement assays performed with detailed chemistry on PM₁₀ samples from the city of Chamonix (France), Atmospheric Chemistry and Physics, 18, 7863-7875, 2018.

Carvalho, T. C., Peters, J. I., and Williams III, R. O.: Influence of particle size on regional lung deposition–what evidence is there?, International journal of pharmaceutics, 406, 1-10, 2011.

Chen, Q., Sun, H., Mu, Z., Wang, Y., Li, Y., Zhang, L., Wang, M., and Zhang, Z.: Characteristics of environmentally persistent free radicals in PM2. 5: Concentrations, species and sources in Xi'an, Northwestern China, Environmental Pollution, 247, 18-26, 2019a.

Chen, Q., Sun, H., Wang, M., Wang, Y., Zhang, L., and Han, Y.: Environmentally persistent free radical (EPFR) formation by visible-light illumination of the organic matter in atmospheric particles, Environ Sci Technol, 2019b.

Church, D. F., and Pryor, W. A.: Free-Radical Chemistry of Cigarette Smoke and Its Toxicological Implications, Environmental Health Perspectives, 64, 111-126, 1985.

Cohen, A. J., Brauer, M., Burnett, R., Anderson, H. R., Frostad, J., Estep, K., Balakrishnan, K., Brunekreef, B., Dandona, L., Dandona, R., Feigin, V., Freedman, G., Hubbell, B., Jobling, A., Kan, H., Knibbs, L., Liu, Y., Martin, R., Morawska, L., Pope, C. A., Shin, H., Straif, K., Shaddick, G., Thomas, M., van Dingenen, R., van Donkelaar, A., Vos, T., Murray, C. J. L., and Forouzanfar, M. H.: Estimates and 25-year trends of the global burden of disease attributable to ambient air pollution: an analysis of data from the Global Burden of Diseases Study 2015, The Lancet, 389, 1907-1918, 2017.

Davies, M. J.: Detection and characterisation of radicals using electron paramagnetic resonance (EPR) spin trapping and related methods, Methods, 109, 21-30, 2016.

Dellinger, B., Pryor, W. A., Cueto, R., Squadrito, G. L., Hegde, V., and Deutsch, W. A.: Role of Free Radicals in the Toxicity of Airborne Fine Particulate Matter, Chemical Research in Toxicology, 14, 1371-1377, 2001.

Dellinger, B., Lomnicki, S., Khachatryan, L., Maskos, Z., Hall, R. W., Adounkpe, J., McFerrin, C., and Truong, H.: Formation and stabilization of persistent free radicals, Proceedings of the Combustion Institute, 31, 521-528, 2007.

Deng, R., Luo, H., Huang, D., and Zhang, C.: Biochar-mediated Fenton-like reaction for the degradation of sulfamethazine: Role of environmentally persistent free radicals, Chemosphere, 126975, 2020.

Dowding, J. M., Dosani, T., Kumar, A., Seal, S., and Self, W. T.: Cerium oxide nanoparticles scavenge nitric oxide radical (NO), Chem Commun (Camb), 48, 4896-4898, 2012.

Dowding, J. M., Seal, S., and Self, W. T.: Cerium oxide nanoparticles accelerate the decay of peroxynitrite (ONOO(-)), Drug Deliv Transl Res, 3, 375-379, 2013.

Dunnick, K. M., Pillai, R., Pisane, K. L., Stefaniak, A. B., Sabolsky, E. M., and Leonard, S. S.: The Effect of Cerium Oxide Nanoparticle Valence State on Reactive Oxygen Species and Toxicity, Biol. Trace Elem. Res., 166, 96-107, 2015.

Fang, T., Zeng, L., Gao, D., Verma, V., Stefaniak, A. B., and Weber, R. J.: Ambient Size Distributions and Lung Deposition of Aerosol Dithiothreitol-Measured Oxidative Potential: Contrast between Soluble and Insoluble Particles, Environ Sci Technol, 51, 6802-6811, 2017.

Gehling, W., and Dellinger, B.: Environmentally persistent free radicals and their lifetimes in PM2.5, Environ Sci Technol, 47, 8172-8178, 2013.

Gerson, F., and Huber, W.: Electron spin resonance spectroscopy of organic radicals, John Wiley & Sons, 2003.

Grulke, E., Reed, K., Beck, M., Huang, X., Cormack, A., and Seal, S.: Nanoceria: factors affecting its pro- and anti-oxidant properties, Environ. Sci.: Nano, 1, 429-444, 2014.

Halliwell, B., and Gutteridge, J. M. C.: Free Radicals in Biology and Medicine, 5th Edition, Oxford university press, United States of America, 905 pp., 2015.

Harmon, A. C., Hebert, V. Y., Cormier, S. A., Subramanian, B., Reed, J. R., Backes, W. L., and Dugas, T. R.: Particulate matter containing environmentally persistent free radicals induces AhR-dependent cytokine and reactive oxygen species production in human bronchial epithelial cells, PLoS One, 13, e0205412, 2018.

Hawkins, C. L., and Davies, M. J.: Detection and characterisation of radicals in biological materials using EPR methodology, Biochimica et Biophysica Acta (BBA)-General Subjects, 1840, 708-721, 2014.

Heard, D. E.: Field Masurements of Atmospheric Composition, in: Analytical Techniques for Atmospheric Measurement, 1-71, 2006.

Highwood, E. J., and Kinnersley, R. P.: When smoke gets in our eyes: The multiple impacts of atmospheric black carbon on climate, air quality and health, Environment international, 32, 560-566, 2006.

Huang, W., Wang, G., Lu, S. E., Kipen, H., Wang, Y., Hu, M., Lin, W., Rich, D., Ohman-Strickland, P., Diehl, S. R., Zhu, P., Tong, J., Gong, J., Zhu, T., and Zhang, J.: Inflammatory and oxidative stress responses of healthy young adults to changes in air quality during the Beijing Olympics, Am J Respir Crit Care Med, 186, 1150-1159, 2012.

Jaligama, S., Patel, V. S., Wang, P., Sallam, A., Harding, J., Kelley, M., Mancuso, S. R., Dugas, T. R., and Cormier, S. A.: Radical containing combustion derived particulate matter enhance pulmonary Th17 inflammation via the aryl hydrocarbon receptor, Part Fibre Toxicol, 15, 20, 2018.

Janssen, N. A., Hoek, G., Simic-Lawson, M., Fischer, P., van Bree, L., ten Brink, H., Keuken, M., Atkinson, R. W., Anderson, H. R., Brunekreef, B., and Cassee, F. R.: Black carbon as an additional indicator of the adverse health effects of airborne particles compared with PM10 and PM2.5, Environ Health Perspect, 119, 1691-1699, 2011.

Karakoti, A., Singh, S., Dowding, J. M., Seal, S., and Self, W. T.: Redox-active radical scavenging nanomaterials, Chem Soc Rev, 39, 4422-4432, 2010.

Khachatryan, L., Vejerano, E., Lomnicki, S., and Dellinger, B.: Environmentally persistent free radicals (EPFRs). 1. Generation of reactive oxygen species in aqueous solutions, Environmental science & technology, 45, 8559-8566, 2011.

Korschelt, K., Schwidetzky, R., Pfitzner, F., Strugatchi, J., Schilling, C., von der Au, M., Kirchhoff, K., Panthofer, M., Lieberwirth, I., Tahir, M. N., Hess, C., Meermann, B., and Tremel, W.: CeO2-x nanorods with intrinsic urease-like activity, Nanoscale, 10, 13074-13082, 2018.

Krug, H. F., and Wick, P.: Nanotoxicology: an interdisciplinary challenge, Angew. Chem. Int. Ed., 50, 1260-1278, 2011.

Künzli, N., Kaiser, R., Medina, S., Studnicka, M., Chanel, O., Filliger, P., Herry, M., Horak Jr, F., Puybonnieux-Texier, V., and Quénel, P.: Public-health impact of outdoor and traffic-related air pollution: a European assessment, The Lancet, 356, 795-801, 2000.

Lakey, P. S., Berkemeier, T., Tong, H., Arangio, A. M., Lucas, K., Poschl, U., and Shiraiwa, M.: Chemical exposure-response relationship between air pollutants and reactive oxygen species in the human respiratory tract, Sci Rep, 6, 32916, 2016.

Lelieveld, J., Evans, J. S., Fnais, M., Giannadaki, D., and Pozzer, A.: The contribution of outdoor air pollution sources to premature mortality on a global scale, Nature, 525, 367-371, 2015.

Lelieveld, J., Klingmüller, K., Pozzer, A., Pöschl, U., Fnais, M., Daiber, A., and Münzel, T.: Cardiovascular disease burden from ambient air pollution in Europe reassessed using novel hazard ratio functions, European Heart Journal, 2019.

Lelieveld, J., Pozzer, A., Pöschl, U., Fnais, M., Haines, A., and Münzel, T.: Loss of life expectancy from air pollution compared to other risk factors: a worldwide perspective, Cardiovascular Research, 2020.

Li, H., Guo, H., Pan, B., Liao, S., Zhang, D., Yang, X., Min, C., and Xing, B.: Catechol degradation on hematite/silica-gas interface as affected by gas composition and the formation of environmentally persistent free radicals, Sci Rep, 6, 24494, 2016.

Li, X., Shen, C., Zhao, H., Jiang, J., Ban, Z., Chen, Z., and Qu, B.: Photoformation of persistent free radicals on a montmorillonite-humic acid complex simulated as particulate organic matter in an aqueous solution, Environmental Science: Processes & Impacts, 2020.

Lyu, Y., Guo, H., Cheng, T., and Li, X.: Particle Size Distributions of Oxidative Potential of Lung-Deposited Particles: Assessing Contributions from Quinones and Water-Soluble Metals, Environ Sci Technol, 52, 6592-6600, 2018.

Ma, Y., Cheng, Y., Qiu, X., Cao, G., Fang, Y., Wang, J., Zhu, T., Yu, J., and Hu, D.: Sources and oxidative potential of water-soluble humic-like substances (HULIS_{WS}) in fine particulate matter (PM_{2.5}) in Beijing, Atmospheric Chemistry and Physics, 18, 5607-5617, 2018.

Magalhaes, S., Baumgartner, J., and Weichenthal, S.: Impacts of exposure to black carbon, elemental carbon, and ultrafine particles from indoor and outdoor sources on blood pressure in adults: a review of epidemiological evidence, Environmental research, 161, 345-353, 2018.

Martinelli, N., Olivieri, O., and Girelli, D.: Air particulate matter and cardiovascular disease: a narrative review, Eur J Intern Med, 24, 295-302, 2013.

Nawrot, T. S., Kuenzli, N., Sunyer, J., Shi, T., Moreno, T., Viana, M., Heinrich, J., Forsberg, B., Kelly, F. J., Sughis, M., Nemery, B., and Borm, P.: Oxidative properties of ambient PM2.5 and elemental composition: Heterogeneous associations in 19 European cities, Atmospheric Environment, 43, 4595-4602, 2009.

Organization, W. H.: Ambient air pollution: A global assessment of exposure and burden of disease, 2016.

Park, E. J., Choi, J., Park, Y. K., and Park, K.: Oxidative stress induced by cerium oxide nanoparticles in cultured BEAS-2B cells, Toxicology, 245, 90-100, 2008.

Patterson, M. C., DiTusa, M. F., McFerrin, C. A., Kurtz, R. L., Hall, R. W., Poliakoff, E. D., and Sprunger, P. T.: Formation of environmentally persistent free radicals (EPFRs) on ZnO at room temperature: Implications for the fundamental model of EPFR generation, Chem Phys Lett, 670, 5-10, 2017.

Plakhova, T. V., Romanchuk, A. Y., Yakunin, S. N., Dumas, T., Demir, S., Wang, S., Minasian, S. G., Shuh, D. K., Tyliszczak, T., Shiryaev, A. A., Egorov, A. V., Ivanov, V. K., and Kalmykov, S. N.: Solubility of Nanocrystalline Cerium Dioxide: Experimental Data and Thermodynamic Modeling, The Journal of Physical Chemistry C, 120, 22615-22626, 2016.

Rajeshkumar, S., and Naik, P.: Synthesis and biomedical applications of Cerium oxide nanoparticles - A Review, Biotechnol Rep (Amst), 17, 1-5, 2018.

Reed, J. R., Cawley, G. F., Ardoin, T. G., Dellinger, B., Lomnicki, S. M., Hasan, F., Kiruri, L. W., and Backes, W. L.: Environmentally persistent free radicals inhibit cytochrome P450 activity in rat liver microsomes, Toxicol Appl Pharmacol, 277, 200-209, 2014.

Rohr, A. C., and Wyzga, R. E.: Attributing health effects to individual particulate matter constituents, Atmospheric Environment, 62, 130-152, 2012.

Schraufnagel, D. E., Balmes, J. R., Cowl, C. T., De Matteis, S., Jung, S. H., Mortimer, K., Perez-Padilla, R., Rice, M. B., Riojas-Rodriguez, H., Sood, A., Thurston, G. D., To, T., Vanker, A., and Wuebbles, D. J.: Air Pollution and Noncommunicable Diseases: A Review by the Forum of International Respiratory Societies' Environmental Committee, Part 1: The Damaging Effects of Air Pollution, Chest, 155, 409-416, 2019.

Seinfeld, J. H., and Pandis, S. N.: Atmospheric chemistry and physics: from air pollution to climate change, John Wiley & Sons, 2016.

Sies, H.: Hydrogen peroxide as a central redox signaling molecule in physiological oxidative stress: Oxidative eustress, Redox Biol, 11, 613-619, 2017.

Stone, V., Miller, M. R., Clift, M. J., Elder, A., Mills, N. L., Møller, P., Schins, R. P., Vogel, U., Kreyling, W. G., and Alstrup Jensen, K.: Nanomaterials versus ambient ultrafine particles: an opportunity to exchange toxicology knowledge, Environmental Health Perspectives, 125, 106002, 2017.

Szalai, A.: The use of time: Daily activities of urban and suburban populations in twelve countries, 1972.

Valavanidis, A., Fiotakis, K., Bakeas, E., and Vlahogianni, T.: Electron paramagnetic resonance study of the generation of reactive oxygen species catalysed by transition metals and quinoid redox cycling by inhalable ambient particulate matter, Redox Rep, 10, 37-51, 2005.

Valavanidis, A., Fiotakis, K., and Vlachogianni, T.: Airborne particulate matter and human health: toxicological assessment and importance of size and composition of particles for oxidative damage and carcinogenic mechanisms, Journal of Environmental Science and Health, Part C, 26, 339-362, 2008.

Vejerano, E. P., Rao, G., Khachatryan, L., Cormier, S. A., and Lomnicki, S.: Environmentally persistent free radicals: insights on a new class of pollutants, Environmental science & technology, 52, 2468-2481, 2018.

Wang, G., Wang, H., Yu, Y., Gao, S., Feng, J., Gao, S., and Wang, L.: Chemical characterization of water-soluble components of PM10 and PM2. 5 atmospheric aerosols in five locations of Nanjing, China, Atmospheric Environment, 37, 2893-2902, 2003.

Wang, Y., Li, S., Wang, M., Sun, H., Mu, Z., Zhang, L., Li, Y., and Chen, Q.: Source apportionment of environmentally persistent free radicals (EPFRs) in PM2. 5 over Xi'an, China, Science of The Total Environment, 689, 193-202, 2019.

Wason, M. S., Colon, J., Das, S., Seal, S., Turkson, J., Zhao, J., and Baker, C. H.: Sensitization of pancreatic cancer cells to radiation by cerium oxide nanoparticle-induced ROS production, Nanomedicine, 9, 558-569, 2013.

Weil, J. A., and Bolton, J. R.: Electron paramagnetic resonance: elementary theory and practical applications, John Wiley & Sons, 2007.

West, J. J., Cohen, A., Dentener, F., Brunekreef, B., Zhu, T., Armstrong, B., Bell, M. L., Brauer, M., Carmichael, G., Costa, D. L., Dockery, D. W., Kleeman, M., Krzyzanowski, M., Kunzli, N., Liousse, C., Lung, S. C., Martin, R. V., Poschl, U., Pope, C. A., 3rd, Roberts, J. M., Russell, A. G., and Wiedinmyer,

C.: "What We Breathe Impacts Our Health: Improving Understanding of the Link between Air Pollution and Health", Environ Sci Technol, 50, 4895-4904, 2016.

World-Health-Organization: WHO Air quality guidelines for particulate matter, ozone, nitrogen dioxide and sulfur dioxide: global update 2005: summary of risk assessment, World Health Organization, 2006.

Xu, M., Wu, T., Tang, Y.-T., Chen, T., Khachatryan, L., Iyer, P. R., Guo, D., Chen, A., Lyu, M., and Li, J.: Environmentally persistent free radicals in PM 2.5: a review, Waste Disposal & Sustainable Energy, 1-21, 2019.

Xue, Y., Luan, Q., Yang, D., Yao, X., and Zhou, K.: Direct Evidence for Hydroxyl Radical Scavenging Activity of Cerium Oxide Nanoparticles, The Journal of Physical Chemistry C, 115, 4433-4438, 2011.

Yang, Y., Mao, Z., Huang, W., Liu, L., Li, J., Li, J., and Wu, Q.: Redox enzyme-mimicking activities of CeO2 nanostructures: Intrinsic influence of exposed facets, Sci Rep, 6, 35344, 2016.

Zhao, S., Gao, P., Miao, D., Wu, L., Qian, Y., Chen, S., Sharma, V. K., and Jia, H.: Formation and Evolution of Solvent-Extracted and Non-Extractable Environmentally Persistent Free Radicals in Fly Ash of Municipal Solid Waste Incinerators, Environmental science & technology, 2019.

Appendix A: Personal List of Publications

Published Journal Articles

1. Lammel, G., Kitanovski, Z., Kukucka, P., Novak, J., Arangio, A. M., Codling, G. P., Filippi, A., Hovorka, J., Leoni, C., Příbylová, P., Prokeš, R., Sáňka, O., Shahpoury, P., Tong, H. and Marco Wietzoreck, R., & Pribylova, P.: Oxygenated and Nitrated Polycyclic Aromatic Hydrocarbons in Ambient Air—Levels, Phase Partitioning, Mass Size Distributions, and Inhalation Bioaccessibility. *Environmental Science & Technology,* **54(5)**, 2615-2625, (2020).

2. Tong, H., Zhang, Y., Filippi, A., Wang, T., Li, C., Liu, F., Leppla, D., Kourtchev, I., Wang, K., Keskinen, H.M., Levula, J. T., Arangio, A. M., Shen, F., Ditas, F., Berkemeier, T., Wang, Y., Su, H., Cheng, Y., Pope, F. D., Fu, P., Yao, M., Pöhlker, C., Petäjä, T., Kulmala, M., Andreae, M. O., Shiraiwa, M., Pöschl, U., Hoffmann, T. and Kalberer, M.: Radical formation by fine particulate matter associated with highly oxygenated molecules. *Environmental science & technology,* **53(21)**, 12506-12518, (2019).

3. Filippi, A., Liu, F., Wilson, J., Lelieveld, S., Korschelt, K., Wang, T., Wang, Y., Reich, T., Pöschl, U., Tremel, W., and Tong, H.: Antioxidant activity of cerium dioxide nanoparticles and nanorods in scavenging hydroxyl radicals. *RSC advances,* **9(20)**, 11077-11081, (2019).

4. Kampf, C. J., Filippi, A., Zuth, C., Hoffmann, T., and Opatz, T.: Secondary brown carbon formation via the dicarbonyl imine pathway: nitrogen heterocycle formation and synergistic effects. *Physical Chemistry Chemical Physics,* **18(27)**, 18353-18364, (2016).

Oral Presentations

1. Filippi, A.: Size Distribution of Environmentally Persistent Free Radicals in Ambient Aerosols, Doktorandenseminar (DoSe), Mainz, Germany, 13th January 2020.

2. Filippi, A.: Redox Chemistry and Health Effects of Atmospherically Relevant Reactive Species, MPGC PhD Seminar, Mainz, Germany, 12th December, 2018.

Poster Presentations

1. Filippi, A., Wietzoreck, M., Wilson, J., Lelieveld, S., Berkemeier, T., Pöschl, U., Lammel , G., Tong, H.: Reduction potential as an indicator for H_2O_2 productivity of organic aerosols, General Assembly of the European Geosciences Union, Vienna, Austria, 7th - 12nd April 2019.

2. Filippi, A., Wietzoreck, M., Wilson, J., Lelieveld, S., Berkemeier, T., Pöschl, U., Lammel , G., Tong, H.: Reduction potential as an indicator for H_2O_2 productivity of organic aerosols, International Conference on Carbonaceous Particles in the Atmosphere, Vienna, Austria, 3rd – 6th April 2019.

3. Filippi, A., Li, C., Lelieveld, S., Wilson, J., Wietzoreck, M., Lammel, G., Pöschl, U., and Tong, H.: H_2O_2 yield of atmospherically relevant quinones in surrogate lung fluid, Biennial Meeting of the Society for Free Radical Research International, Lisbon, Portugal, 4th – 7th June 2018.

4. Filippi, A., Liu, F., Pöschl, U., Tong, H.: Adverse Health Effect of Atmospheric aerosols: The Role of Radicals, Sino-European Summer School on Atmospheric Chemistry, Fudan University Shanghai, China, 21st – 30th November 2017.